Electronic Theses and Dissertations

Theses, Dissertations, and Major Papers

1-1-2007

Reconfigurable kinematics, dynamics and control process for industrial robots.

Ana Djuric
University of Windsor

Follow this and additional works at: https://scholar.uwindsor.ca/etd

RECONFIGURABLE KINEMATICS, DYNAMICS AND CONTROL PROCESS FOR INDUSTRIAL ROBOTS

by

Ana Djuric

Dissertation
Submitted to the Faculty of Graduate Studies through
Mechanical, Automotive, and Materials Engineering in Partial Fulfillment of the
Requirements for
the Degree of Doctor of Philosophy at the
University of Windsor

Windsor, Ontario, Canada
2007
© 2007 Ana Djuric

Library and
Archives Canada

Published Heritage
Branch

395 Wellington Street
Ottawa ON K1A 0N4
Canada

Bibliothèque et
Archives Canada

Direction du
Patrimoine de l'édition

395, rue Wellington
Ottawa ON K1A 0N4
Canada

Canada

ABSTRACT

This work, aims at developing a highly reconfigurable control system which intelligently unifies the reconfiguration and manages the interaction of individual robotics control systems within a reconfigurable manufacturing system (RMS). For performing any reconfigurable control process, a reconfigurable plant model that represents different robotic systems was developed.

Instead of modeling and creating new reconfigurable systems, new modular robots and machines, the existing systems, robots and machines were defined as reconfigurable systems, modular robots and machines according to their reconfigurable aspects. From the study of existing robotic software and reviewing the literature, the idea of grouping robots according to their kinematic similarities was conceived and the Reconfigurable PUMA-Fanuc (RPF) model was developed.

A generic solution module called the Unified Kinematic Modeler and Solver (UKMS) implements the geometric approach for solving the inverse kinematic problem for the (RPF) model.

A Reconfigurable PUMA-Fanuc Jacobian Matrix (RPFJM) and reduced Reconfigurable PUMA-Fanuc Singularity Matrix (RPFSM) were developed.

The Reconfigurable Robot Workspace (RRW) was developed using the Filtering Boundary Points (FBP) method.

For the symbolic calculation of the RPF dynamics equations, named Reconfigurable PUMA-Fanuc Dynamic Model (RPFDM), the recursive Newton-Euler algorithm was employed, using the symbolic algebra package MAPLE 10®. The simplification of the model was done using the Automatic Separation Method (ASM). The significance of the RPFDM is that it automatically generates each element of the inertia matrix A, Coriolis torques matrix B, centrifugal torques

matrix C, and gravity torques vectors G. This model was extended to include the robot actuator dynamics and the complete electro-mechanical model named RPFDM+ is presented.

The Reconfigurable Control Platform (RCP) was developed using Matlab/Simulink® software. As a case study, the PUMA 560 robot was selected and the reconfigurable "PI" controller was designed as a function of the motor parameters.

All eight modules (RPF, UKMS, RPGJM, RPFSM, RRW, RPFDM, RPFDM+, and RCP) can be reconfigured by changing the parameters K_1, K_2, K_3, K_4, K_5, and K_6. These parameters represent the sinus and cosines of the robot twist angles. Using the ABB, Fanuc and PUMA 560 robots, the examples were performed.

DEDICATION

To my mother Ljubinka Vulovic.

ACKNOWLEDGEMENTS

I would like to express my sincerest and deepest appreciation to my supervisor Professor Waguih ElMaraghy for giving me the opportunity, his guidance, and for helping me throughout the course of my Ph.D program. I would also like to extend my thanks to my Supervisory Committee, Dr. Waguih ElMaraghy, Dr. Robert Gaspar, Dr. Bruce Minaker, Dr. Nader Zamani, and Dr. Jonathan Wu, for their comments and time in reviewing my dissertation.

I would like to acknowledge the great help and insight that I received from the IMS Centre directors, Professor Hoda ElMaraghy and Professor Waguih ElMaraghy, for giving me the chance to discuss the research topics with other members through the regular meetings they arranged for us. I learned a lot from these meetings. I would like to extend my thanks to all other members in IMS Centre especially to Dr. R. Jill Urbanic, Biljana Marinkovic and my college Dr. Mirjana Filipovic for their suggestions and encouragement.

I would like to thank the Staff of both, the Department of Mechanical, Materials and Automotive Engineering and Industrial and Manufacturing Systems Engineering Department: Ms. Jacquie Mummery, Mr. Ram Barakat, Ms. Zaina Batal, and Ms. Rosemarie Gignac and Ms. Barbara Denomey for their support and kind assistance during my study.

TABLE OF CONTENTS

viii

x

LIST OF TABLES

xii

LIST OF FIGURES

xiv

xvi

xvii

NOMENCLATURE

Abbreviations

A:	Arm.
ASP:	Automatic Separation Procedure.
AA:	Above arm.
BA:	Below arm.
D:	Down.
DD:	Dynamic Damping.
DF:	Do not flip.
D-H:	Denavit – Hartenberg.
DOF:	Degree of Freedom.
E:	Elbow.
EA:	Elbow Above.
EB:	Elbow Below.
F:	Flip.
FBP:	Filtering Boundary Points.
HIC:	Hybrid Impedance Control.
LA:	Left Arm.
L&A:	Left and Above.

L&B:	Left and Below.
NSERC:	Natural Science and Engineering Council of Canada.
OOP:	Objected Oriented Programming.
PD:	Proportional Differential.
PI:	Proportional Integral.
PID:	Proportional Integral Differential.
PUMA:	Programmable Universal Machine for Assembly.
RA:	Right arm.
R&A:	Right and Above.
R&B:	Right and Below.
RCP:	Reconfigurable Control Platform.
RMS:	Reconfigurable Manufacturing System.
RPF:	Reconfigurable Puma-Fanuc.
RPFJM:	Reconfigurable Puma-Fanuc Jacobian Matrix.
RPFSM:	Reconfigurable Puma-Fanuc Singularity Matrix.
RRW:	Reconfigurable Robot Workspace.
RPFDM:	Reconfigurable Puma-Fanuc Dynamic Model.
RPFDM+:	Reconfigurable Puma-Fanuc Dynamic Model Plus.
RNE:	Recursive Newton-Euler Algorithm.

RRP:	Reconfigurable Robot Platform.
SCARA:	Selective Compliant Articulated Robot Arm.
U:	Up.
UKMS:	Unified Kinematic Modeler and Solver.
UROCA:	Unified Reconfigurable Open Control Architecture.
W:	Wrist.
WD:	Wrist down.
WU:	Wrist up.

Symbols

A:	6×6 Inertia matrix.
$\hat{A}$:	Diagonal matrix.
a:	Approach vector
a_i:	i^{th} Link offset.
a_{ij}:	Matrix A elements.
$^{i}(^{0}a_i)$:	i^{th} Linear acceleration.
$^{i}(^{0}a_{ci})$:	i^{th} Linear acceleration of the center of mass.
B:	6×15 Coriolis torques matrix.
B_L:	Load Damping Coefficient.
B_m:	Armature Damping Coefficient.

$\hat{B}$:   Diagonal matrix.

$b_{i,ij}$:   Matrix B elements.

C : 6×6 Centrifugal torques matrix.

$\hat{C}$:   Diagonal matrix.

C_b :   Boundary singularities.

C_i :   Interior singularities.

c_{ij} :   Matrix C elements.

d_i : i^{th} Link length.

E :   Center of the end-effector.

E_g :   Back electromotive force.

e :   Efficiency.

$^{i}(f_i^{*})$:   Joint forces.

$^{6}(^{6}f_{Tool}) = 0$:   End-effector force.

G : 6×1 Gravity torques vector.

^{i}g : i^{th} Gravity vector.

I_i : i^{th} Moment of inertia about center of mass of each link.

i_m :   Armature current.

J :	The Jacobian matrix.
J_{11} :	3×3 block of the Jacobian matrix.
J_{22} :	3×3 block of the Jacobian matrix.
J_E :	End-effector Jacobian matrix.
J_L :	Load Inertia.
J_m :	Armature Inertia.
J_W :	Wrist Jacobian matrix.
K_b :	Voltage constant.
K_i :	i^{th} Configuration parameter of the ith twist angel α_i.
K_t :	Torque constant.
L_m :	Armature Inductance.
M :	Parameter.
m_i :	i^{th} Link mass.
N :	Gear ratio.
n :	Normal vector.
$^i(n_i^*)$:	Joint moments.
N_L :	Number of teeth of the output gear (load gear).
N_m :	Number of teeth of the input gear (motor gear).

xxii

$^6(^6n_{Tool}) = 0$:　　　　　End-effector moment.

O_3, O_4, O_5, O_6 :　　　　　Centers of the 3th, 4th, 5th and 6th joints coordinate frames.

$O_{3\times3}$:　　　　　3×3 zero matrix.

p :　　　　　Position vector which points from the origin of the shoulder coordinate system (x_0, y_0, z_0) to the point where the last three joints are intersecting.

p_6 :　　　　　Position vector which points from the origin of the shoulder coordinate system (x_0, y_0, z_0) to the position of the end-effector.

P_{ci} :　　　　　i^{th} Radial distance to the center of mass of each link.

p_E :　　　　　Position vector of the end-effector center E.

P_{IN} :　　　　　Input power.

$^{i-1}P_i$:　　　　　i^{th} Position matrix.

P_i :　　　　　Point on the 2-3 envelope

$P_{i1}, P_{i2}, P_{i3}, P_{i4}$:　　　　　Points in each quadrant of the local coordinate system.

P_{OUT} :　　　　　Output power.

p_x, p_y, p_z :　　　　　Coordinates of the position vector p with respect to the (x_0, y_0, z_0).

p_W :　　　　　Position vector of the spherical wrist W.

q :　　　　　Vector of generalized joint coordinates.

xxiii

$\dot{q}$:   Vector of joint velocities.

$\ddot{q}$:   Vector of joint acceleration.

RPM :   Rotation per Minute.

r :   Parameter.

r_i :   Center of mass for i^{th} link.

$^{i-1}R_i$: i^{th} Rotational matrix.

$(^{i-1}R_i)^T$:   Transpose of all rotational matrices.

R_m :   Armature Resistance.

S :   Parameter.

s :   Sliding vector.

$^0T_6$:   Homogeneous transformation matrix, which specifies the position and orientation of the end point of manipulator with respect to the base coordinate system.

$^{i-1}T_i$:   Homogeneous transformation matrix from $(i-1)^{th}$ link to i^{th} link.

T_M :   Motor generated torque.

T_{stall} :   Stall Torque.

V :   Armature Voltage.

$^i(^0V_i)$: i^{th} Linear velocity.

xxiv

V_{max} :	Maximum voltage.
w :	Parameter.
W :	Center of the spherical wrist.
$\dot{X}_E$:	End-effector velocity.
$\dot{X}_W$:	Wrist velocity.
x_i :	Vector of generalized Cartesian coordinates.
$\dot{x}_i$:	Vector of Cartesian velocities.
$\ddot{x}_i$:	Vector of Cartesian acceleration.
$z - w$:	Local coordinate system.
α_i :	i^{th} Twist angle.
${}^i({}^0\alpha_i)$:	i^{th} Angular acceleration.
β :	Angle.
δ :	Small distance from P_i.
ϕ :	Angle.
φ :	Angle.
θ_i :	i^{th} Joint angle.
θ_i^L :	i^{th} Joint angle for Left Arm configuration.

xxv

$\theta_i^R:$ i^{th} Joint angle for Right Arm configuration.

$^{i-1}\dot{\theta}_i:$ i^{th} Angular velocity vector.

$\theta_m:$ Angular position of armature.

$\tau:$ Load torque.

$\Omega:$ Parameter.

$\omega:$ Angular velocity of armature.

$^i(^0\omega_i):$ i^{th} Angular velocity.

$\psi:$ Parameter.

CHAPTER ONE

1. INTRODUCTION

A generic, reconfigurable kinematic module was an important need for the Unified Reconfigurable Control Architecture (UROCA) an architecture developed as part of the Strategic Research Project at the University of Windsor, supported by the Natural Science and Engineering Council of Canada (NSERC) Strategic Project Grant in "Reconfigurable Control Process for Manufacturing" provided to Prof. W. ElMaraghy.

Previous research investigations, for the sake of having several generic solutions, classified robot kinematic groups according to their twist angles, which are fixed for each group (Balkan M. T., et al., 2001). Accordingly, a different solution was provided for each group. The UKMS, unlike the others, accepts all the possible orientations for each joint within the RPF model, and therefore, it discards any classification that is based on having fixed twist angles. Instead, the UKMS unifies the model and generalizes the solution for robots of different twist angles rather than having different solutions for small groups of 6R robots with fixed twist angles.

There are different approaches for solving the inverse kinematic problem: algebraic, iterative and geometric. Different investigators used the following methods: the screw algebra (Kohil D., and A. H. Soni, 1975), the inverse transform (Paul P.R., 1981), the dual matrices (Pennock G. R. and Yang A. T., 1985), the dual number quaterian (Yang A. T., and R. Freudenstein, 1964), the iterative method (Uicker J. J. Jr., et al., 1964), and the homogeneous matrix approach (Legnani G., et al., part 1, 1996), (Legnani G., et al., part 2, 1996). Tsai L.W., 1985, presented an analytical approach for the inverse kinematic problem that requires solving a system of eight second-order equations in eight unknowns. A semi-analytical method for solving the inverse kinematics for the Fanuc Arc Mate

1

Series was presented by Balkan M. T., *et al.*, 2000. It is based on parameterised joint variables and analytical inverse kinematic solutions, which were proposed for some classes of robots according to a classification made by the authors. Bekir K. and Serkan A., 2000 have implemented the artificial neural-network approach for solving the inverse kinematics of one type of six-joint robot. The well-known fixed-point iteration algorithm for solving a non-linear system of equations was applied by Tourassis V. D. and Ang M. H. Jr, 1989 for solving the inverse kinematic problem of 6R robots. Manseur R. and Doty K. L. made a series of publications (Manseur R. and Doty K. L., 1996), (Manseur R. and Doty K. L., 1992), (Manseur R. and Doty K. L., 1989), (Manseur R. and Doty K. L., 1988) for solving the inverse kinematics of 6R manipulators by applying iterative and one-dimensional numerical approaches. A unified kinematic approach for solving robot kinematics has been applied on the PUMA 560 robot, (Gu Y. L. and Ho J. S., 1990).

The geometric approach for solving the inverse kinematic problem was applied for three-joint placeable robots with either rotational or translational joints by Fu H., *et al.*, 1998. Fischer I.S., 2000 extended the geometric method for application to the seven-joints Space Station Remote Manipulator System (SSRMS). Fu H., *et al.*, 2000 have presented four new geometric invariants for the 6R manipulators in order to eliminate the joint variables in closure equations developed for solving this type of manipulator. These four invariants replace the Gaussian elimination process that was frequently used by other researchers. (Chapelle F., and Bidaud P., 2000) implemented an evolutionary symbolic regression algorithm for approximating the inverse kinematic model of any generic 6R manipulators. Her M. G., *et al.*, 2002 presented a paper that concerned the inverse kinematic approximation by using a fuzzy logic method tuned by a genetic algorithm. A common deficiency in the above mentioned methods occurs when one attempts to select the most appropriate solution among all the possible ones. Pashkevich A., 1997, used the geometric approach for solving the inverse kinematics for robots with an offset wrist. His work concerned a group of robots which do not belong to

2

the RPF model for the moment. The RPF model will be extended in future to include this type of robot.

In this work, solving the inverse kinematic problem of the RPF model, which has the first three joints rotating and the last three joint axes intersecting at a point, is performed by the geometric approach (Lee C. S. G., and Ziegler M., 1984). This approach, as was more elaborated by Fu K.S., *et al.*, 1987 and Owens J. P., 1994, is generalized for application to a wide class of 6R industrial robots that fall within the scope of our RPF model. Some modifications and adjustments made to the geometric approach were necessary in order to generalize it for application to the RPF model. In the first place, have chosen to implement this approach because it is much simpler than the other methods for application to different robotic systems having rotational joints. The resulting unified geometric-based solution can be used for any robotic manipulator that has a kinematic structure falling within the scope of the RPF model. The main feature of this solution is that one can use the same equations, which include newly introduced configuration parameters, for solving a wide variety of 6R kinematic groups in the RPF model.

Currently there is interest in research on the modeling and creation of reconfigurable systems, modular robots and machines (Matsumaru T., 1995), (Kelmar L. and Khosla P., 1988), (Benhabib B., *et al.*, 1989), (Chen I. M. and Yang G., 1996), (Podhorodeski R. P. and Nokleby S. B., 2000). This work is based on the power of comparison between different robotic systems, and the result is the development of reconfigurable parameters for solving their inverse kinematics. Future research will extend the unified approach to reconfigurable robots.

The RPF and UKMS modules require the development of their Jacobian matrix. Previous research investigations were on developing the Jacobian by using different methods. These methods are compared in terms of their computational efficiency since the Jacobian must be computed in real time for control. A review of these methods is given by Orin D. E. and Schrader W. W. 1984.

3

A comparison, using three different methods for calculating, the Jacobian of 6 DOF robots with rotary or sliding joints are presented by Fu K.S., *et al.*, 1987 and applied on the PUMA robot. By employing symbolic reduction techniques in conjunction with the separation of the resultant equations into on-line, temporary variables and off-line constraints, efficient formulations of the Jacobian, inverse Jacobian, and inverse Jacobian multiplied by a vector have been developed by Leathy M. B., *et al.*, 1987. The Jacobian can be obtained by a simple method explained in (Spong M. W. and Vidyasagar M. 1989. The study and resolution of singularities for the PUMA robot were analyzed in detail by Cheng F. T., *et al.*, 1997, Oenny D., *et al.*, 2000, and Yuan J., 2001.

An important step for robot singularity analysis is task decoupling. This concept has been known since Pieper's pioneering work (Pieper, D. L, 1968). The complete analysis of task decoupling was done in detail by Tourassis V. D. and Ang M. H. Jr, 1995.

The structural synthesis and the singularity analysis of six different families of orthogonal anthropomorphic robotic manipulators with 6R degrees of freedom, were presented by Gogu G., 2002. The kinematics singularities of each family were analyzed and interpreted both algebraically and geometrically. The singular configurations of 6R robots with spherical wrist in general and the KUKA KR-15/2 industrial robot in particular, are analytically described and classified by Hayes M. J. D., *et al.*, 2002.

Symbolic inversion of the Jacobian matrix for the robots with spherical wrist was investigated by Fijany A. and Antal K. Bejczy 1988 and the examples were performed on PUMA, Stanford and 6R joints coplanar robot.

The next reconfigurable solution for the RPF is the robot work envelope. This problem attracted researchers for many investigations for calculation of the robot envelope for different types of robots with 2, 3 and more degrees of freedom and different types of joints (rotational or translational). The algorithm for calculating the

4

workspace volume was developed for manipulators which consist of revolute or prismatic joints at any stage but the first (Shaik M. A. and Datreis P., 1986).

Calculation for the exterior boundary and interior boundary (boundary to voids) for n-DOF manipulators has been developed by Abdel-Malek K., *et al.*, 2000. The formulation of the workspace boundary for n-DOF rotational joint manipulator was presented by Ceccarelli M., 1996. The examples of up to 6R manipulators have been used to demonstrate a procedure. A general 4R manipulator's workspace boundary was algebraically calculated. Effects of link lengths and link offsets on the 2D workspace were analyzed (Ceccarelli M., and Vinciguerra A., 1995). The workspace calculation of the n-DOF redundant manipulator with rotating base was presented by Kwan S. J., *et al.*, 1991 and Hansen J. A., *et al.*, 1983.

For seven different kinematic structures (PPP, RPP, PRP, PPR, PRR, RPR and RRR), where R is for rotational joints and P is for prismatic joints, regional structures were calculated for the workspace analysis (Spanos J., and Kohil D., 1985). Kohil D., and Spanos J., 1985 used polynomial discriminants for workspace analysis. This is applied on robots with spherical wrists.

Determination of the workspace, envelope volume, bifurcation analysis, and cross sectional views of the workspace for 3, 4, and 5 DOF manipulators is presented by Abdel-Malek K., *et al.*, 1999. The calculation of the workspace for 2-DOF planar robot was done by Zhang H., *et al.*, 1991. There is no work on the workspace calculation using a reconfigurable approach applied on a reconfigurable model.

The RPFDM represents the next important module that UROCA requires. For robotic systems with few degrees of freedom, direct application of Lagrangian, Newton-Euler, or other methods can be used for the development of the equations of motion.

Two identification methods: the "step-by-step method" and the "simultaneous method" were experimentally examined to estimate the parameters of the dynamic

5

model of the PUMA 560, (Yoshida K., *et al.*, 1992). Using the Lagrangian energy method, the dynamic equations were calculated, and simplified by using general conditions on the link parameters (Park H. S., and Cho H. C., 1991). Three algebraic methods (Lagrange's method, Kane's method and Wittenburg's method) for developing the equations of motion for a three-degree-of-freedom PUMA robot were compared on the basis of computational efficiency (Ju M. S., and Mansour J. M., 1989). An efficient structure for the computation of robot dynamics in real time was presented by Izaguirre A., *et al.*, 1992, and the results agree with the PUMA 260 robot. The equations of motion for serial-link manipulators were calculated in symbolic form using a recursive Newton-Euler algorithm and the symbolic algebra package MAPLE 7®, (Corke P. I., 1998). For this general technique the investigation was particularly concerned with the PUMA 560 robot. Use of the same recursive Newton-Euler algorithm for dynamic calculation of an open-loop kinematic chain was presented by Walker M. W., and Orin D. E., 1982. They compare the computational complexity of four different methods for calculation of the joint variable: joint position, velocity, acceleration and input torques or forces. A deterministic simplification procedure of the PUMA 560 robot has been introduced by Armstrong B., *et al.*, 1986. A numerical comparison of different kinematic, dynamic and electrical parameters for the PUMA 560 robot were presented by Corke P. I., and Armstrong B., 1994.

The Efficient Manipulator Dynamic Equation Generator (EMDEG) has been used for generation of dynamic equations in symbolic form, and the example of the PUMA 560 has been generated (Burdick J. W., 1986). The reduced PUMA 600 dynamic model has been developed using Newton-Euler and Lagrange-Euler algorithms (Leathy M. B., *et al.*, 1986). The Newton-Euler recursive algorithm was used by other researchers for inverse dynamics calculations for robotic systems (Rajagopalan R.,1996) (Yamakita M., *et al.*, 1991), (Featherstone R., and Orin D., 2000), (Palaz H., *et al.*, 1993). A computer aided design package called Robotica was developed by Nathery J. F. and Spong M., 1994, for symbolic and numeric

6

calculation of kinematic and dynamic equations for multi-degree-of-freedom manipulators.

After developing seven reconfigurable modules: RPF, UKMS, RPFJM, RPFSM, RRW, RPFDM, and RPFDM+, which together represent the robot plant model, the next step is to design matching controller.

A nonlinear feedback robot control was implemented for the coupled robot manipulator dynamics and robot joint actuator dynamics. The controller was experimentally evaluated on the PUMA 560 robot. The comparison between a nonlinear feedback robot control based on the robot dynamics only and control of the coupled dynamics system showed that the second one has better performance (Tarn T. J., *et al.*, 1991).

A dynamic damping (DD) control law introduced by (Anderson J. Robert, 1990) was implemented for robot control and compared with the computed torque and "PD" control laws. The advantage of the DD control laws granted stability, greater bandwidth, for small inertias, and more efficient utilization of torque. The DD control law is recommended for PUMA 560 robot because this robot has extensively varying inertia. A unification of different approaches to force and position control of robots was named Hybrid Impedance Control (HIC), (Anderson J. Robert and Mark W. Spong, 1988). The HIC use a duality condition which allows to select a control for different type of environment.

The controller for a PUMA 512 robot was replaced with a PC based controller that can achieve real time direct control of a six joint robot. The values of the proportional joint controllers are presented (Katupitiya J., *et al.*, 1997). The "PI" and "PID" controllers were designed for independent robot joint control. The PUMA 560 was used as an example for the experimental evaluation of the controllers (Hsia T. C., *et al.*, 1988). The nonlinear model-based predictive control and computed torque control were compared using a PUMA 560 robot. The predictive control gives better results, (Vivas A., and Mosquera V., 2005).

7

Different control designs for the PUMA 560 have been done by many researchers, (Sokolov A. and Sandor J. Toth, 1999), (Nagy P. V., 1988), (Dixon W. E., *et al.*, 2001), (Moreira N., *et al.*, 1996), (Goldenberg A. A. and Chan L., 1988). However, none of this research considered reconfigurable control design for reconfigurable robot models.

Table 1.1 presents a literature review summary. The highlighted area under the 6R reconfigurable twist angles robot family represents the area that was not covered in literature and was investigated and solved in this research.

Table 1.1: Literature Review Summary Matrix

Modeling	Specific Robot Family					
	PUMA	Fixed Twist angles	6R Reconfigurable Twist Angles	6, 5, 4, 3, 2 DOF General	Reconfigurable Robots	Flexible Joints and Links Robots
Kinematics (Geometry Method)	KG_1	KG_2		KG_3	KG_4	KG_5
Kinematics (Other methods)	KO_1	KO_2		KO_3	KO_4	KO_5
Jacobian	J_1	J_2		J_3	J_4	J_5
Singularity	S_1	S_2		S_3	S_4	S_5
Workspace	W_1	W_2		W_3	W_4	W_5
Dynamics	D_1	D_2		D_3	D_4	D_5
Control	C_1	C_2		C_3	C_4	C_5

KG_1: (Lee C. S. G., and Ziegler M., 1984), (Fu K.S., *et al.*, 1987), (Owens J. P., 1994)

KG_2: (Owens J. P., 1994)

8

KG_3: (Pashkevich A., 1997)

KG_4: No references found.

KG_5: No references found.

KO_1: (Gu Y. L. and Ho J. S., 1990).

KO_2: (Balkan M. T., *et al.*, 2000), (Balkan M. T., *et al.*, 2001), (Kohil D., and A. H. Soni, 1975), (Paul P.R., 1981), (Pennock G. R. and Yang A. T., 1985), (Yang A. T., and R. Freudenstein, 1964), (Uicker J. J. Jr., *et al.*, 1964), (Legnani G., *et al.*, part 1, 1996), (Legnani G., *et al.*, part 2, 1996). (Tsai L.W., 1985), (Bekir K. and Serkan A., (2000))

KO_3 : (Tourassis V. D. and Ang M. H. Jr, 1989), (Manseur R. and Doty K. L., 1996), (Manseur R. and Doty K. L., 1992), (Manseur R. and Doty K. L., 1989), (Manseur R. and Doty K. L., 1988), (Fu H., *et al.*, 1998). (Fischer I.S., 2000), (Fu H., *et al.*, 2000), (Chapelle F., and Bidaud P., 2001), . (Her M. G., *et al.*, 2002)

KO_4: (Matsumaru T., 1995), (Kelmar L. and Khosla P., 1988), (Benhabib B., *et al.*, 1989), (Chen I. M. and Yang G., 1996), (Podhorodeski R. P. and Nokleby S. B., 2000).

KO_5: (Filipovic M., *at al.*, 2007).

J_1 : (Orin D. E. and Schrader W. W. 1984), (Fu K.S., *et al.*, 1987), (Corke P. I. 1998).

J_2 : (Orin D. E. and Schrader W. W. 1984), (Leathy M. B., *et al.*, 1987), (Spong M. W. and Vidyasagar M. 1989)

J_4 : No references found.

J_5 : No references found.

9

S_1 : (Cheng F. T., *et al.*, 1997), (Oenny D., *et al.*, 2000), and (Yuan J., 2001), (Fijany A. and Antal K. Bejczy 1988), (Corke P. I. 1998)

S_2 : (Tourassis V. D. and Ang M. H. Jr, 1995), (Gogu G., 2002), (Hayes M. J. D., *et al.*, 2002)

S_4 : No references found.

S_5 : No references found.

W_1: No references found.

W_2, W_3: (Shaik M. A. and Datreis P., 1986), (Abdel-Malek K., *et al.*, 2000), (Ceccarelli M., and Vinciguerra A., 1995). (Ceccarelli M., 1996), (Kwan S. J., *et al.*, 1991), (Hansen J. A., *et al.*, 1983) , (Spanos J., and Kohil D., 1985). (Kohil D., and Spanos J., 1985), (Abdel-Malek K., *et al.*, 1999), (Zhang H., *et al.*, 1991)

W_4: No references found.

W_5: No references found.

D_1: (Yoshida K., *et al.*, 1992), (Izaguirre A., *et al.*, 1992), (Corke P. I., and Armstrong B., 1994), (Corke P. I., 1998), (Walker M. W., and Orin D. E., 1982), (Armstrong B., *et al.*, 1986), (Burdick J. W., 1986), (Leathy M. B., *et al.*, 1986),

D_2: (Park H. S., and Cho H. C., 1991), (Ju M. S., and Mansour J. M., 1989), (Rajagopalan R.,1996) (Yamakita M., *et al.*, 1991), (Featherstone R., and Orin D., 2000), (Palaz H., *et al.*, 1993), (Nathery J. F. and Spong M., 1994)

D_4: No references found.

D_5: (Filipovic M., *at al.*, 2007).

C_1: (Anderson J. R., 1990), (Tarn T. J., *et al.*, 1991), (Katupitiya J., *et al.*, 1997), (Hsia T. C., *et al.*, 1988), (Vivas A., and Mosquera V., 2005), (Sokolov A. and

Sandor J. Toth, 1999), (Nagy P. V., 1988), (Dixon W. E., *et al.*, 2001), (Moreira N., *et al.*, 1996), (Goldenberg A. A. and Chan L., 1988).

C_2: This was not investigated.

C_3: No references found.

C_4: No references found.

C_5: No references found.

1.1. Problem Statement

A reconfigurable approach to modeling and designing new manufacturing processes, production, automated machines, software, hardware, and etc., is a current research trend. Automated machines are the essentials of reconfigurable manufacturing. To be able to use them in future reconfigurable manufacturing systems, there is a need to treat them as reconfigurable automated machines. However according to a literature review, the reconfigurable robotic software does not exist yet.

Most of the simulation and off-line programming software is designed so as to provide only robot kinematic models. Usually they have a library of some robots, and if user needs a new robot, they have the option to buy it or to model it with software that they have. This process is sometimes complex and long. The current simulation and off-lining programming software can not be used to perform any reconfigurable control process.

This problem can be solved using the new approach of designing a reconfigurable plant model which can be used for reconfigurable control process. First step in creation of the reconfigurable modules is unification of different robotic systems. Unification is done by comparing different robotic systems and

11

developing reconfigurable parameters. The analysis was done using simulation and off-line programming software Workspace 5®. The eight developed reconfigurable modules (RPF, UKMS, RPGJM, RPFSM, RRW, RPFDM, RPFDM+, and RCP) represent a reconfigurable robot plant model. This solution can be used for any robot that belongs to the RPF group of robots. By simply putting robot information, these eight reconfigurable modules will automatically generate a robot model and its controller.

1.2. Background of Robotics

The development of the industrial robot-arm was of particular importance. Its ability to emulate the serial-link manipulator nature of the human-arm has led to a whole new class of production tasks that may be profitably automated. Examples are paint-spraying, welding, assembly, and pick-and-place operations. More recently, advances in image-recognition, tactile-sensing, and artificial-intelligence have expanded the number of potential applications into those areas where sensory feedback from the environment is required, such as picking up objects which have been randomly placed on a conveyor-belt.

'Dumb' manipulators (controlled directly by a human instead of following a computer program) have found further applications in carrying out tasks that might be potentially hazardous to humans. Examples are handling radioactive materials, and manipulating objects underwater or in space (Owens, 1990).

The first robots were introduced in the manufacturing industry in the USA in 1961. Since that time there has been a significant growth in the number of robots in use and the range of applications in which they are used. Today robots play a key role in industrial and manufacturing engineering. In developed countries, many large-scale national and international robot related research and development programs have been launched and are still underway (Ulrich, 1990). There are over 100 robot manufacturers around the world (Djuric A., 1999).

12

In general, robots may substitute for human operators in the following situations (Groover, 1987):

- Hazardous work environment for human operators

- Repetitive and heavy work cycles

- Parts difficult to handle by human operators

- Infrequent product changeovers

- Part positioning and orientating

Many commercially available industrial robots are widely used in manufacturing and assembly tasks, such as material handling, spot/arc welding, parts assembly, paint spraying, loading, and unloading numerically controlled machines. Some robots are also used in space and undersea exploration, and prosthetic arm research.

1.2.1. Description of a Robot Model

From the study of robotic software Workspace 5® (Workspace 5®, User Manual, 2000) and reviewing literature (Djuric A., 1999), (Armstrong B., *et al.*, 1986), the following characteristics are commonly used to describe a robot model:

- Robot name

- Number of joints

- Type of joints

- Joint's positive directions (twist angles α_i and joint angles θ_i)

- Base frame

13

- Tool frame

- Link's lengths d_i

- Link's offsets a_i

- Link's mass m_i

- Radial distance to the center of mass of each link P_{ci}

- Moment of inertia about a center of mass of each link I_i

The structure of the robot consists of a number of links and joints; a joint will allow relative motion between two links. Two types of joints are used, a revolute joint to produce rotation and a translational joint to produce translation. To achieve complete control of the end effector's position and orientation, a minimum of six joints are required. The basic robot arm has three joints; this allows the tool at the end of the arm to be positioned anywhere in the robot's working envelope. Even though there are a large number of robot configurations that are possible, only five configurations are commonly used in industrial robotics. These are Polar, Cylindrical, Cartesian, Jointed Arm, SCARA (Selective Compliant Articulated Robot Arm) in Figure 1.1.

14
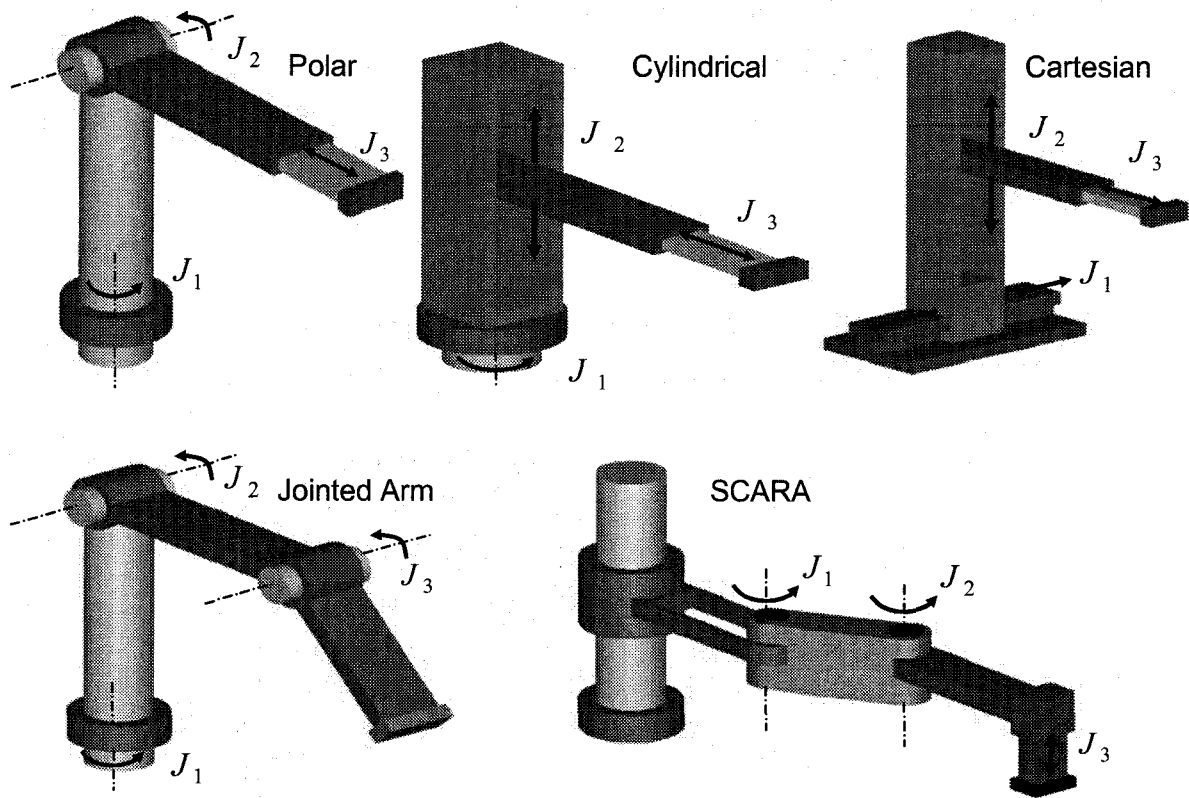
Figure 1.1: Polar, Cylindrical, Cartesian, Jointed Arm, SCARA

For the Polar configuration, the linear extending arm is capable of being rotated around the horizontal and vertical axes. For the Cylindrical configuration, the linear extending arm can be moved vertically up and down in a rotating column. For the Cartesian (Gantry) configuration, there are three orthogonal sliding or prismatic joints. For the Jointed Arm configuration, there are three joints arranged in an anthropomorphic configuration. For the SCARA configuration, there are two rotary axes and a linear joint.

1.2.2. Robot Geometry

The study of robot kinematics requires a unified methodology to identify the variables of a robot's or manipulator's joints and links. Robot arm kinematics deals with the analytical study of the geometry of motion of a robot arm with respect to the fixed reference coordinate system as a function of time, without regard to the forces/moments that cause the motion. Thus, it deals with the analytical

15

description of the spatial displacement of the robot as a function of time, in particular the relations between the joint variable space and the position and orientation of the end-effector of a robot arm.

1.2.2.1 Tool and Base Coordinate frame

Robotic kinematics depends on the use of right handed Cartesian frames of reference. Accordingly, the Tool and Base frames are shown on Figure 1.2.
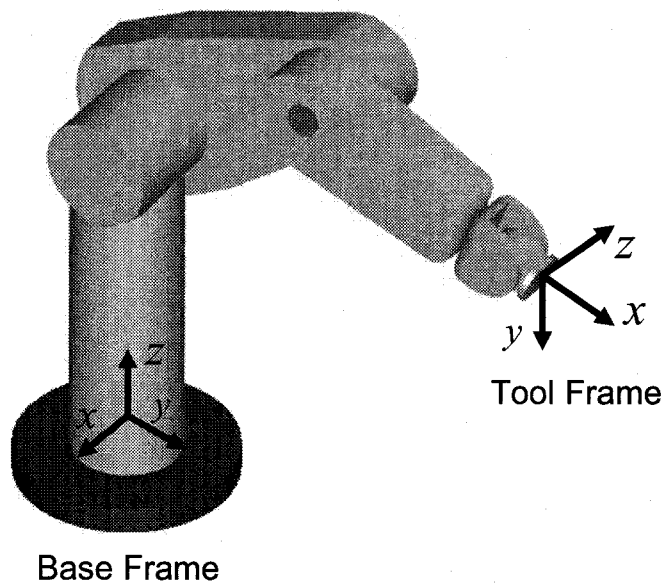
Figure 1.2: Tool and Base frames for the PUMA 560 robot

1.2.2.2 Joints

Two types of joints are commonly found in robots: revolute joints, and prismatic joints. Unlike the joints in the human arm, the joints in a robot are normally restricted to one degree of freedom, to simplify the mechanics, kinematics, and control of the manipulator. In general, two links are connected by a lower-pair joint which has two surfaces sliding over one another while remaining in contact. Only six different lower-pair joints are possible: revolute, cylindrical, spherical, planar, prismatic, and screw, Figure 1.3.

16

Revolute   Cylindrical   Spherical

Planar   Prismatic   Screw
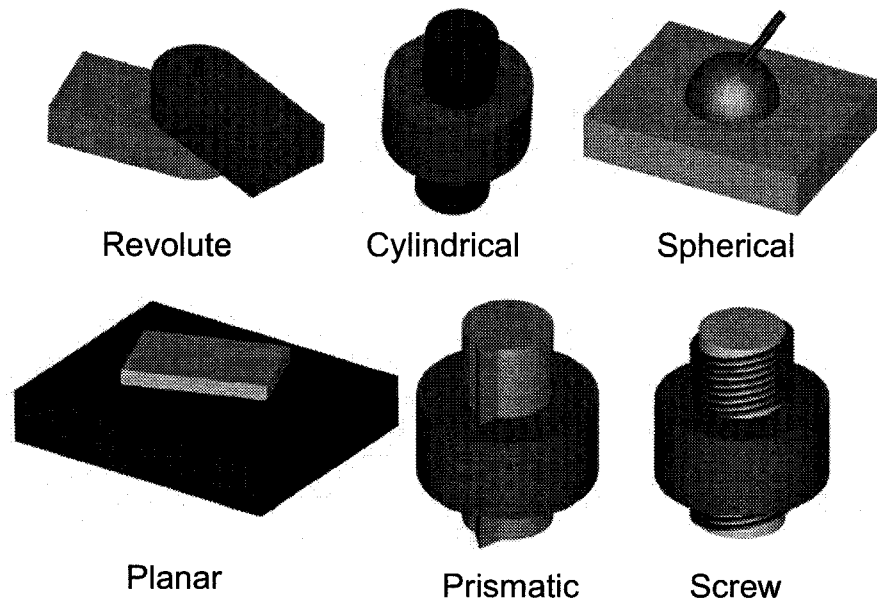
Figure 1.3: The lower pair joints

1.2.2.3 Links

A link is a solid mechanical structure, which connects two joints. The main purpose of a link is to maintain a fixed relationship between the joints at its ends. The last link of a manipulator has only one joint, located at the proximal end (the end closest to the base) of the link. At the distal end of this link (the end furthest away from the base) instead of a joint, there is usually a place to attach a gripper: a tool plate. Between the axes of the joints at the ends of any link there can be two degrees of translation and two degrees of rotation. These degrees of freedom are called the link parameters.

1.2.3. Fundamentals of Robot Kinematics

Kinematics is the relationships between the positions, velocities, and accelerations of the links of a manipulator, where a manipulator is a robot arm. The transformation, between a coordinate frame located in the end-effector of the robot (known as the tool frame) and a coordinate frame located in the base of the robot

17

(known as the base frame) will be studied in detail. This transformation specifies the location (position and orientation) of the hand in space with respect to the base of the robot, but it does not tell us which configuration of the arm is required to achieve this location. As we will see, it is often possible to achieve the same end-effector position with many arm configurations.

A serial link manipulator is a series of links, which connects the end-effector to the base, with each link connected to the next by an actuated joint. If a coordinate frame is attached to each link, the relationship between two links can be described with a homogeneous transformation matrix using D-H rules (Denavit J., and Hartenberg R. S, 1955), and they are named $^{i-1}T_i$, where i is number of joints. The first matrix $^0T_1$ relates the first link to the base frame, and the last $^5T_6$ matrix relates the hand frame to the last link. A sequence of these matrices called the forward kinematic transform of the manipulator is used to describe the transform from the base to the hand of the manipulator.

In the kinematic analysis of manipulator position, there are two separate problems to solve: direct kinematics, and inverse kinematics. Direct kinematics involves solving the forward transformation equation to find the location of the hand in terms of the angles and displacements between the links. The angles and displacements between the links are called joint coordinates and are described with link variables, while the location of the hand in space is described with Cartesian coordinates. Inverse kinematics involves solving the inverse transformation equation to find the relationships between the links of the manipulator from the location of the hand in space. Inverse kinematics is the most difficult problem to solve and, for some manipulators, closed form solutions cannot be found. However, constraints are usually placed on manipulator design so that the inverse solution can be found; without this, the robot is difficult to control in Cartesian space. The inverse kinematic solution for a manipulator is usually derived from the direct kinematic transform; so direct kinematics will be discussed first. Before the direct kinematic algorithm is in detail, discussed a method for

18

assigning coordinate frames to links will be developed. To assign a coordinate frame to a link, the relationship between it and the previous link must be understood. This relationship comprises the rotations and translations that occur at the joints.

1.2.3.1 Denavit - Hartenberg Notation

Each joint is assigned a coordinate frame. Using the Denavit-Hartenberg notation (Denavit J., and Hartenberg R. S, 1955), 4 parameters are needed to describe how a frame i relates to a previous frame $i-1$.

As seen in Figure 1.4, the z_i- axis points along the ith axis. The origin of the ith frame is on the ith axis at the point of the common perpendicular with the $i+1$ frame. The x_i- axis points along the perpendicular, or if the axes intersect, x_i is normal to the plane containing the two axes. The y_i- axis completes a right-handed coordinate system.

After assigning coordinate frames the four D-H parameters can be defined as following (Figure 1.4):

a_i- Link length is the distance along the common normal between the joint axes

α_i-Twist angle is the angle between the joint axes

θ_i-Joint angle is the angle between the links

d_i- Link offset is the displacement, along the joint axes between the links
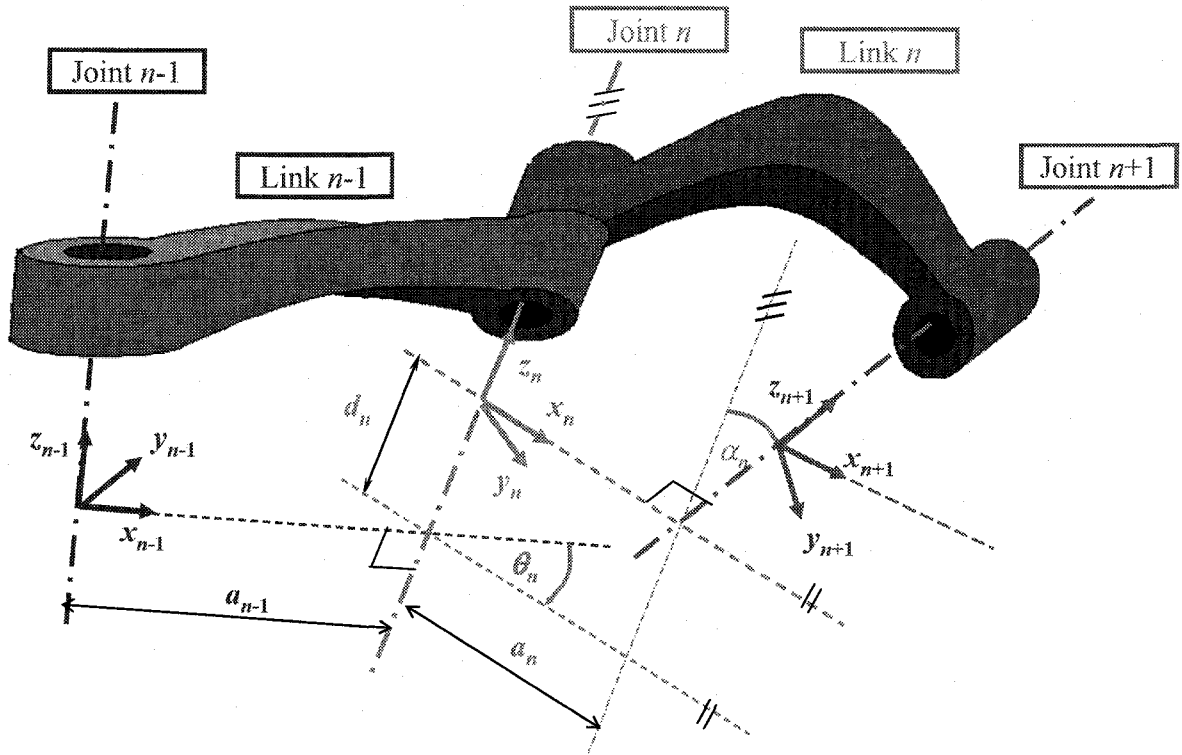
Figure 1.4: Coordinate frames and D-H parameters

Between two frames we have a kinematic relationship, two translations and two rotations:

- Translate along x_{i-1} a length a_{i-1}

- Rotate about x_{i-1} the twist angle α_{i-1}

- Rotate about d_i an angle θ_i

- Translate along z_i a distance d_i

This relationship is mathematically represented by a 4×4 Homogeneous Transformation Matrix in Equation 1.

$$T_x(a_{i-1})R_x(\alpha_{i-1})R_z(\theta_i)T_z(d_i) = \begin{bmatrix} \cos\theta_i & -\cos\alpha_i \sin\theta_i & \sin\alpha_i \sin\theta_i & a_i \cos\theta_i \\ \sin\theta_i & \cos\alpha_i \cos\theta_i & -\sin\alpha_i \cos\theta_i & a_i \sin\alpha_i \\ 0 & \sin\alpha_i & \cos\alpha_i & d_i \\ 0 & 0 & 0 & 1 \end{bmatrix} \quad (1)$$

20

The robot can now be kinematically modeled by using the link transforms:

$$^0T_n = {}^0T_1\,{}^1T_2\,{}^2T_3 \cdots {}^{i-1}T_i \cdots {}^{n-1}T_n \qquad (2)$$

Where ^0T_n is the pose of the end-effector relative to base; $^{i-1}T_i$ is the link transform for the ith joint; and n is the number of links.

1.3. Research Approach

To compare and contrast the different solutions for robot modeling, robot kinematics, dynamics and control, first a literature review was performed, which is covered in Chapter 1.

The reconfigurable robot modeling approach and reconfigurable inverse kinematic solution is presented in detail in Chapter 2. The examples of the ABB IRB1400 and the Fanuc ARCMate120iL robots are used to show the capability of UKMS and to verify inverse kinematic results.

In a Chapter 3, two reconfigurable modules are developed. The first one is the RPFJM. All elements of this matrix are presented in Appendix A. The examples of PUMA group Jacobian named RPJM and the example of the Fanuc group Jacobian named RFJM are presented in Appendix B and Appendix C respectively, second reconfigurable module is the RPFSM. The complete result is in Appendix D. The example for the PUMA and Fanuc cases are the RPSM and the RFSM and their results are in Appendix E and Appendix F respectively. The complete reconfigurable calculation program for RPFJM written in MAPLE 10® is presented in a Technical Document (Djuric 2007).

In a Chapter 4 the reconfigurable robot workspace (RRW) is obtained. The examples of ABB IRB1400 and Fanuc ARCMate120iL robots are used to show the capability of creating workspace in 2D and 3D.

21

The reconfigurable PUMA-Fanuc dynamic model (RPFDM) is developed in Chapter 5. The reduced reconfigurable PUMA 560 dynamic parameters as a function of the K_6 parameter are given in Appendix G. The complete reconfigurable calculation program for RPFDM model written in MAPLE 10® is presented in a Technical Document (Djuric 2007). The extended RPFDM+ model includes DC motors for each link. All motor information is shown in Chapter 6.

The design of the Reconfigurable Control Platform (RCP) for the PUMA 560 is done in Chapter 6. The sizing of the DC motors is done in detail. The reconfigurable "PI" controller for joint position control is designed as a function of robot motor parameters. Simulation is done using Matlab/Simulink ® software. The future work and conclusions are presented in Chapters 7 and 8 respectively.

2. GENERALIZED RECONFIGURABLE 6 - JOINT ROBOT MODELING

2.1. Introduction to Unified Reconfigurable Open Control Architecture (UROCA)

This research is a part of the UROCA (Unified Reconfigurable Open Control Architecture) project, which aims to develop a highly reconfigurable control system that intelligently unifies the reconfiguration and manages the interaction of individual robotics control systems performing in a reconfigurable manufacturing system. As UROCA is intended for controlling a wide variety of industrial machines, it has the feature of easy reconfiguration from one machine to another as well as from one application to another with the lowest amount of change (ElBeheiry E.M., et al., 2004), Figure 2.1.
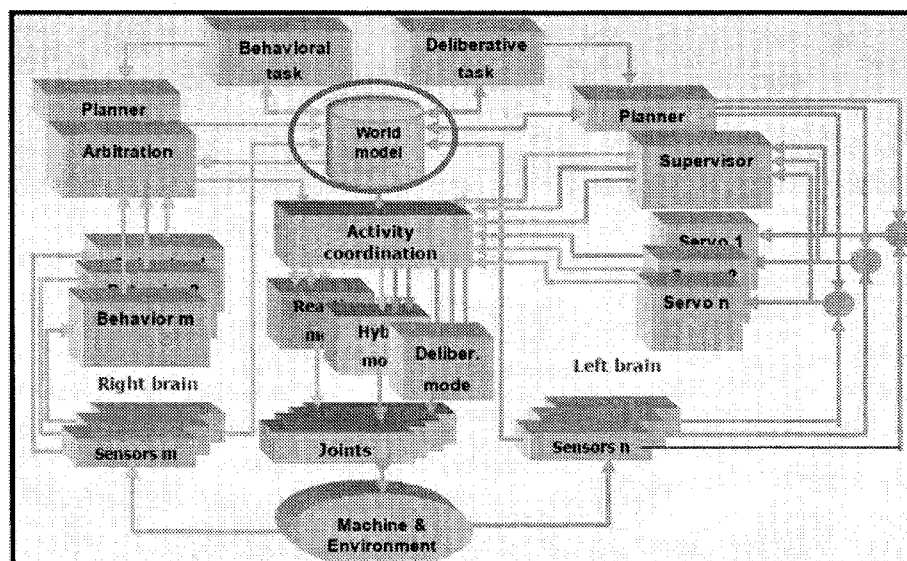
Figure 2.1: UROCA Architecture

23

The goal of this research is to develop reconfigurable World Models for robotic applications, and its position in UROCA is circled in Figure 2.1.

The graphical representation of the UROCA architecture in Figure 2.1 is inspired by human learning principles and the right brain, left brain and whole brain design methodologies. For robotic applications, the left planner, using a world model, performs tasks related to command decoupling, path generation, trajectory planning, kinematics inversion, dynamics calculation, etc. To be able to perform any reconfigurable control process, a reconfigurable plant model that represents different robotic systems, needs to be develop.

2.2. Reconfigurable Aspects of Industrial Robotic Systems

There is a strong possibility here for the UROCA architecture to switch from one template to another, rather than switch from one individual robot model to another.

Most of the current research has been done in the area of modeling modular and reconfigurable robots, machines, reconfigurable controls and software for the modular systems. There is no reconfigurable software or controller designed for existing industrial robots.

To be able to design a reconfigurable controller for existing robots, no one must know what is reconfigurable; the robot's reconfigurable aspects must be found. From the analysis of many industrial robots came with the classification presented in Figure 2.2. This classification has four reconfiguration levels and each level has its own groups of robots:

Level 1: All Industrial robots belong to one group.

Level 2: Robots that has six rotational joints (6R) belong to one group, and robots with combination of rotational and translational joints are in a second group.

24

Level 3: The first group is 6R PUMA type robots, and the second group is 6R Fanuc type robots.

Level 4: Specific single robots from each of the two groups in Level 3 represent their own groups.

LAVEL 1

Industrial Robots

$(^1K_i)^r = f(^ia_i, ^id_i)$

LAVEL 2

6R Puma-Fanuc type robots

Joint	θ_i	d_i	l_i	α_i
1	θ_1	d_1	l_1	±90
2	θ_2	d_2	l_2	±180; 0
3	θ_3	d_3	l_3	±90
4	θ_4	d_4	0	±90
5	θ_5	0	0	±90
6	θ_6	d_6	l_6	±180; 0

Translational and/or rotational 3-4-5 DOF type robots

LAVEL 3

6R Puma type robots

Joint	θ_i	d_i	l_i	α_i
1	θ_1	d_1	l_1	-90
2	θ_2	d_2	l_2	0
3	θ_3	d_3	l_3	90
4	θ_4	d_4	0	-90
5	θ_5	0	0	90
6	θ_6	d_6	l_6	±180; 0

6R Fanuc type robots

Joint	θ_i	d_i	l_i	α_i
1	θ_1	d_1	l_1	-90
2	θ_2	d_2	l_2	180
3	θ_3	d_3	l_3	90
4	θ_4	d_4	0	-90
5	θ_5	0	0	90
6	θ_6	d_6	l_6	±180; 0

LAVEL 4

ABB IRB 1400 robot

$(^1K_i)^r = const$
$\theta_i, d_i, l_i = const$

Joint	Theta	D	A	Alpha
1	-360.00	475.00	150.00	-90.00
2	-90.00	0.00	600.00	0.00
3	180.00	0.00	-120.00	90.00
4	0.00	720.00	0.00	-90.00
5	0.00	0.00	0.00	90.00
6	0.00	85.00	0.00	0.00

Fanuc ARC Mate 120iL robot

$(^2K_i)^r = const$
$\theta_i, d_i, l_i = const$

Joint	Theta	D	A	Alpha
1	0.00	700.00	200.00	-90.00
2	-90.00	0.00	800.00	180.00
3	180.00	0.00	-75.00	90.00
4	0.00	-813.00	0.00	-90.00
5	0.00	0.00	0.00	90.00
6	0.00	-100.00	0.00	0.00

Figure 2.2: Classification of Industrial robots

The reconfigurable controller, for example, is supposed to control the path for different robots, which includes position, velocity and acceleration (forward and inverse kinematics). To be able to control the path for different robots, there is a

25

need to develop a reconfigurable kinematic module using all the information from the analysis of the robots' similarities and differences, and the robots' reconfigurable parameters. From Figure 2.2 can be recognized a group of 6R PUMA-type and Fanuc-type robots which represent RPF model.

2.3. Development of the RPF Model

As a preliminary step towards having the RPF model, kinematic structures of 197 different industrial robots from 11 different manufacturers where analyzed: ABB, Adept, Comau, Fanuc, Kawasaki, Kuka, Motoman, Nachi, Panasonic, Staubli, and Daihen. The results are reported in Table 2.1. Listed robots in bold are PUMA type, underlined are Fanuc type and italic are others.

From the analysis of similarities and differences between different robotic systems, can be concluded: most of 6 rotational joints industrial robots have either PUMA or Fanuc kinematic structure. The most noticeable difference between the two kinematic groups is in the direction of joint 3, which is reflected by having two different values for the twist angle α_2. This twist angle is $\alpha_2 = 0°$ for PUMA type and $\alpha_2 = 180°$ for Fanuc type. On Figure 2.3 we can see Fanuc and ABB robots which are Fanuc-type and PUMA-type robots and their kinematic structures respectively.
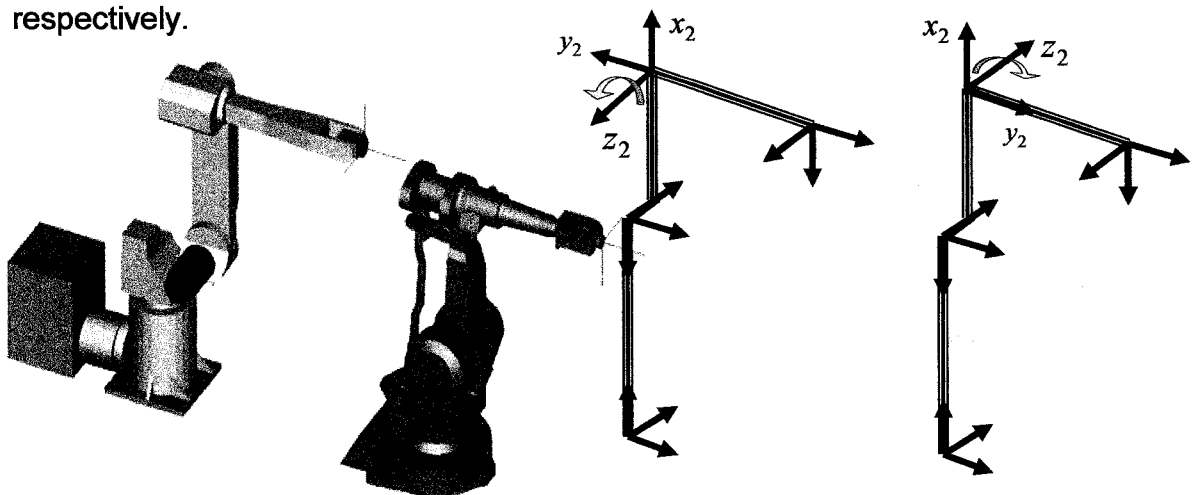
Figure 2.3: Fanuc-type and PUMA -type robots and their joint three directions

26

Table 2.1: Kinematic type classification of robotic systems from 11 different manufacturers.

Manufacturers

ABB	ADEPT	COMAU	FANUC		KAWASAKI
IRB2400_L	ADEPT604S	SMART H3XL	M6iB	S430il	FS 10E
IRB6000_2.4	ADEPT1	SMART_M1	S420iF 2.85	A520i	FS30L
IRB6000_2.8	ADEPT3	OFFSET	S420iW 2.85	A600	FS10N
IRB6000_3.0	ADEPT550	SMART 3	ARCMate120i	ARCMate100	FS20N
IRB6400_2.4	ADEPT604	SMART M1	S430iF	ARCMate100i	FS10C
IRB6400_2.8	Cobra 600	INLINE	S900iH	LR Mate	FS30N
IRB6400_3.0		6125	S900iL	LRMate200i	FS20C
IRB4400_L10		SMART H1	S420iL	LRMate200il	FS10L
IRB4400_L30		SMART H1XL	S6	M 16iT	UX150
IRB3000_10		SMART H2	S420iF 3.0	M16i	FS06N
IRB3400_10		SMART H3L	S430iR	M16iL	UX200
IRB2400_10			S420iS	M6i	FS 06L
IRB4400_60			S420iW 2.4	P155	FS45N
IRB3200			S900iW	P200e12L	FS45C
IRB1500			S430iW	P200e12R	ZX165U
IRB2000			ARCMate50il	R2000iA 165F	JS30
IRB4400_45			ARCMate100iB	R2000iA 200F	JS40
IRB2400_16			S700	S200	UX70
IRB60			S500	S400	KF193
IRB6400_PE			S900W	S420FD	EE10C
IRB6600-175_2.8			ARCMate120iL	S420iF	FA06L
IRB1000			S900H		FA06N
IRB140			S900L		FA 20N
IRB1400			M710i		JS 5
					JS10

Table 2.1. (Continued).

Manufacturers

KUKA	MOTOMAN		NACHI	PANASONIC	STAUBLI	DAIHEN
KR 150-2	K30S	SK120	SF200	VR120	RX 90L	DR 500s
KR 200-2	SK16-6	UP200	SF133	VR032	RX 90	V20S
KR 150L120-2	SV3XL	UP6-C	SC35F	VR016	RX 130L	
KR 30L15-2	UP165-100	UP20M	SC80LF	VR008L	RX 60	
KR 150L150-2	UP6R	SK150	SC300F	VR004	RX 60L	
KR 6-2	K3S	UP130	SC06F	VR006	PUMA 560	
KR 200L120-2	SV3X	SK16M	SC120F	VR006L	PUMA 761	
KR 15-2	K60CSH	UP165	SC120LF	VR008		
KR 30-2	SK45-30	SV3CR	SC15F			
KR 45-2	SK6	K30SH	SF133T			
KR 200L150-2	UP6	K100RSH	SF200T			
KR 125L90-3	SK120-80	K100S				
KR 15L6-2	SV3	K10M				
KR125_2	SV16-640	K10S				
KR 350L280-2	K120S					
KR 150K	SK120-75					
KR 150L110K	SV16-650					
KR 150L130K	UP50					
KR 125-2	UP20					
KR 125-3	SK45					
KR 125L100-2	SK120-150					
KR 125L90-2	SK16					

27

From this table, the most recognizable (in-common) feature is that 174 robots are of 6Rotational joints with either PUMA or Fanuc groups. The significance of this comparison is shown in Figure 2.4.
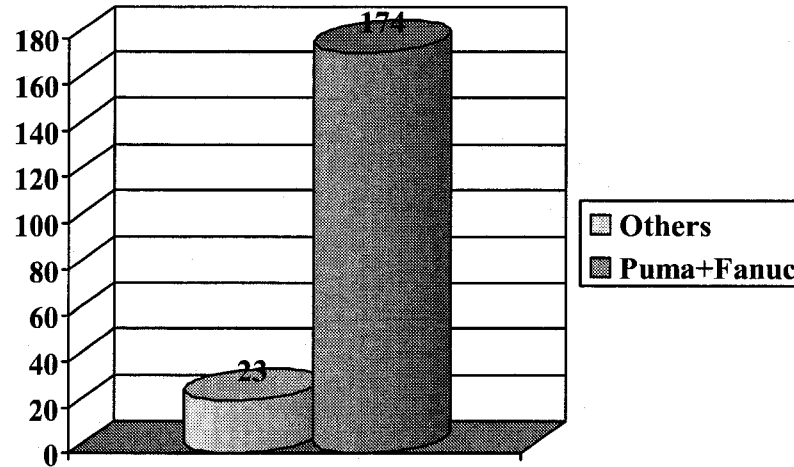
Figure 2.4: Comparison between PUMA-Fanuc type of robots and other robots

Because of the results from the comparison, this work is focused on generating unified robot model that represents these two groups.

2.3.1. The Design of Configuration Parameters K_i

The RPF model has six rotational joints. Each joint can have either left or right positive directions. To make the relationship between each coordinate system, all combinations of their orientations were expressed with equations.

Joint 1 has either a left or right positive direction. This means that z_0 axis of the Joint 1 coordinate system $x_0 y_0 z_0$ can point up or down. To get forward and backward directions for Joint 2, there are four different orientations of the $x_1 y_1 z_1$ coordinate system. The relationship between Joint 1 coordinate system $x_0 y_0 z_0$ and Joint 2 coordinate system $x_1 y_1 z_1$ is given in Figure 2.5. If the direction of vector z_0

28

is opposite to the direction of vector y_1, then the first twist angle is $\alpha_1 = -90°$. If the directions of these two vectors are the same, then $\alpha_1 = +90°$.

θ_1	α_1
$\pm 90°$	$\pm 90°$
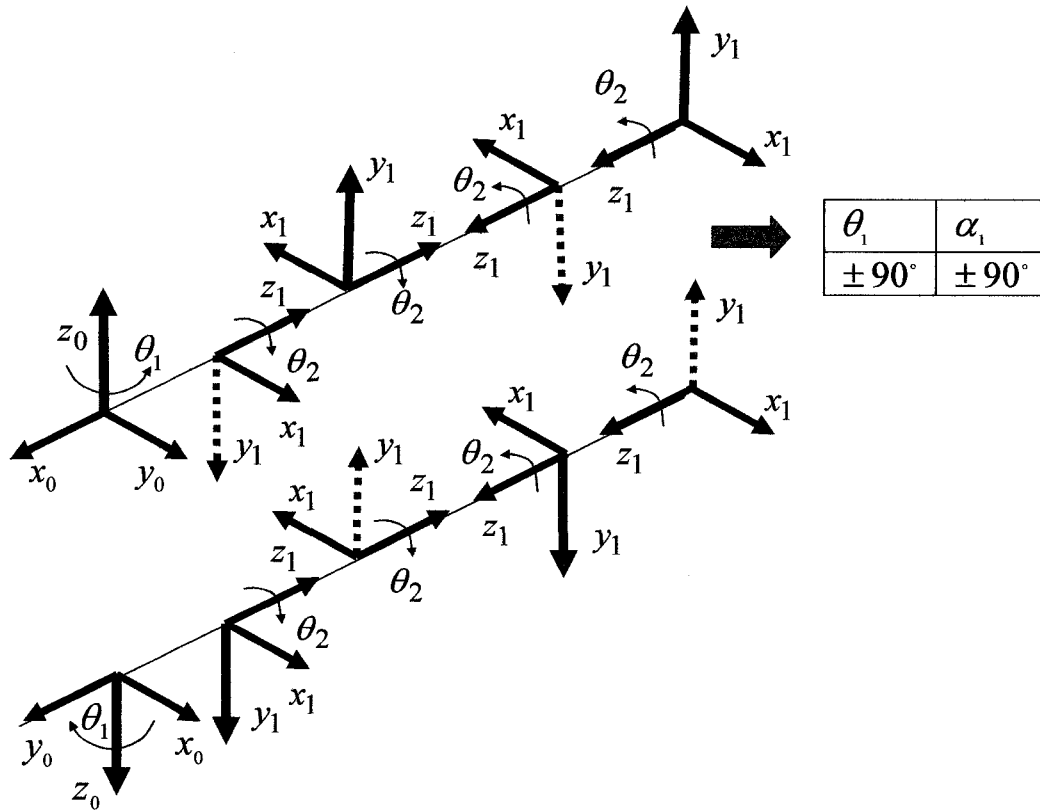
Figure 2.5: Relation between directions of Joint 1 and Joint 2

Joint 2 has either a forward or backward direction, and it can be achieved with four different orientations of the $x_1 y_1 z_1$ coordinate system. The relationship between the Joint 2 coordinate system $x_1 y_1 z_1$ and the Joint 3 coordinate system $x_2 y_2 z_2$ is given in Figure 2.6. Vectors z_1 and z_2 are always parallel. If their directions are the same, the second twist angle is $\alpha_2 = 0°$, but if the directions are opposite then $\alpha_2 = \pm 180°$.

29

θ_2	α_2
0°,±90°,±180°	0°

θ_2	α_2
0°,±90°,±180°	±180°
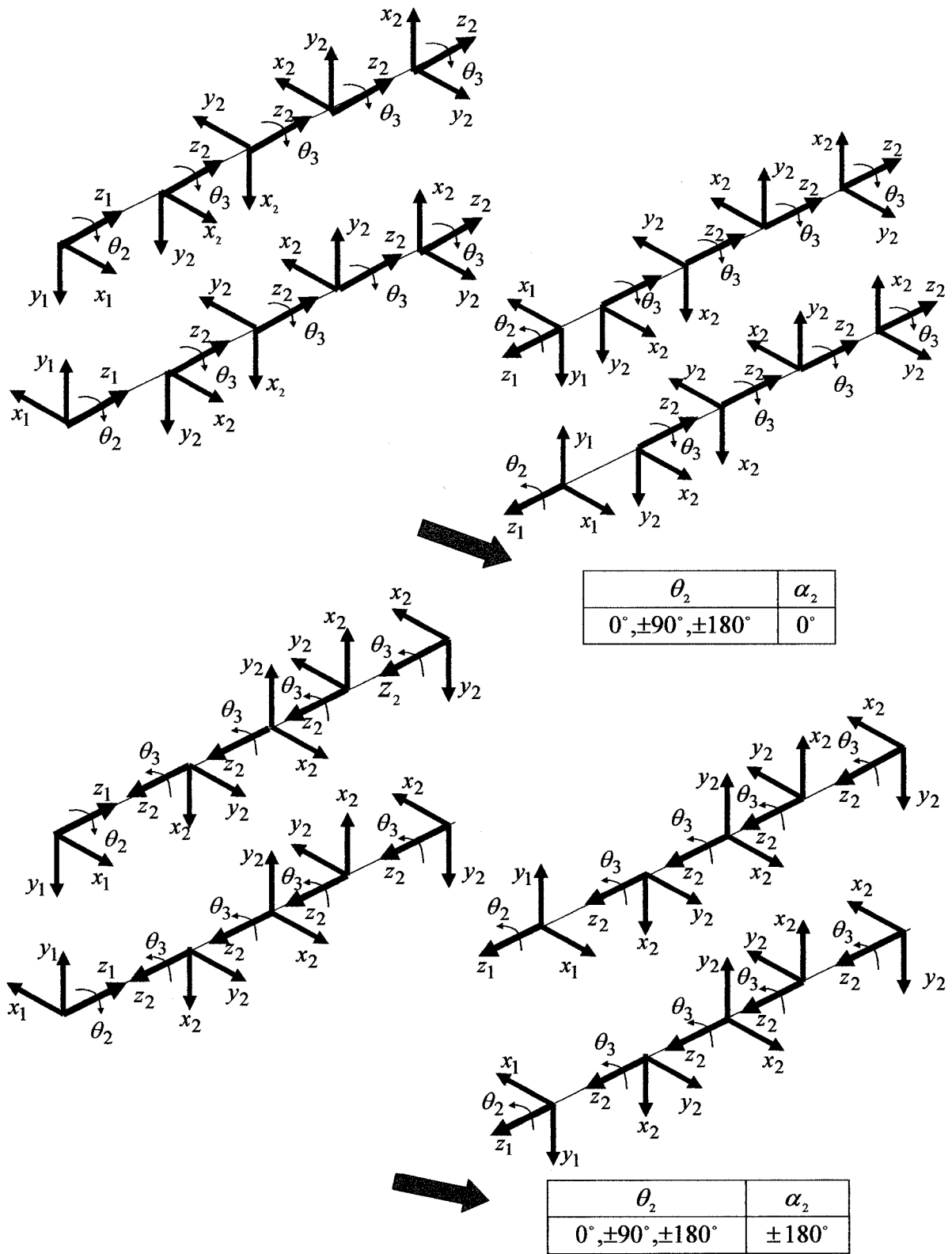
Figure 2.6: Relation between directions of Joint 2 and Joint 3

30

Joint 3 has either a forward or backward direction, and it can be achieved with only two different orientations of the $x_2 y_2 z_2$ coordinate system. The relationship between the Joint 3 coordinate system $x_2 y_2 z_2$ and the Joint 4 coordinate system $x_3 y_3 z_3$ is given in Figure 2.7. Vector z_2 is not parallel with vector z_3, but z_2 must be parallel with y_3 and their directions can be the same or opposite. If their directions are the same the third twist angle is $\alpha_3 = +90°$, but if the directions are opposite then $\alpha_3 = -90°$.

θ_3	α_3
$0°, \pm 180°$	$\pm 90°$
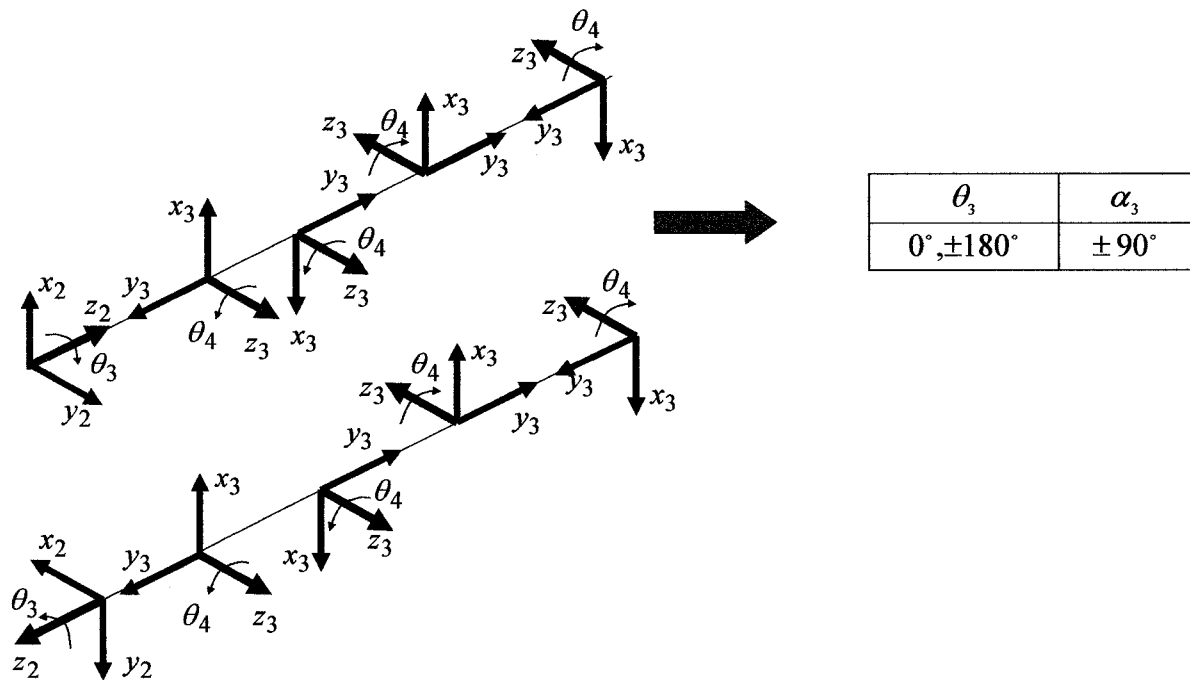
Figure 2.7: Relation between directions of Joint 3 and Joint 4

Joint 4 has either left or right direction and it can be achieved with only four different orientations of the $x_3 y_3 z_3$ coordinate system. The relationship between the Joint 4 coordinate system $x_3 y_3 z_3$ and the Joint 5 coordinate system $x_4 y_4 z_4$ is given in Figure 2.8. Vector z_3 is not parallel with vector z_4, but z_3 must be parallel with y_4, and their directions can be the same or opposite. If their directions are the same the fourth twist angle is $\alpha_4 = +90°$, but if the directions are opposite then $\alpha_4 = -90°$.

31
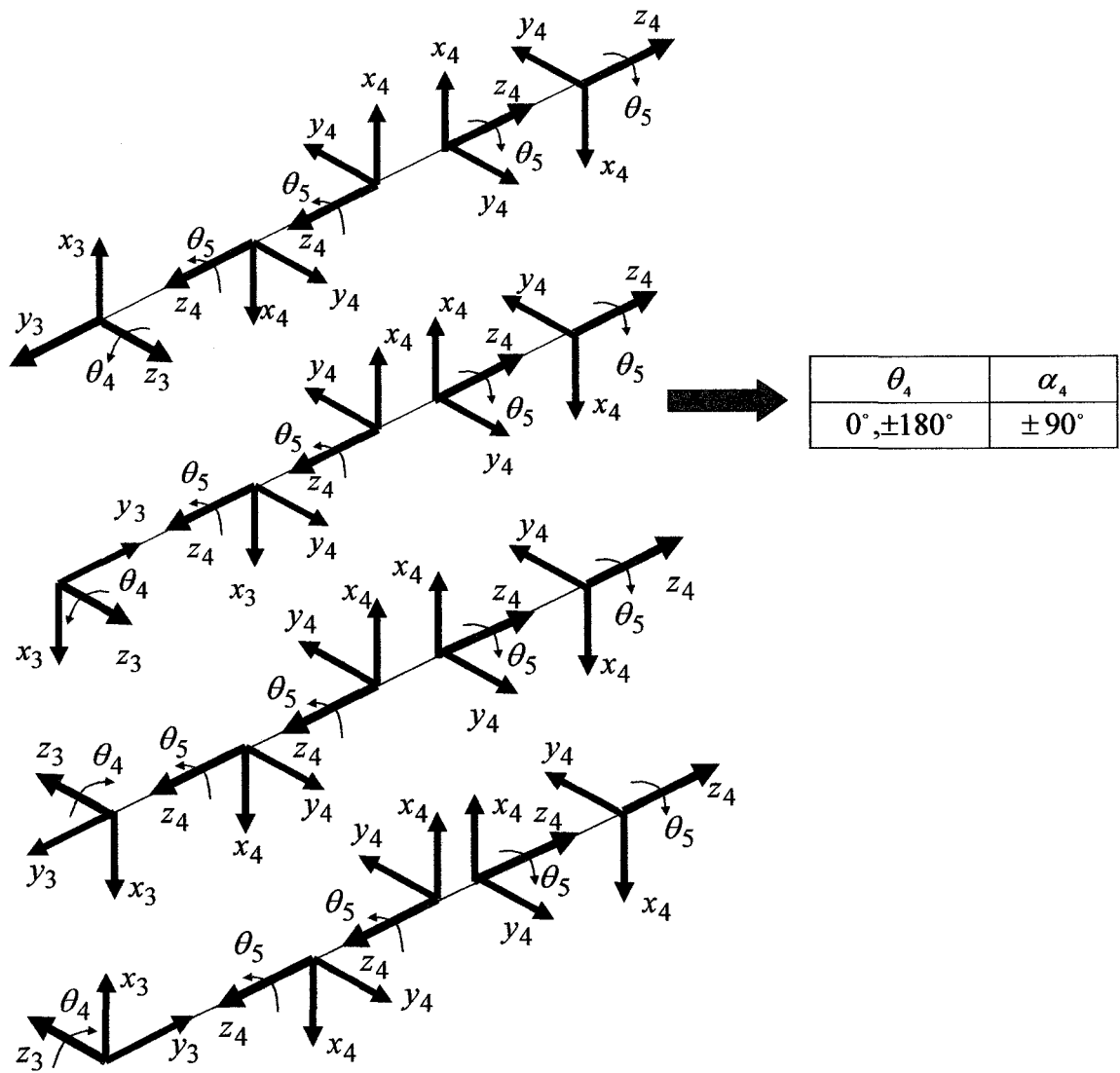
Figure 2.8: Relation between directions of Joint 4 and Joint 5

Joint 5 has either a forward or backward direction and it can be achieved with only four different orientations of the $x_4 y_4 z_4$ coordinate system. The relationship between the Joint 5 coordinate system $x_4 y_4 z_4$ and the Joint 6 coordinate system $x_5 y_5 z_5$ is given in Figure 2.9. Vector z_4 is not parallel with vector z_5, but z_4 must be parallel with y_5 and their directions can be the same or opposite. If their directions are the same the fifth twist angle is $\alpha_5 = +90°$, but if the directions are opposite then $\alpha_5 = -90°$.

32

θ_s	α_s
$0°,\pm180°$	$\pm90°$
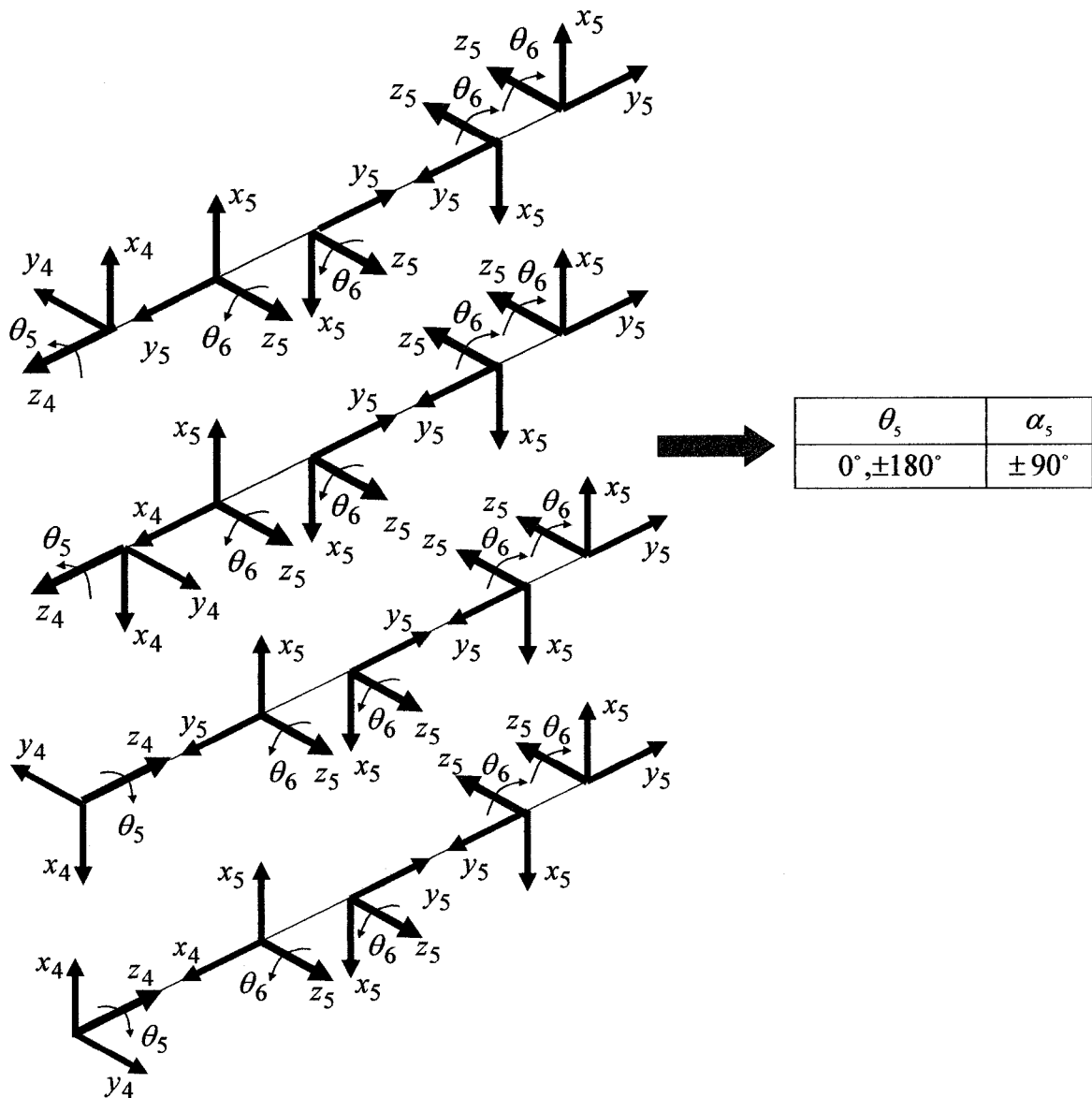
Figure 2.9: Relation between directions of Joint 5 and Joint 6

Joint 6 has either a left or right direction and it can be achieved with four different orientations of the $x_5 y_5 z_5$ coordinate system. The relationship between the Joint 6 coordinate system $x_5 y_5 z_5$ and approach vector coordinate system $x_6 y_6 z_6$ is given in Figure 2.10. Vectors z_5 and z_6 are always parallel. If their directions are the same the then the sixth twist angle is $\alpha_6 = 0°$, but if the directions are opposite then $\alpha_6 = \pm180°$.

33
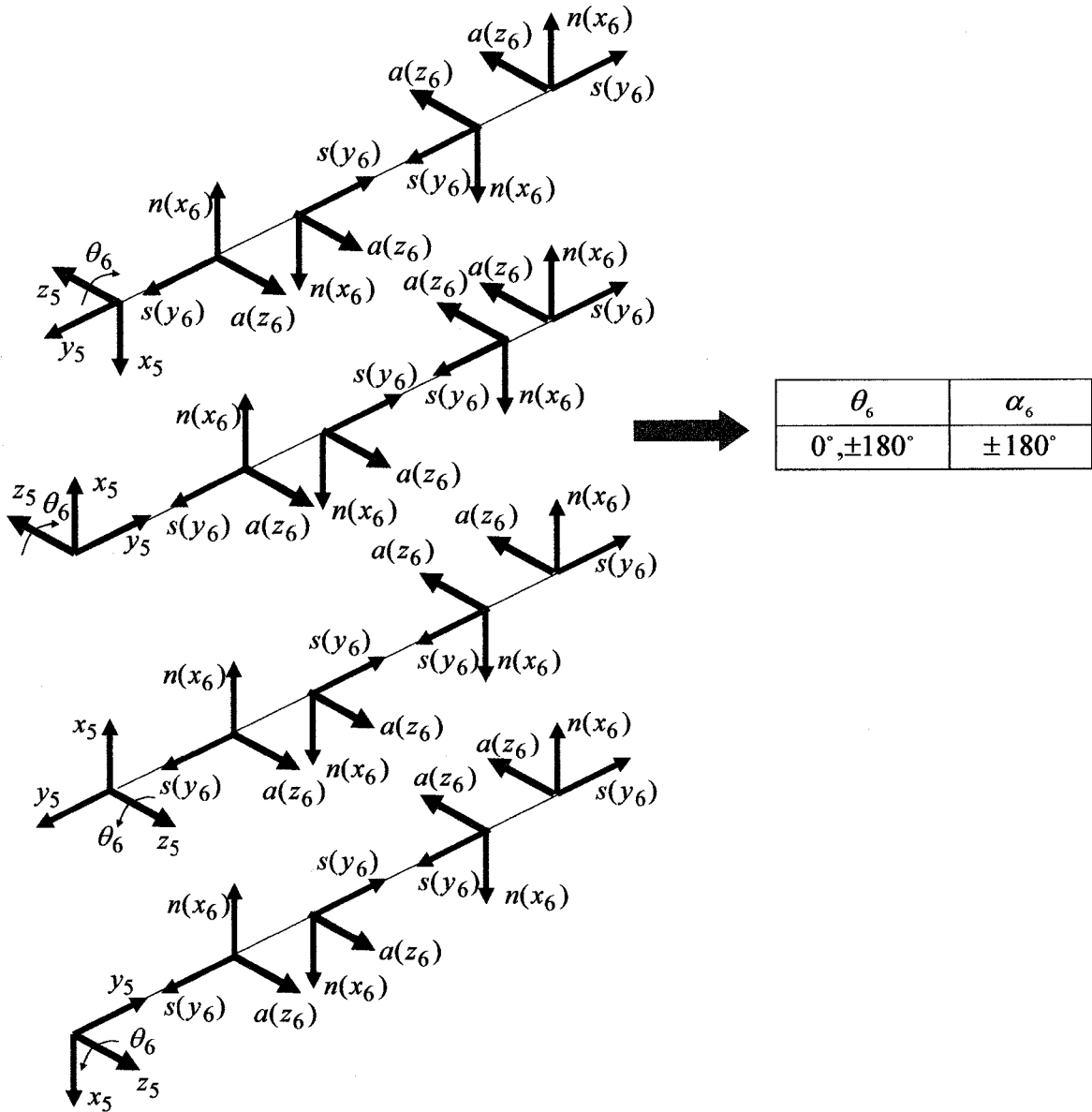
Figure 2.10: Relation between directions of Joint 6 and approach vector

The RPF model can be reconfigured from one kinematic group to another or from one application to another by using configuration parameters K_1, K_2, K_3, K_4, K_5, and K_6 as defined in Equation 3:

$$K_1 = \sin\alpha_1, \quad K_2 = \cos\alpha_2, \quad K_3 = \sin\alpha_3, \quad K_4 = \sin\alpha_4, \quad K_5 = \sin\alpha_5, \quad K_6 = \cos\alpha_6 \qquad (3)$$

These parameters are used to determine the signs in the joint's equations, of the different robot configurations by calculating sine and cosine of the twist angles

34

which are different for all the robots that belong to the two main kinematic groups (PUMA and Fanuc) in the RPF model as shown in Table 2.4. Except for K_2, all the other parameters (K_1, K_3, K_4, K_5, K_6) are used for configuring all the PUMA and Fanuc groups in the RPF model. K_2 totally switches the modeling process from PUMA type to Fanuc type and vice versa within the RPF model. K_1 controls the direction of joint 1 relative to joint 2 by controlling the sign of their twist angle α_1 as shown in Figure 2.5. Thus, one can say that K_1 provides eight different combinations of joints 1 and 2 orientations by having two different values for their embraced twist angle. Note here that α_1 is one of the important D-H parameters. Similarly, the other configuration parameters K_3, K_4, K_5, and K_6 control the relative directions between the joints (3,4), (4,5), (5,6), and (6, flange), respectively. This is possible by letting K_3, K_4, K_5, and K_6 control the signs of the twist angles α_3, α_4, α_5, and α_6, respectively.

Generic PUMA and Fanuc type robots are graphically presented in Figures 2.11 and 2.12, respectively.
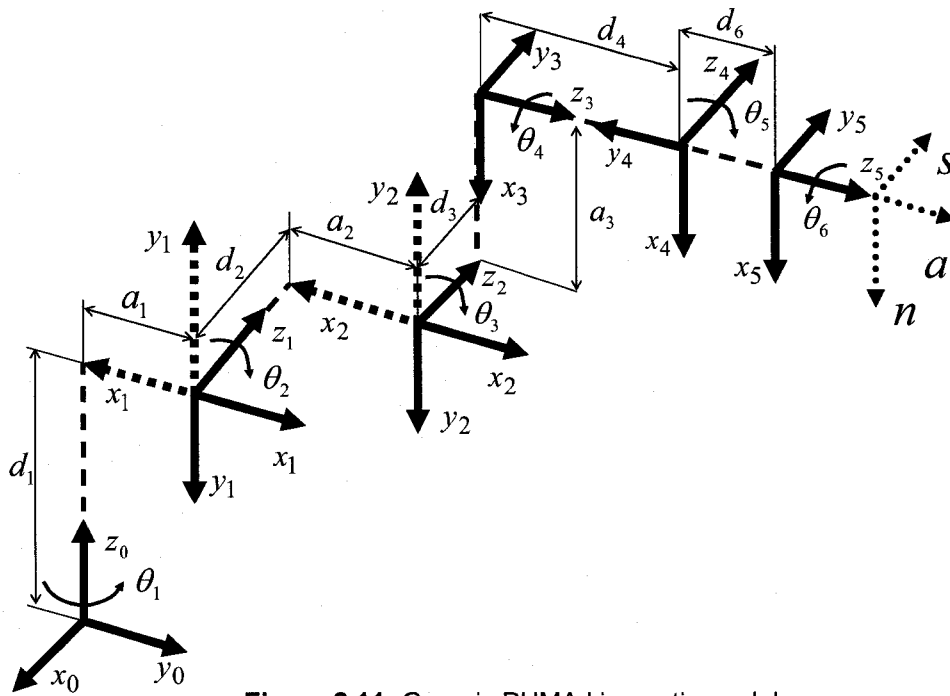
Figure 2.11: Generic PUMA kinematic model

35
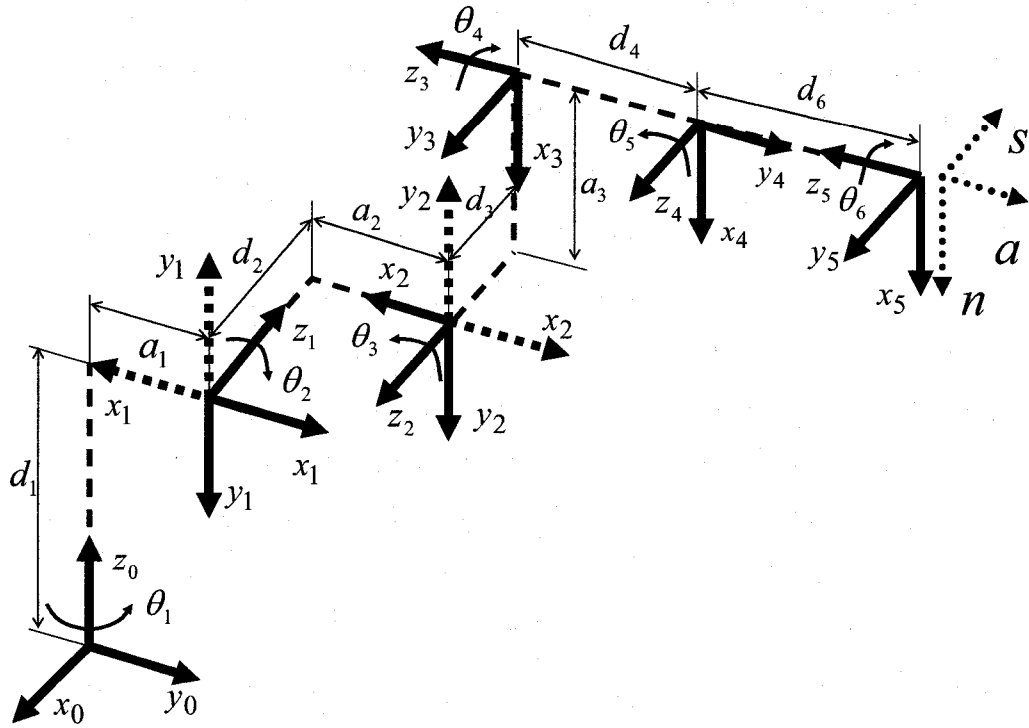
Figure 2.12: Generic PUMA kinematic model

The D-H parameters for two groups of robots are in Tables 2.2 and 2.3.

Table 2.2: D-H parameters for PUMA -like kinematic model.

Joint	θ_i	d_i	a_i	α_i
1	θ_1	d_1	a_1	$-90°$
2	θ_2	d_2	a_2	$0°$
3	θ_3	d_3	a_3	$90°$
4	θ_4	d_4	0	$-90°$
5	θ_5	0	0	$90°$
6	θ_6	d_6	a_6	$\pm180°;0$

Table 2.3: D-H parameters for Fanuc-like kinematic model.

Joint	θ_i	d_i	a_i	α_i
1	θ_1	d_1	a_1	$-90°$
2	θ_2	d_2	a_2	$180°$
3	θ_3	d_3	a_3	$90°$
4	θ_4	d_4	0	$-90°$
5	θ_5	0	0	$90°$
6	θ_6	d_6	a_6	$\pm180°;0$

The result obtained above is of great importance, since the majority of industrial robots have either six or five rotational joints, and belong to either the PUMA or Fanuc group. Among those robots, there are too many commonalities and one major difference (in the direction of joint 3) that would inhibit the

36

generalization of any solution for these robots. It further complicates the automation of any procedural inverse kinematic computations. In fact, this is the main issue where the UKMS module merges the two kinematic groups into one RPF structure through graphical and concurrent computational means. The RPF (Figure 2.13) contains all the possible link lengths and offsets that are non-zero, except for d_5, a_4, and a_5 which are zero. Retaining the condition of having the last three joint's axes intersecting at a point (Pieper D. L, 1968) produces these zero parameters. Based on investigations on the PUMA-like and Fanuc-like robots, it was found that Pieper's condition applies to both of them. In other words, the 174 robots in Table 2.1 that belong to either the PUMA or Fanuc group all have an inline wrist and satisfy Pieper's condition. Hence, it applies to the RPF model by inspection. The two kinematic (structures) models in Figures 2.11 and 2.12 are now merged together into a unified, reconfigurable kinematic model as illustrated in Figure 2.13.
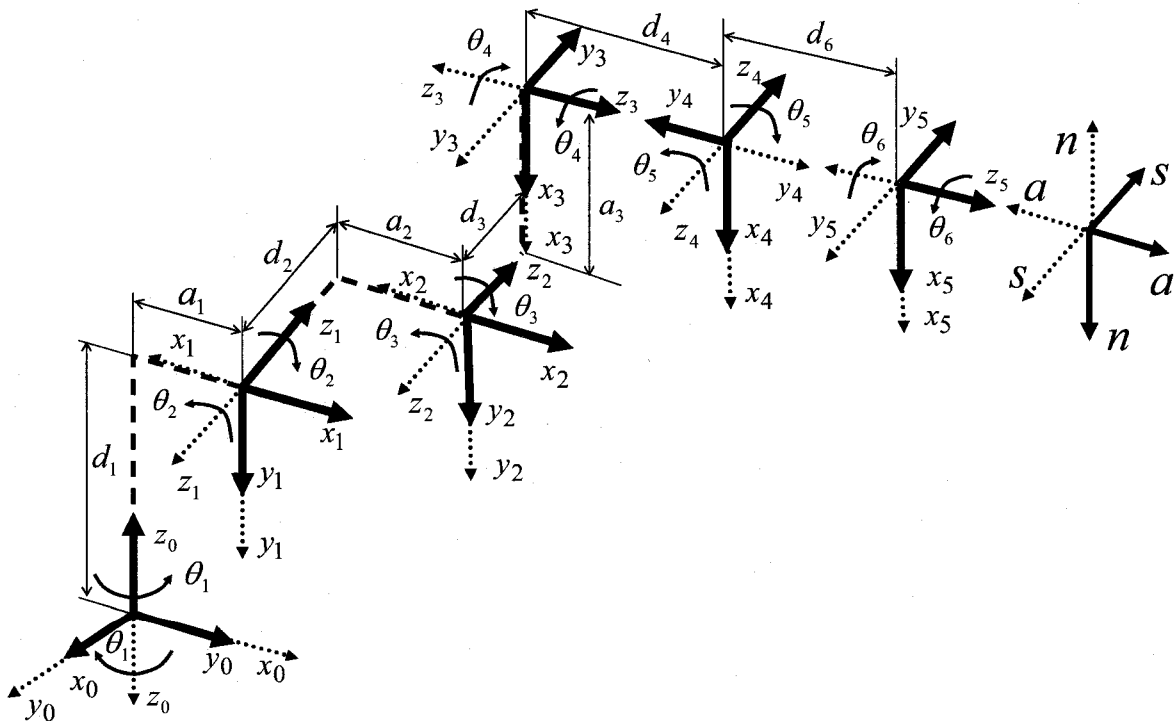
Figure 2.13: RPF kinematic model.

37

This RPF model has the feature of having different joint directions that are reflected by different twist angles, as indicated in Table 2.4.

Table 2.4: D-H parameters for the RPF model.

Joint	θ_i	d_i	a_i	α_i
1	θ_1	d_1	a_1	$\pm 90°$
2	θ_2	d_2	a_2	$\pm 180°;0$
3	θ_3	d_3	a_3	± 90
4	θ_4	d_4	0	± 90
5	θ_5	0	0	± 90
6	θ_6	d_6	a_6	$\pm 180°;0$

The key idea of having this RPF kinematic model is to have both directions for each joint (Figure 2.13) available for solving a generic inverse kinematic problem with the aid of the D-H rules in Table 2.4. This necessarily means the development of generic mathematical equations for solving all the possible configurations of the RPF model.

Once the RPF kinematic model is established as in Figure 2.13, need to solve the kinematics problem which consists of two sub-problems: (i) the direct kinematic problem and (ii) the inverse kinematics problem. The direct kinematics problem is to find the position and orientation of the robot's end effector relative to the base coordinate frame for a given set of joint angles. The inverse kinematics problem is to calculate the robot's joint angles for a given position and orientation of the robot's end effector. The rest of this work is devoted to developing a geometry based generic inverse kinematic solution for all possible configurations of the RPF model.

2.4. A Unified Geometry-Based Solution

According to the different joint coordinate systems as well as the human arm geometry, the various arm configurations of the RPF model can be described with three configuration indicators: Arm (A), Elbow (E), and Wrist (W) in addition to an extra Flip (F) indicator, as shown in Figure 2.14. The first two configuration indicators determine one solution from four possible solutions for the first three joints. The third indicator doubles the number of possible solutions.

| Left and Above | Right and Above | Left and Below | Right and Below |
| Arm (L&A) | Arm (R&A) | Arm (L&B) | Arm (R&B) |
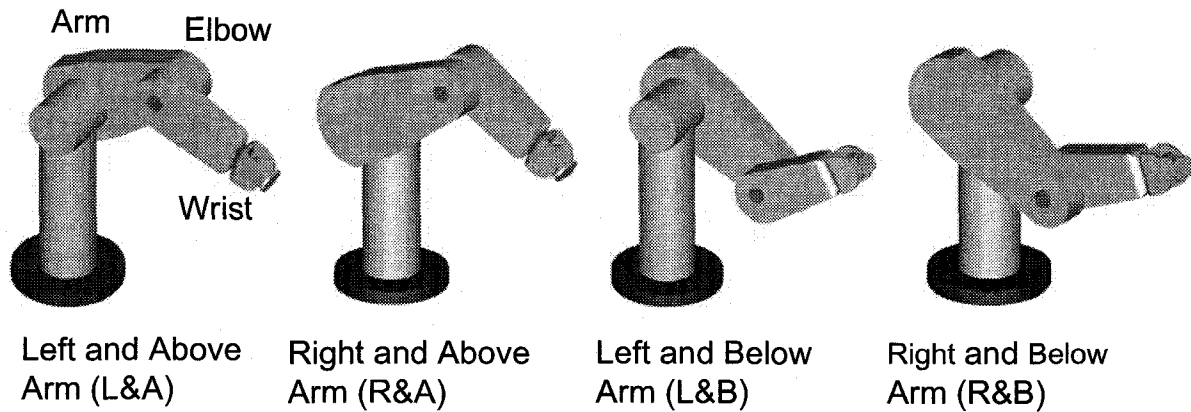
Figure 2.14. Definition of various arm configurations.

The required robot path is given by a set of points. Each point is defined with a coordinate system. The coordinate system has its own position and orientation. We need to calculate the robot joint values for each point depending on its position and orientation as described by Equation 4. Based on the position of each point, the values for the first three joints can be calculated. Hence, the values of the last three joints are calculated from the orientation vector and joint values of the first three joints (Lee C. S. G., and Ziegler M., 1984). The arm transformation matrix, $^{0}T_{6}$, which is valid for any 6R robotic system, is normally given by:

$$^{0}T_{6} = \begin{bmatrix} n_x & s_x & a_x & p_x \\ n_y & s_y & a_y & p_y \\ n_z & s_z & a_z & p_z \\ 0 & 0 & 0 & 1 \end{bmatrix}$$

(4)

39

Lee C. S. G., and Ziegler M., 1984 introduced the definitions of the various configurations according to the human arm geometry as follows: (i) Right Arm (RA) is defined as when positive θ_2 moves the wrist in the positive z_0 direction, while θ_3 is not active, (ii) Left Arm (LA) is defined as when positive θ_2 moves wrist in negative z_0 direction while θ_3 is not active, (iii) Above Arm (AA) (elbow above wrist) is defined as when the position of the wrist of the *Right/Left Arm* with respect to the shoulder coordinate system has a negative/positive coordinate value along the y_2 axis, (iv) Below Arm (BA) (elbow below wrist) is defined as when the position of the wrist of the *Right/Left Arm* with respect to the shoulder coordinate system has a positive/negative coordinate value along the y_2 axis, (v) Wrist Down (WD) is defined as when the s unit vector of the hand coordinate system and the y_5 unit vector of the (x_5, y_5, z_5) coordinate system have a positive dot product, $s \cdot y_5 > 0$, and (vi) Wrist Up (WU) is defined when the s unit vector of the hand coordinate system and the y_5 unit vector of the (x_5, y_5, z_5) coordinate system have a negative dot product, $s \cdot y_5 < 0$. The fourth indicator is introduced as a Flip (F) indicator or Do not Flip (DF) indicator.

According to the previous definitions of the robot configurations have the following basic definitions:

$$A = \left\{ \begin{array}{l} +1, \text{RA} \\ -1, \text{LA} \end{array} \right\}, \ E = \left\{ \begin{array}{l} +1, \text{AA} \\ -1, \text{BA} \end{array} \right\}, \ W = \left\{ \begin{array}{l} +1, \text{D} \\ -1, \text{U} \end{array} \right\}, \ F = \left\{ \begin{array}{l} +1, \text{F} \\ -1, \text{DF} \end{array} \right\} \quad (5)$$

The user must specify the signed values of the indicators in Equation 5 to be able to find the inverse kinematics solution. These indicators can be calculated from the values of the joint angles of the robot. The equations for calculating these indicators are:

40

$$A = sign[-d_4 K_3 \sin(K_2 \theta_2 + \theta_3) - a_3 \cos(\theta_2 + K_2 \theta_3) - a_1 - a_2 \cos \theta_2] = \begin{cases} +1 \Rightarrow RA \\ -1 \Rightarrow LA \end{cases} \quad (6)$$

$$E = A \cdot sign(-a_4 \sin \theta_3 \cos \theta_4 + K_3 d_4 \cos \theta_3 - a_3 \sin \theta_3) = \begin{cases} +1 \Rightarrow EAW \\ -1 \Rightarrow EBW \end{cases} \quad (7)$$

$$W = \begin{cases} sign(s \cdot z_4) & if \ s \cdot z_4 \neq 0 \\ sign(n \cdot z_4) & if \ s \cdot z_4 = 0 \end{cases} = \begin{cases} +1 \Rightarrow WD \\ -1 \Rightarrow WU \end{cases} \quad (8)$$

2.4.1. Arm Solution for the First Three Joints

For the calculation of the first three joints, the position vector p, which points from the origin of the shoulder coordinate system (x_0, y_0, z_0) to the point where the last three joints axis are intersecting. These types of robots are known as robots with a spherical wrist.
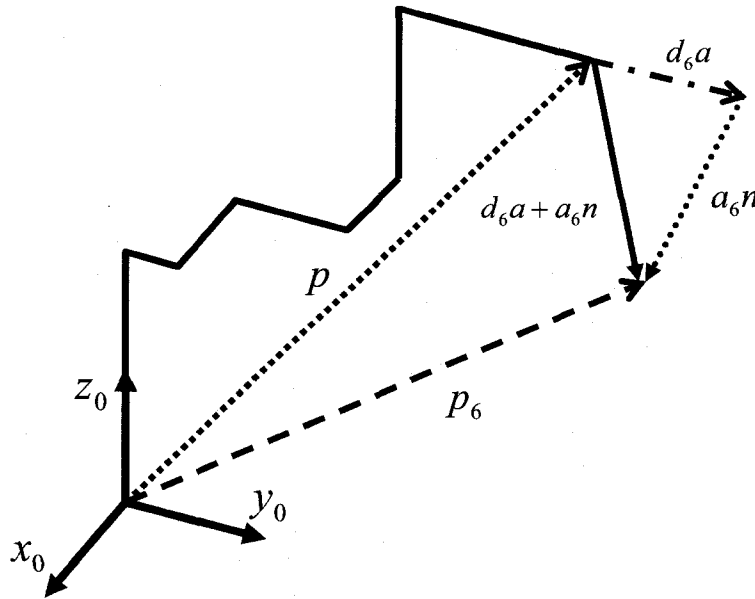
Figure 2.15: Position vector p for spherical wrist robots.

From Figure 2.15, the position vector $p = p_6 - (d_6 a + a_6 n) = (p_x, p_y, p_z)^T$, which corresponds to the position vector $^0 T_4$, can be found. It can be calculated from the right hand side of Equation 9:

41

$$\begin{bmatrix} p_x \\ p_y \\ p_z \end{bmatrix} =$$

$$\begin{bmatrix} \cos\theta_1[d_4K_3\sin(K_2\theta_2 + \theta_3) + a_3\cos(\theta_2 + K_2\theta_3) + a_1 + a_2\cos\theta_2] + K_1(d_2 + K_2d_3)\sin\theta_1 \\ \sin\theta_1[d_4K_3\sin(K_2\theta_2 + \theta_3) + a_3\cos(\theta_2 + K_2\theta_3) + a_1 + a_2\cos\theta_2] - K_1(d_2 + K_2d_3)\cos\theta_1 \\ -d_4K_1K_3\cos(K_2\theta_2 + \theta_3) + a_3K_1\sin(\theta_2 + K_2\theta_3) + a_2K_1\sin\theta_2 + d_1 \end{bmatrix} \quad (9)$$

2.4.1.1 Solution for Joint 1

To calculate the angle θ_1 of Joint 1, need to have the projections of the position vector p onto the x_0y_0 plane as depicted in Figures 2.16 and 2.17. For the two values of the A configurations have two different solutions for θ_1: θ_1^L as shown in Figure 2.16 and θ_1^R as shown in Figure 2.17. According to the similarities and differences that exist between the PUMA and Fanuc kinematic groups within the RPF model, developed the equations for calculating θ_1. Strictly speaking, the main difference between PUMA -like and Fanuc-like kinematic groups is that directions of Joints 2 and 3 are the same for PUMA type and opposite to each other for Fanuc type. When the joints are in the same directions it means that their rotational vectors are equal, $z_1 = z_2$, and for the opposite direction they have opposite sign, $z_1 = -z_2$.
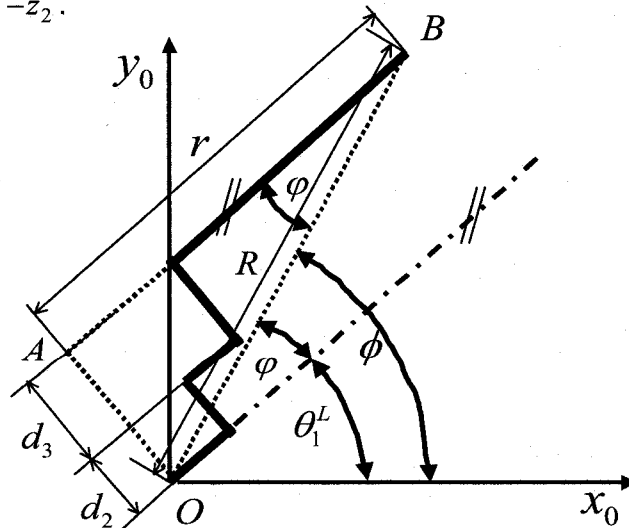
Figure 2.16: LA (Left Arm) projections of the position vector p onto the x_0y_0 plane.

42
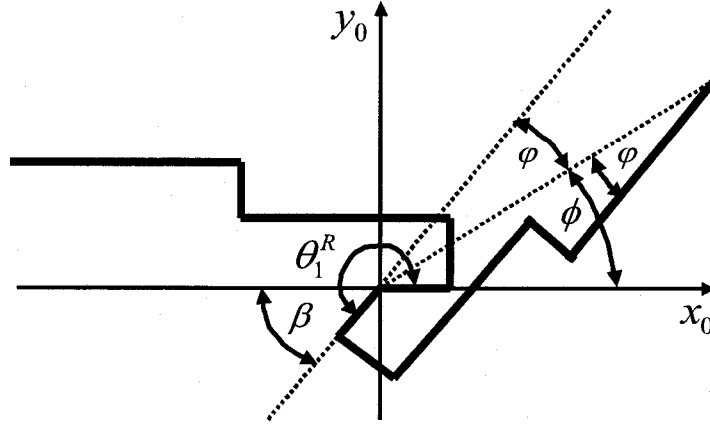
Figure 2.17: RA (Right Arm) projections of the position vector p onto the $x_0 y_0$ plane.

From Figure 2.16, equations for calculating the angle θ_1^L can be derived. To calculate the distance OA in Figure 2.17 as in Equation 12, use the configuration parameter K_2 (which controls the sign of d_3) as previously introduced in Equation 3:

$$\theta_1^L = \phi - \varphi \tag{10}$$

$$\sin\varphi = \frac{OA}{R}, \quad \cos\varphi = \frac{AB}{R}, \quad \sin\phi = \frac{p_y}{R}, \quad \cos\phi = \frac{p_x}{R} \tag{11}$$

$$OA = d_2 + K_2 d_3, \quad OB = R = \sqrt{p_x^2 + p_y^2} \tag{12}$$

$$AB = r = \sqrt{R^2 - OA^2} = \sqrt{p_x^2 + p_y^2 - (d_2 + K_2 d_3)^2} \tag{13}$$

$$\sin\theta_1^L = \sin(\phi - \varphi) = \frac{p_y r - p_x (d_2 + K_2 d_3)}{R^2} \tag{14}$$

$$\cos\theta_1^L = \cos(\phi - \varphi) = \frac{p_x r + p_y (d_2 + K_2 d_3)}{R^2} \tag{15}$$

Now solve for θ_1^R. From Figure 2.17, obtained the following equations for the angle θ_1^R.

43

$$\theta_1^R = 180° + \beta, \quad \beta = \varphi + \phi \tag{16}$$

Combining Equations 10 - 16, obtain the sine and cosine functions of θ_1^R :

$$\sin \theta_1^R = \sin(180° + \varphi + \phi) = \frac{-p_y r - p_x (d_2 + K_2 d_3)}{R^2} \tag{17}$$

$$\cos \theta_1^R = \cos(180° + \varphi + \phi) = \frac{-p_x r + p_y (d_2 + K_2 d_3)}{R^2} \tag{18}$$

Combining the solutions for the LA (Left Arm), θ_1^L, and the RA (Right Arm), θ_1^R, obtain solution for θ_1 as expressed below:

$$\theta_1 = \text{atan} 2 \left(\frac{-A\, p_y r - p_x (d_2 + K_2 d_3)}{-A\, p_x r + p_y (d_2 + K_2 d_3)} \right) \tag{19}$$

2.4.1.2 Solution for Joint 2

To calculate the angle θ_2 of joint 2, the projections of the position vector p onto the $x_1 y_1$ plane should be defined as shown in Figures 2.18 and 2.19. From Figure 2.18, the equations for calculating the joint angle θ_2 can be easily deduced as follows:

$$r = AE = \sqrt{BE^2 - AB^2} = \sqrt{(p_x - a_1 \cos \theta_1)^2 + (p_y - a_1 \sin \theta_1)^2 - (d_2 + K_2 d_3)^2} \tag{20}$$

$$S = AD = \sqrt{r^2 + DE^2} = \\ \sqrt{(p_x - a_1 \cos \theta_1)^2 + (p_y - a_1 \sin \theta_1)^2 - (d_2 + K_2 d_3)^2 + (p_z - |d_1|)^2} \tag{21}$$

$$AF = a_2 \tag{22}$$

$$FC = a_3 \tag{23}$$

44
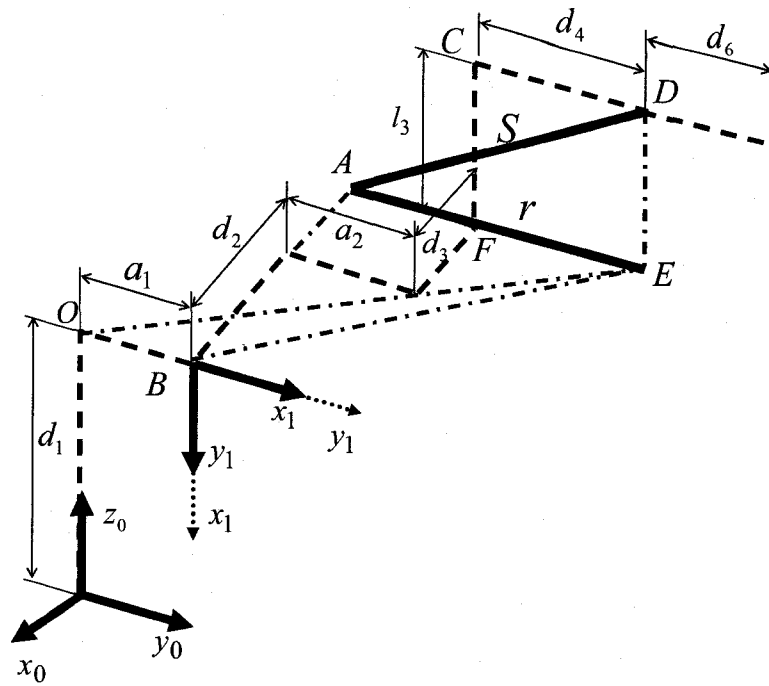
Figure 2.18: Projections of the position vector p onto the $x_1 y_1$ plane.
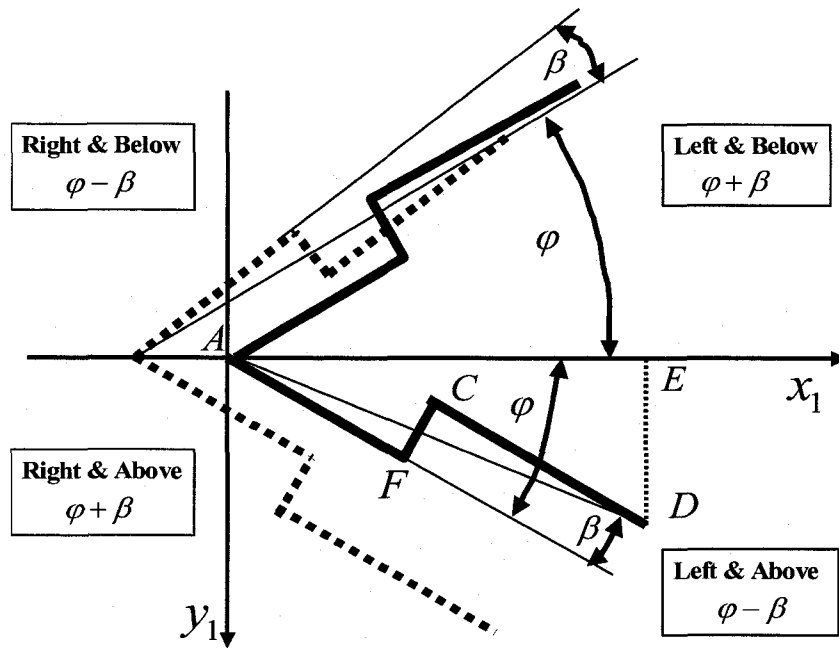
Figure 2.19: Four combinations of A and E configurations for joint 2 solution.

For the two combinations LA and RA and the two combinations EA and EB that are shown in Figure 2.19, there are four solutions for Joint 2. In Figure 2.19, four possible solutions for Joint 2 are indicated. These four solutions are defined in

45

Table 2.5. To include two different directions for Joint 1 one more sign parameter, which depends on the z_0 direction must be included. When z_0 is pointing up, as it is shown on the Figure 2.19, d_1 will be a positive number. For the case when z_0 is pointing down, d_1 will have a negative sign in Equation 24. The sign control parameter ω is expressed in Equation 24 and included in Equation 25.

$$\omega = sign(d_1) \tag{24}$$

Table 2.5: Possible arm configurations for Joint 2 (Lee C. S. G., and Ziegler M., 1984).

Configurations	θ_2	A	E
L&A	$\varphi - \beta$	-1	+1
L&B	$\varphi + \beta$	-1	-1
R&A	$\varphi + \beta$	+1	+1
R&B	$\varphi - \beta$	+1	-1

$$\theta_2 = (\varphi + A \cdot E \beta)\omega \tag{25}$$

Considering *AFCD* in Figure 2.19 as well as Equations 20 – 25, the sine and cosine functions of the angle φ can be found to be:

$$\sin\varphi = \frac{(|d_1| - |p_z|)}{S} \quad , \quad \cos\varphi = -\frac{r}{S} \cdot A \tag{26, 27}$$

Applying the cosine theorem on triangle *AFD* in Figure 2.19, the angle β can be found:

$$\cos\beta = \frac{S^2 + a_2^2 - a_3^2 - d_4^2}{2Sa_2} \quad , \quad \sin\beta = \sqrt{1 - \cos^2\beta} \tag{28, 29}$$

With some algebraic manipulation of Equations 20 - 29, one can obtain θ_2 as follows:

$$\sin\theta_2 = \omega(\sin\varphi\cos\beta + A \cdot E \cos\varphi\sin\beta) \tag{30}$$

46

$$\cos\theta_2 = \cos\varphi\cos\beta - A\cdot E\sin\varphi\sin\beta \tag{31}$$

$$\theta_2 = \operatorname{atan}2\left(\frac{\sin\theta_2}{\cos\theta_2}\right) \tag{32}$$

2.4.1.3 Solution for Joint 3

The calculation of the angle θ_3 (between the axes x_2 and x_3) for joint 3 requires projecting the position vector p onto the x_2y_2 plane as shown in Figures 2.20 and 2.21.
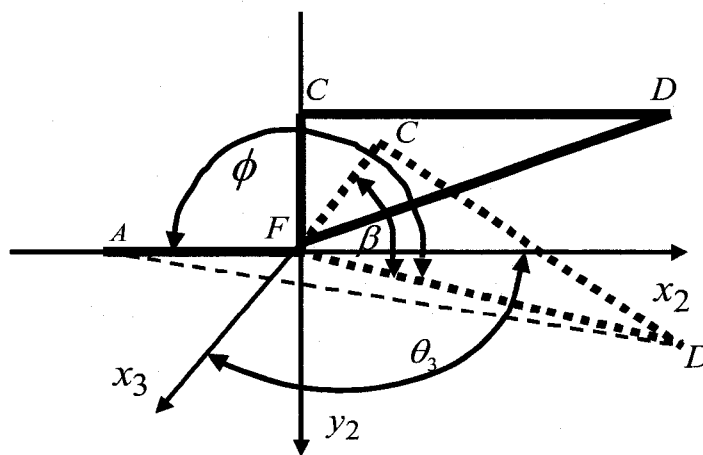
Figure 2.20: Joint 3 angle for PUMA group
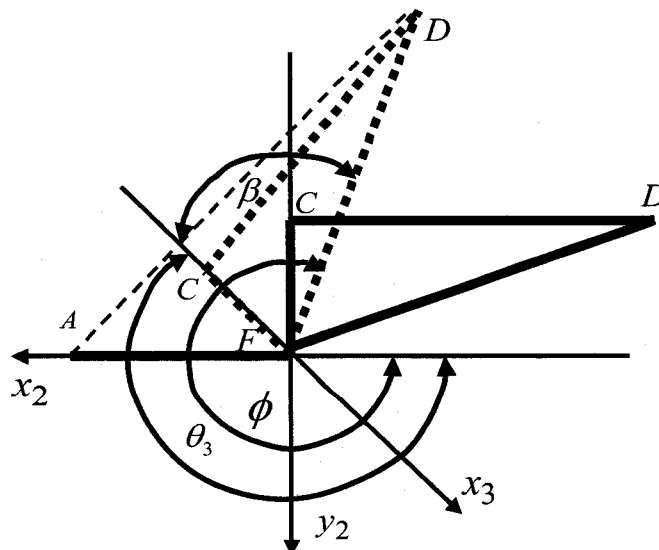
Figure 2.21: Joint 3 angle for Fanuc group

47

For the PUMA and Fanuc kinematic groups the angle θ_3 is, respectively, given by:

$$\theta_3 = \phi - \beta \tag{33}$$

$$\theta_3 = 360° - (\phi - \beta) \tag{34}$$

From Figures 2.20 and 2.21 it can be seen that the $x_2 y_2$ coordinate system for the PUMA group is different from the Fanuc one. The difference between the two groups is imparted by the difference in the directions of joint 2 and joint 3 with respect to each other. The directions of these two joints are the same for the PUMA type and they oppose each other for the Fanuc type. This fact is clearly described in Tables 2.6 and 2.7. As discussed above, this difference can be accommodated with the control parameter K_2. Considering *AFCD* in Figures 2.20 and 2.21, the angle β can be calculated as follows:

$$AF = a_2, FC = a_3, \; CD = d_4 \tag{35}$$

$$\sin\beta = \frac{CD}{FD} = \frac{d_4}{\sqrt{a_3^2 + d_4^2}}, \; \cos\beta = \frac{FC}{FD} = \frac{|a_3|}{\sqrt{a_3^2 + d_4^2}} \tag{36}$$

Applying the cosine theorem to the triangle *AFD* in Figure 2.20 or Figure 2.21, the angle ϕ can be calculated as follows:

$$\cos\phi = \frac{a_2^2 + a_3^2 + d_4^2 - S^2}{2a_2 BD} = \frac{a_2^2 + a_3^2 + d_4^2 - S^2}{2a_2\sqrt{a_3^2 + d_4^2}} \tag{37}$$

Table 2.6 provides, for a PUMA group, the four possible combinations, while in Table 2.7 all the possible arm configurations for Fanuc group are given. To calculate the sinus of the angle ϕ, the control parameter K_2 is used as follows:

$$\sin\phi = K_2 \omega A \cdot E \sqrt{1 - \cos^2\phi} \tag{38}$$

48

Table 2.6: Arm configurations for PUMA type robots.

Arm configurations		ϕ	θ_3	$\sin\phi$	A	E	$K_2(\text{A}\cdot\text{E})$	K_2
L & A,	$p_{y_2} > 0$	$<180°$	$\phi - \beta$	$\sin\phi$	-1	+1	-(-1) = +1	-1
L & B,	$p_{y_2} < 0$	$>180°$	$\phi - \beta$	$-\sin\phi$	-1	-1	-(+1) = -1	-1
R & A,	$p_{y_2} > 0$	$<180°$	$\phi - \beta$	$-\sin\phi$	+1	+1	-(+1) = -1	-1
R & B,	$p_{y_2} < 0$	$>180°$	$\phi - \beta$	$\sin\phi$	+1	-1	-(-1) = +1	-1

Table 2.7: Arm configurations for Fanuc type robots.

Arm configuration		ϕ	θ_3	$\sin\phi$	A	E	$K_2(\text{A}\cdot\text{E})$	K_2
L & A,	$p_{y_2} > 0$	$>180°$	$\phi - \beta$	$-\sin\phi$	-1	+1	-1	1
L & B,	$p_{y_2} < 0$	$<180°$	$\phi - \beta$	$\sin\phi$	-1	-1	+1	1
R & A,	$p_{y_2} > 0$	$>180°$	$\phi - \beta$	$\sin\phi$	+1	+1	+1	1
R & B,	$p_{y_2} < 0$	$<180°$	$\phi - \beta$	$-\sin\phi$	+1	-1	-1	1

Finding the parameters S and r given by Equations 20 and 21, using Equations 33-38, the following equations for calculating the joint angle θ_3 can be derived:

$$\sin\theta_3 = \sin(\phi - \beta) \tag{39}$$

$$\cos\theta_3 = \cos(\phi - \beta) \tag{40}$$

$$\theta_3 = \operatorname{atan}2\left(\frac{\sin\theta_3}{\cos\theta_3}\right) \tag{41}$$

2.4.2. Arm Solution for the Last Three Joints

The solution of the last three joints for the RPF model can be acquired from the joint values of the first three joints (i.e., calculation of matrix $^0T_3$) and by setting these joints to meet the following criterion (Lee C. S. G., and Ziegler M., 1984):

49

$$z_4 = \frac{\pm(z_3 \times a)}{\|z_3 \times a\|}, \qquad a = (a_x, a_y, a_z)^T \tag{42}$$

$$a = \pm z_5, \qquad a = (a_x, a_y, a_z)^T \tag{43}$$

$$s = y_6, \quad s = (s_x, s_y, s_z)^T, \text{ where } \quad n = (n_x, n_y, n_z)^T \tag{44}$$

The condition in Equation 42 is used to set Joint 4 such that a rotation about Joint 5 will align the coordinate system of joint 6 with the approach vector a. If the vector cross product from Equation 42 is zero, it will create the degenerate case. This problem appears when joint 4 and joint 6 are parallel. The second condition in Equation 43 sets Joint 5 to align the coordinate system of joint 6 with the approach vector. Equation 44 is used to align the axis of joint 6 with the sliding and normal vectors.

2.4.2.1 Solution for Joint 4

The orientations for the wrist are given in Equation 8 and shown in Table 2.8. The sign of the vector z_4 is defined with Ω, and is described by the orientation of either the n or s unit vector with respect to the y_5 unit vector. More details are given by Lee C. S. G., and Ziegler M., 1984.

Table 2.8: Various orientations for the wrist.

Wrist orientation	$\Omega = s \cdot y_5$ or $n \cdot y_5$	ψ	$M = \psi \cdot sign(\Omega)$
D	≥ 0	+1	+1
D	< 0	+1	-1
U	≥ 0	-1	-1
U	< 0	-1	+1

Projections of the (x_4, y_4, z_4) coordinate frame on the (x_3, y_3) plane, for two different directions of θ_4, are shown in Figure 2.22.
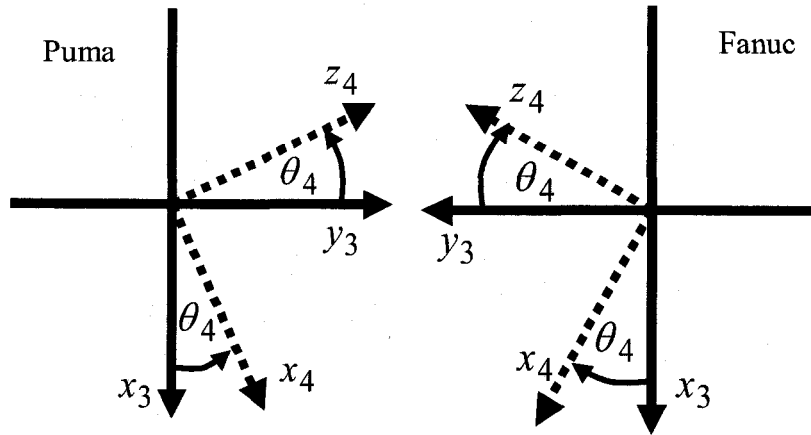
Figure 2.22: Joint 4 angle for PUMA and Fanuc groups.

Considering the wrist orientations as given in Table 2.8, the following equations for calculating the joint angle θ_4 can be found:

$$z_4 \cdot y_3 = \cos\theta_4 \tag{45}$$

$$z_4 \cdot x_3 = \cos(\theta_4 + 90°) = -\sin\theta_4 \tag{46}$$

$$\sin\theta_4 = -M(z_4 \cdot x_3) \tag{47}$$

$$\cos\theta_4 = K_2 M(z_4 \cdot y_3) \tag{48}$$

The vectors x_3 and y_3 are the x- and y-column vectors of the matrix $^0T_3$, which is obtained by plugging the D-H parameters (Table 2.4) into the homogeneous transformation matrices as in Equations 49 and 50:

$$^{i-1}T_i = \begin{bmatrix} \cos\theta_i & -\cos\alpha_i \sin\theta_i & \sin\alpha_i \sin\theta_i & a_i \cos\theta_i \\ \sin\theta_i & \cos\alpha_i \cos\theta_i & -\sin\alpha_i \cos\theta_i & a_i \sin\theta_i \\ 0 & \sin\alpha_i & \cos\alpha_i & d_i \\ 0 & 0 & 0 & 1 \end{bmatrix} \tag{49}$$

$$^0T_3 = {}^0T_1 {}^1T_2 {}^2T_3 \tag{50}$$

51

$$\theta_4 = \operatorname{atan} 2\left(\frac{\sin\theta_4}{\cos\theta_4}\right) \tag{51}$$

Combining Equations 45 - 51, one can obtain θ_4:

$$\theta_4 =$$
$$\operatorname{atan} 2\left(\frac{MK_2[(\cos\theta_1\cos(\theta_2 + K_2\theta_3)a_x + \sin\theta_1\cos(\theta_2 + K_2\theta_3)a_y + K_1\sin(\theta_2 + K_2\theta_3)a_z]}{MK_1K_2K_3(\sin\theta_1 a_x - \cos\theta_1 a_y)}\right) \tag{52}$$

where the configurations parameters K_1, K_2, K_3 are as defined in Equation 3. The resulting Equation 52 is used to solve for both directions of θ_4. For the degenerate case can set any value for θ_4 with the proper wrist orientation (U/D). It can start by setting θ_4 equal to its current value. Using the F indicator in Equation 5, can be obtained the other solutions for θ_4 including $\theta_4 = \theta_4 + 180°$ (Lee C. S. G., and Ziegler M., 1984).

2.4.2.2 Solution for Joint 5

To calculate θ_5, the axis of rotation of Joint 6 have to be align with the approach vector ($a = \pm z_5$). The projections of (x_5, y_5, z_5) coordinate frame onto (x_4, y_4) plane, for two different directions of θ_5, are shown in Figure 2.23 and expressed in Equations 53 and 54. The sine and cosine of θ_5 will have different signs, which will depend on the relation between the approach vector a and the vector y_4. The sign is expressed in Equation 3 and both cases are shown in Figure 2.23:

$$\sin\theta_5 = K_6 x_4 \cdot a \tag{53}$$

$$\cos\theta_5 = -K_6 y_4 \cdot a \tag{54}$$

52

$$^0T_4 = {}^0T_1{}^1T_2{}^2T_3{}^3T_4 \tag{55}$$

where x_4 and y_4 are the x- and y-column vectors of the matrix $^0T_4$ in Equation 55, respectively.
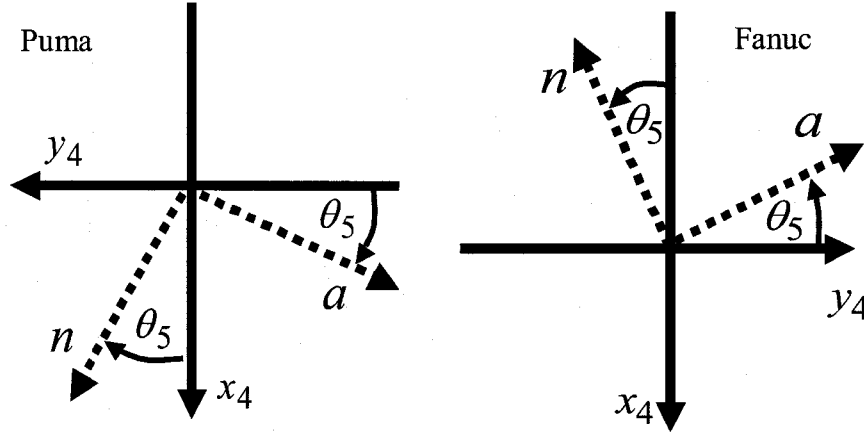
Figure 2.23: Solution for Joint 5 (PUMA and Fanuc groups respectively).

From Equations 53 - 54, the sine and cosine of θ_5 are calculated as follows:

$$\sin\theta_5 = K_6\{[\cos\theta_1\cos(\theta_2 + K_2\theta_3)\cos\theta_4 + K_1K_2K_3\sin\theta_1\sin\theta_4]a_x$$
$$+ [\sin\theta_1\cos(\theta_2 + K_2\theta_3)\cos\theta_4 - K_1K_2K_3\cos\theta_1\sin\theta_4]a_y \tag{56}$$
$$+ K_1(\sin(\theta_2 + K_2\theta_3)\cos\theta_4)a_z\}$$

$$\cos\theta_5 = -K_6\{[K_3K_4\cos\theta_1\sin(K_2\theta_2 + \theta_3)]a_x + K_3K_4[\sin\theta_1\sin(K_2\theta_2 + \theta_3)]a_y$$
$$- [K_1K_2K_3K_4\cos K_2\theta_2 + \theta_3)]a_z\} \tag{57}$$

The parameter K_4 is defined as in Equation 1. Combining Equations 55 to 57, θ_5 is found to be:

$$\theta_5 = \operatorname{atan}2\left(\frac{\sin\theta_5}{\cos\theta_5}\right) \tag{58}$$

The resulting solution (Equation 58) is used to solve for both directions of θ_5. Note here that if $\theta_5 \approx 0$, the degenerate case occurs.

53

2.4.2.3 Solution for Joint 6

The rotation axis of joint 6 is aligned with the approach vector a. Also, need to align the orientation of the end effector, in order to facilitate applications like picking up an object, by setting $s = y_6$. The projection of the flange (n, s, a) coordinate frame onto the (x_5, y_5) plane, for two different directions of θ_6, are shown in Figure 2.24 and expressed in Equations 60 and 61. When $a = -z_5$, the twist angle α_6 is equal to zero, making θ_6 have a negative cosine. In the cases when $a = z_5$, the angle θ_6 will have a positive cosine. The parameter K_6 in Equation 3 controls this difference.
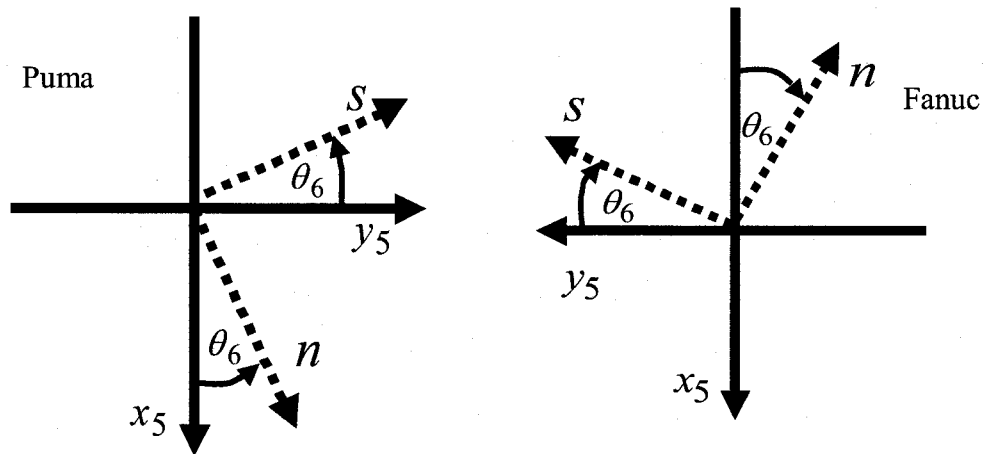
Figure 2.24: Solution for Joint 6

$$\sin\theta_6 = n \cdot y_5 \tag{59}$$

$$\cos\theta_6 = K_6 s \cdot y_5 \tag{60}$$

The parameter K_6 is defined as in Equation 3. The vector y_5 is the y-column vector of the $^0T_5$ matrix, while n and s are the normal and sliding vectors of the $^0T_6$ matrix, respectively:

$$^0T_5 = {}^0T_1\,{}^1T_2\,{}^2T_3\,{}^3T_4\,{}^4T_5 \tag{61}$$

54

$$\sin\theta_6 = [K_4 K_5 (\cos\theta_1 \cos(\theta_2 + K_2\theta_3)\sin\theta_4 - K_1 K_2 K_3 K_4 K_5 \sin\theta_1 \cos\theta_4)]n_x$$
$$+ [K_4 K_5 (\sin\theta_1 \cos(\theta_2 + K_2\theta_3)\sin\theta_4 + K_1 K_2 K_3 K_4 K_5 \cos\theta_1 \cos\theta_4)]n_y \qquad (62)$$
$$+ [K_1 K_4 K_5 \sin(\theta_2 + K_2\theta_3)\sin\theta_4]n_z$$

$$\cos\theta_6 = K_6 \{[K_4 K_5 (\cos\theta_1 \cos(\theta_2 + K_2\theta_3)\sin\theta_4 - K_1 K_2 K_3 K_4 K_5 \sin\theta_1 \cos\theta_4)]s_x$$
$$+ [K_4 K_5 (\sin\theta_1 \cos(\theta_2 + K_2\theta_3)\sin\theta_4 + K_1 K_2 K_3 K_4 K_5 \cos\theta_1 \cos\theta_4)]s_y \qquad (63)$$
$$+ [K_1 K_4 K_5 \sin(\theta_2 + K_2\theta_3)\sin\theta_4]s_z\}$$

Combining Equations 59 to 63, the angle θ_6 can be obtained:

$$\theta_6 = \operatorname{atan}2\left(\frac{\sin\theta_6}{\cos\theta_6}\right) \qquad (64)$$

The solution procedure outlined above provides eight solutions for the inverse kinematics problem of the six-joints RPF robots. The first three solutions $(\theta_1, \theta_2, \theta_3)$ represent the position of the end-effector, whereas the last three solutions $(\theta_4, \theta_5, \theta_6)$ represent the orientation of the end-effector. The results are applicable for all types of robots that can be included within the RPF model. Note here that all the six angles are in the range of $(-\pi, +\pi)$.

2.5. Simulation Results and Discussions

A generic geometry-based solution for solving the inverse kinematic problem of the RPF model has been presented in the preceding section.

The solutions for the joint angles contain proposed configuration parameters $K_1, K_2, K_3, K_4, K_5, K_6$ and all the non-zero D-H parameters. This provided a systematic approach for constructing the RPF model and enabled the development of the UKMS by using a hybrid graphical and computational method. With the UKMS that is based on the RPF model in software, are able to represent most of the 6R industrial robots and to solve their inverse kinematic problem. A

55

simple graphical user interface will be used for fast robot modeling and simulation of different industrial applications. To represent a robot in UROCA software, one needs to define all the joint coordinate systems with their orientations and positions relative to the base frame. This is accomplished by using a simple drag-and-drop feature that is available via the graphical interface. Arm lengths and offsets are systematically generated according the chosen positions of the axis systems. Figures 2.25 schematically explains this procedure, in three major steps, with an application to the ABB IRB1400 robot arm which represents a PUMA -type robot. The solution module was written as an OOP (Objected Oriented Programming) in Visual C++ code.

Each robot path as shown in Figure 2.26 and 2.27 consists of five points and a home position. In the simulation obtained the inverse kinematic for all the designated path points as well as the robot's home position. Two examples from each kinematic group are presented.
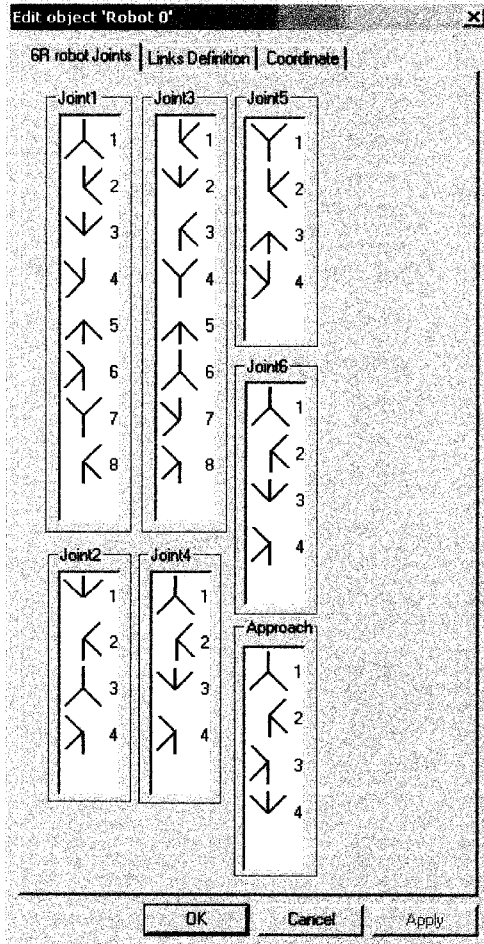
56
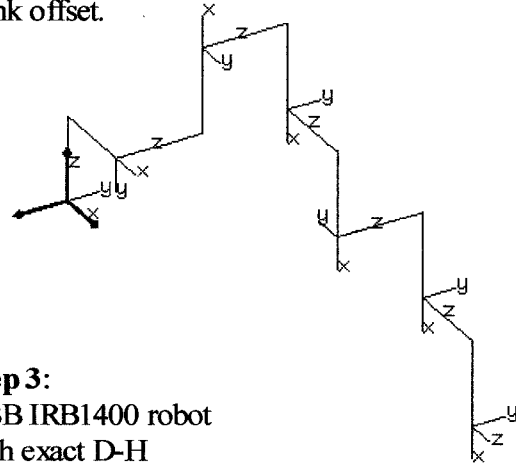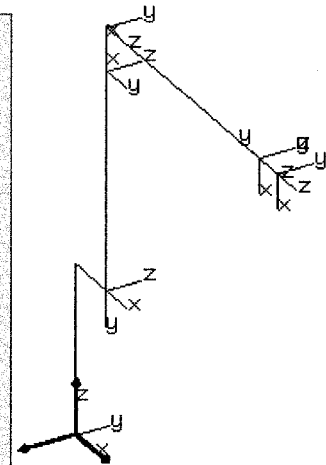
Figure 2.25: Three major steps for representing the kinematics model of a robot in UROCA

57

Example 1: ABB IRB 1400

This example considers the ABB IRB1400 arm with its generalized D-H parameters and path as shown in Figure 2.26. A coordinate system for each joint has been assigned in order to define the D-H parameters as previously shown in Figure 2.25.

Joint	θ_i (deg)	d_i (mm)	a_i (mm)	α_i (deg)
1	0.00	475.00	150.00	-90.00
2	-90.00	0.00	600.00	0.00
3	180.00	0.00	-120.00	90.00
4	0.00	720.00	0.00	-90.00
5	0.00	0.00	0.00	90.00
6	0.00	85.00	0.00	0.00
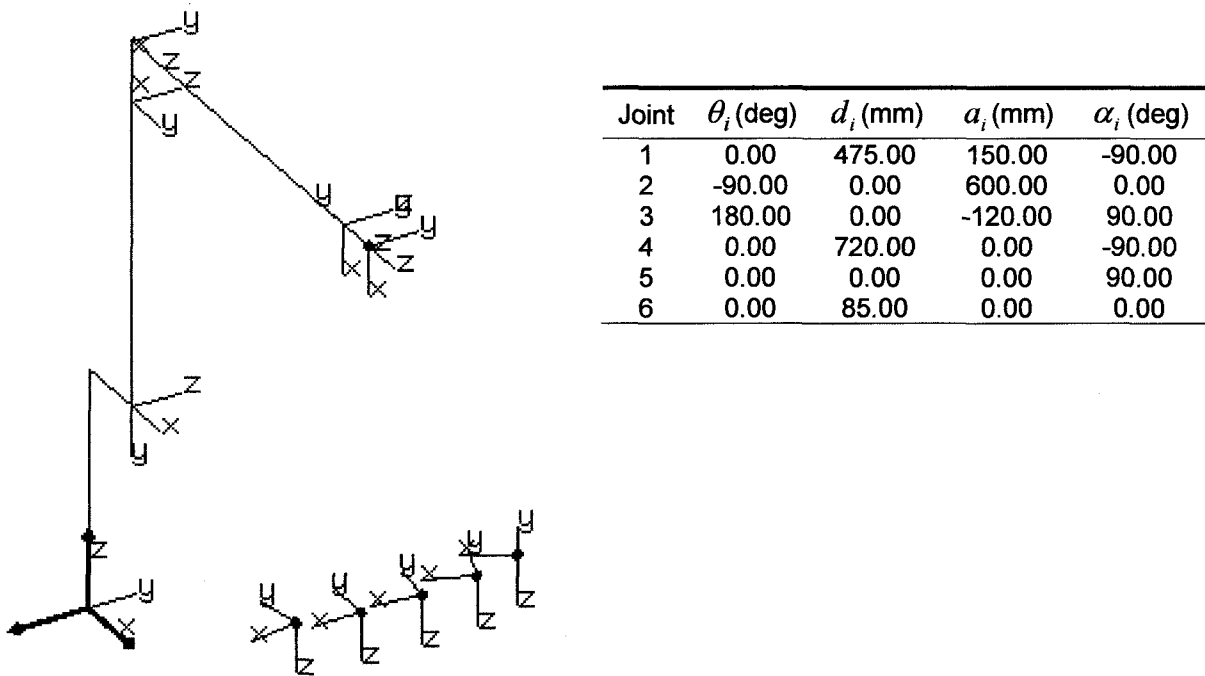
Figure 2.26: Fanuc ABB IRB 1400 with points on the path and its D-H parameters

For the given path, which includes five poses and the home position, the inverse kinematics for each pose were calculated. The poses are defined with their positions $P = (p_x, p_y, p_z)$ and orientations (n,s,a), as shown in Table 2.9.

Table 2.9: Various points on the ABB IRB 1400 robot Path

Points	px	py	pz	$n = (n_x, n_y, n_z)$	$s = (s_x, s_y, s_z)$	$a = (a_x, a_y, a_z)$
1	1045.54	240.32	559.44	-0.52, 0.85, 0.00	0.85, 0.52, 0.00	0.00, 0.00, -1.00
2	1072.93	146.64	559.44	-0.32, 0.94, 0.00	0.94, 0.32, 0.00	0.00, 0.00, -1.00
3	1085.12	31.86	559.44	-0.12, 0.99, 0.00	0.99, 0.12, 0.00	0.00, 0.00, -1.00
4	1081.42	- 86.70	559.44	0.01, 0.99, 0.00	0.99, -0.01, 0.00	0.00, 0.00, -1.00
5	1059.54	-202.24	559.44	0.16, 0.98, 0.00	0.98, -0.16, 0.00	0.00, 0.00, -1.00
6	955.00	0.00	1195.00	0.00, 0.00, -1.00	0.00, 1.00, 0.00	1.00, 0.00, 0.00

58

The results, as expected, are not unique. Solutions for Joint 1 are presented graphically, Figure 2.27. The solutions for points 2, 3, 4, 5, and 6 are given in Tables 2.10-2.14.
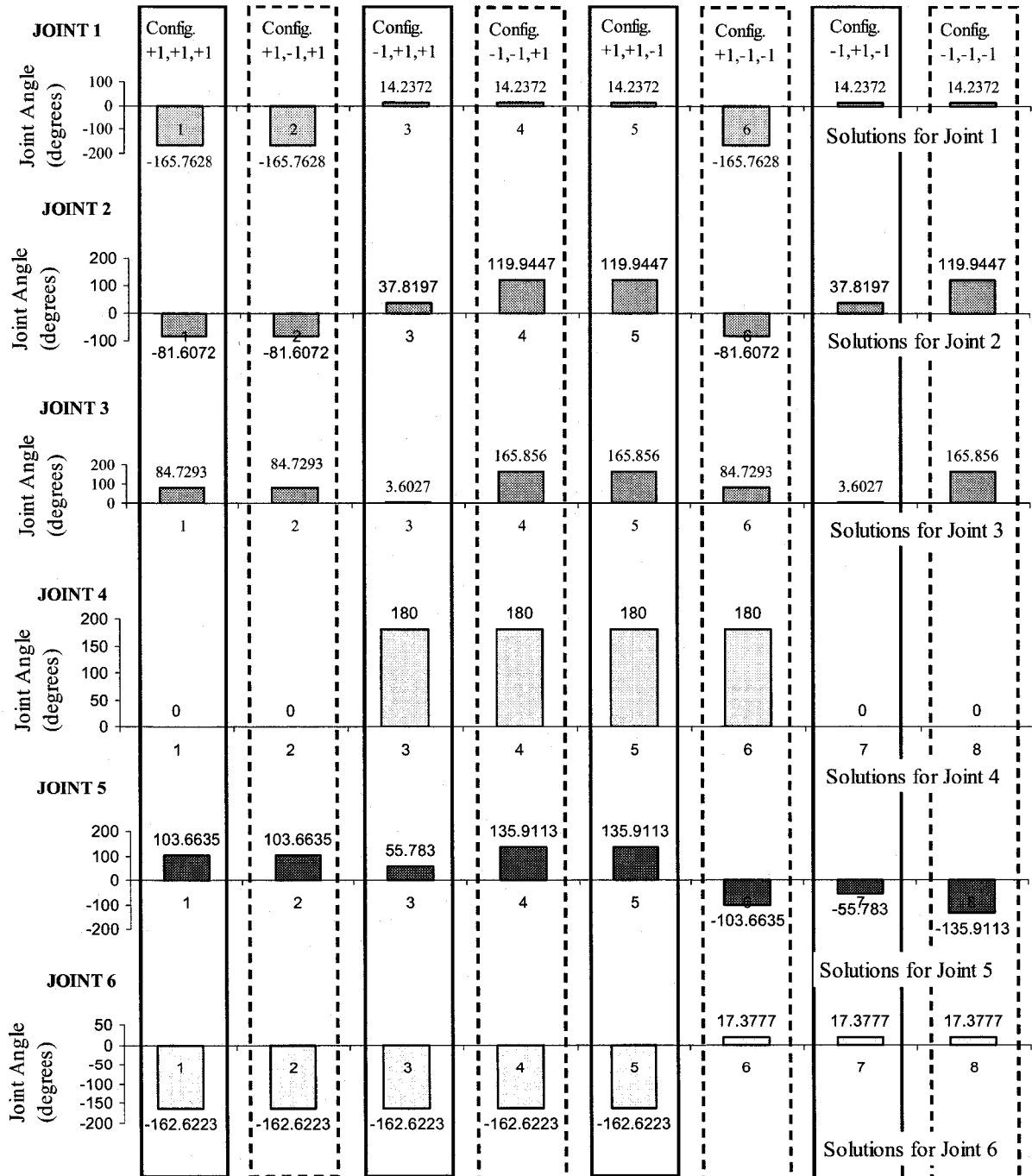
Figure 2.27: Joint solutions for point 1.

59

Table 2.10: Joint solutions for point 2.

Solutions	Point #2							
	1	2	3	4	5	6	7	8
A, E, W	+1, +1, +1	+1, -1, +1	**-1, +1, +1**	-1, -1, +1	+1, +1, -1	+1, -1, -1	-1, +1, -1	-1, -1, -1
JOINT1	-172.2175	-172.2175	**7.7825**	7.7825	-172.2175	-172.2175	7.7825	7.7825
JOINT2	-59.3014	254.9523	**29.3682**	130.0427	-59.3014	254.9523	29.3682	130.0427
JOINT3	-122.0437	-39.0317	**9.0554**	-170.1308	-122.0437	-39.0317	9.0554	-170.1308
JOINT4	180.0000	180.0000	**0**	0	0	0	180.0000	180.0000
JOINT5	88.6549	125.9207	**51.5764**	130.0880	-88.6549	-125.9207	-51.5764	-130.0880
JOINT6	78.9125	78.9125	**78.9125**	78.9125	-101.0875	-101.0875	-101.0875	-101.0875

Table 2.11: Joint solutions for point 3.

Solutions	Point #3							
	1	2	3	4	5	6	7	8
A, E, W	+1, +1, +1	+1, -1, +1	**-1, +1, +1**	-1, -1, +1	+1, +1, -1	+1, -1, -1	-1, +1, -1	-1, -1, -1
JOINT1	-178.3182	-178.3182	**1.6818**	1.6818	-178.3182	-178.3182	1.6818	1.6818
JOINT2	-59.6845	255.3018	**29.5929**	129.8760	-59.6845	255.3018	29.5929	129.8760
JOINT3	-121.3845	-39.6908	**8.7269**	-169.8023	-121.3845	-39.6908	8.7269	-169.8023
JOINT4	180.0000	180.000	**0**	0	0	0	180.000	180.000
JOINT5	88.9310	125.6109	**51.6802**	129.9263	-88.9310	-125.6109	-51.6802	-129.9263
JOINT6	84.4949	84.4949	**84.4949**	84.4949	-95.5051	-95.5051	-95.5051	-95.5051

Table 2.12: Joint solutions for point 4.

Solutions	Point #4							
	1	2	3	4	5	6	7	8
A, E, W	+1, +1, +1	+1, -1, +1	**-1, +1, +1**	-1, -1, +1	+1, +1, -1	+1, -1, -1	-1, +1, -1	-1, -1, -1
JOINT1	175.4159	175.4159	**-4.5841**	-4.5841	175.4159	175.4159	-4.5841	-4.5841
JOINT2	-59.5843	255.2103	**29.5344**	129.9194	-59.5843	255.2103	29.5344	129.9194
JOINT3	-121.5571	-39.5183	**8.8125**	-169.8879	-121.5571	-39.5183	8.8125	-169.8879
JOINT4	180.0000	180.0000	**0**	0	0	0	180.0000	180.0000
JOINT5	88.8587	125.6920	**51.6531**	129.9684	-88.8587	-125.6920	-51.6531	-129.9684
JOINT6	85.9264	85.9264	**85.9264**	85.9264	-94.0736	-94.0736	-94.0736	-94.0736

Table 2.13: Joint solutions for point 5.

Solutions	Point #5							
	1	2	3	4	5	6	7	8
A, E, W	+1, +1, +1	+1, -1, +1	**-1, +1, +1**	-1, -1, +1	+1, +1, -1	+1, -1, -1	-1, +1, -1	-1, -1, -1
JOINT1	169.1933	169.1933	**-10.8067**	-10.8067	169.1933	169.1933	-10.8067	-10.8067
JOINT2	-58.7096	254.4137	**29.0154**	130.3039	-58.7096	254.4137	29.0154	130.3039
JOINT3	-123.0603	-38.0150	**9.5700**	-170.6454	-123.0603	-38.0150	9.5700	-170.6454
JOINT4	180.0000	180.0000	**0**	0	0	0	180.0000	180.0000
JOINT5	88.2301	126.3987	**51.4146**	130.3415	-88.2301	-126.3987	-51.4146	-130.3415
JOINT6	88.4083	88.4083	**88.4083**	88.4083	-91.5917	-91.5917	-91.5917	-91.5917

60

Table 2.14: Joint solutions for point 6.

	Point #6(HOME POSITION)							
Solutions	1	2	3	4	5	6	7	8
A, E, W	+1, +1, +1	+1, -1, +1	-1, +1, +1	-1, -1, +1	+1, +1, -1	+1, -1, -1	-1, +1, -1	-1, -1, -1
JOINT1	-180.0000	-180.0000	0	0	-180.0000	-180.0000	0	0
JOINT2	-32.4652	-77.0996	0	90.0000	-32.4652	-77.0996	0	90.0000
JOINT3	-121.0430	-40.0323	0	-161.0754	-121.0430	-40.0323	0	-161.0754
JOINT4	180.0000	180.0000	0	0	0	0	0	180.0000
JOINT5	26.4917	62.8681	0	71.0754	-26.4917	-62.8681	0	-71.0754
JOINT6	0.0000	0.0000	0	0	180.0000	180.0000	0	-180.0000

Example 2: Fanuc ARCMate120iL

This example considers the ARCMate120iL arm with its generalized D-H parameters. A path similar to the one used in the previous example is used as shown in Figure 2.28.

Joint	θ_i (deg)	d_i (mm)	l_i (mm)	α_i (deg)
1	0.00	700.00	200.00	-90.00
2	-90.00	0.00	800.00	180.00
3	180.00	0.00	-75.00	90.00
4	0.00	-813.00	0.00	-90.00
5	0.00	0.00	0.00	90.00
6	0.00	-100.00	0.00	0.00
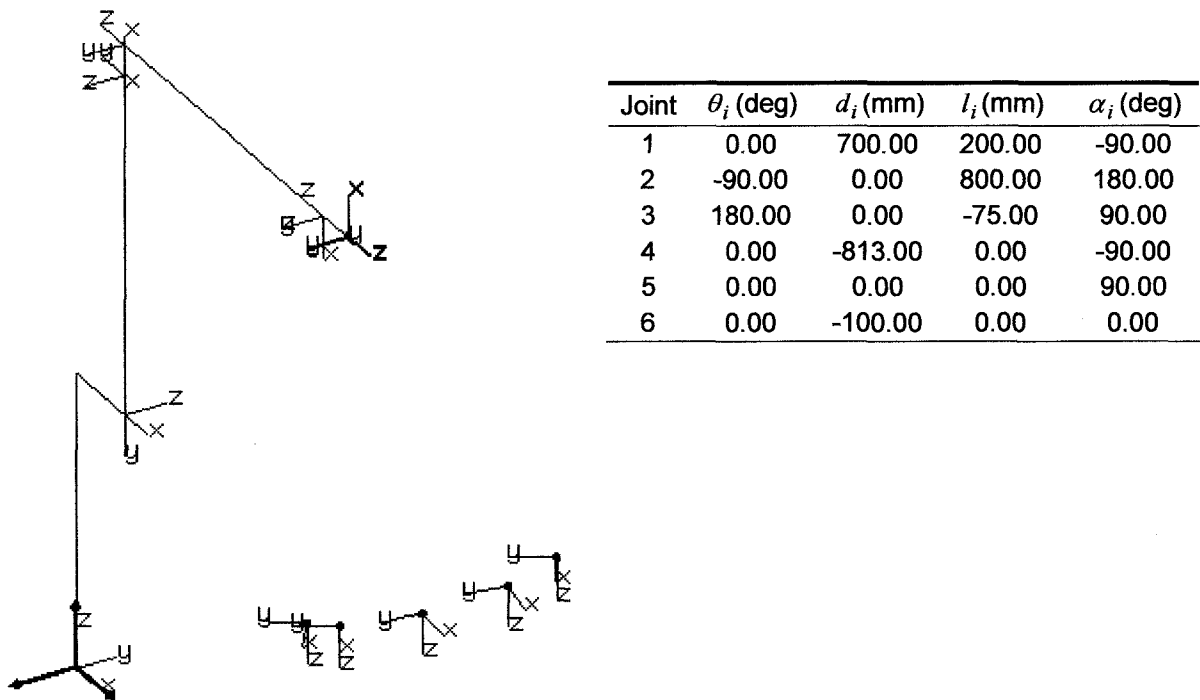
Figure 2.28: Fanuc ARCMate120iL with points on the path and its D-H parameters

61

For the given path, which includes five poses and the home position, the inverse kinematics for each pose were calculated. The poses are defined with their positions $P = (p_x, p_y, p_z)$ and orientations (n,s,a) as in Table 2.15.

Table 2.15: Various points on the ARCMate120iL robot Path

Points	px	py	pz	$n = (n_x, n_y, n_z)$	$s = (s_x, s_y, s_z)$	$a = (a_x, a_y, a_z)$
1	1361.84	345.54	836.80	0.85, 0.52, 0.00	0.52, -0.85, 0.00	0.00, 0.00, -1.00
2	1411.94	202.91	836.80	0.98, 0.18, 0.00	0.18, -0.98, 0.00	0.00, 0.00, -1.00
3	1419.28	-3.11	836.80	0.99, -0.08, 0.00	-0.08, -0.99, 0.00	0.00, 0.00, -1.00
4	1380.35	-174.26	836.80	0.85, -0.51, 0.00	-0.51, -0.85, 0.00	0.00, 0.00, -1.00
5	1337.16	-226.66	836.80	0.80, -0.58, 0.00	-0.58, -0.80, 0.00	0.00, 0.00, -1.00
6	1113.00	0.00	1575.00	0.00,0.00,1.00	0.00,-1.00,0.00	1.00,0.00,0.00

The results, as expected, are not unique. Solutions for Joint 1 are presented graphically, Figure 2.29. The solutions for points 2, 3, 4, 5, and 6 are given in Tables 2.16-2.20.

62

Figure 2.29: Joint solutions for point 1

63

Table 2.16: Joint solutions for point 2.

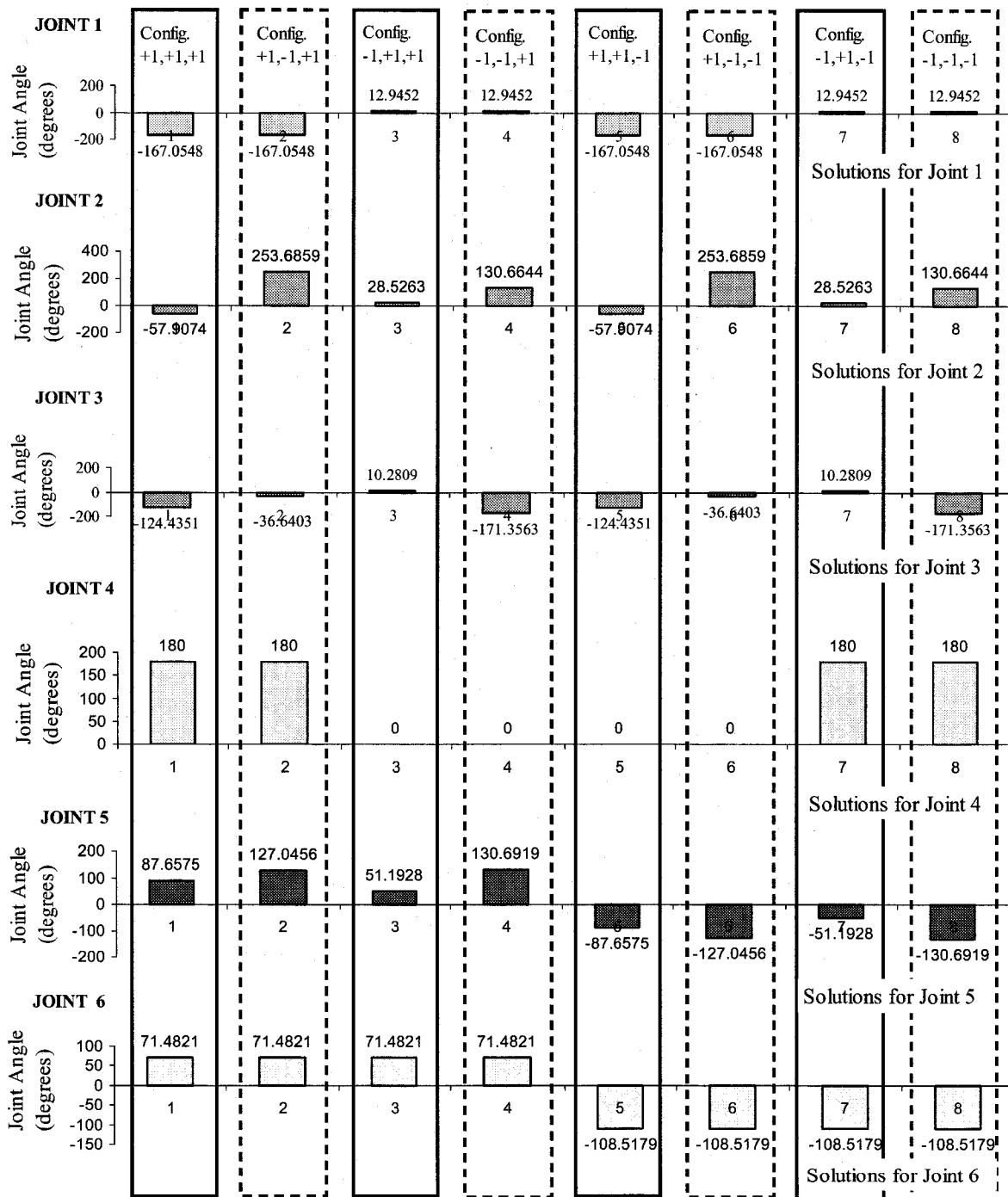| Solutions	Point #2							
	1	2	3	4	5	6	7	8
A, E, W	+1, +1, +1	+1, -1, +1	**-1, +1, +1**	-1, -1, +1	+1, +1, -1	+1, -1, -1	-1, +1, -1	-1, -1, -1
JOINT1	-171.8218	-171.8218	**8.1782**	8.1782	-171.8218	-171.8218	8.1782	8.1782
JOINT2	-81.7163	-81.7163	**39.1914**	118.9525	-81.7163	-81.7163	39.1914	118.9525
JOINT3	84.7293	84.7293	**5.9263**	163.5324	84.7293	84.7293	5.9263	163.5324
JOINT4	0	0	**180.0000**	180.0000	180.0000	180.0000	0	0
JOINT5	103.5543	103.5543	**56.7349**	134.5799	-103.5543	-103.5543	-56.7349	-134.5799
JOINT6	-177.2633	-177.2633	**-177.2633**	-177.2633	2.7367	2.7367	2.7367	2.7367

Table 2.17: Joint solutions for point 3.

Solutions	Point #3							
	1	2	3	4	5	6	7	8
A, E, W	+1, +1, +1	+1, -1, +1	**-1, +1, +1**	-1, -1, +1	+1, +1, -1	+1, -1, -1	-1, +1, -1	-1, -1, -1
JOINT1	179.8743	179.8743	**-0.1257**	-0.1257	179.8743	179.8743	-0.1257	-0.1257
JOINT2	-81.6802	-81.6802	**38.7306**	119.2879	-81.6802	-81.6802	38.7306	119.2879
JOINT3	84.7293	84.7293	**5.1435**	164.3152	84.7293	84.7293	5.1435	164.3152
JOINT4	0	0	**180.0000**	180.0000	180.0000	180.0000	0	0
JOINT5	103.5905	103.5905	**56.4129**	135.0273	-103.5905	-103.5905	-56.4129	-135.0273
JOINT6	175.1117	175.1117	**175.1117**	175.1117	-4.8883	-4.8883	-4.8883	-4.8883

Table 2.18: Joint solutions for point 4.

Solutions	Point #4							
	1	2	3	4	5	6	7	8
A, E, W	+1, +1, +1	+1, -1, +1	**-1, +1, +1**	-1, -1, +1	+1, +1, -1	+1, -1, -1	-1, +1, -1	-1, -1, -1
JOINT1	172.8046	172.8046	**-7.1954**	-7.1954	172.8046	172.8046	-7.1954	-7.1954
JOINT2	-75.9132	-87.1588	**36.9555**	120.5599	-75.9132	-87.1588	36.9555	120.5599
JOINT3	95.8612	73.5974	**2.1492**	167.3095	95.8612	73.5974	2.1492	167.3095
JOINT4	0	0	**180.0000**	180.0000	180.0000	180.0000	0	0
JOINT5	98.2255	109.2438	**55.1937**	136.7496	-98.2255	-109.2438	-55.1937	-136.7496
JOINT6	156.3917	156.3917	**156.3917**	156.3917	-23.6083	-23.6083	-23.6083	-23.6083

Table 2.19: Joint solutions for point 5.

Solutions	Point #5							
	1	2	3	4	5	6	7	8
A, E, W	+1, +1, +1	+1, -1, +1	**-1, +1, +1**	-1, -1, +1	+1, +1, -1	+1, -1, -1	-1, +1, -1	-1, -1, -1
JOINT1	170.3793	170.3793	**-9.6207**	-9.6207	170.3793	170.3793	-9.6207	-9.6207
JOINT2	-68.0757	-94.6206	**34.7758**	122.0759	-68.0757	-94.6206	34.7758	122.0759
JOINT3	111.0020	58.4566	**-1.4792**	170.9379	111.0020	58.4566	-1.4792	170.9379
JOINT4	0	0	**180.0000**	180.0000	180.0000	180.0000	0	0
JOINT5	90.9223	116.9229	**53.7451**	138.8621	-90.9223	-116.9229	-53.7451	-138.8621
JOINT6	153.5417	153.5417	**153.5417**	153.5417	-26.4583	-26.4583	-26.4583	-26.4583

64

				Point #6 (Home position)				
Solutions	1	2	3	4	5	6	7	8
A, E, W	+1, +1, +1	+1, -1, +1	**-1, +1, +1**	-1, -1, +1	+1, +1, -1	+1, -1, -1	-1, +1, -1	-1, -1, -1
JOINT1	-180.0000	-180.0000	**0**	0	-180.0000	-180.0000	0	0
JOINT2	-31.6643	-76.7260	**0**	85.7930	-31.6643	-76.7260	0	85.7930
JOINT3	129.3129	40.1458	**0**	169.4587	129.3129	40.1458	0	169.4587
JOINT4	180.0000	180.0000	**0**	0	0	0	0	180.0000
JOINT5	-19.0229	-63.1282	**0**	-83.6657	19.0229	63.1282	0	83.6657
JOINT6	0	0	**0**	0	-180.0000	-180.0000	0	-180.0000

65

CHAPTER THREE

3. SINGULARITY ANALYSIS OF A RECONFIGURABLE PUMA -FANUC ROBOTIC MODEL VIA A RECONFIGURABLE JACOBIAN MATRIX APPROACH

Robot control processes can sometimes run into difficulties, since the inverse mapping from a Cartesian space to a joint space may cause problems. These are robot positions that are referred to as singularities or degeneracy. Upon solving the inverse kinematics for the RPF model, the singularity problem should be the next priority.

This work is based on the power of comparing the similarities between different robotic systems and the result is the development of reconfigurable parameters for solving their inverse kinematics and singularity problems. Instead of calculating a Jacobian Matrix for every individual robot and solving for their singularities, a Reconfigurable PUMA - Fanuc Jacobian Matrix (RPFJM) was developed.

3.1. Reconfigurable PUMA -Fanuc Jacobian Matrix (RPFJM)

This model requires a development of its Jacobian matrix. Let:

$$x_i = f_i(q_1, q_2, q_3, \ldots, q_n), \quad i = 1, 2, \ldots, m \tag{65}$$

be a set of 'm' equations, each being a function of 'n' independent variables. Then the time derivate of x_i can be written as a function of $\dot{q}_i$ as follows:

$$\dot{x}_i = \frac{\partial f_i}{\partial q_1}\dot{q}_1 + \frac{\partial f_i}{\partial q_2}\dot{q}_2 + \frac{\partial f_i}{\partial q_3}\dot{q}_3 + \ldots + \frac{\partial f_i}{\partial q_n}\dot{q}_n, \quad i = 1, 2, \ldots, m \tag{66}$$

66

The Jacobian J is an 'm x n' linear transformation matrix that maps an n-dimensional velocity vector $\dot{q}_i$ into an m-dimensional velocity vector $\dot{x}_i$, Equation 67.

$$\dot{X} = J\dot{q} \tag{67}$$

Equation 67 is presented in vectors form with Equation 68.

$$\begin{bmatrix} \dot{x}_1 \\ \dot{x}_2 \\ \vdots \\ \dot{x}_m \end{bmatrix} = \begin{bmatrix} \dfrac{\partial f_1}{\partial q_1} & \dfrac{\partial f_1}{\partial q_2} \cdots & \dfrac{\partial f_1}{\partial q_n} \\ \dfrac{\partial f_2}{\partial q_1} & \dfrac{\partial f_2}{\partial q_2} \cdots & \dfrac{\partial f_2}{\partial q_n} \\ \vdots & \vdots & \vdots \\ \dfrac{\partial f_m}{\partial q_1} & \dfrac{\partial f_m}{\partial q_2} \cdots & \dfrac{\partial f_m}{\partial q_n} \end{bmatrix} \begin{bmatrix} \dot{q}_1 \\ \dot{q}_2 \\ \vdots \\ \dot{q}_n \end{bmatrix} \tag{68}$$

For robot manipulators, the Jacobian is defined as the coefficient matrix of any set of equations that relates the velocity state of the end-effector described in the Cartesian space to the actuated joint rates in the joint velocity space.

$$\text{The joint rates are: } \dot{q}_i = \begin{cases} \dot{\theta}_i, & \text{For revolute joints} \\ \dot{d}_i, & \text{For prismatic joints} \end{cases} \tag{69}$$

The RPF model has only rotational joints, which means that:

$$\dot{q}_i = \dot{\theta}_i \tag{70}$$

In this thesis the Newton-Euler recursive method was used, (Spong M. W. and Vidyasagar M. 1989) for the Reconfigurable PUMA -Fanuc Jacobian Matrix (RPFJM) calculation. The end effector velocity state is expressed in terms of the linear velocity of the origin of the end effector coordinate frame, V_n and the angular velocity of the end effector ω_n, and thus we have:

67

$$\dot{X} = \begin{bmatrix} V_n \\ \omega_n \end{bmatrix} \tag{71}$$

The linear velocity for revolute joints is:

$$^{n}(^{0}V_{n}) = {}^{n}R_{n-1}{}^{n-1}(^{0}V_{n-1}) + {}^{n}(^{0}\omega_{n}) \times {}^{n}R_{n-1}{}^{n-1}r_{n} \tag{72}$$

The angular velocity for revolute joints is:

$$^{n}(^{0}\omega_{n}) = {}^{n}R_{n-1}{}^{n-1}[^{n-1}(^{0}\omega_{n-1}) + {}^{n-1}\omega_{n}] \tag{73}$$

Applying previously given Equations 71-73 for 6R robots provides the following equation:

$$\begin{bmatrix} ^{6}(^{0}V_{6})_{x} \\ ^{6}(^{0}V_{6})_{y} \\ ^{6}(^{0}V_{6})_{z} \\ ^{6}(^{0}\omega_{6})_{x} \\ ^{6}(^{0}\omega_{6})_{y} \\ ^{6}(^{0}\omega_{6})_{z} \end{bmatrix} = {}^{6}(^{0}J) \begin{bmatrix} \dot{\theta}_{1} \\ \dot{\theta}_{2} \\ \dot{\theta}_{3} \\ \dot{\theta}_{4} \\ \dot{\theta}_{5} \\ \dot{\theta}_{6} \end{bmatrix} \tag{74}$$

where the $^{6}(^{0}J)$ 6 x 6 matrix is the solution given with Equation 75.

$$^{6}(^{0}J) = \begin{bmatrix} J_{11} & J_{12} & J_{13} & J_{14} & J_{15} & J_{16} \\ J_{21} & J_{22} & J_{23} & J_{24} & J_{25} & J_{26} \\ J_{31} & J_{32} & J_{33} & J_{34} & J_{35} & J_{36} \\ J_{41} & J_{42} & J_{42} & J_{43} & J_{45} & J_{46} \\ J_{51} & J_{52} & J_{53} & J_{54} & J_{55} & J_{56} \\ J_{61} & J_{62} & J_{63} & J_{64} & J_{65} & J_{66} \end{bmatrix} \tag{75}$$

Using Equations 72-75, the Reconfigurable PUMA-Fanuc Jacobian Matrix (RPFJM) is calculated, Equation 76:

68

$$
{}^{6}({}^{0}J) = \begin{bmatrix} J_{11} & J_{12} & J_{13} & J_{14} & J_{15} & 0 \\ J_{21} & J_{22} & J_{23} & J_{24} & J_{25} & J_{26} \\ J_{31} & J_{32} & J_{33} & J_{34} & J_{35} & 0 \\ J_{41} & J_{42} & J_{43} & J_{44} & J_{45} & 0 \\ J_{51} & J_{52} & J_{53} & J_{54} & J_{55} & 0 \\ J_{61} & J_{62} & J_{63} & J_{64} & 0 & K_{6} \end{bmatrix} \tag{76}
$$

The developed Jacobian matrix (Equation 76), depends on the configuration parameters K_1, K_2, K_3, K_4, K_5, and K_6 and can be used for all robots that belong to the RPF model. The elements of the matrix in Equation 76 are given in Appendix A and the calculation is provided by Ana M. Djuric (2007).

The above calculation was done manually and by using the MAPLE 10 software. Manual calculations provide better results because of the equation's simplification.

The RPFJM helps for an easy Jacobian calculation for different robotic systems by only changing configuration parameters. Using this model, we can analyze singularity problem(s) for single robots of robot families at the time.

3.1.1. Example of PUMA Jacobian Matrix

D-H parameters were adopted from (Fu K.S., *et al.*, 1987) and presented in Table 2.4. According to the twist angles, the configuration parameters are:

$$
K_1 = -1, \ K_2 = 1, \ K_3 = 1, \ K_4 = -1, \ K_5 = 1, \ K_6 = 1 \tag{77}
$$

The Jacobian matrix was developed before for this well-known model, (Leathy M. B., *et al.*, 1987). This example is used to prove the validity of the RPFJM and its result is given in Equation 78, and all elements are in Appendix B.

69

$$
{}^6({}^0J)_{PUMA} = \begin{bmatrix} J_{11} & J_{12} & J_{13} & J_{14} & J_{15} & 0 \\ J_{21} & J_{22} & J_{23} & J_{24} & J_{25} & 0 \\ J_{31} & J_{32} & J_{33} & 0 & 0 & 0 \\ J_{41} & J_{42} & J_{43} & J_{44} & J_{45} & 0 \\ J_{51} & J_{52} & J_{53} & J_{54} & J_{55} & 0 \\ J_{61} & J_{62} & J_{63} & J_{64} & 0 & 1 \end{bmatrix}
\tag{78}
$$

3.1.2. Example of Fanuc Matrix

To explore the reconfigurabiliy of the RPFJM model, another example of the Fanuc-type robot is presented. According to the twist angles, Table 2.4, the configuration parameters are:

$$
K_1 = -1, \ K_2 = -1, \ K_3 = 1, \ K_4 = -1, \ K_5 = 1, \ K_6 = 1
\tag{79}
$$

Equation 80, which is the same as Equation 78, represents the Fanuc type robot's Jacobian matrix. Differences between these two equations are in the expressions of their matrix elements, which can be seen in detail in Appendix C.

$$
{}^6({}^0J)_{FANUC} = \begin{bmatrix} J_{11} & J_{12} & J_{13} & J_{14} & J_{15} & 0 \\ J_{21} & J_{22} & J_{23} & J_{24} & J_{25} & 0 \\ J_{31} & J_{32} & J_{33} & 0 & 0 & 0 \\ J_{41} & J_{42} & J_{43} & J_{44} & J_{45} & 0 \\ J_{51} & J_{52} & J_{53} & J_{54} & J_{55} & 0 \\ J_{61} & J_{62} & J_{63} & J_{64} & 0 & 1 \end{bmatrix}
\tag{80}
$$

The RPFJM matrix, Equation 80, is showing that some elements in the Jacobian matrix are equal to zero: $J_{16} = J_{26} = J_{36} = J_{46} = J_{56} = J_{65} = 0$, and one element is constant: $J_{66} = K_6$. For the two examples for PUMA -type and Fanuc-type robots the results show that the same elements are equal to zero: $J_{16} = J_{26} = J_{36} = J_{46} = J_{56} = J_{34} = J_{35} = J_{65}$ and one is equal to one: $J_{66} = 1$. The differences between the other elements of Jacobian matrices for PUMA and Fanuc

70

groups of robots are in their expressions that depend on the different D-H parameters.

3.2. Reduced Reconfigurable PUMA -Fanuc Singularity Matrix (RPFSM)

In general terms, a singularity occurs when two or more robot joints are pointing in the same direction. This means that a position has multiple solutions, which causes problems for motion in certain directions. For example, a typical 6R robot such as the ABB 6400 has a singularity when joint 5 is zero, meaning that joints 4 and 6 are aligned. Robot control processes can sometimes run into difficulties, since the inverse mapping from a Cartesian space to a joint space may fail robot positions that are referred to as singularities or degeneracy.

Suppose that the RPF model consists of a 3-DOF forearm with a 3-DOF spherical wrist. The configuration of the 6×6 Jacobian matrix is singular if and only if:

$$\det(J) = 0 \tag{81}$$

In order to simplify the analysis, matrix J can be divided into four blocks of 3×3 matrices.

$$J = \begin{bmatrix} J_{11} & J_{12} \\ J_{21} & J_{22} \end{bmatrix} \tag{82}$$

Equation 74 represents a relationship between joint rates and end-effector velocities of RPF model, and can be written as:

$$\dot{X}_E = J_E \dot{\theta} \tag{83}$$

71

The end-effector center E is presented with position vector p_E, while the center of the spherical wrist W is presented with vector p_W, Figure 3.1.
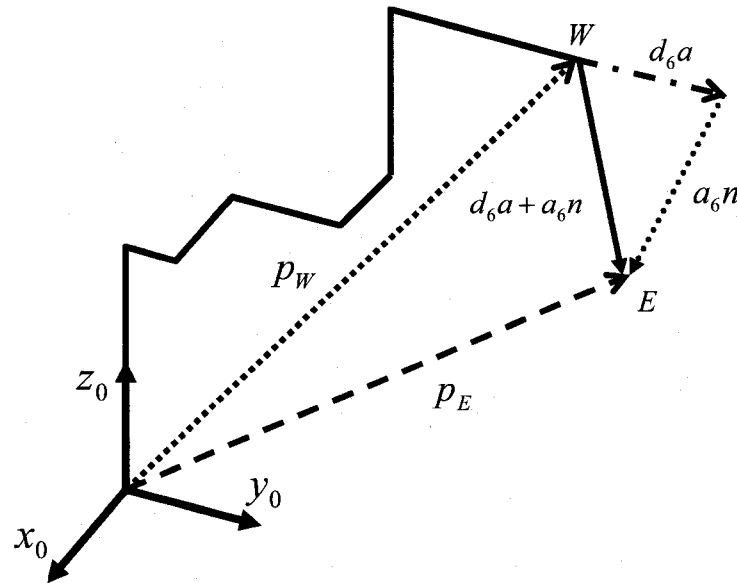

Figure 3.1: Position vector p_E for spherical wrist robots.

If the velocity reference point is selected at the center of the wrist, then the relationship between the joint rates and the velocity of the wrist become:

$$\dot{X}_W = J_W \dot{\theta} \tag{84}$$

Referring to Tourassis V. D. and Ang M. H. Jr, 1995 and Cheng F. T., *et al.*, 1997, the Jacobian matrix J_W will have the block triangular form:

$$J_W = \begin{bmatrix} J_{11} & 0_{3\times3} \\ J_{21} & J_{22} \end{bmatrix} \tag{85}$$

It is typical in the literature to use the vector method for calculating the Jacobian matrix, and decoupling it by choosing the coordinate frames, so that their centers are $O_3 = O_4 = O_5 = O_6$, which produces $J_{12} = O_{3\times3}$, (Orin D. E. and Schrader W. W. 1984).

72

To simplify the singularity analysis the Recursive Newton-Euler and vector methods are used. The Recursive Newton-Euler method produces a very simple J_{22} matrix and a very complex J_{11} matrix. Because of that, a simple vector method is used for developing J_{11}, (Cheng F. T., *et al.*, 1997). This method results in a simpler J_{11} matrix and a more complex J_{22} matrix.

The determinant of the Jacobian matrix is always the same, and that allows the combination of the different methods. To decouple the Jacobian matrix will use the following two conditions: $d_6 = 0$ and $a_6 = 0$. It can be seen from Figure 3.1 that the end-effector point will move to the wrist point if these conditions are satisfied. The resulting matrix is in Appendix D.

Referring to Orin D. E. and Schrader W. W. 1984, the determinant of the Jacobian is independent of the velocity reference point selected. From this conclusion can write Equation 86:

$$\det(J_W) = \det(J_E) \tag{86}$$

From Equations 85 and 86 have:

$$\det(J_W) = \det(J_{11})\det(J_{22}) \tag{87}$$

From Equations 81 and 87, the condition of singularity of the RPF model can be decoupled into two determinates:

$$\det(J_{11}) = 0 \text{ or } \det(J_{22}) = 0 \tag{88}$$

3.2.1. Forearm Singularity of the RPF Model

The forearm singularities can be identified by checking the determinant of the matrix J_{11}. The reduced reconfigurable J_{11} was developed by using the simple matrix method. Referring to Cheng F. T., *et al.*, 1997 there are two conditions, for forearm singularities. One is boundary singularities, Equation 89,

73

$$C_b = -a_3 \sin(K_2\theta_3) + K_3 d_4 \cos(K_2\theta_3) = 0 \qquad (89)$$

and the other one is the interior singularity, Equation 90,

$$C_i = -K_1 K_2 a_1 - K_1 K_2 a_2 \cos(\theta_2) - K_1 K_2 a_3 \cos(\theta_2 + K_2\theta_3)$$
$$- K_1 K_3 d_4 \sin(\theta_2 + K_2\theta_3) = 0 \qquad (90)$$

These two condition equations depend of the same reconfigurable parameters, Equation 3. From the previous research work by Cheng F. T., *et al.*, 1997, Oenny D., et al., 2000, and Yuan J., 2001, can see that boundary singularity happens when the wrist point is located on the x_2 axis. This can be identified by mapping J_{11} into the x_2, y_2, z_2 coordinate system, which can be seen in Figure 2.13. The interior singularity happens when the wrist locates at the $y_1 - z_1$ plane, (Cheng F. T., *et al.*, 1997), (Oenny D., *et al.*, 2000), and (Yuan J., 2001). Then one of the axes in z_1, or z_2, or y_3 can be seen as the singular direction.

3.2.2. Wrist Singularity of the RPF Model

The wrist singularities can be identified by checking the determinant of the matrix J_{22}. This result came from decoupling the Jacobian matrix derived using the Newton-Euler recursive method. This matrix is much simpler than the one derived by the vector method. The determinate of J_{22} is given in Equation 91:

$$\det(J_{22}) = K_4 K_5 \sin(\theta_5) = 0 \qquad (91)$$

This is true when $\theta_5 = 0°$, or $\theta_5 = 180°$. Physically, this means that joints 4 and 6 are aligned. This result is the same for all robots in the RPF group.

The matrices J_{11} and J_{22} give the Reduced Reconfigurable PUMA -Fanuc Singularity Matrix (RPFSM) which can be easily reconfigured by only changing the configuration parameters from Equation 3.

3.2.3. Example of PUMA Reduced Singularity Matrix

Using the D-H parameters for PUMA robots from Table 2.4, the PUMA Reduced Singularity Matrix can be calculated. This example is used to prove the validity of the RPFSM model, and can be compared with references in the literature (Cheng F. T., *et al.*, 1997), (Oenny D., *et al.*, 2000), (Yuan J., 2001), and (Fu K.S., *et al.*, 1987). The resulting matrix is in Appendix E.

3.2.4. Example of Fanuc Reduced Singularity Matrix

Using the D-H parameters for Fanuc robots from Table 2.4, the Fanuc Reduced Singularity Matrix can also be calculated. The resulting matrix is in Appendix F.

75

CHAPTER FOUR

4. ROBOT WORK ENVELOPE

The work envelope, also known as the robot operating envelope or workspace is the set of points representing the maximum extent or reach of the robot tool in all directions, (Nof S. Y., 1999).

The inner and outer reachable workspace surfaces are created with the tool frame. The travel limits for the first 3 positioning joints in the kinematic chain are used to generate the limits of the surface, (Anon. 1999).

The workspace of the manipulator is defined as the set of all end-effector locations (position and orientations of the end-effector frame) that can be reached by arbitrary choices of joint variables within the corresponding range. If both end-effector position and orientation are considered, the workspace is the complete workspace; disregarding the orientation of the end-effector gives the reachable workspace. The subject of the reachable workspace that can be attained with arbitrary orientations of the end-effector is the dexterous workspace (Nof S. Y., 1999).

4.1. Calculation of Reconfigurable Robot Workspace (RRW)

For the workspace calculation, the first three joints are used. By varying their joint limits from minimum to maximum, the complete 3-D reachable workspace is described. This 3-D envelope can be called the 1-2-3 envelope. Excluding Joint 1, we get a 2-D envelope, called the 2-3 envelope. The most difficult part is to calculate the 2-3 envelope using one control algorithm. The reason is the differences in Joint 2 and Joint 3 directions, which depend on the robot manufacturer.

76

Analyzing the Joint 2 and Joint 3 motion for different robots, a unique control algorithm can be developed. Rotating the 2-3 envelope about Joint 1 for the given limits, the result will be the 1-2-3 envelope. The 2-3 envelope, which includes all reachable points, by varying Joint 2 and Joint 3 for robot model IRB6400-24, is presented in Figure 4.1.
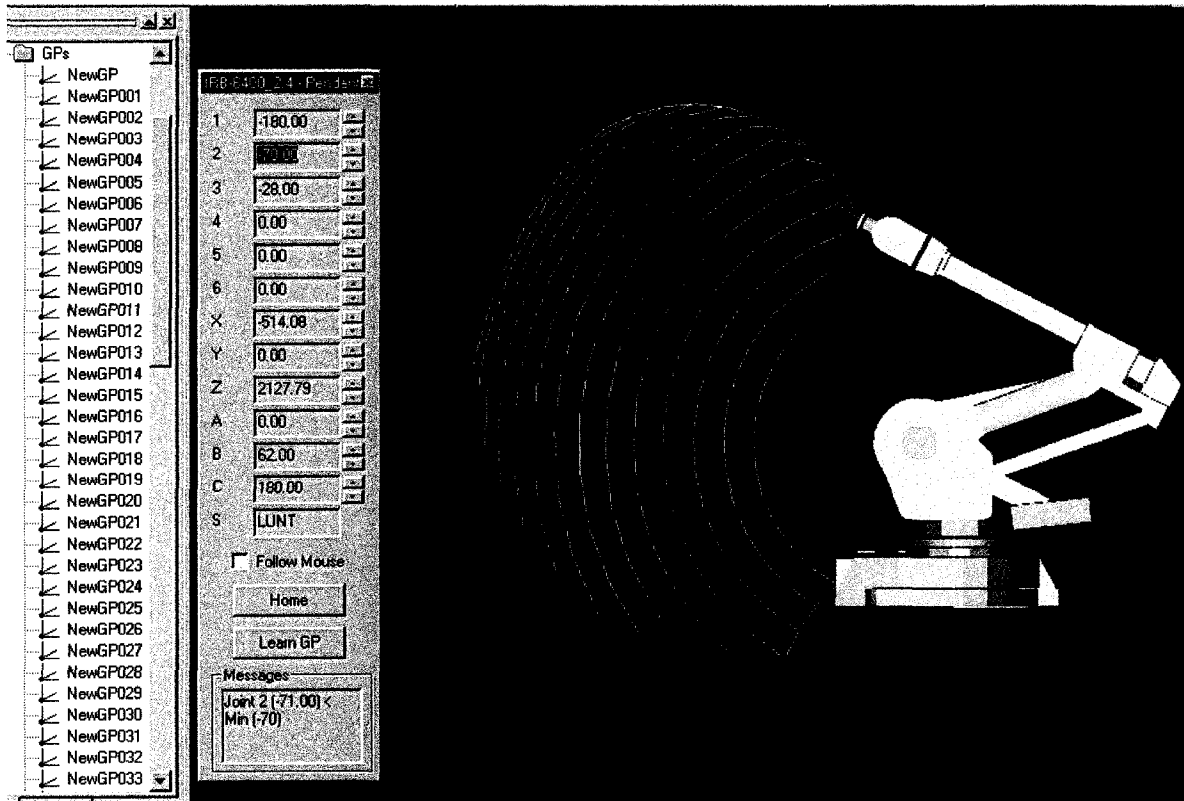

Figure 4.1: Envelope Boundary for Joint 2 and Joint 3 IRB6400-24 (**Workspace 4® software**)

The 2-3 envelope developed by varying Joint 1 and Joint 2 for their given joint limits, will produce an area with the inside points and the points on the boundary of the area. The working envelope has two parts: **Boundary Envelope** (contains only points on the workspace boundary) and **Interior Envelope** (contains all other points inside of the boundary). See Figure 4.2.
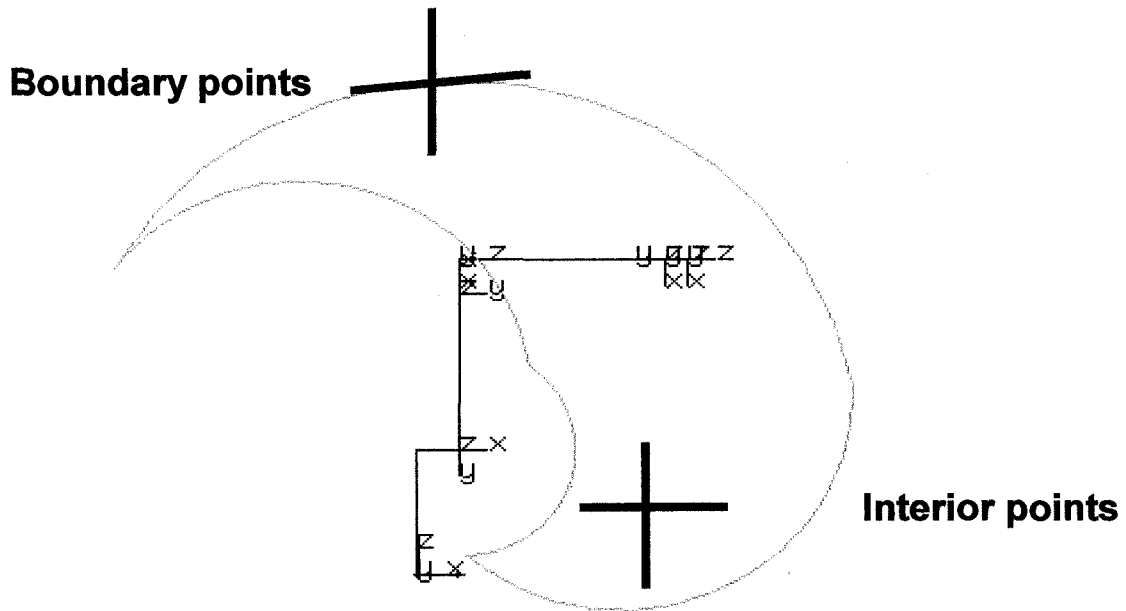
77

Figure 4.2: Boundary and Interior points

To get the 3-D surface by rotating the 2-3 envelope about Joint 1, we need only the boundary of the 2-3 envelope. To be able to separate the boundary envelope from the complete envelope, need to know which points are on the boundary and which are inside of the boundary. To check the points need some mathematical analysis. The procedure for selecting the boundary points is called Filtering Boundary Points (FBP).

4.2. Filtering Boundary Points (FBP) Method

Consider a point P_i on the 2-3 envelope, that can be inside of the boundary or on the boundary, as shown in the side view in Figure 4.3. Place a local coordinate system $z - w$ with its centre at the selected point P_i. In each quadrant of the local coordinate system, create a point: P_{i1}, P_{i2}, P_{i3}, P_{i4}, a small distance δ from P_i.
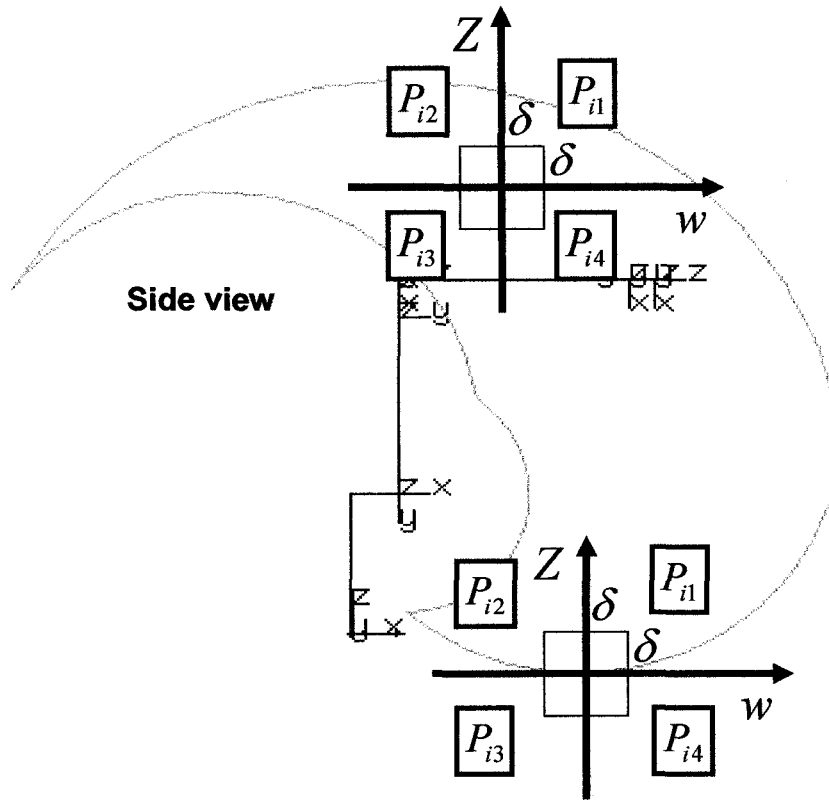
78

Figure 4.3: Side view of the area around the P_i point in the Robot Workspace

To get new coordinates for the four points, need to analyze them in 3D. Because of that the top view of the envelope is created and presented in Figure 4.4.
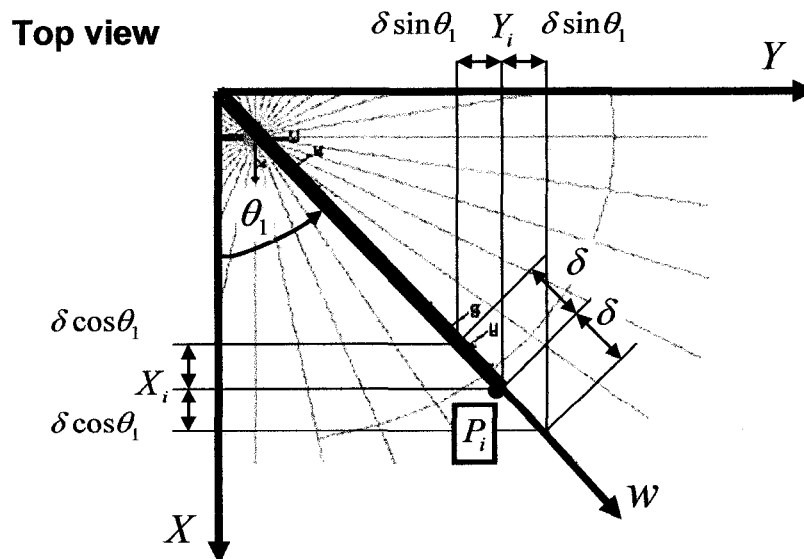

Figure 4.4: Top view of the area around the P_i point in the robot workspace

79

These points will have new locations, and their coordinates are expressed in Equations 92-95:

$$P_{i2}(X_i - \delta\cos\theta_1; Y_i - \delta\sin\theta_1; Z_i + \delta) \tag{92}$$

$$P_{i1}(X_i + \delta\cos\theta_1; Y_i + \delta\sin\theta_1; Z_i + \delta) \tag{93}$$

$$P_{i3}(X_i - \delta\cos\theta_1; Y_i - \delta\sin\theta_1; Z_i - \delta) \tag{94}$$

$$P_{i4}(X_i + \delta\cos\theta_1; Y_i + \delta\sin\theta_1; Z_i - \delta) \tag{95}$$

If $P_i(x,y)$ is an interior point then all four local points P_{i1}, P_{i2}, P_{i3}, and P_{i4} will be reachable by the robot. If $P_i(x,y)$ is boundary point then at least one of the four local points P_{i1}, P_{i2}, P_{i3}, and P_{i4} will be an unreachable point for the robot.

All points on the boundary must be connected with lines to form the closed polyline. This polyline represents the 2-3 envelope. Rotating the 2-3 envelope about Joint 1, will produce 1-2-3 envelope, which represents the robot's workspace. This is shown in Figure 4.5.
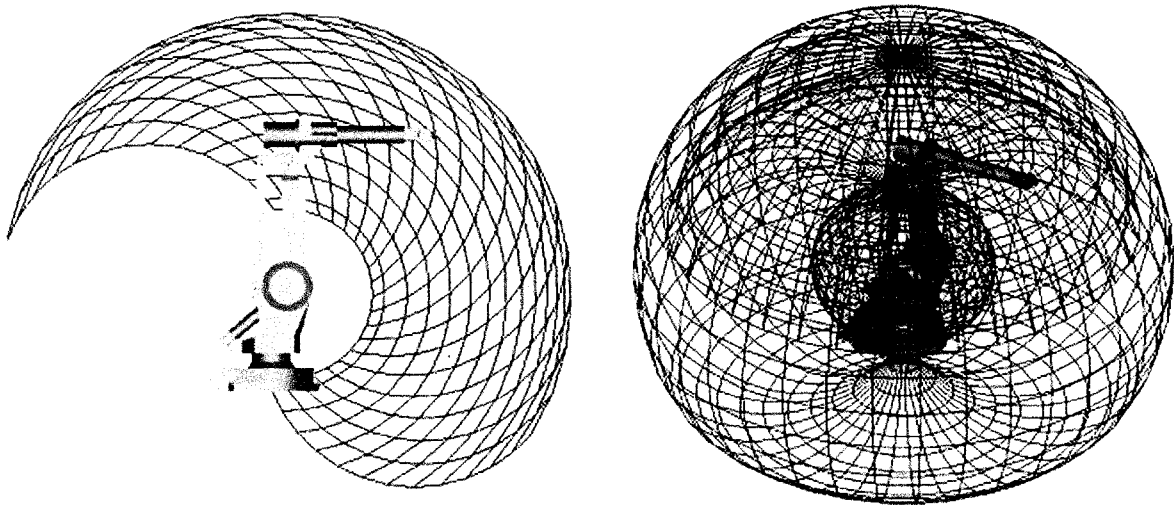

Figure 4.5: 2-3 envelope and 1-2-3 envelope

80

4.2.1. Envelope for the ABB IRB 1400 robot

In Figure 4.6, the 2-3 envelope and 1-2-3 envelope for the ABB IRB 1400 robot are shown.
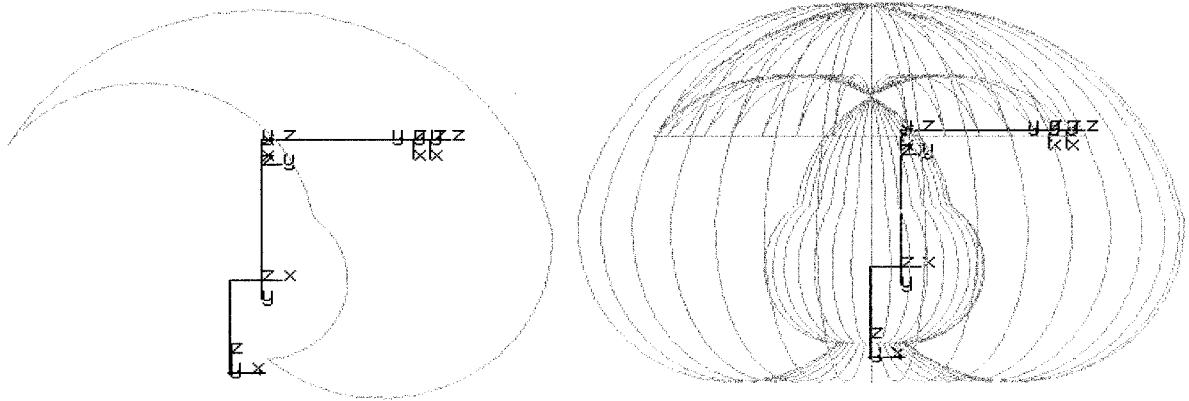

Figure 4.6: 2-3 envelope and 1-2-3 envelope for the ABB IRB 1400 robot

4.2.2. Envelope for the Fanuc ARC Mate 120iL robot

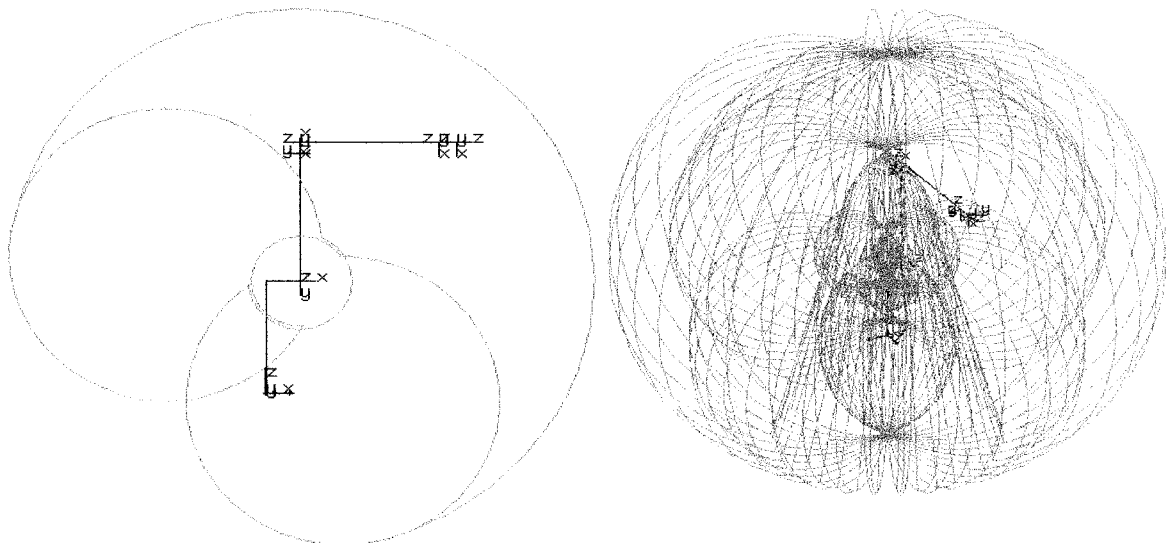In Figure 4.7, the 2-3 envelope and 1-2-3 envelope for the Fanuc ARC Mate 120iL robot are shown.

Figure 4.7: 2-3 envelope and 1-2-3 envelope for the Fanuc ARC Mate 120iL robot

81

CHAPTER FIVE

5. GENERALIZED RECONFIGURABLE 6 - JOINT ROBOT DYNAMICS

This work is based on the power of comparing the similarities between different robotic systems and the result of it is the development of reconfigurable parameters for solving their inverse kinematics, singularity problems and dynamic equations, previously shown. The software package MAPLE 10® and the recursive Newton-Euler (RNE) algorithm were used for developing symbolic dynamic equations of the RPF model. The full dynamic model is calculated, including the dynamics of the robot actuators.

5.1. Description of the RPFDM

For the previously developed the RPF model, the dynamic equations are solved. This dynamic model, called the RPFDM, can be reconfigured from one dynamic group to another or from one application to another by using the configuration parameters $K_1, K_2, ..., K_6$, as defined in Equation 3. This model is graphically shown in Figure 5.1.

Each joint is presented with a different coordinate system; all six links are shown as spheres for simplifications of the calculation. Each link has mass m_1, $m_2, ..., m_6$ respectively.
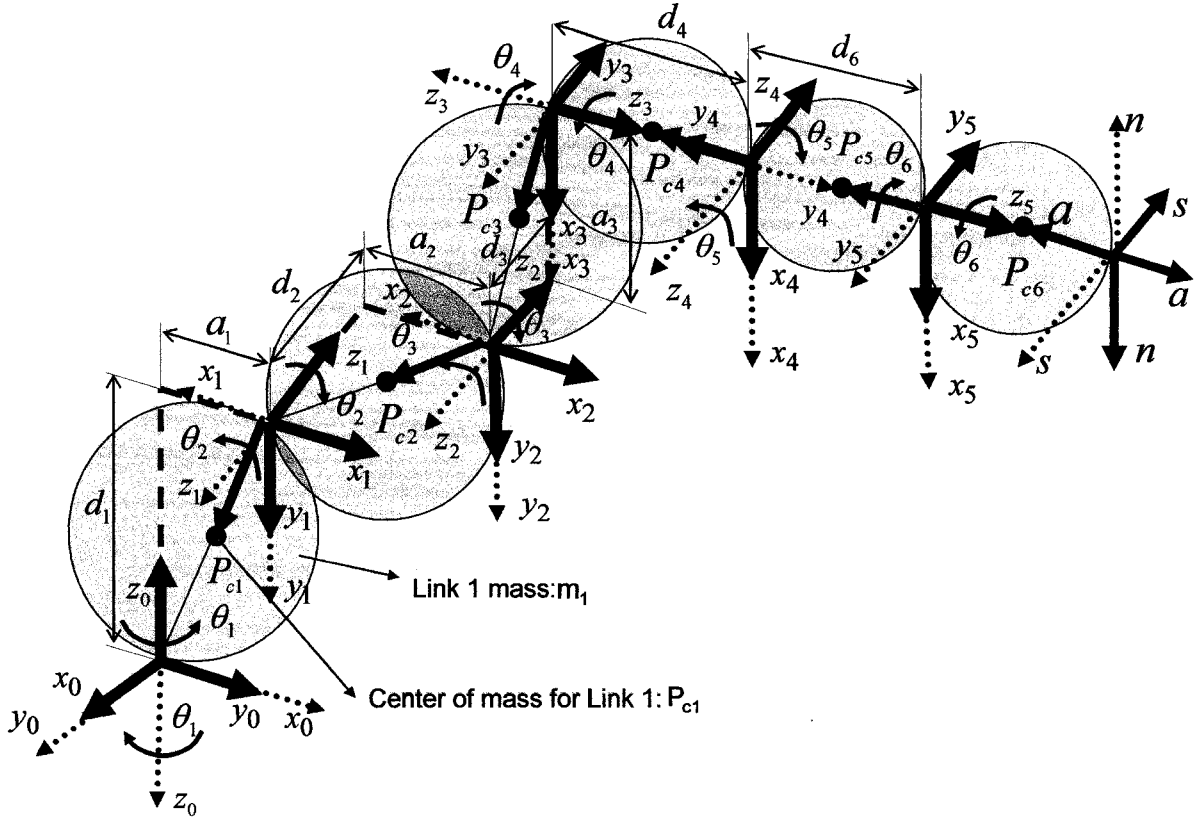
Figure 5.1: Generic PUMA -Fanuc Dynamic Model (RPFDM).

The radial distance to the center of mass for each link is: P_{c1}, P_{c2},..., P_{c6} respectively. These parameters are defined in Equation 96.

$$P_{c1} = \begin{bmatrix} K_1 \dfrac{a_1}{2} \\ \dfrac{d_1}{2} \\ 0 \end{bmatrix}, P_{c2} = \begin{bmatrix} K_2 \dfrac{a_2}{2} \\ 0 \\ K_2 \dfrac{d_2}{2} \end{bmatrix}, P_{c3} = \begin{bmatrix} \dfrac{a_3}{2} \\ K_3 \dfrac{d_3}{2} \\ 0 \end{bmatrix}, P_{c4} = \begin{bmatrix} 0 \\ K_4 \dfrac{d_4}{2} \\ 0 \end{bmatrix}, P_{c5} = \begin{bmatrix} 0 \\ 0 \\ 0 \end{bmatrix}, P_{c6} = \begin{bmatrix} 0 \\ 0 \\ K_6 \dfrac{d_6}{2} \end{bmatrix} \quad (96)$$

The D-H parameters (Denavit J., and Hartenberg R. S, 1955) for the RPFDM are the same as for the RPF model, and are presented in Table 2.4.

The RPFDM satisfies Pieper's condition (Pieper D. L, *et al.*, 1968), that the last three joints axes intersect at a point, which produces parameters d_5, a_4, a_5 equal to zero. This is shown in Figure 2.13. Both PUMA -type and Fanuc-type robots

83

have been investigated and it was found that Pieper's condition applies to both robot structures.

The moment of inertia about the center of mass (highlighted in Figure 5.1) for each link is related to the inertia of the center of the mass of the sphere, as shown in Equation 97.

$$I_i = \frac{2}{3}m_i r_i^2 \begin{bmatrix} 1 & 0 & 0 \\ 0 & 1 & 0 \\ 0 & 0 & 1 \end{bmatrix}, \ i = 1,2,\ldots,6 \tag{97}$$

The RPFDM is calculated from the presented information. The equations of motion for a 6-DOF manipulator are given by (98).

$$A(q)\ddot{q} + B(q)[\dot{q}\dot{q}] + C(q)[\dot{q}^2] + G(q) = \tau \tag{98}$$

Equation 98 represents the dynamics of the ideal rigid bodies (links) connected with the joints, where there is a generalized force/torque vector τ acting at the each joint. In the case where have 6R joints, the vector τ is a torque about each axis of rotation, produced by an actuator that is usually a DC motor (Spong M. W. and Vidyasagar M. 1989).

The matrix A is the 6×6 inertia matrix, B is the 6×15 Coriolis torque matrix, C is 6×6 the centrifugal torque matrix, and G is a 6×1 gravity torque vector. Vector q is the vector of generalized joint coordinates: $q = [q_1 \ q_2 \ \cdots \ q_6]^T$. Vectors $\dot{q}$, $\ddot{q}$ are the vectors of joint velocities and acceleration respectively.

Vector $[\dot{q}\dot{q}]$ is a 15×1 vector of velocity products and it is given as $[\dot{q}\dot{q}] = [\dot{q}_1\dot{q}_2 \ \dot{q}_1\dot{q}_3 \ \cdots \ \dot{q}_1\dot{q}_6 \ \dot{q}_2\dot{q}_3 \ \cdots \ \dot{q}_2\dot{q}_6 \ \dot{q}_3\dot{q}_4 \ \cdots \ \dot{q}_5\dot{q}_6]$.

Vector $[\dot{q}^2] = [\dot{q}_1^2 \ \dot{q}_2^2 \ \cdots \ \dot{q}_6^2]$ is vector of squared velocity.

84

The calculation of the complete electro-mechanical model (RPFDM+) was done in two steps. The first step consists of using the RNE (Recursive Newton-Euler) algorithm for calculating the dynamics of the mechanical part (RPFDM). In the second step, the dynamic parameters for all six actuators are included.

5.2. RNE Algorithm for the RPFDM

The RPFDM calculation is performed using the RNE Algorithm (Spong M. W. and Vidyasagar M. 1989), (Fu K.S., *et al.*, 1987), (Owens J. P., 1990), to calculate the velocity and accelerations for all the joints. This is called forward computation. The next step is the backward computation of joints' torques and forces, which are computed one link at a time starting from the end-effector link and ending at the base of the manipulator. The forward and backward flow computation is graphically presented in Figure 5.2.
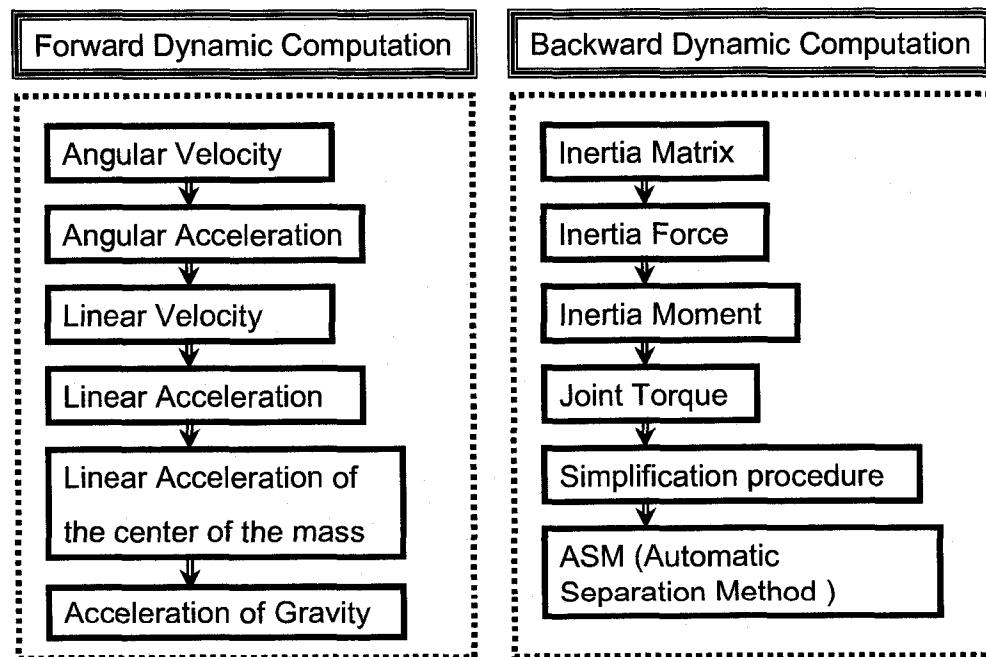
Forward Dynamic Computation	Backward Dynamic Computation
Angular Velocity	Inertia Matrix
Angular Acceleration	Inertia Force
Linear Velocity	Inertia Moment
Linear Acceleration	Joint Torque
Linear Acceleration of the center of the mass	Simplification procedure
Acceleration of Gravity	ASM (Automatic Separation Method)

Figure 5.2: Forward and Backward Dynamic Flowchart

85

5.2.1. Forward Computation of Velocity and Accelerations

The joint coordinate frames (Figure 2.13) are assigned using the D-H notation (Table 2.4) and are expressed with their homogeneous transformation matrices $^{i-1}T_i$ ($i = 1,2...6$), as shown in Equation 99.

$$
^0T_1 = \begin{bmatrix} \cos\theta_1 & 0 & K_1\sin\theta_1 & a_1\cos\theta_1 \\ \sin\theta_1 & 0 & -K_1\cos\theta_1 & a_1\sin\theta_1 \\ 0 & K_1 & 0 & d_1 \\ 0 & 0 & 0 & 1 \end{bmatrix}, \quad
^1T_2 = \begin{bmatrix} \cos\theta_2 & -K_2\sin\theta_2 & 0 & a_2\cos\theta_2 \\ \sin\theta_2 & K_2\cos\theta_2 & 0 & a_2\sin\theta_2 \\ 0 & 0 & K_2 & d_2 \\ 0 & 0 & 0 & 1 \end{bmatrix}
$$

$$
^2T_3 = \begin{bmatrix} \cos\theta_3 & 0 & K_3\sin\theta_3 & a_3\cos\theta_3 \\ \sin\theta_3 & 0 & -K_3\cos\theta_3 & a_3\sin\theta_3 \\ 0 & K_3 & 0 & d_3 \\ 0 & 0 & 0 & 1 \end{bmatrix}, \quad
^3T_4 = \begin{bmatrix} \cos\theta_4 & 0 & K_4\sin\theta_4 & a_4\cos\theta_4 \\ \sin\theta_4 & 0 & -K_4\cos\theta_4 & a_4\sin\theta_4 \\ 0 & K_4 & 0 & d_4 \\ 0 & 0 & 0 & 1 \end{bmatrix}
$$

$$
^4T_5 = \begin{bmatrix} \cos\theta_5 & 0 & K_5\sin\theta_5 & a_5\cos\theta_5 \\ \sin\theta_5 & 0 & -K_5\cos\theta_5 & a_5\sin\theta_5 \\ 0 & K_5 & 0 & d_5 \\ 0 & 0 & 0 & 1 \end{bmatrix}, \quad
^5T_6 = \begin{bmatrix} \cos\theta_6 & -K_6\sin\theta_6 & 0 & a_6\cos\theta_6 \\ \sin\theta_6 & K_6\cos\theta_6 & 0 & a_6\sin\theta_6 \\ 0 & 0 & K_2 & d_6 \\ 0 & 0 & 0 & 1 \end{bmatrix} \quad (99)
$$

The upper $3X3$ sub matrices of the each homogeneous transformation matrices represent the rotational matrices for each joint, and they are presented in Equation 100:

$$
^0R_1 = \begin{bmatrix} \cos\theta_1 & 0 & K_1\sin\theta_1 \\ \sin\theta_1 & 0 & -K_1\cos\theta_1 \\ 0 & K_1 & 0 \end{bmatrix}, \quad
^1R_2 = \begin{bmatrix} \cos\theta_2 & -K_2\sin\theta_2 & 0 \\ \sin\theta_2 & K_2\cos\theta_2 & 0 \\ 0 & 0 & K_2 \end{bmatrix},
$$

$$
^2R_3 = \begin{bmatrix} \cos\theta_3 & 0 & K_3\sin\theta_3 \\ \sin\theta_3 & 0 & -K_3\cos\theta_3 \\ 0 & K_3 & 0 \end{bmatrix}, \quad
^3R_4 = \begin{bmatrix} \cos\theta_4 & 0 & K_4\sin\theta_4 \\ \sin\theta_4 & 0 & -K_4\cos\theta_4 \\ 0 & K_4 & 0 \end{bmatrix},
$$

$$
^4R_5 = \begin{bmatrix} \cos\theta_5 & 0 & K_5\sin\theta_5 \\ \sin\theta_5 & 0 & -K_5\cos\theta_5 \\ 0 & K_5 & 0 \end{bmatrix}, \quad
^5R_6 = \begin{bmatrix} \cos\theta_6 & -K_6\sin\theta_6 & 0 \\ \sin\theta_6 & K_6\cos\theta_6 & 0 \\ 0 & 0 & K_2 \end{bmatrix} \quad (100)
$$

The next step is to find the transpose of all rotational matrices: $({}^{0}R_{1})^{T},({}^{1}R_{2})^{T},...,({}^{5}R_{6})^{T}$.

The upper right $3X1$ sub matrices for each homogeneous transformation matrices represent the position vectors for each joint and is stated in Equation 101:

$$
{}^{0}P_{1} = \begin{bmatrix} a_{1}\cos\theta_{1} \\ a_{1}\sin\theta_{1} \\ d_{1} \end{bmatrix}, \quad {}^{1}P_{2} = \begin{bmatrix} a_{2}\cos\theta_{2} \\ a_{2}\sin\theta_{2} \\ d_{2} \end{bmatrix}, \quad {}^{2}P_{3} = \begin{bmatrix} a_{3}\cos\theta_{3} \\ a_{3}\sin\theta_{3} \\ d_{3} \end{bmatrix},
$$

$$
{}^{3}P_{4} = \begin{bmatrix} a_{4}\cos\theta_{4} \\ a_{4}\sin\theta_{4} \\ d_{4} \end{bmatrix}, \quad {}^{4}P_{5} = \begin{bmatrix} a_{5}\cos\theta_{5} \\ a_{5}\sin\theta_{5} \\ d_{5} \end{bmatrix}, \quad {}^{5}P_{6} = \begin{bmatrix} a_{6}\cos\theta_{6} \\ a_{6}\sin\theta_{6} \\ d_{6} \end{bmatrix} \tag{101}
$$

The angular velocity vectors for all six joints are presented in Equation 102.

$$
{}^{0}\dot{\theta}_{1} = \begin{bmatrix} 0 \\ 0 \\ \dot{\theta}_{1} \end{bmatrix}, \quad {}^{1}\dot{\theta}_{2} = \begin{bmatrix} 0 \\ 0 \\ \dot{\theta}_{2} \end{bmatrix}, \quad {}^{2}\dot{\theta}_{3} = \begin{bmatrix} 0 \\ 0 \\ \dot{\theta}_{3} \end{bmatrix}, \quad {}^{3}\dot{\theta}_{4} = \begin{bmatrix} 0 \\ 0 \\ \dot{\theta}_{4} \end{bmatrix}, \quad {}^{4}\dot{\theta}_{5} = \begin{bmatrix} 0 \\ 0 \\ \dot{\theta}_{5} \end{bmatrix}, \quad {}^{5}\dot{\theta}_{6} = \begin{bmatrix} 0 \\ 0 \\ \dot{\theta}_{6} \end{bmatrix} \tag{102}
$$

Using the appropriate rotation matrices and angular velocity vectors, the angular and linear velocities for all six joints can be calculated from Equations 103 and 104 respectively:

$$
{}^{i}({}^{0}\omega_{i})={}^{i}R_{i-1}[{}^{i-1}({}^{0}\omega_{i-1})+{}^{i-1}\dot{\theta}_{i}], \quad i=1,2,...,6 \tag{103}
$$

$$
{}^{i}({}^{0}V_{i})={}^{i}R_{i-1}{}^{i-1}({}^{0}V_{i-1})+{}^{i}({}^{0}\omega_{i})\times{}^{i}R_{i-1}{}^{i-1}P_{i}, \quad i=1,2,...,6 \tag{104}
$$

The linear and angular acceleration for all six joints is calculated from Equations 105 and 106 respectively

$$
\begin{aligned} {}^{i}({}^{0}a_{i})={}^{i}R_{i-1}[{}^{i-1}({}^{0}a_{i-1})+{}^{i-1}({}^{0}\alpha_{i-1})\times{}^{i-1}P_{i}+{}^{i-1}({}^{0}\omega_{i-1})\times({}^{i-1}({}^{0}\omega_{i-1})\times{}^{i-1}P_{i}) \\ +2{}^{i-1}({}^{0}\omega_{i-1})\times({}^{i-1}\dot{\theta}_{i}\times{}^{i-1}P_{i})+{}^{i-1}\ddot{\theta}_{i}\times{}^{i-1}P_{i}+{}^{i-1}\dot{\theta}_{i}\times({}^{i-1}\dot{\theta}_{i}\times{}^{i-1}P_{i}) \end{aligned}, \quad i=1,2,...,6 \tag{105}
$$

87

$$^i(^0\alpha_i)=^iR_{i-1}[^{i-1}(^0\alpha_{i-1})+^{i-1}(^0\omega_{i-1})\times^{i-1}\omega_i+^{i-1}\alpha_i], \; i=1,2,\ldots,6 \tag{106}$$

The linear acceleration of the center of mass is calculated from Equation 107:

$$^i(^0a_{ci})=^i(^0a_i)+^i(^0\alpha_i)\times^i(^iP_{ci})+^i(^0\omega_i)\times[^i(^0\omega_i)\times^i(^iP_{ci})], \; i=1,2,\ldots,6 \tag{107}$$

5.2.2. Backward Computation of Forces and Moments

The general gravity vectors for the RPFM model are expressed:

$$^ig=^iR_0\,^0g, \; i=1,2,\ldots,6 \tag{108}$$

From the Figure 5.1, gravity vector for the first link is: $^0g=\begin{bmatrix} 0 \\ 0 \\ -g \end{bmatrix}$, where

$g=9.81m/s^2$.

Once the velocities and accelerations of the links are found, the joint forces and moments can be computed one link at a time starting from the end-effector link and ending at the base link. It is assumed that there is no load at the end-effector; therefore, $^6(^6f_{Tool})=0$, and $^6(^6n_{Tool})=0$.

$$^i(f_i^*)=-m_i\,^i(^0a_{ci}), \; i=1,2,\ldots,6 \tag{109}$$

$$^i(n_i^*)=-^iI_i\,^i(^0\alpha_{ci})-^i(^0\omega_{ci})\times[^iI_i\,^i(^0\omega_{ci})], \; i=1,2,\ldots,6 \tag{110}$$

Where ^iI_i is the inertia tensor. This is simply expressed in Equation 97.

The force and moment balance equations about the center of mass of link i in recursive form can be written as:

$$^i(f_i^*)+^i(^{i-1}f_i)-^i(^if_{i+1})+m_i\,^ig=0, \; i=1,2,\ldots,6 \tag{111}$$

88

$$^i(n_i^*)+{}^i({}^{i-1}n_i)-{}^i({}^in_{i+1})-[{}^i({}^{i-1}P_i)+{}^i({}^iP_{ci})]\times{}^i({}^{i-1}f_i)+{}^i({}^iP_{ci})\times{}^i({}^if_{i+1})=0\,,i=1,2,\ldots,6 \quad (112)$$

Once the reaction forces and moments are computed in the ith link frame, they are converted into the $(i-1)^{th}$ link frame by the following equations:

$$^i({}^{i-1}f_i)={}^{i-1}R_i\,{}^i({}^{i-1}f_i)\,,\ i=1,2,\ldots,6 \quad (113)$$

$$^i({}^{i-1}n_i)={}^{i-1}R_i\,{}^i({}^{i-1}n_i)\,,\ i=1,2,\ldots,6 \quad (114)$$

Actuator torques and forces τ_i are obtained by projecting the forces onto their corresponding joint axes:

$$\tau_i={}^i({}^{i-1}n_i)^{T\ i-1}z_{i-1}\,,\ i=1,2,\ldots,6 \quad (115)$$

The RNE procedure produced the final six expressions of the actuators torques and forces τ_i, $i=1,2,\ldots,6$. Each of these six equations contains sums of products of matrices elements A, B, C, G, and trigonometric terms. To be able to get a dynamic equation in a form of Equation 98, need to generate each matrix A, B, C, and G, which means need to calculate their elements: a_{11}, a_{12},..., a_{16}, ...,a_{66}, b_{112}, b_{113},...,b_{156}, ...,b_{656}, c_{11}, c_{12},..., c_{16},...,c_{66}, $g_1,g_2,\ldots,g_6$. To avoid complications when factoring out each element in each τ_i expression, the Automatic Separation Procedure (ASP) is used, which produces an automatic generation of the matrix elements. This method is explained in the next section.

5.3. Automatic Separation Method (ASM)

To avoid calculation complexity and reach the final goal of the dynamic equation in the form of Equation 98, the Automatic Separation Procedure (ASP) was used. This procedure has three steps.

89

The first step is to simplify and organize the angular and linear velocity equations. To overcome these problems it is necessary to implement the basic trigonometric rules expressed in Equations 116 – 118:

$$\sin\theta_i\cos\theta_j + K_i\cos\theta_i\sin\theta_j = \sin(\theta_i + K_i\theta_j)\,,\ i=1,2,...,6\,,\ j=1,2,...,6\,,\ K_i=\pm1 \quad (116)$$

$$\cos\theta_i\cos\theta_j - K_i\sin\theta_i\sin\theta_j = \cos(\theta_i + K_i\theta_j)\,,\ i=1,2,...,6\,,\ j=1,2,...,6\,,\ K_i=\pm1 \quad (117)$$

$$\sin^2\theta_i + \cos^2\theta_i = 1\,,\ i=1,2,...,6 \quad (118)$$

Two more simplifications can be applied, as shown in Equations 119 and 120.

$$K_i^{\,2} = 1\,,\ i=1,2,...,6 \quad (119)$$

$$K_i^{\,3} = K_i\,,\ i=1,2,...,6 \quad (120)$$

To be able to apply Equations 119 and 120 using MAPLE 10®, the command "algsubs", must be used. This command substitute sub-expressions into an expression. In Equation 121 the example of simplifying a_{11}, the first element of matrix A is given:

$$\text{algsubs}\,(K_6^{\,3} = K_6, a_{11}) \quad (121)$$

The second step consists of ordering parameters of each element of the equation, which will help to continue the calculation without much complexity. The form is given in Equation 122.

$$ELEMENT = K_i a_i d_i \sin\theta_i \cos\theta_i\,, i=1,2,...,6 \quad (122)$$

The third step is separation of elements, and it is important for further calculations. This method is first applied to the angular acceleration $^i(^0\alpha_i)_i$ and linear acceleration of the center of mass $^i(^0a_{ci})$, such that its these expressions

90

are written as a sum of separated elements, as a function of the parameters of the vectors $[\ddot{q}]$, $[\dot{q}\dot{q}]$, $[\dot{q}^2]$.

$$^i(^0\alpha_i)_{i(\alpha_i)} = \begin{bmatrix} ^i(^0\alpha_i)_{i(\alpha_i)1} \\ ^i(^0\alpha_i)_{i(\alpha_i)2} \\ ^i(^0\alpha_i)_{i(\alpha_i)3} \end{bmatrix}, \ i = 1,2,\ldots,6 \tag{123}$$

$$^i(^0\alpha_i)_{i(\omega_i^2)} = \begin{bmatrix} ^i(^0\alpha_i)_{i(\omega_i^2)1} \\ ^i(^0\alpha_i)_{i(\omega_i^2)2} \\ ^i(^0\alpha_i)_{i(\omega_i^2)3} \end{bmatrix}, \ i = 1,2,\ldots,6 \tag{124}$$

$$^i(^0\alpha_i)_{i(\omega_{ij})} = \begin{bmatrix} ^i(^0\alpha_i)_{i(\omega_{ij})1} \\ ^i(^0\alpha_i)_{i(\omega_{ij})2} \\ ^i(^0\alpha_i)_{i(\omega_{ij})3} \end{bmatrix}, \ i = 1,2,\ldots,6, \ j = 1,2,\ldots,6 \tag{125}$$

$$^i(^0a_{ci}) = \begin{bmatrix} ^i(^0a_{ci})_{i(\alpha_i)1} \\ ^i(^0a_{ci})_{i(\alpha_i)2} \\ ^i(^0a_{ci})_{i(\alpha_i)3} \end{bmatrix}, \ i = 1,2,\ldots,6 \tag{126}$$

$$^i(^0a_{ci}) = \begin{bmatrix} ^i(^0a_{ci})_{i(\omega_i^2)1} \\ ^i(^0a_{ci})_{i(\omega_i^2)2} \\ ^i(^0a_{ci})_{i(\omega_i^2)3} \end{bmatrix}, \ i = 1,2,\ldots,6 \tag{127}$$

$$^i(^0a_{ci}) = \begin{bmatrix} ^i(^0a_{ci})_{i(\omega_{ij})1} \\ ^i(^0a_{ci})_{i(\omega_{ij})2} \\ ^i(^0a_{ci})_{i(\omega_{ij})3} \end{bmatrix}, \ i = 1,2,\ldots,6, \ j = 1,2,\ldots,6 \tag{128}$$

The calculation of the inverse dynamics can be done such that all elements of the matrices from Equation 98 can be automatically generated. Using the Equations 109 -115 and 123 -128, the automatic generation of all matrix elements can be produced, as shown below

91

$$a_{ij} = {}^{i}({}^{i-1}n_{i(\alpha_i)})^{T}\,{}^{i-1}z_{i-1}, \quad i = 1,2,\ldots,6, \quad j = 1,2,\ldots,6 \qquad (129)$$

$$b_{i,ij} = {}^{i}({}^{i-1}n_{i(\omega_{ij})})^{T}\,{}^{i-1}z_{i-1}, \quad i = 1,2,\ldots,6, \quad j = 1,2,\ldots,6 \qquad (130)$$

$$c_{ij} = {}^{i}({}^{i-1}n_{i(\omega_i^2)})^{T}\,{}^{i-1}z_{i-1}, \quad i = 1,2,\ldots,6, \quad j = 1,2,\ldots,6 \qquad (131)$$

$$g_i = {}^{i}({}^{i-1}n_{i(GR_i)})^{T}\,{}^{i-1}z_{i-1}, \quad i = 1,2,\ldots,6, \quad j = 1,2,\ldots,6 \qquad (132)$$

From the Equations 129 -132, all four matrices A, B, C, and G can be assembled. By selecting any robot that belongs to the RPF group of robots, and entering all essential information, the dynamic model can be automatically generated. This provides a fundamental basis for subsequent control strategies.

5.4. Coupling Motor Dynamics with Link Dynamics

The dynamic model in Equation 98 presents only the mechanical part of the complete robot dynamic model. The other part that should be considered is the dynamics of the joint actuators. These two dynamic systems need to be coupled to present more realistic behavior of different robotic systems. The importance of coupling the robot manipulator dynamics and robot joint actuators is presented by Tarn T. J., et al., 1991.

When considering DC motors in series with a gear train with gear ratio $\dfrac{1}{N}$ and connected to a manipulator link, as shown in Figure 5.3, the Equation of motion is expressed as in Equation 134.

Knowing this, generic dynamic models that contain the dynamic elements for both systems can be developed, (Vukobratovic M., et al., 1986), (Spong M. W. and Vidyasagar M. 1989).
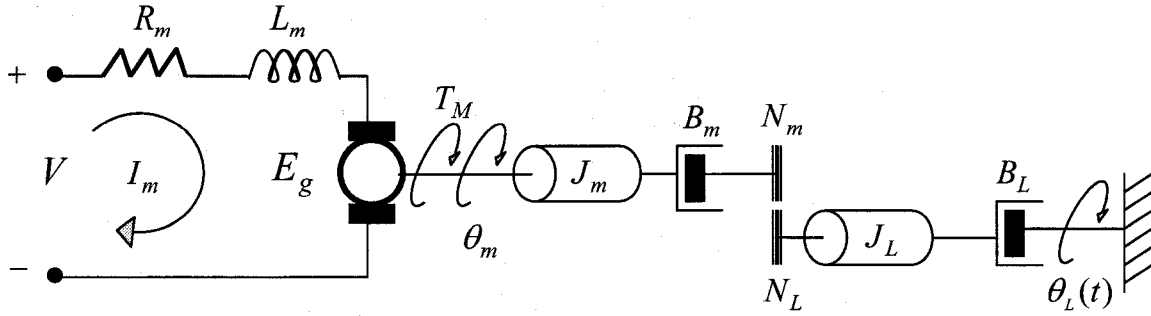
Figure 5.3: Lumped model of link with DC Motor and gear

It is essential that an analytical mathematical model for the DC motor that contains the mechanical and electrical parameters (Figure 5.3), be established.

The DC motor electrical and mechanical equations are expressed in Equations 133 and 134.

$$V = L_m \frac{di_m}{dt} + R_m i_m + E_g \,, \quad E_g = K_b \omega \tag{133}$$

$$T_M = J_m \frac{d\omega}{dt} + B_m \omega + N\tau \,, \quad T_M = K_t i_m \tag{134}$$

Armature inductance can be neglected for the model simplification, (Vukobratovic M., *et al.*, 1986), (Spong M. W. and Vidyasagar M. 1989), therefore:

$$L_m \approx 0 \tag{135}$$

Equation 136 is derived from equations 133-135:

$$V \frac{K_t}{R_m} = J_m \ddot{\theta}_m + (B_m + \frac{K_t}{R_m} K_b) \dot{\theta}_m + N\tau \tag{136}$$

An important relationship is expressed in Equation 137:

$$\theta_m = \frac{1}{N} q \,, \quad N = \frac{N_m}{N_L} \tag{137}$$

93

Dividing Equation 136 by N, and combining Equation 137, gives:

$$\frac{K_t}{NR_m}V = \frac{J_m}{N^2}\ddot{q} + (\frac{B_m}{N^2} + \frac{K_tK_b}{N^2R_m})\dot{q} + \tau \tag{138}$$

For the 6-DOF RPF model, Equation 138 must be expressed in a vector form. This is presented in Equations 139 – 142:

$$V = \begin{bmatrix} V_1 & V_2 & V_3 & V_4 & V_5 & V_6 \end{bmatrix}^T \tag{139}$$

$$\hat{A} = diag(\frac{J_{mi}}{N_i^2}), \quad i = 1,2,\ldots,6 \tag{140}$$

$$\hat{B} = diag(\frac{B_{mi}}{N_i^2} + \frac{K_{ti}K_{bi}}{N_i^2R_{mi}}), \quad i = 1,2,\ldots,6 \tag{141}$$

$$\hat{C} = diag(\frac{K_{ti}}{N_i^2R_{mi}}), i = 1,2,\ldots,6 \tag{142}$$

From Equations 139 – 142 generate Equation 143:

$$\hat{C}V = \hat{A}\ddot{q} + \hat{B}\dot{q} + \tau \tag{143}$$

From Equations 98 and 143, the complete general electro-mechanical dynamic equation of the RPF robot model can be developed. The resultant Equation is shown below.

$$\hat{C}V = \hat{A}\ddot{q} + \hat{B}\dot{q} + A(q)\ddot{q} + B(q)[\dot{q}\dot{q}] + C(q)[\dot{q}^2] + G(q) \tag{144}$$

This model is named RPFDM+.

94

5.5. Example of Some Matrix Elements for the RPFDM and PUMA 560

Using the available information, the dynamic model for the PUMA 560 is presented here. (Armstrong B., *et al.* 1986) presented kinematic, dynamic and electrical parameters for the PUMA 560. The DH parameters are in Table 5.5, and masses in Table 5.6.

Figure 5.4: PUMA 560 DH parameters

Joint	θ_i (deg)	d_i (mm)	a_i (mm)	α_i (deg)
1	θ_1	0	0	-90
2	θ_2	149.09	431.8	0
3	θ_3	0	-20.32	90
4	θ_4	433.07	0	-90
5	θ_5	0	0	90
6	θ_6	56.25	0	0

Figure 5.5: PUMA 560 DH link mass value

Joint	m_i (kg)
1	4.33
2	10.20
3	4.80
4	1.18
5	0.32
6	0.13

The calculated dynamic equation for the RPF model is very complex and the results are difficult to show. Because of this only specific elements from the output are presented. These elements are a_{16}, $b_{6.56}$, c_{64}, Gg_3 from the matrices A, B, C, and G, respectively. This is presented in Equations 145 – 148:

95

$$a_{16} = \frac{1}{6} K_1 K_5 m_6 d_6^2 \alpha_6 \left(\sin(\theta_2) \cos(\theta_3) \cos(\theta_4) \sin(\theta_5) \right.$$
$$- \sin(\theta_2) K_3 \sin(\theta_3) K_4 \cos(\theta_5)$$
$$+ K_2 \cos(\theta_2) \sin(\theta_3) \cos(\theta_4) \sin(\theta_5)$$
$$\left. + K_2 \cos(\theta_2) K_3 \cos(\theta_3) K_4 \cos(\theta_5) \right)$$

(145)

$$b_{6,56} = \frac{1}{4} d_6^2 m_6 \omega_5 \omega_6 K_6 K_5 \left(2 K_5 \sin(\theta_6) K_2 K_3 \sin(\theta_1) \right.$$
$$\sin(\theta_2 + K_2 \theta_3) K_4 \cos(\theta_5)$$
$$- 2 K_5 \sin(\theta_6) \sin(\theta_5) \sin(\theta_1) \cos(\theta_2 + K_2 \theta_3) \cos(\theta_4)$$
$$+ 2 K_5 \sin(\theta_6) \sin(\theta_5) K_1 \cos(\theta_1) K_2 K_3 \sin(\theta_4)$$
$$- K_4 \cos(\theta_5) \cos(\theta_6) \sin(\theta_5) \cos(\theta_1) \cos(\theta_2 + K_2 \theta_3)$$
$$\cos(\theta_4) K_6 - K_4 \cos(\theta_5) \cos(\theta_6) \sin(\theta_5) K_1 \sin(\theta_1) K_2$$
$$K_3 \sin(\theta_4) K_6 +$$
$$\cos(\theta_5)^2 \cos(\theta_6) K_2 K_3 \cos(\theta_1) \sin(\theta_2 + K_2 \theta_3) K_6 - 4$$
$$\left. + 4 \cos(\theta_6)^2 \right)$$

(146)

$$Gg_3 = \frac{1}{2} m_3 g K_3 K_1 \left(2 K_2 K_3 \cos(\theta_2 + K_2 \theta_3) a_3 \right.$$
$$+ K_2 K_3 \cos(\theta_2 + K_2 \theta_3)^2 \cos(\theta_1) a_3$$
$$+ K_3 \cos(\theta_2 + K_2 \theta_3) K_1 \sin(\theta_1) d_3$$
$$+ K_1 a_3 - K_1 a_3 \cos(\theta_2 + K_2 \theta_3)^2$$
$$\left. + 2 \sin(\theta_2 + K_2 \theta_3) d_3 \cos(\theta_3) \right)$$

(147)

96

$$c_{64} = -\frac{1}{4} \cos\left(\theta_5\right) m_6 \, \omega_4^2 \, d_6^2 \, K_6 \, K_5 \left(3 \, K_5 \cos\left(\theta_5\right) \sin\left(\theta_5\right) \sin\left(\theta_6\right)\right.$$
$$K_2 \, K_3 \cos\left(\theta_1\right) \sin\left(\theta_2 + K_2 \, \theta_3\right) K_4 \, K_6$$
$$+ 3 \, K_5 \sin\left(\theta_6\right) \cos\left(\theta_1\right) \cos\left(\theta_2 + K_2 \, \theta_3\right) \cos\left(\theta_4\right)$$
$$\cos\left(\theta_5\right)^2 K_6 - 3 \, K_5 \sin\left(\theta_6\right) \cos\left(\theta_1\right) \cos\left(\theta_2 + K_2 \, \theta_3\right)$$
$$\cos\left(\theta_4\right) K_6 + 3 \, K_5 \sin\left(\theta_6\right) K_1 \sin\left(\theta_1\right) K_2 \, K_3 \sin\left(\theta_4\right)$$
$$\cos\left(\theta_5\right)^2 K_6 - 3 \, K_5 \sin\left(\theta_6\right) K_1 \sin\left(\theta_1\right) K_2 \, K_3 \sin\left(\theta_4\right) K_6$$
$$+ 2 \, K_5 \sin\left(\theta_1\right) \cos\left(\theta_2 + K_2 \, \theta_3\right) \cos\left(\theta_4\right) \cos\left(\theta_6\right)$$
$$\cos\left(\theta_5\right)^2 + 2 \, K_2 \, K_3 \sin\left(\theta_1\right) \sin\left(\theta_2 + K_2 \, \theta_3\right) K_4 \, K_5 \tag{148}$$
$$\cos\left(\theta_5\right) \sin\left(\theta_5\right) \cos\left(\theta_6\right)$$
$$+ 2 \, K_5 \, K_1 \cos\left(\theta_1\right) K_2 \, K_3 \sin\left(\theta_4\right) \cos\left(\theta_6\right)$$
$$- 2 \, K_5 \sin\left(\theta_1\right) \cos\left(\theta_2 + K_2 \, \theta_3\right) \cos\left(\theta_4\right) \cos\left(\theta_6\right)$$
$$+ K_5 \sin\left(\theta_5\right) K_1 \cos\left(\theta_1\right) K_2 \, K_3 \sin\left(\theta_4\right) \cos\left(\theta_5\right) \sin\left(\theta_6\right)$$
$$- K_5 \sin\left(\theta_5\right) \sin\left(\theta_1\right) \cos\left(\theta_2 + K_2 \, \theta_3\right) \cos\left(\theta_4\right) \cos\left(\theta_5\right)$$
$$\sin\left(\theta_6\right) + K_2 \, K_3 \sin\left(\theta_1\right) \sin\left(\theta_2 + K_2 \, \theta_3\right) K_4 \, K_5 \cos\left(\theta_5\right)^2$$
$$\sin\left(\theta_6\right) - 2 \, K_5 \, K_1 \cos\left(\theta_1\right) K_2 \, K_3 \sin\left(\theta_4\right) \cos\left(\theta_6\right) \cos\left(\theta_5\right)^2$$
$$- 2 \cos\left(\theta_5\right) + 2 \cos\left(\theta_5\right) \cos\left(\theta_6\right)^2$$
$$- 4 \sin\left(\theta_6\right) \sin\left(\theta_5\right) \cos\left(\theta_6\right)\Big)$$

The same matrices elements for PUMA 560, according to the information from (Armstrong B., et al. 1986) are presented in Equations 149 – 152:

$$a_{16} = -0.00004000000000 \, \alpha_6 \left(\sin\left(\theta_2\right) \cos\left(\theta_3\right) \cos\left(\theta_4\right) \sin\left(\theta_5\right)\right.$$
$$+ \sin\left(\theta_2\right) \sin\left(\theta_3\right) \cos\left(\theta_5\right) \tag{149}$$
$$+ \cos\left(\theta_2\right) \sin\left(\theta_3\right) \cos\left(\theta_4\right) \sin\left(\theta_5\right)$$
$$- 1.\cos\left(\theta_2\right) \cos\left(\theta_3\right) \cos\left(\theta_5\right)\Big)$$

97

$$
\begin{aligned}
b_{6,56} = -\ & 10^{-13}\,\omega_5\,\omega_6\,\Big(-1.028320312\ 10^9\ \cos(\theta_5)\ \cos(\theta_6)\ \sin(\theta_5) \\
& \cos(\theta_1)\ \cos(\theta_2+\theta_3)\ \cos(\theta_4) \\
& +1.028320312\ 10^9\ \cos(\theta_5)\ \cos(\theta_6)\ \sin(\theta_5)\ \sin(\theta_1) \\
& \sin(\theta_4)-1.028320312\ 10^9\ \cos(\theta_5)^2\ \cos(\theta_6)\ \cos(\theta_1) \\
& \sin(\theta_2+\theta_3)+2.056640625\ 10^9\ \sin(\theta_6)\ \sin(\theta_5)\ \sin(\theta_1) \\
& \cos(\theta_2+\theta_3)\ \cos(\theta_4) \\
& +2.056640625\ 10^9\ \sin(\theta_6)\ \sin(\theta_5)\ \cos(\theta_1)\ \sin(\theta_4) \\
& +2.056640625\ 10^9\ \sin(\theta_6)\ \sin(\theta_1)\ \sin(\theta_2+\theta_3)\ \cos(\theta_5) \\
& +4.113281250\ 10^9-4.113281250\ 10^9\ \cos(\theta_6)^2\Big)
\end{aligned}
$$

(150)

$$
\begin{aligned}
c_{64} = \ & 10^{-13}\,\cos(\theta_5)\,\Big(3.084960938\ 10^9\ \cos(\theta_1)\ \cos(\theta_2+\theta_3) \\
& \cos(\theta_4)\ \sin(\theta_6) \\
& -3.084960938\ 10^9\ \cos(\theta_1)\ \cos(\theta_2+\theta_3)\ \cos(\theta_4)\ \sin(\theta_6) \\
& \cos(\theta_5)^2-3.084960938\ 10^9\ \sin(\theta_1)\ \sin(\theta_4)\ \sin(\theta_6) \\
& +3.084960938\ 10^9\ \sin(\theta_1)\ \sin(\theta_4)\ \sin(\theta_6)\ \cos(\theta_5)^2 \\
& +3.084960938\ 10^9\ \cos(\theta_1)\ \sin(\theta_2+\theta_3)\ \cos(\theta_5)\ \sin(\theta_5) \\
& \sin(\theta_6)+4.113281250\ 10^9\ \sin(\theta_6)\ \sin(\theta_5)\ \cos(\theta_6) \\
& +2.056640625\ 10^9\ \cos(\theta_5) \\
& -2.056640625\ 10^9\ \cos(\theta_5)\ \cos(\theta_6)^2 \\
& +2.056640625\ 10^9\ \sin(\theta_1)\ \cos(\theta_2+\theta_3)\ \cos(\theta_4) \\
& \cos(\theta_6)-2.056640625\ 10^9\ \sin(\theta_1)\ \cos(\theta_2+\theta_3)\ \cos(\theta_4) \\
& \cos(\theta_6)\ \cos(\theta_5)^2 \\
& +1.028320312\ 10^9\ \sin(\theta_5)\ \sin(\theta_1)\ \cos(\theta_2+\theta_3)\ \cos(\theta_4) \\
& \cos(\theta_5)\ \sin(\theta_6) \\
& +2.056640625\ 10^9\ \cos(\theta_1)\ \sin(\theta_4)\ \cos(\theta_6) \\
& -2.056640625\ 10^9\ \cos(\theta_1)\ \sin(\theta_4)\ \cos(\theta_6)\ \cos(\theta_5)^2 \\
& +1.028320312\ 10^9\ \sin(\theta_5)\ \cos(\theta_1)\ \sin(\theta_4)\ \cos(\theta_5) \\
& \sin(\theta_6)+2.056640625\ 10^9\ \sin(\theta_1)\ \sin(\theta_2+\theta_3)\ \cos(\theta_5) \\
& \sin(\theta_5)\ \cos(\theta_6) \\
& +1.028320312\ 10^9\ \sin(\theta_1)\ \sin(\theta_2+\theta_3)\ \cos(\theta_5)^2\ \sin(\theta_6) \\
& \Big)\,\omega_4^2
\end{aligned}
$$

(151)

98

$$Gg_3 = 0.04876800000\, g\left(-1. + \cos\left(\theta_2 + \theta_3\right)^2 + 2.\,\cos\left(\theta_2 + \theta_3\right)\right.$$
$$\left. + \cos\left(\theta_1\right)\cos\left(\theta_2 + \theta_3\right)^2\right) \tag{152}$$

The RPFDM provides a complete dynamic model for any robot from the RPF group. The simplifications applied are only mathematical rules. Applying the simplification rules from (Armstrong B., et al. 1986), the specific matrix elements for PUMA 560 are presented in Equations 153 – 156:

$$a_{16} = 0 \tag{153}$$

$$b_{6,56} = 0 \tag{154}$$

$$c_{64} = 0 \tag{155}$$

$$Gg_3 := \left(-0.048768 \cdot \sin\left(\theta_2 + \theta_3\right)^2\right.$$
$$+ 0.048768 \cdot \cos\left(\theta_1\right)\cos\left(\theta_2 + \theta_3\right)^2$$
$$\left. + 0.097536 \cdot \cos\left(\theta_2 + \theta_3\right)\right) \cdot g: \tag{156}$$

The difference between these two results is only in the number of applied simplifications. From the RPFDM can analyze all the elements and work on their simplifications. For the dynamics of the RPF model can see that the most complex result is for c_{11}.

CHAPTER SIX

6. RECONFIGURABLE CONTROL PLATFORM FOR PUMA 560 ROBOT

For the complete general electro-mechanical dynamic model RPFDM+, and using the available information for the PUMA 560, the design of a controller is presented in this chapter. The additional simplifications of matrices A, B, C, and G, were done according to the work of (Armstrong B., *et al.* 1986). See Appendix G for details. The reason for the additional simplifications is to decrease time for developing the MATLAB/SIMULINK model. The same simplification procedure can be used for other robotic systems.

The control design for the electro-mechanical dynamic model was done in two steps. In the first step the PI (proportional integral) controller was designed for each DC motor. In the second step, these controllers were tuned, and used for the complete electro-mechanical dynamics model for each robot link.

6.1. DC Motor Sizing Procedure

The PUMA 560 is a 6-DOF robotic manipulator that uses six DC servo motors for joint control. Joint positions are measured using encoders and potentiometers. For the first three joints (waist, shoulder and elbow), large motors are used. The last three joints (wrist) are controlled by three small motors.

Using the MATLAB/SIMULINK platform, the complete electro-mechanical dynamic model of PUMA 560 was developed. The control design for each motor position is presented and the results are discussed.

100

For the control design of DC motors the electrical and mechanical equations will be treated separately. Equations 133 and 134 for one DOF can be written as following:

$$V = L_m \frac{di_m}{dt} + R_m i_m + K_b \dot{\theta}_m \qquad (157)$$

$$K_m i_m = J_m \ddot{\theta}_m + B_m \dot{\theta}_m + N\tau \qquad (158)$$

The Laplace transform notation for Equations 157 and 158 is presented in Equations 159 and 160:

$$V(s) = (L_m s + R_m) I_m(s) + K_b s \theta_m(s) \qquad (159)$$

$$K_m I_m(s) = (J_m s^2 + B_m s)\theta_m(s) + T_m(s) \qquad (160)$$

The block diagram for the DC motor is shown schematically in Figure 6.1. The transfer function of the DC motor from input voltage to output was developed and presented in Equation 161.
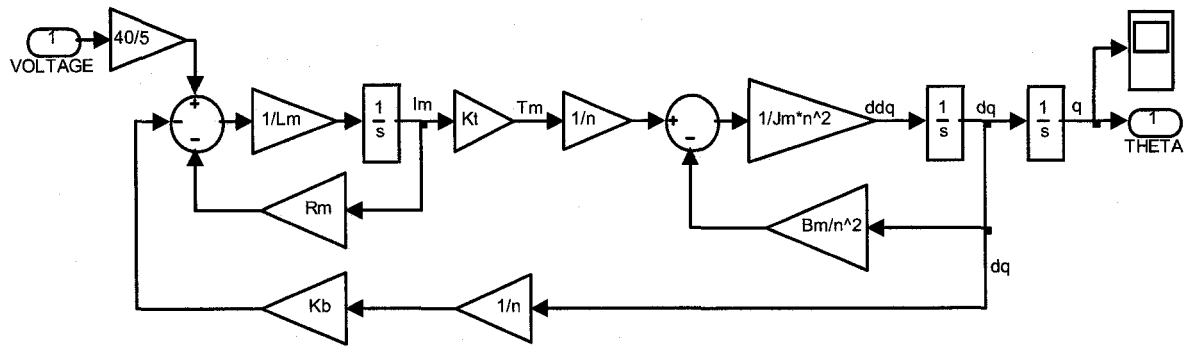
Figure 6.1: DC motor block diagram

$$\frac{\theta_m(s)}{V(s)} = \frac{K_t}{(J_m s^2 + B_m s)(L_m s + R_m) + K_t K_b s} \qquad (161)$$

The eigenvalues are calculated from the characteristic equation, which is the denominator of the transfer function, and presented in the following equations:

101

$$s_{1/2} = \frac{-(B_m L_m + J_m R_m) \pm \sqrt{(B_m L_m + J_m R_m)^2 - 4J_m L_m (B_m R_m + K_t K_b)}}{2 J_m L_m} \qquad (162)$$

$$s_3 = 0 \qquad (163)$$

From the literature (Electro-Craft Corp, 1973), by applying constant voltage V to the motor terminal, the motor shaft will accelerate according to Equation 157 and 158, and achieve a final steady state velocity. Under steady state conditions, the current is constant, and the motor equations become:

$$V = R_m i_m + K_b \dot{\theta}_m \qquad (164)$$

$$T_M = K_t i_a \qquad (165)$$

Combining Equations 164 and 165, the relation between the velocity and generated torque at steady state is given in Equation 166.

$$V = R_m \frac{T_M}{K_t} + K_b \dot{\theta}_m \qquad (166)$$

From the Equation 166, the maximum speed can be calculated if there is no load, (torque is equal to zero).

$$\dot{\theta}_{m(max)} = \frac{V}{K_b} \qquad (167)$$

Maximum RPM is calculated in Equation 168:

$$RPM_{max} = \dot{\theta}_{m(max)} \frac{60}{2\pi} \qquad (168)$$

The generated torque at stall is given from Table 6.1. The relation between the speed and the torque is expressed in Equation 169.

102

$$RPM = RPM_{max} - Slope_{RPM}T_M \qquad (169)$$

Slope is calculated from the relation in Equation 170:

$$Slope_{RPM} = \frac{RPM_{max}}{T_{Stall}} \qquad (170)$$

Figure 6.2 shows the speed-torque curve for DC motor 1.
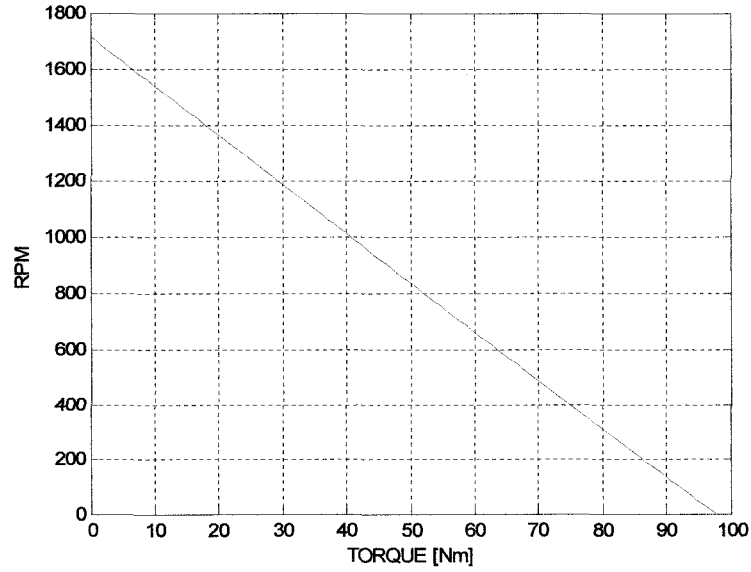
Figure 6.2: DC motor 1 speed-torque curve
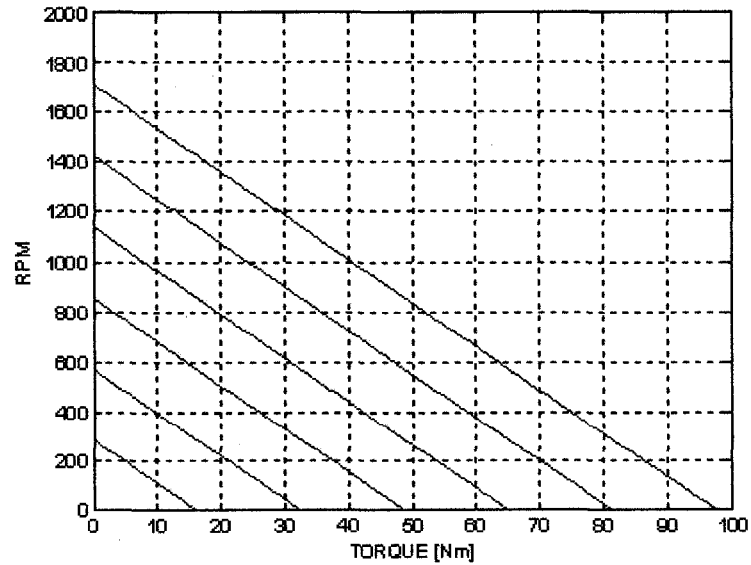
Figure 6.3: Torque lines for different voltages (DC motor 1)

103

Torque lines for different voltages are presented in Figure 6.3.

The current line, presented in Figure 6.4, can be constructed from the known maximum current in Table 6.1.
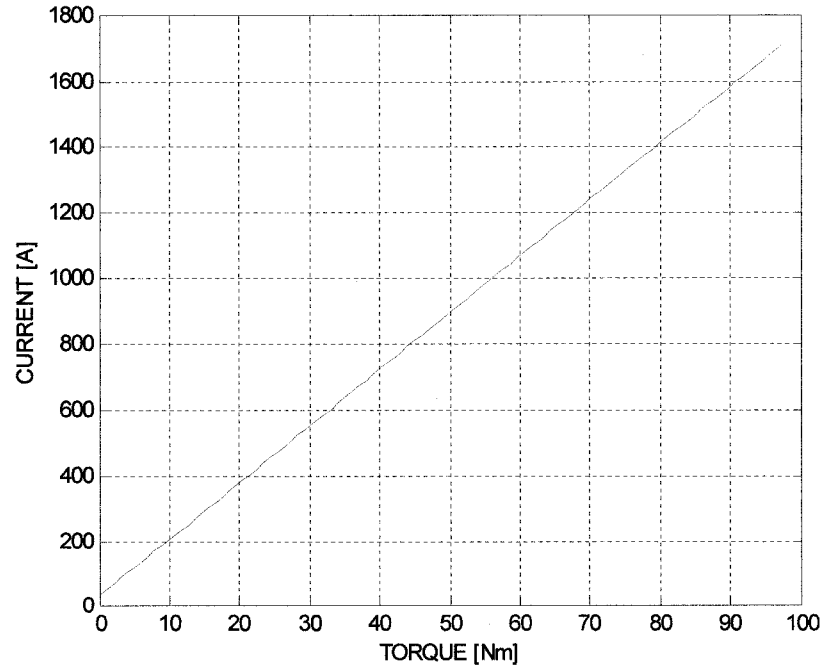
Figure 6.4: Current Line (DC motor 1)

The input power to the motor is given in Equation 171. The maximum voltage is $V_{max} = 40V$. The current line in Figure 6.4 is scaled by the value of $\dfrac{RPM_{max}}{I_{max}}$, where I_{max} is maximum current given in Table 6.1. This is applied later on all motor steady state characteristic diagrams.

$$P_{IN} = V_{max} I_m \tag{171}$$

The output power is the power that is delivered to the load.

$$P_{OUT} = RPM \frac{2\pi}{60} T_m \tag{172}$$

The power curve is shown on Figure 6.5.

104
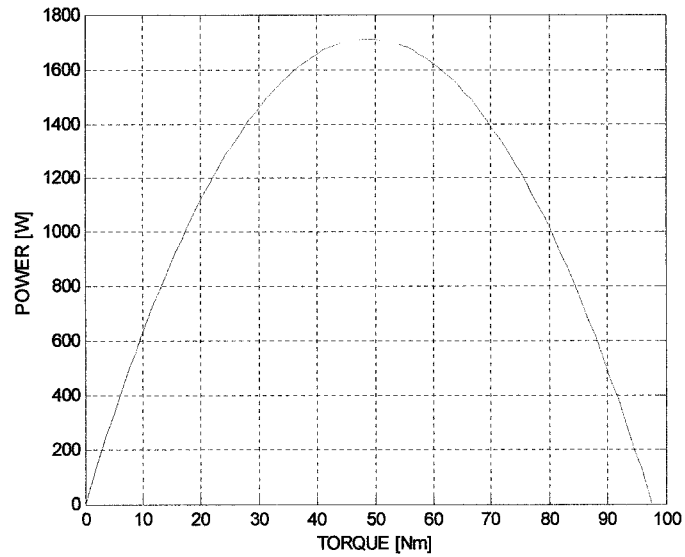
Figure 6.5: Power curve (DC motor 1)
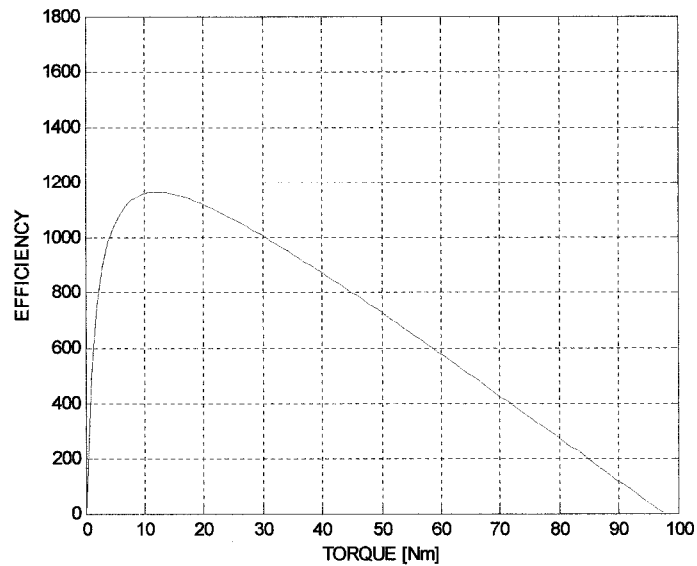
Figure 6.6: Efficiency curve (DC motor 1)

The efficiency can be calculated as a relation between input and output power, Equation 173. The efficiency curve in Figure 6.6 is scaled by the value of RPM_{max}. The efficiency of the DC motor 1 is $e = 0.6786$ and the scaled value is $e = 1162.3$. This is applied later on all motor steady state characteristic diagrams.

$$e = \frac{P_{OUT}}{P_{IN}}$$
(173)

105

From the available literature, (Corke P. I., and Armstrong B., 1994), (Corke P. I., 1994), (Corke P. I., and Armstrong B., 1995), (Armstrong B., *et al.*, 1986), (Leathy M. B., *et al.*, 1986) and some estimation, the PUMA 560 parameters are presented in the Table 6.1. Using the previously explained procedure for calculating the voltage, current, power and efficiency, and information from Table 6.1, all the PUMA 560 motor sizing data are presented graphically in Figures 6.7-6.12.

Table 6.1: PUMA 560 DC motors information

Links	1	2	3	4	5	6
Gear Ratio	$G_1 = 62.61$	$G_2 = 107.36$	$G_3 = 53.69$	$G_4 = 76.01$	$G_5 = 71.91$	$G_6 = 76.93$
Motor Inertia $[Nm^2]$	$J_{m1} = 1.140$	$J_{m2} = 4.710$	$J_{m3} = 0.830$	$J_{m4} = 0.200$	$J_{m5} = 0.179$	$J_{m6} = 0.193$
Armature Resistant $[\Omega]$	$R_{m1} 2.1$	$R_{m2} = 2.1$	$R_{m3} = 2.1$	$R_{m4} = 6.7$	$R_{m5} = 6.7$	$R_{m6} = 6.7$
Maximum current $[A]$	$I_{\max 1} = 8.25$	$I_{\max 2} = 8.25$	$I_{\max 3} = 8.25$	$I_{\max 4} = 4.23$	$I_{\max 5} = 8.25$	$I_{\max 6} = 8.25$
Motor Torque Constant $[Nm/A]$	$K_{t1} = 0.223$	$K_{t2} = 0.226$	$K_{t3} = 0.240$	$K_{t4} = 0.069$	$K_{t5} = 0.072$	$K_{t6} = 0.066$
Motor damping coefficient $[Nms/rad]$	$B_{m1} =$ 0.00148	$B_{m2} =$ 0.000817	$B_{m3} =$ 0.00138	$B_{m4} =$ 0.000712	$B_{m5} =$ 0.00826	$B_{m6} =$ 0.00367
Back EMF constant $[Nm/A]$	$K_{b1} = K_{t1}$	$K_{b2} = K_{t2}$	$K_{b3} = K_{t3}$	$K_{b4} = K_{t4}$	$K_{b5} = K_{t5}$	$K_{b6} = K_{t6}$
Motor Inductance $[\Omega/s]$	$L_{m1} =$ 0.0048	$L_{m2} =$ 0.0048	$L_{m3} =$ 0.0048	$L_{m4} =$ 0.0039	$L_{m5} =$ 0.0039	$L_{m6} =$ 0.0039
RPM	$rpm_1 =$ 1798.5	$rpm_2 =$ 1690.1	$rpm_3 =$ 1591.5	$rpm_4 =$ 5787.5	$rpm_5 =$ 5305.2	$rpm_6 =$ 1798.5
Stall Torque $[Nm]$	$T_{STALL1} = 97.6$	$T_{STALL2} = 186.4$	$T_{STALL3} = 89.4$	$T_{STALL4} = 24.2$	$T_{STALL5} = 20.1$	$T_{STALL6} = 21.3$
Brake Away Torque $[Nm]$	$T_{BA1} = 6.3$	$T_{BA2} = 5.5$	$T_{BA3} = 2.6$	$T_{BA4} = 1.3$	$T_{BA5} = 1.0$	$T_{BA6} = 1.2$

MOTOR1 STEADY STATE CHARACTERISTICS
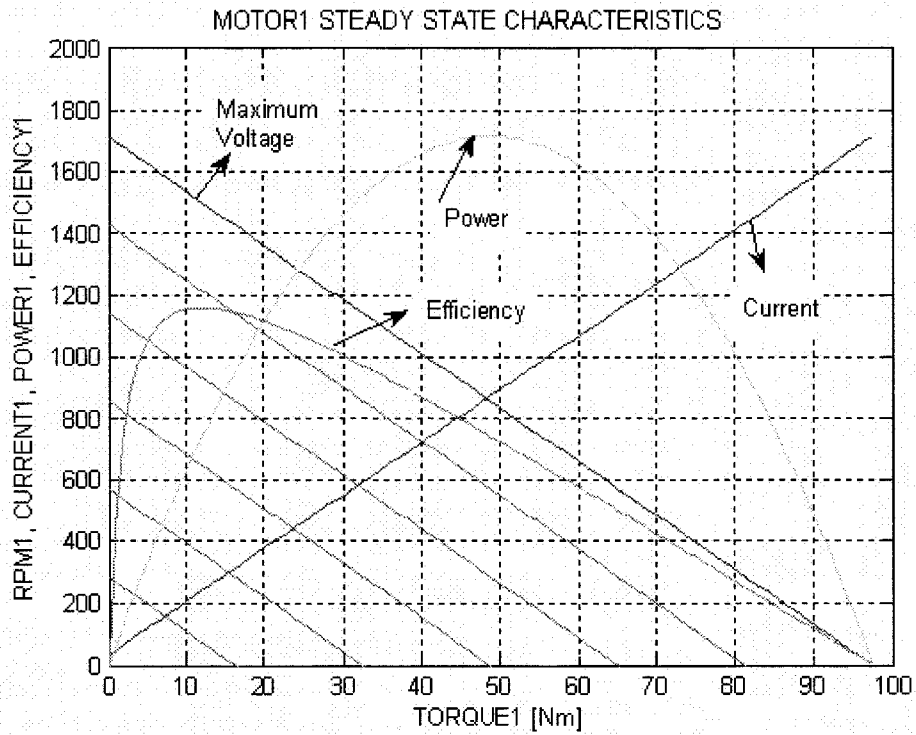
Figure 6.7: DC motor 1 characteristics

MOTOR2 STEADY STATE CHARACTERISTICS
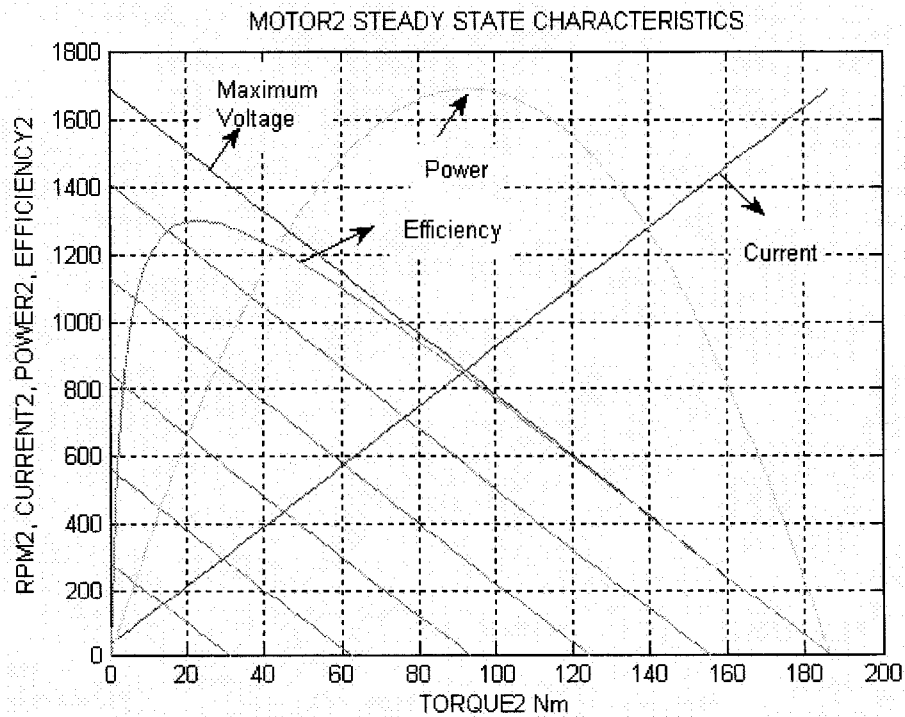
Figure 6.8: DC motor 2 characteristics

107
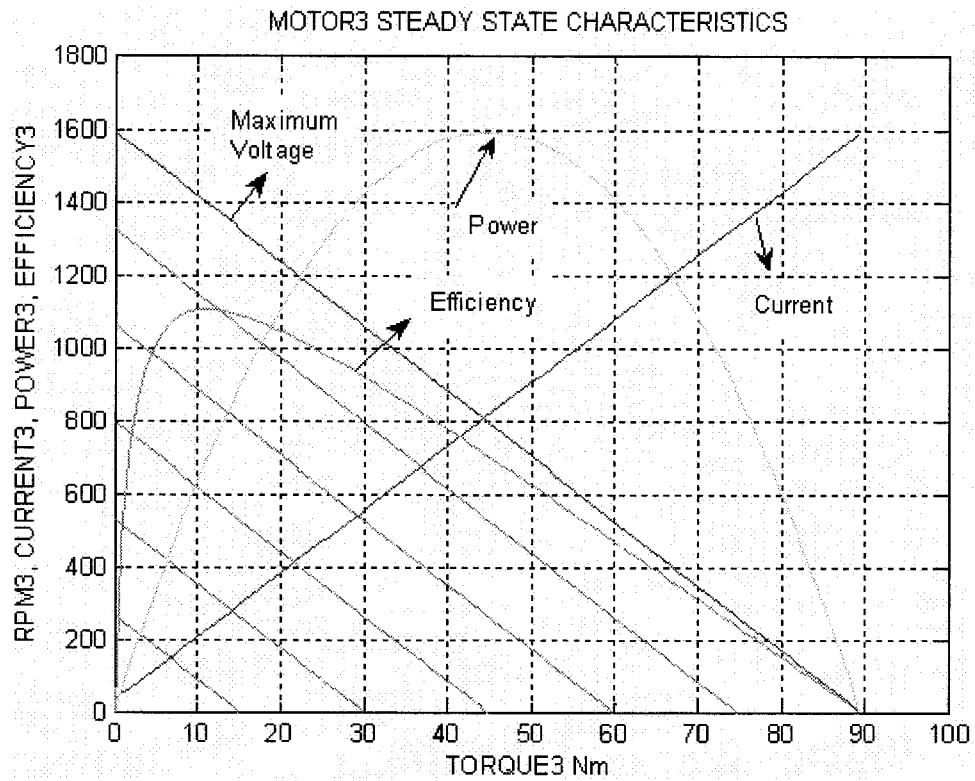
Figure 6.9: DC motor 3 characteristics
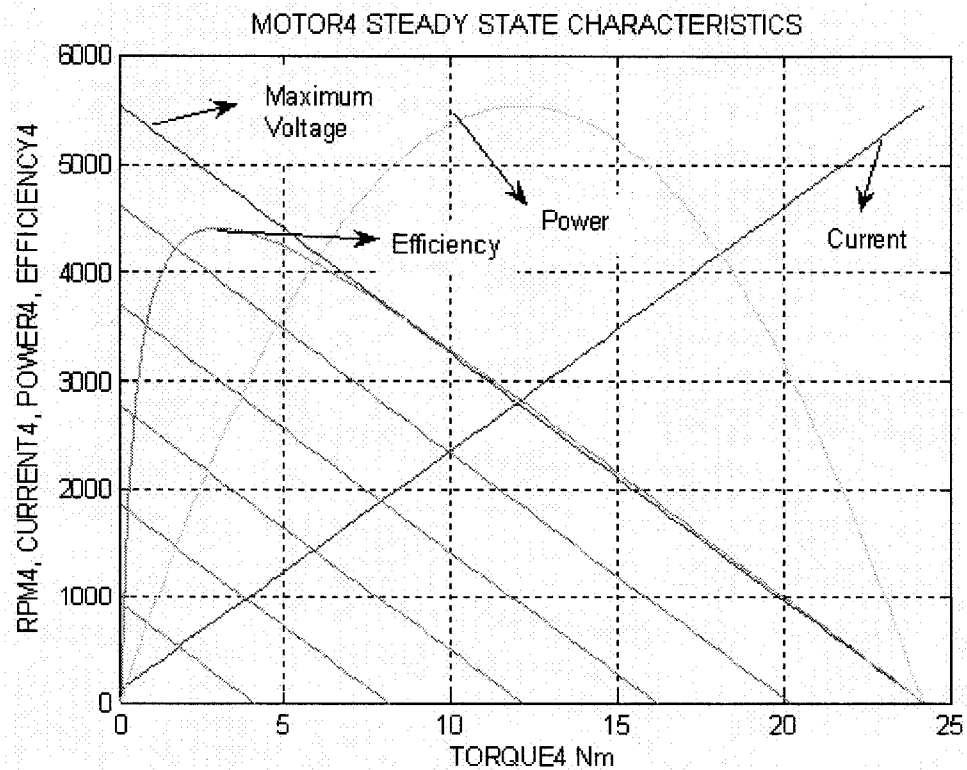

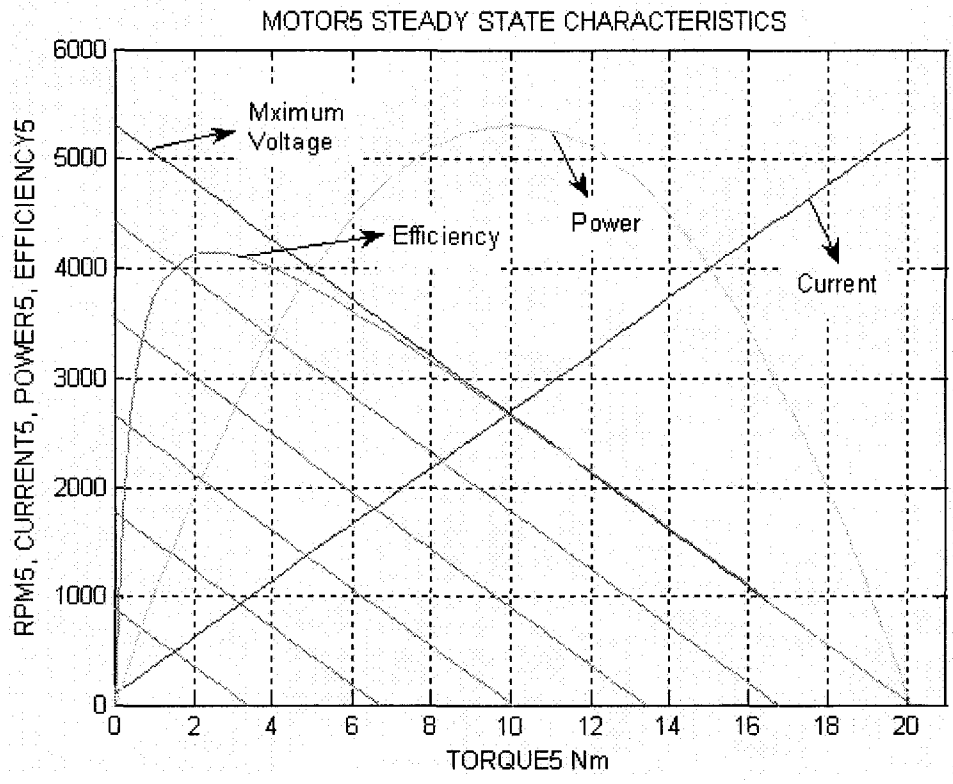**Figure 6.10:** DC motor 4 characteristics
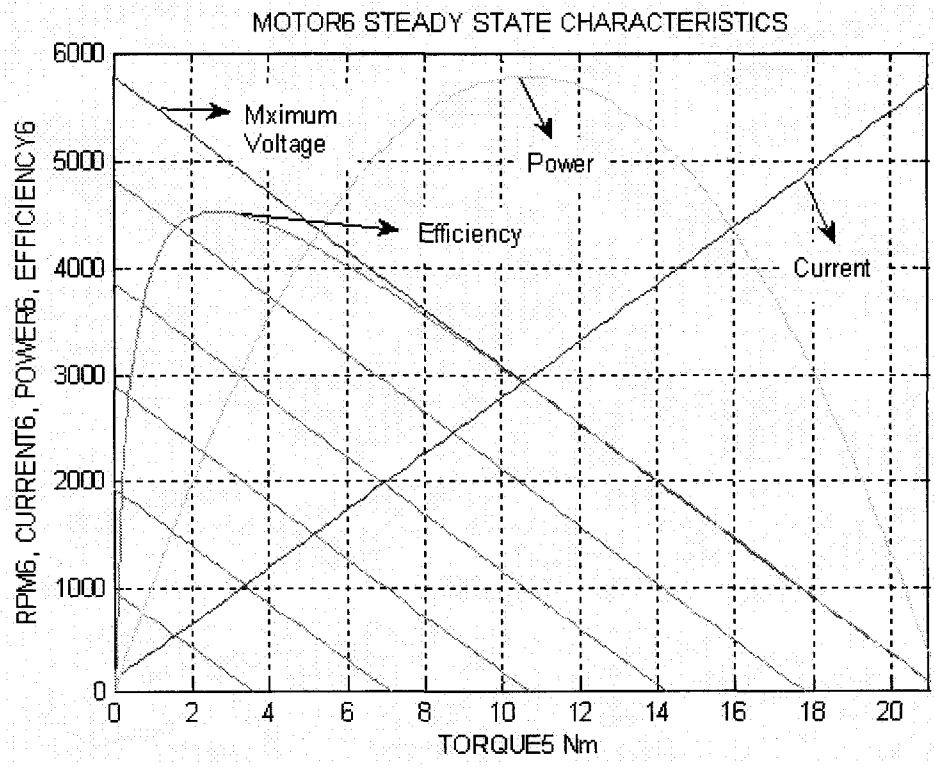
108

Figure 6.11: DC motor 5 characteristics

Figure 6.12: DC motor 6 characteristics

109

The open loop DC motor velocity transfer function can be calculated from Equation 174.

$$\frac{\dot{\theta}_m(s)}{V(s)} = \frac{K_t}{(J_m s + B_m)(L_m s + R_m) + K_t K_b}$$

(174)

The open loop unloaded DC motor velocity root locus for all six motors are presented on Figures 6.13-6.18.

The eigenvalues for all six open loop motor velocity control systems have real negative values. The dominant, slow eigenvalue P_2 is a mechanical one, while the fast eigenvalue P_1 is an electrical one.
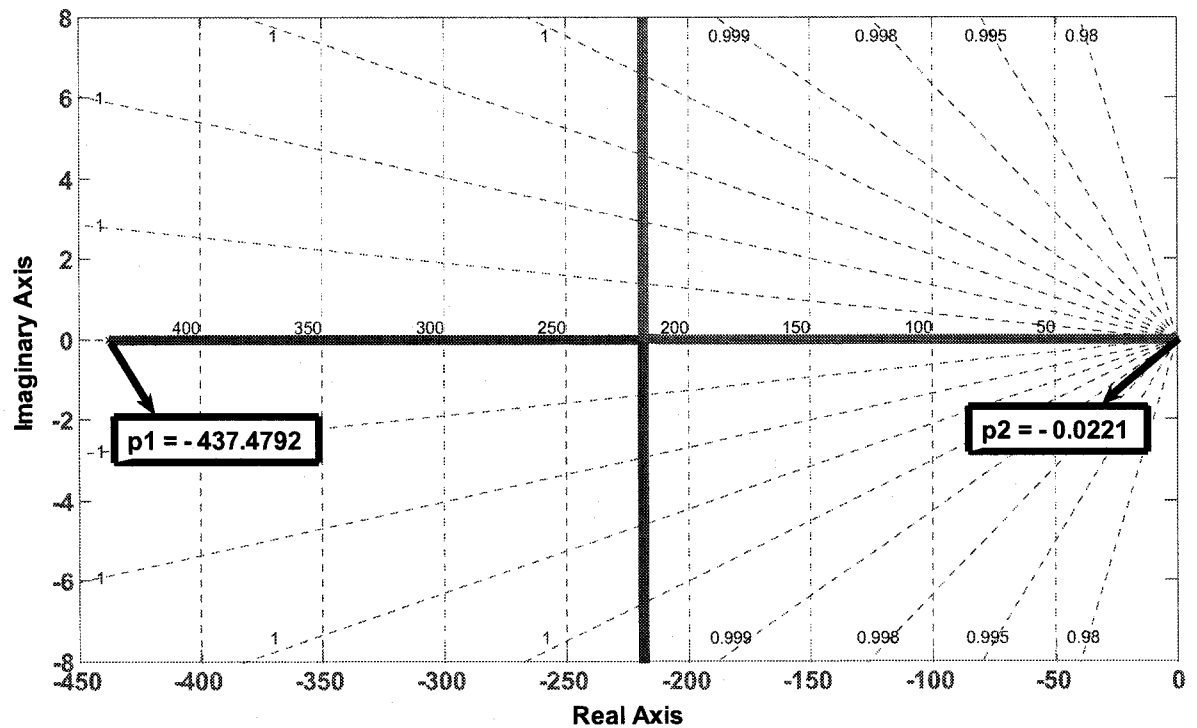
Figure 6.13: Motor 1 velocity dynamics, root locus

110
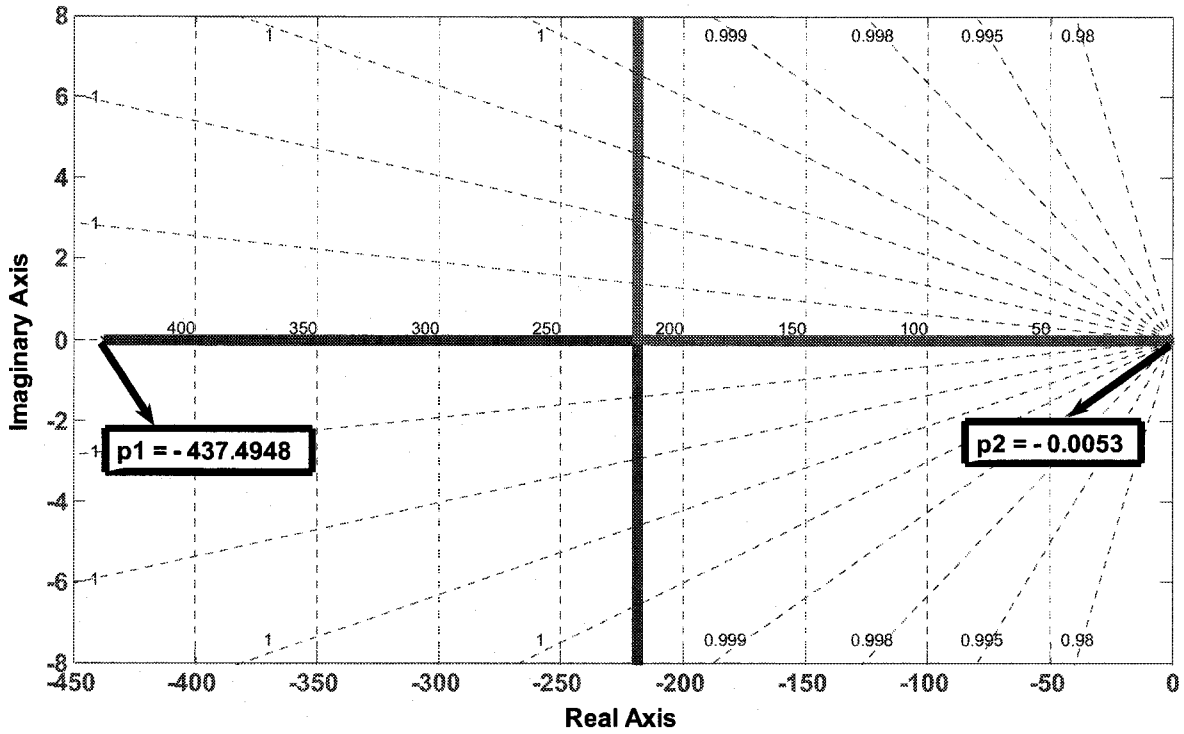
Figure 6.14: Motor 2 velocity dynamics, root locus
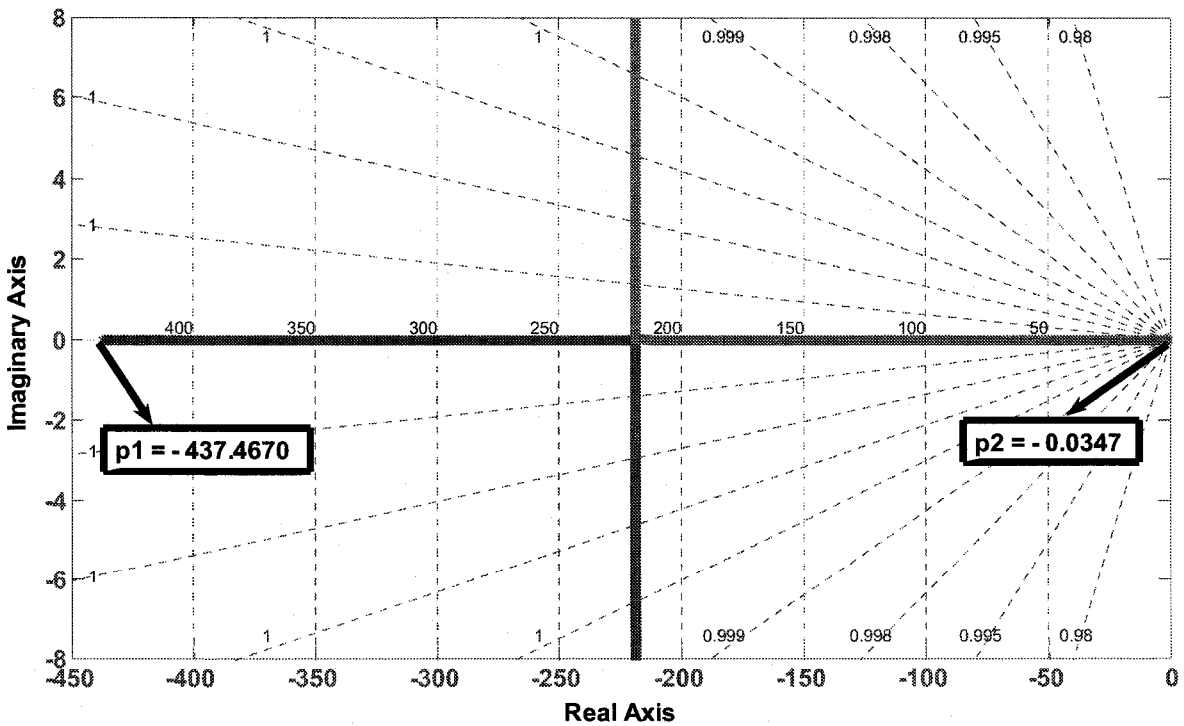
Figure 6.15: Motor 3 velocity dynamics, root locus

111
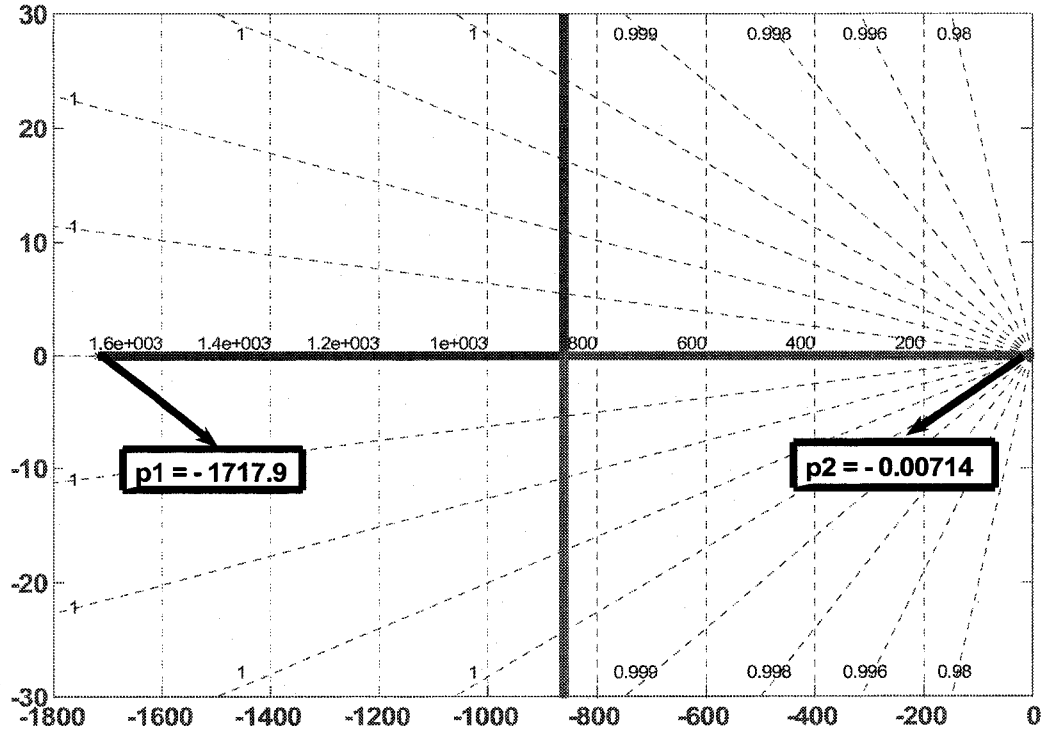
Figure 6.16: Motor 4 velocity dynamics, root locus
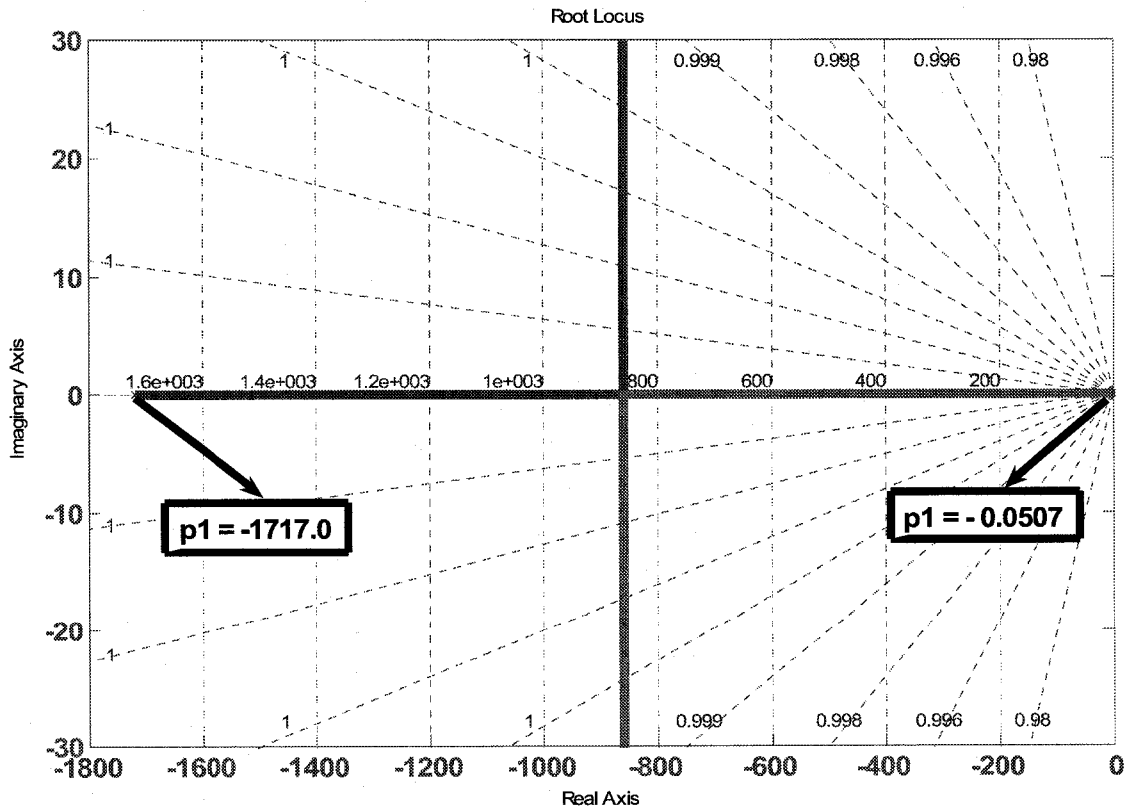
Figure 6.17: Motor 5 velocity dynamics, root locus

112
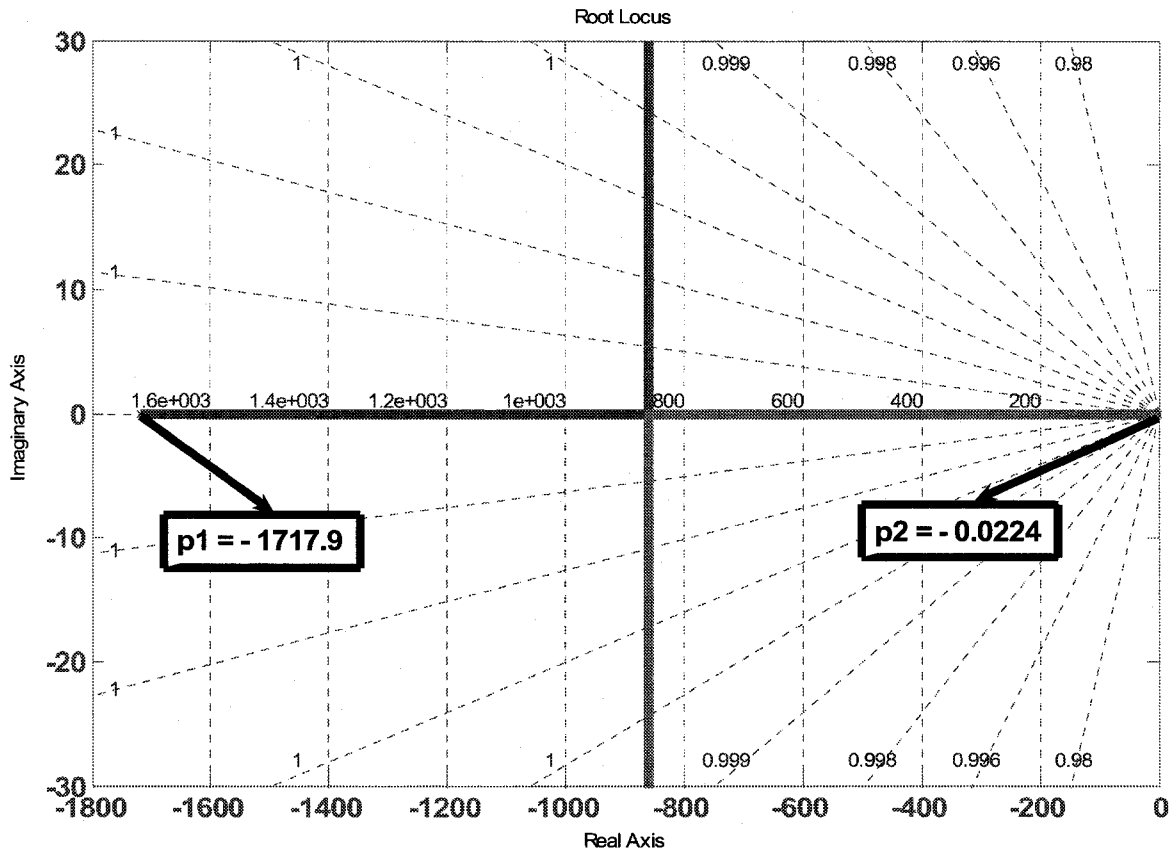
Figure 6.18: Motor 6 velocity dynamics, root locus

6.2. DC Motor Reconfigurable Position Control Design

The reason for position control systems is to control the angular position of the motor shaft. The root loci can be designed from the DC motor position transfer function, Equation 161. The graphical representation is in Figure 6.19.

There are three poles. Two are negative, and one is in zero. A zoom of the two poles close to the zero is shown in Figure 6.20. It can be seen that system becomes oscillatory when gain is increased.

By adding a zero to the open loop transfer function, the root loci will be modified as shown in Figure 6.21. The new configuration can produce better system performance and accommodate higher gain.

113
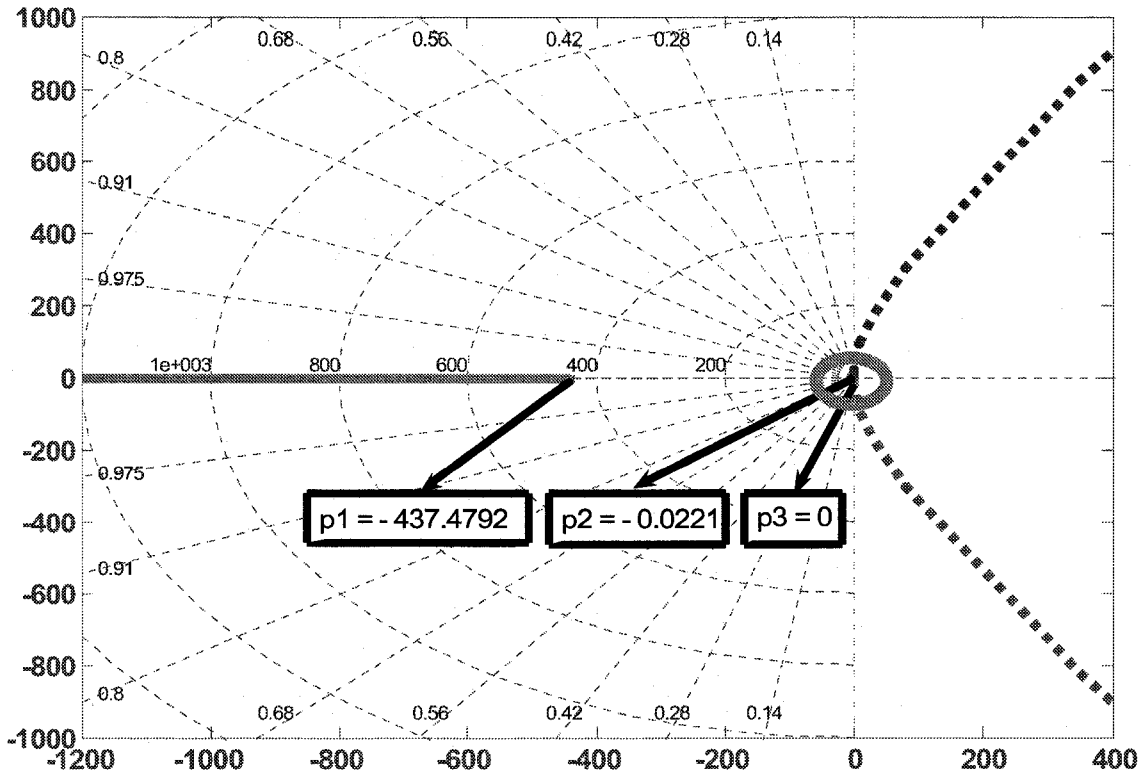
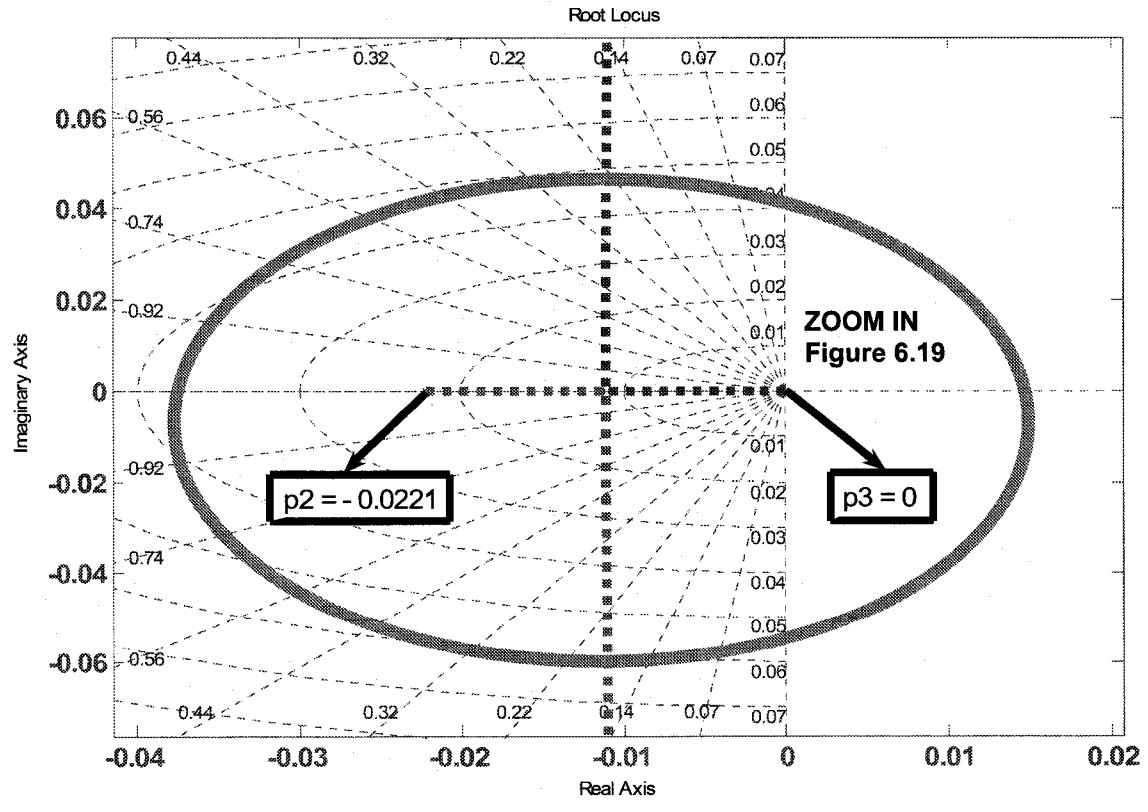**Figure 6.19:** Motor 1: Root locus of position control system

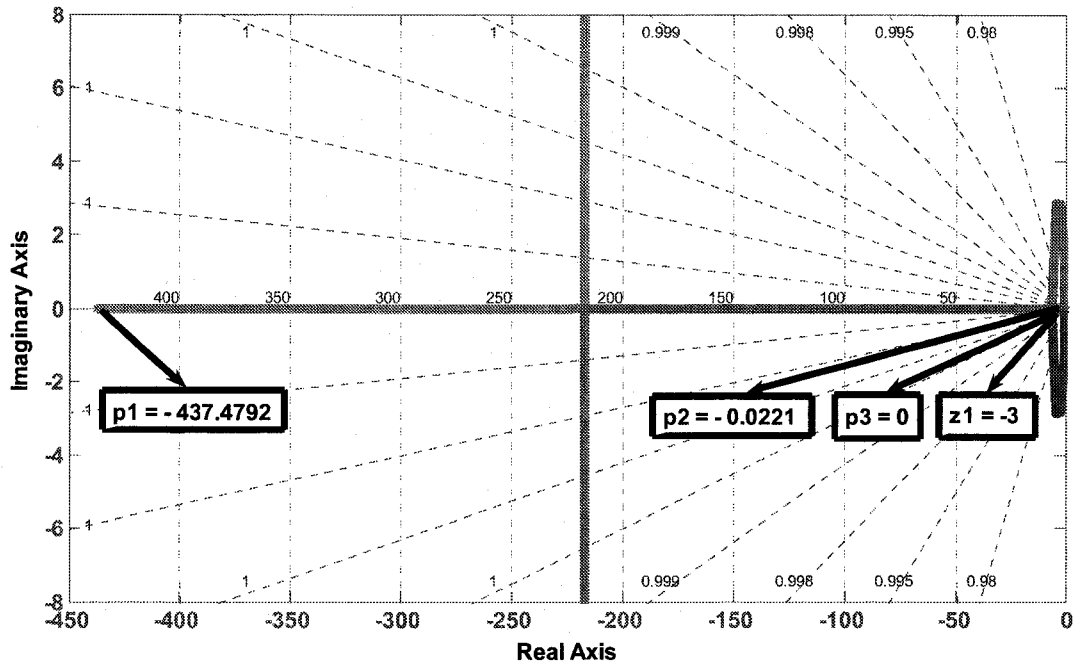**Figure 6.20:** Motor 1: magnified – poles around zero

114

Figure 6.21: Motor 1: Root locus of the position control system with an added zero

The root locus analysis for the other five motors is shown in Figures 6.22-6.36.
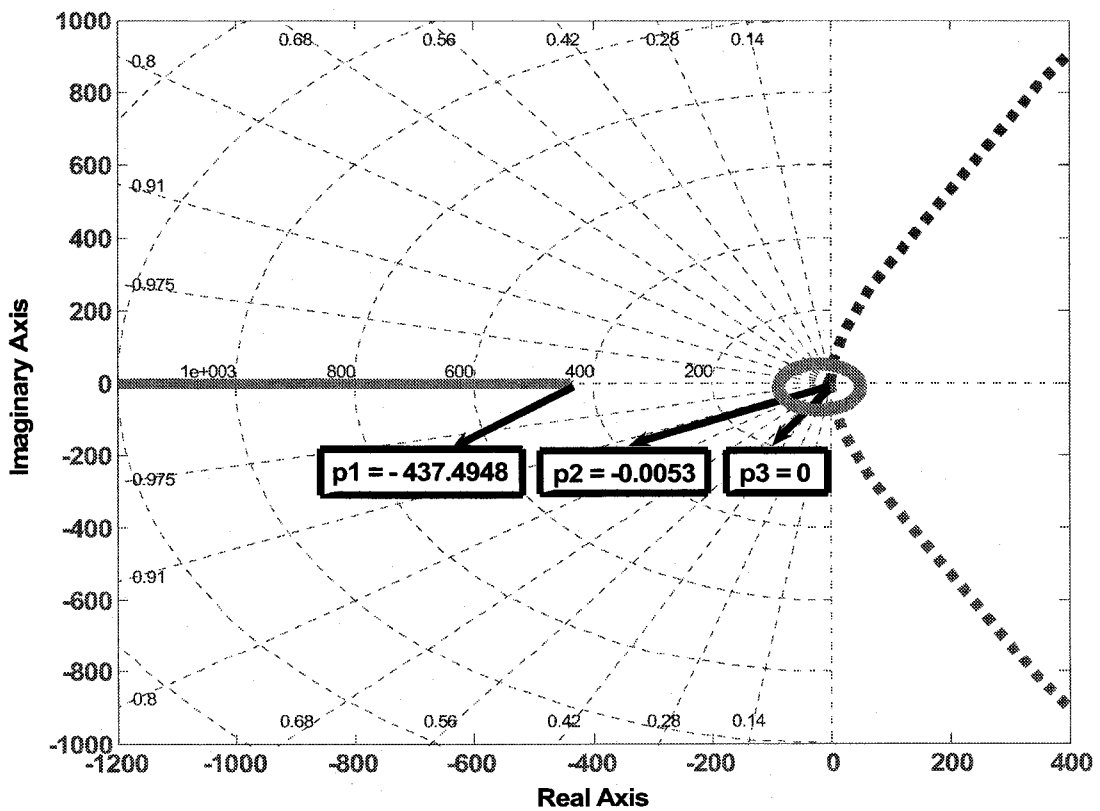

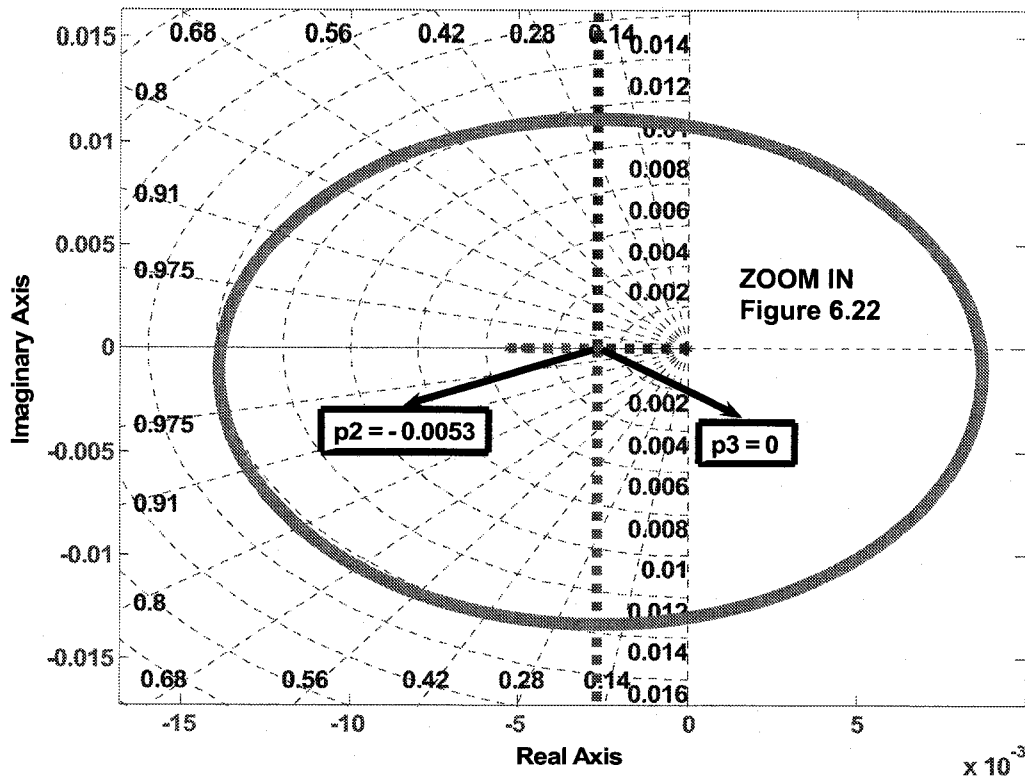**Figure 6.22:** Motor 2: Root locus of position control system

115

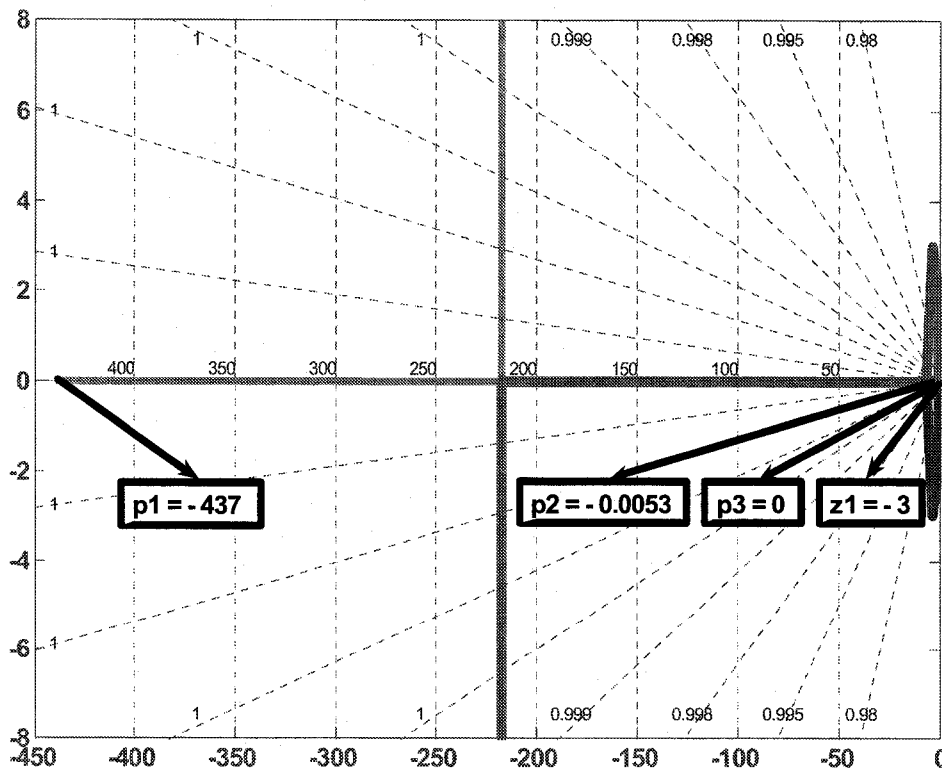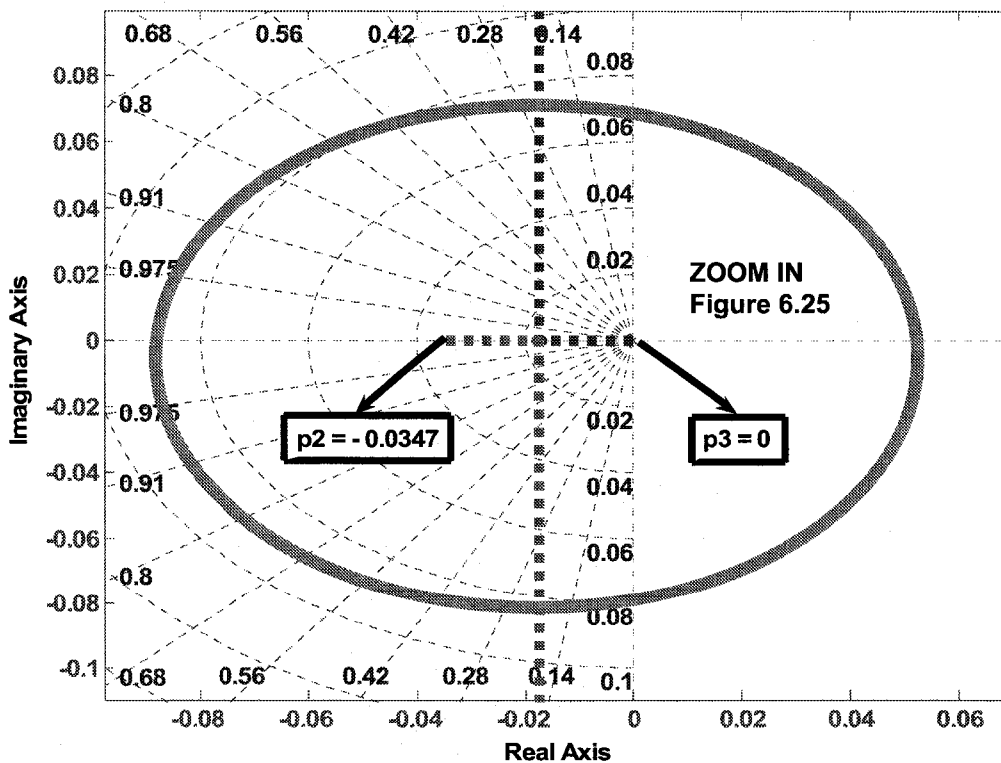**Figure 6.23:** Motor 2: magnified – poles around zero

Figure 6.24: Motor 2: Root locus of the position control system with added a zero

116

Figure 6.25: Motor 3: Root locus of position control system
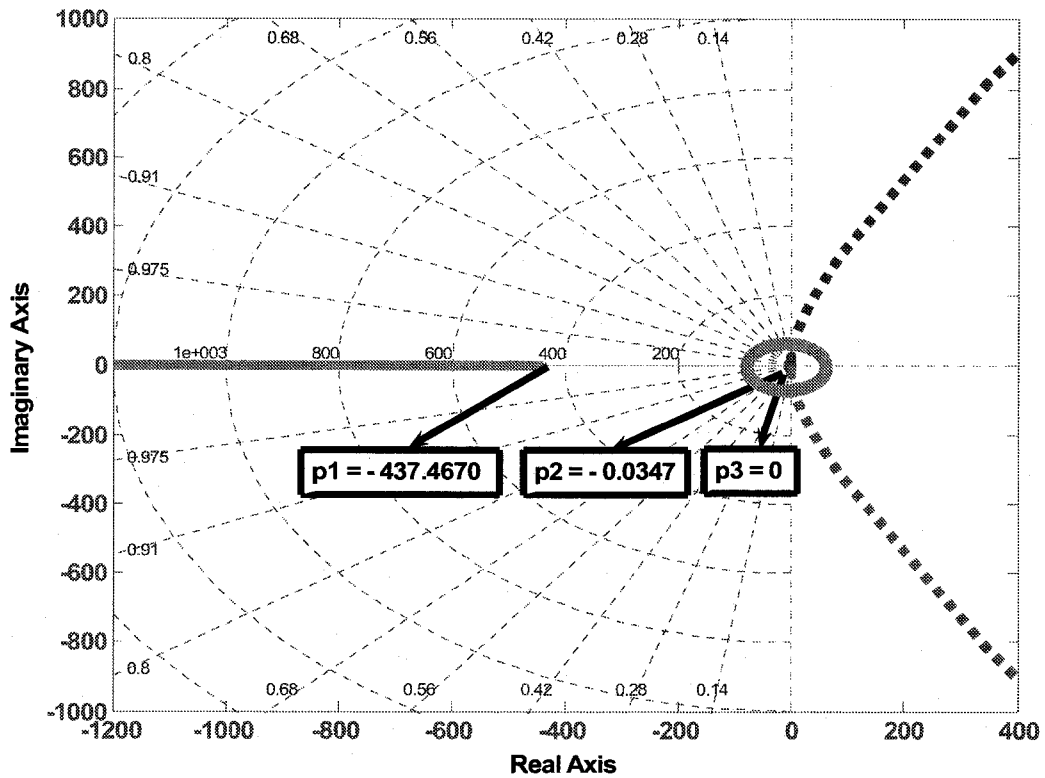

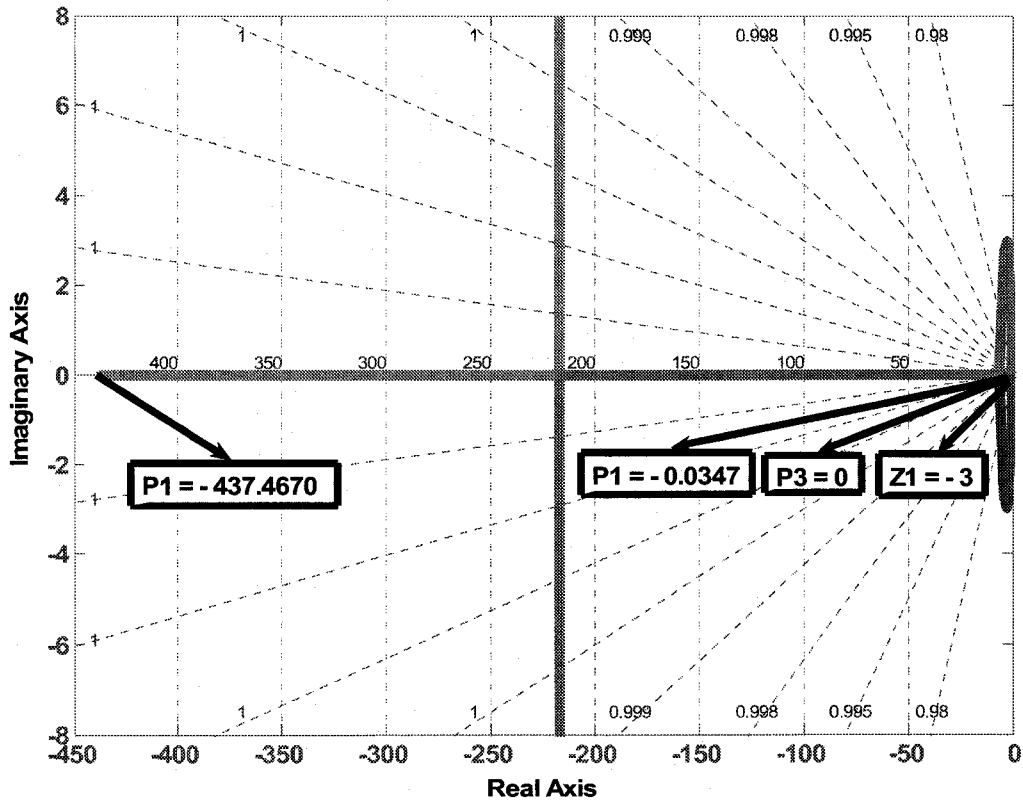**Figure 6.26:** Motor 3: magnified – poles around zero

117

Figure 6.27: Motor 3: Root locus of the position control system with an added zero

Figure 6.28: Motor 4: Root locus of position control system

118

Figure 6.29: Motor 4: magnified – poles around zero

Figure 6.30: Motor 4: Root locus of the position control system with an added zero
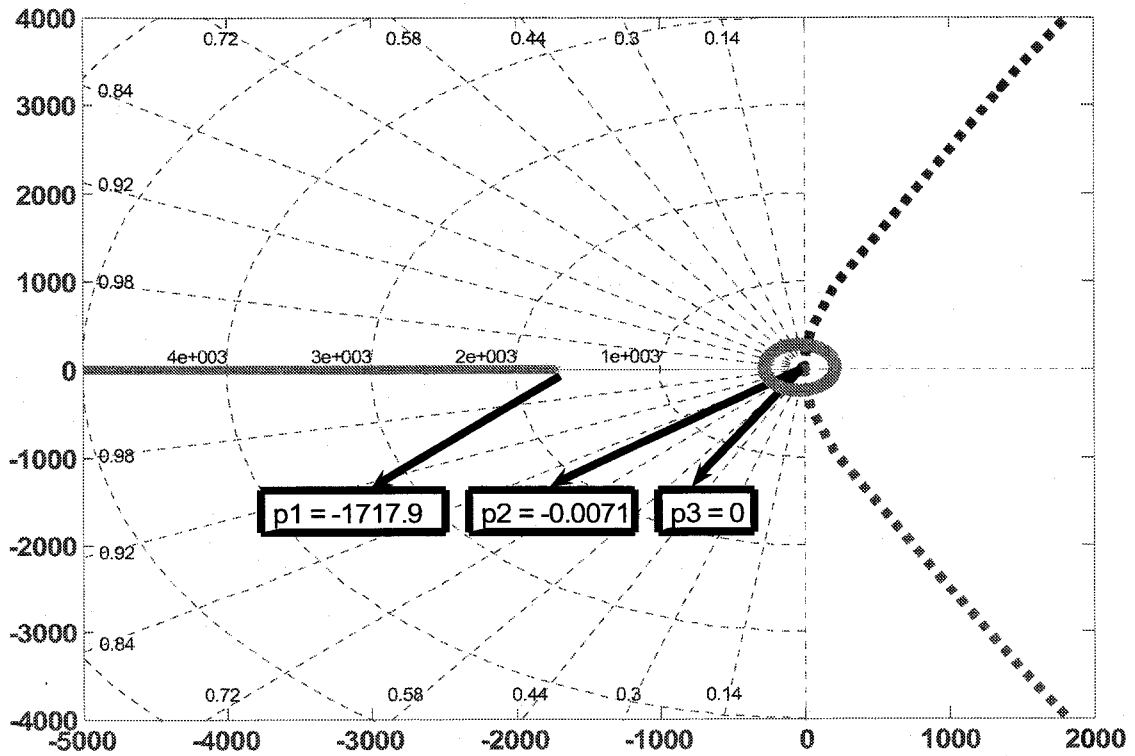
119

Figure 6.31: Motor 5: Root locus of position control system

Figure 6.32: Motor 5: magnified – poles around zero

120

Figure 6.33: Motor 5: Root locus of the position control system with added a zero
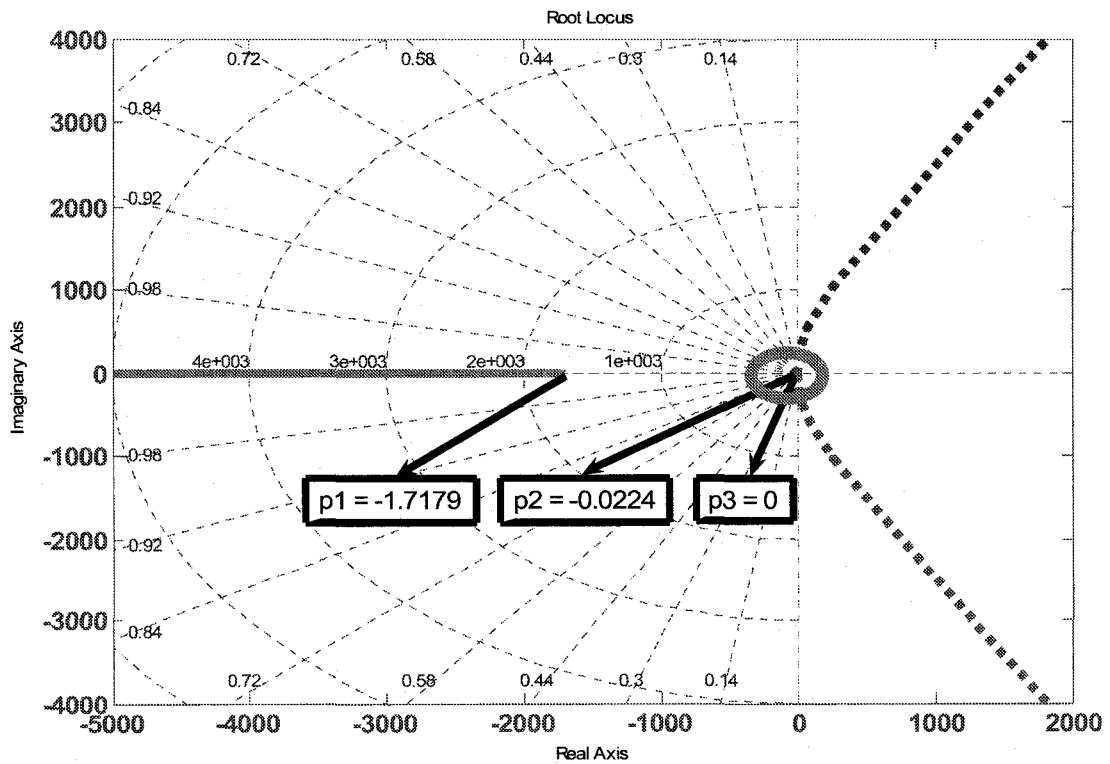
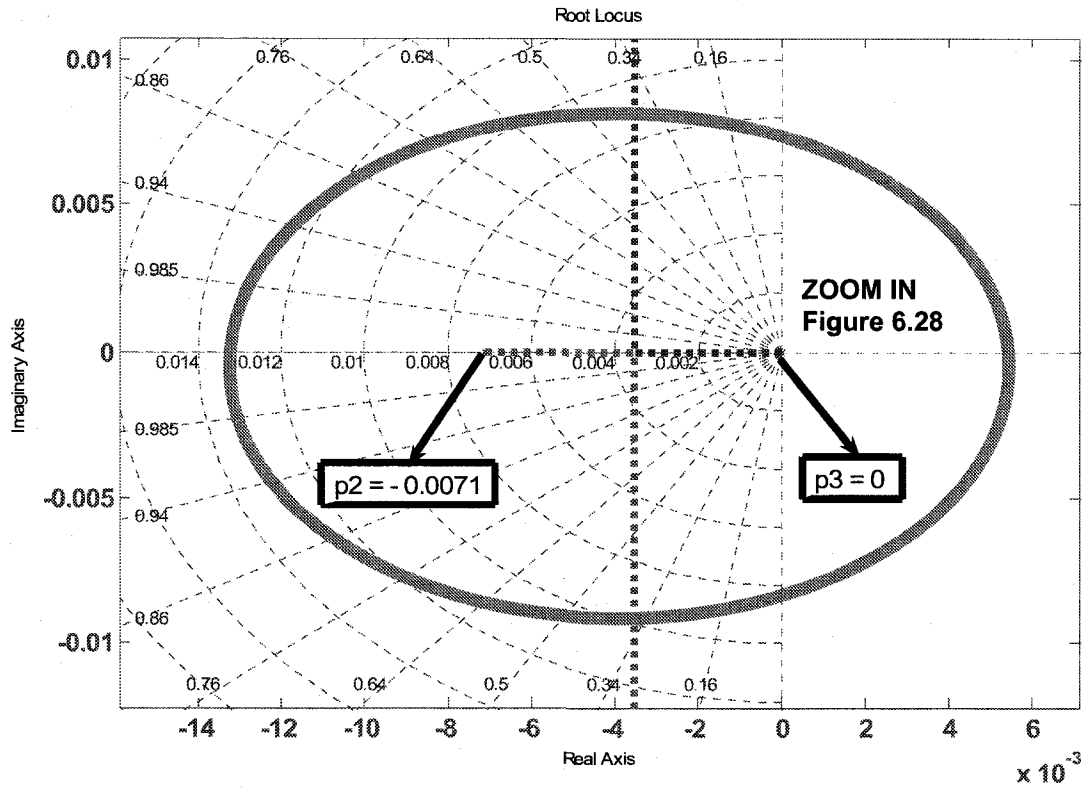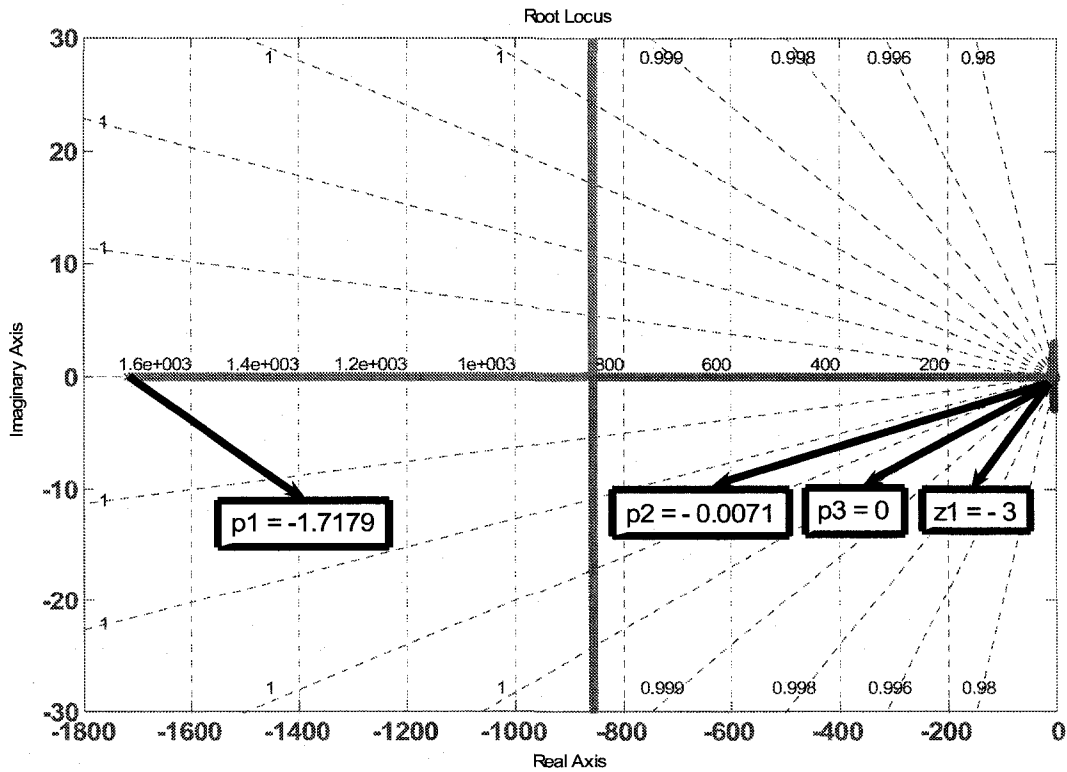**Figure 6.34:** Motor 6: Root locus of position control system

121
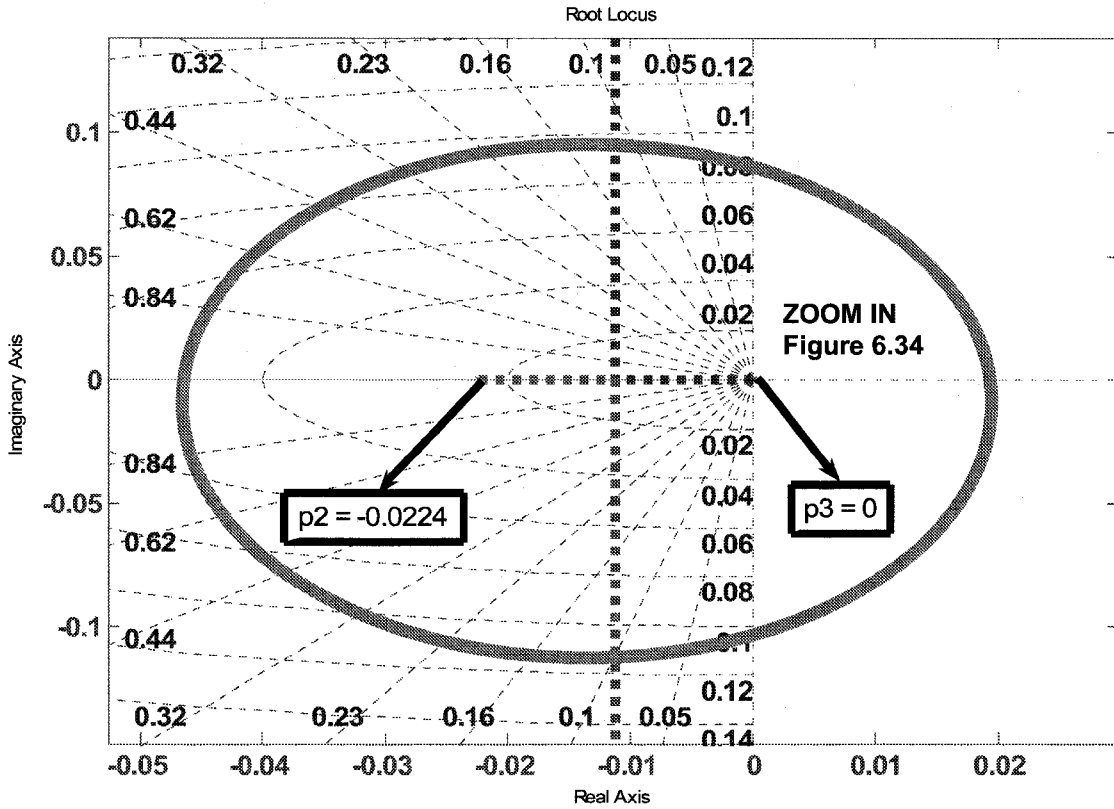
Figure 6.35: Motor 6: magnified – poles around zero

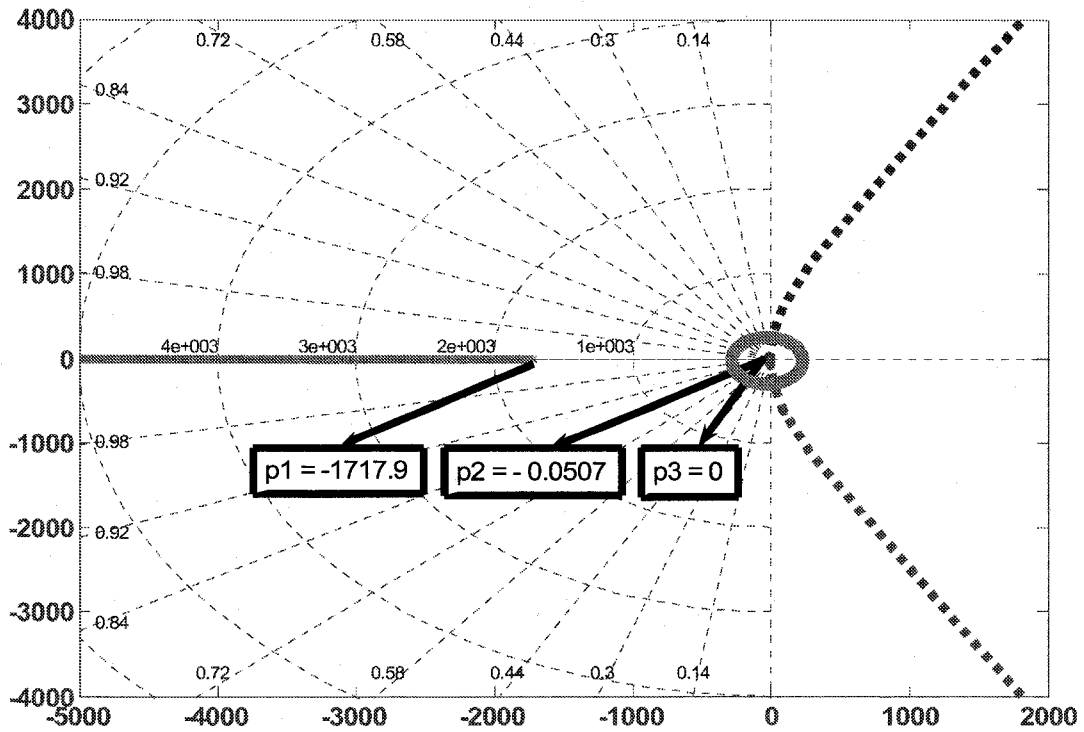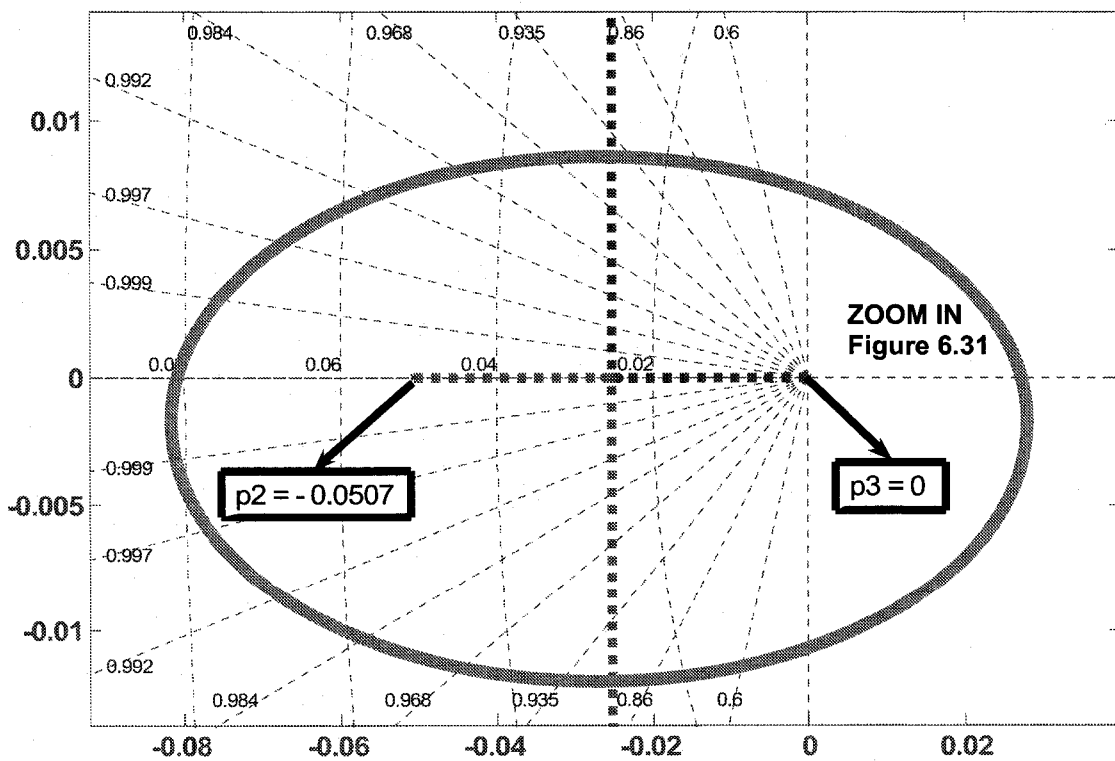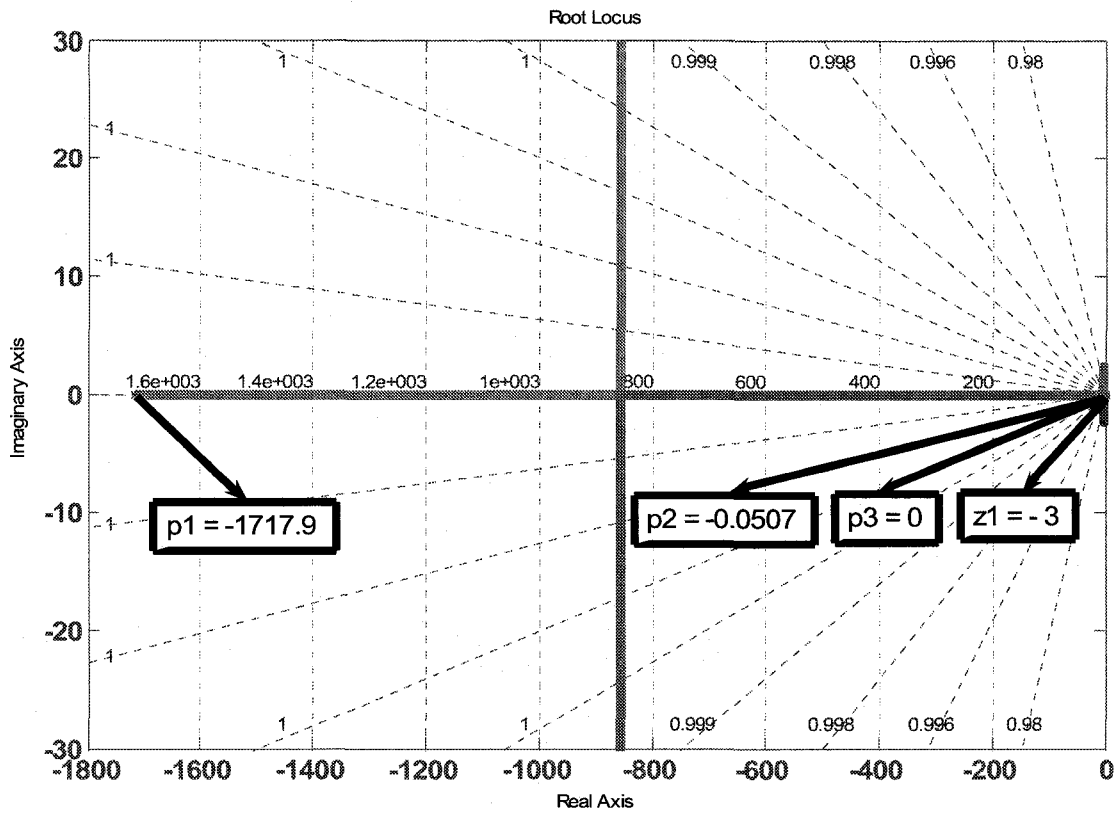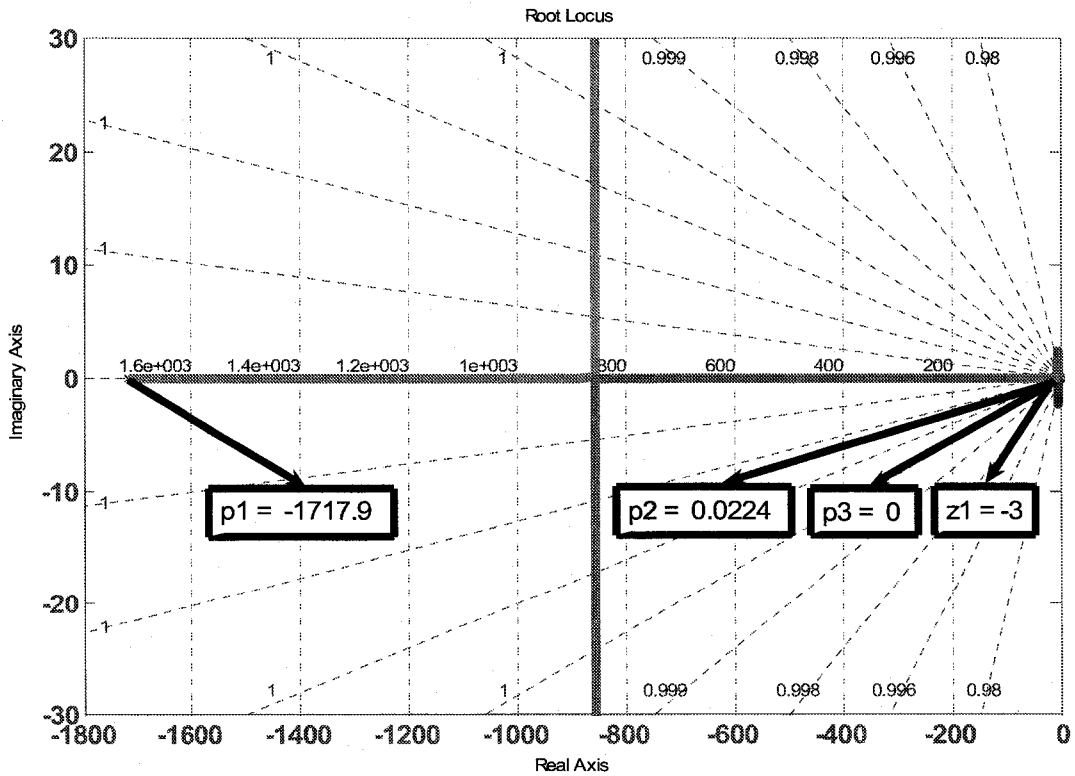**Figure 6.36:** Motor 6: Root locus of the position control system with an added zero

122

From the literature review (Leva A., and Bascetta L., 2006), (Electro-Craft Corp, 1973), (Tewari A., 2002), (Kokotovic V. *et al.*, 1998), (Anderson J. R., 1990), (Anderson J. R. and Spong M. W, 1988), and analysis of the DC motor performances using the root locus method, a PI controller was developed for each motor. The analysis shows that control parameters and gain can be expressed as a function of each of the motor parameters, as in Equations 175 -177.

$$K_{Pi} = R_{mi}, \quad i = 1,2...6 \tag{175}$$

$$K_{Ii} = L_{mi}, \quad i = 1,2...6 \tag{176}$$

$$Gain_i = \frac{V_{max}}{60/2\pi}(\frac{K_{ti}}{B_{mi}R_{mi}} + K_{ti}K_{bi}), \quad i = 1,2...6 \tag{177}$$

The control scheme for the DC motor including gear ratio is presented in Figure 6.37.
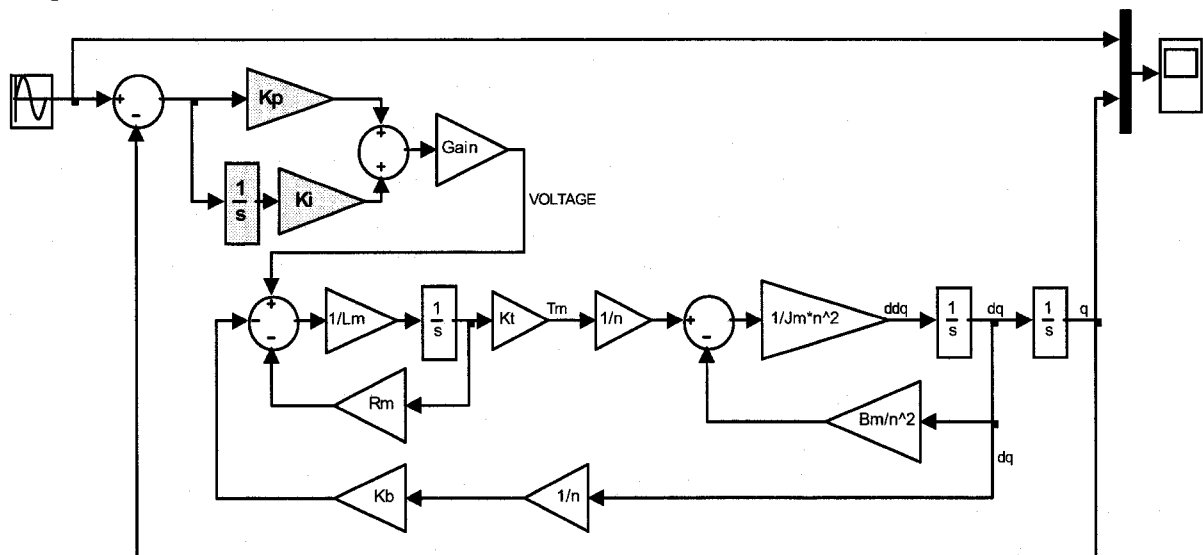
Figure 6.37: PI controller for the DC Motor 1

A Simulink simulation was done for each motor. Using a sinus as an input signal, the system response for motor 1 is shown in Figure 6.38.

123
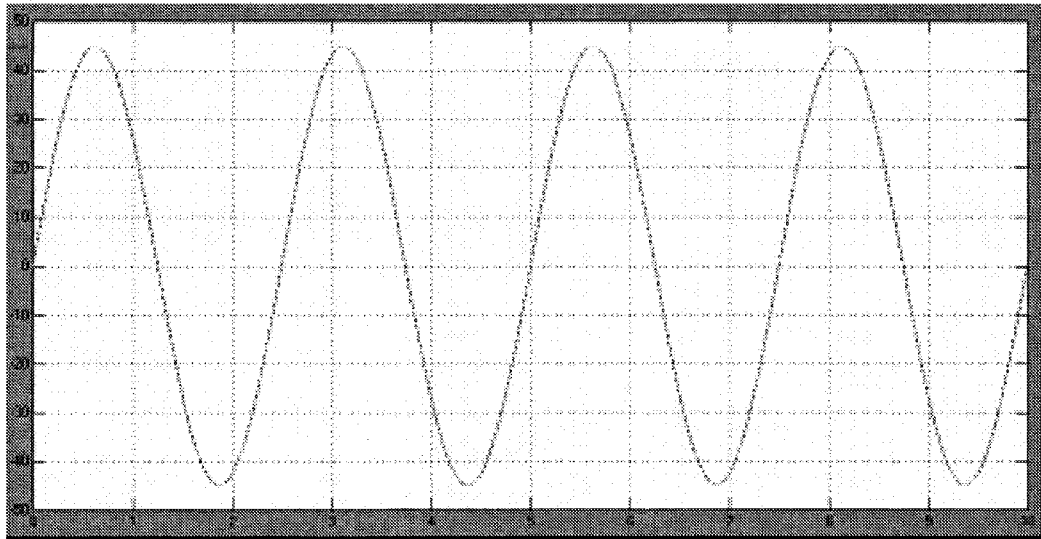
Figure 6.38: DC Motor1 response

6.3. Implementing DC Motor Reconfigurable Position Controller for PUMA 560 Robot

The previously designed reconfigurable controller, Equations 175-177, has been implemented for the PUMA 560 robot.

The MATLAB/SIMULINK scheme is designed such that the electrical part is separate from the mechanical part. From the electrical scheme, the output is $\dfrac{K_{ti}i_{mi}}{N_i}$, and this input to the mechanical part of the scheme. For the complete analysis of the dynamic system the inductance is included:

$$L_{mi} \neq 0 , \quad i = 1,2 \dots 6 \tag{178}$$

From the reviewed literature (Armstrong B., *et al.*, 1986), (Corke P. I., and Armstrong B., 1994), the cross-coupling values have been determined from testing the wrist mechanism and corresponding with numerical value by Breaking Away torque. The relationship between joint and motor angles is given by:

124

$$q = \begin{bmatrix} \dfrac{1}{G_1} & 0 & 0 & & & \\ & & & 0 & 0 & 0 \\ 0 & \dfrac{1}{G_2} & 0 & 0 & 0 & 0 \\ & & & 0 & 0 & 0 \\ 0 & 0 & \dfrac{1}{G_3} & & & \\ & & \dfrac{1}{G_4} & 0 & 0 \\ 0 & 0 & 0 & & & \\ 0 & 0 & 0 & \dfrac{G_{45}}{G_4} & \dfrac{1}{G_5} & 0 \\ 0 & 0 & 0 & \dfrac{G_{46}}{G_4} & \dfrac{G_{56}}{G_5} & \dfrac{1}{G_6} \end{bmatrix} \theta_m$$ (179)

Where G_i ($i = 1,2\ldots6$), is the gear ratio for each joint. Vector q is the vector of generalized joint coordinates: $q = [q_1 \quad q_2 \quad \cdots \quad q_6]^T$. Vector θ_m is the vector of motor angles: $\theta_m = [\theta_{m1} \quad \theta_{m2} \quad \cdots \quad \theta_{m6}]^T$.

In a Section 5.5 the dynamic model of the PUMA 560 robot was developed using the RPFDM. Because of the model complexity, the information from Armstrong B., *et al.* 1986 is applied and the simplified PUMA 560 dynamic model is presented in Appendix G. This model contains reconfigurable parameter K_6, which controls the direction of joint 6.

Each link is treated separately and their equations are as following:

$$a_{i1}\ddot{q}_1 + \ldots + a_{i6}\ddot{q}_6 + b_{i12}\dot{q}_1\dot{q}_2 + \ldots b_{i56}\dot{q}_5\dot{q}_6 + c_{i1}\dot{q}_1 + \ldots + c_{i6}\dot{q}_6 + G_i = \tau_i, \quad i = 1,2\ldots6$$ (180)

The electrical part of the motor, Equation 133 is treated separately. The PI controller for each link is connected to the electrical part of the motor. The output of the electrical part of the motor is motor torque. The mechanical part of the motor, Equation 134 is combined with the link dynamics. It is schematically presented in Figure 6.39.

125

Figure 6.39: Schematic diagram of the PUMA 560 robot first link

The link dynamics from Figure 6.39 are shown in detail in Figure 6.40.

The reconfigurable control block from Figure 6.39 is shown in detail in Figure 6.41. This block has two main sub blocks; the PI control box and the command waveform block.

126
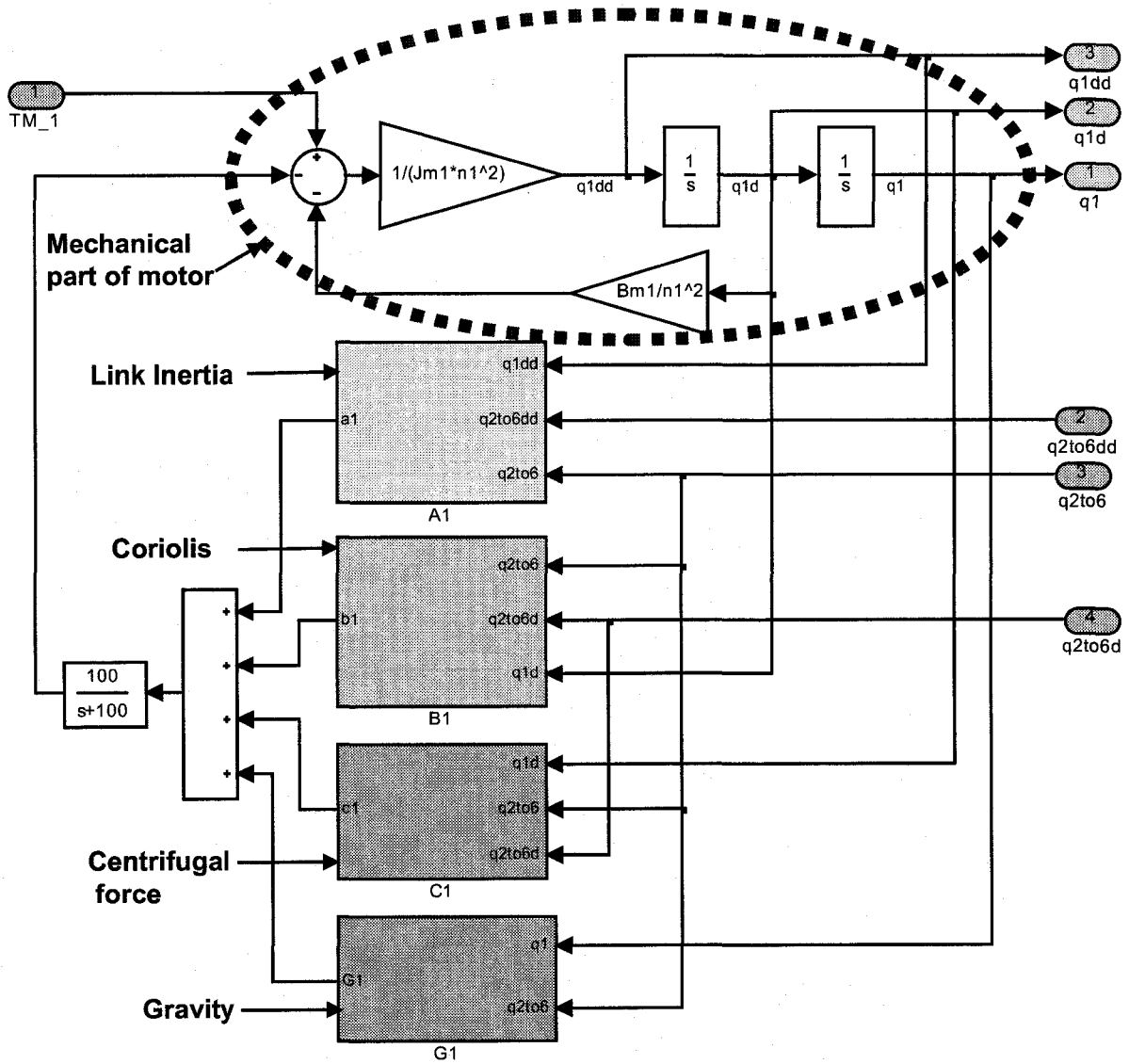
Figure 6.40: Schematic diagram of the first link dynamics and first motor dynamics

127
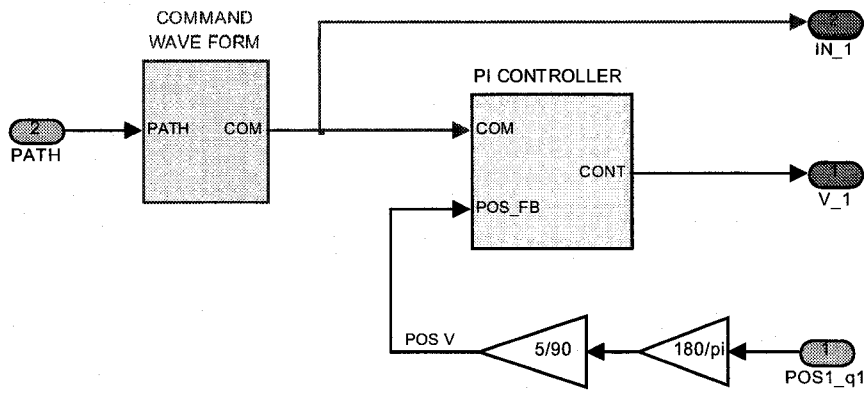
Figure 6.41: Schematic diagram of the Controller with input command

The reconfigurable PI controller is shown in Figure 6.42.
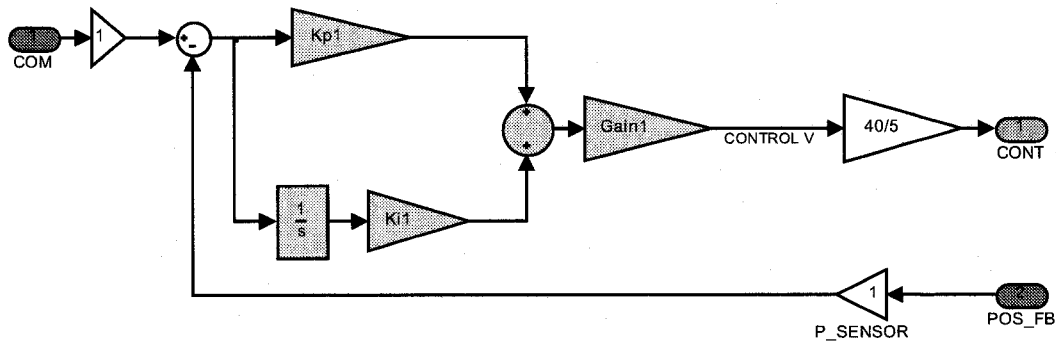
Figure 6.42: Schematic diagram of the PI Controller

The electrical part of the DC motor block from Figure 6.39 is shown in detail in Figure 6.43.
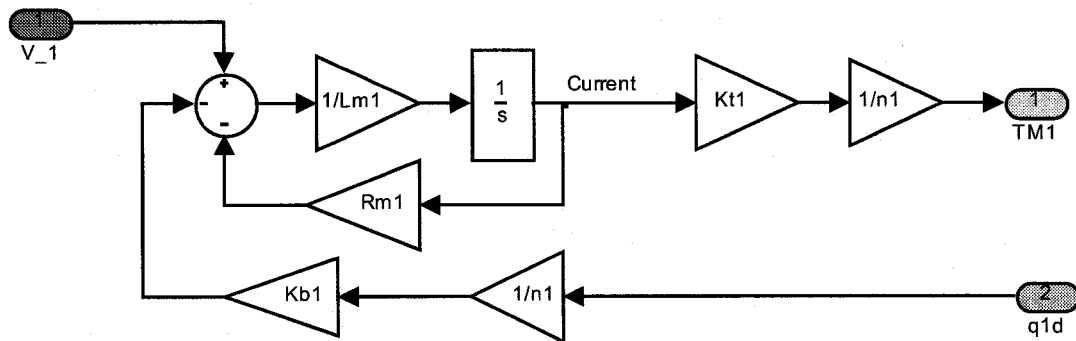
Figure 6.43: Schematic diagram of the electrical part of the DC motor

The complete schematic diagram of the PUMA 560 is presented in Figure 6.44. This diagram has six links, six motors, six reconfigurable controllers, and a block with the robot path.

128
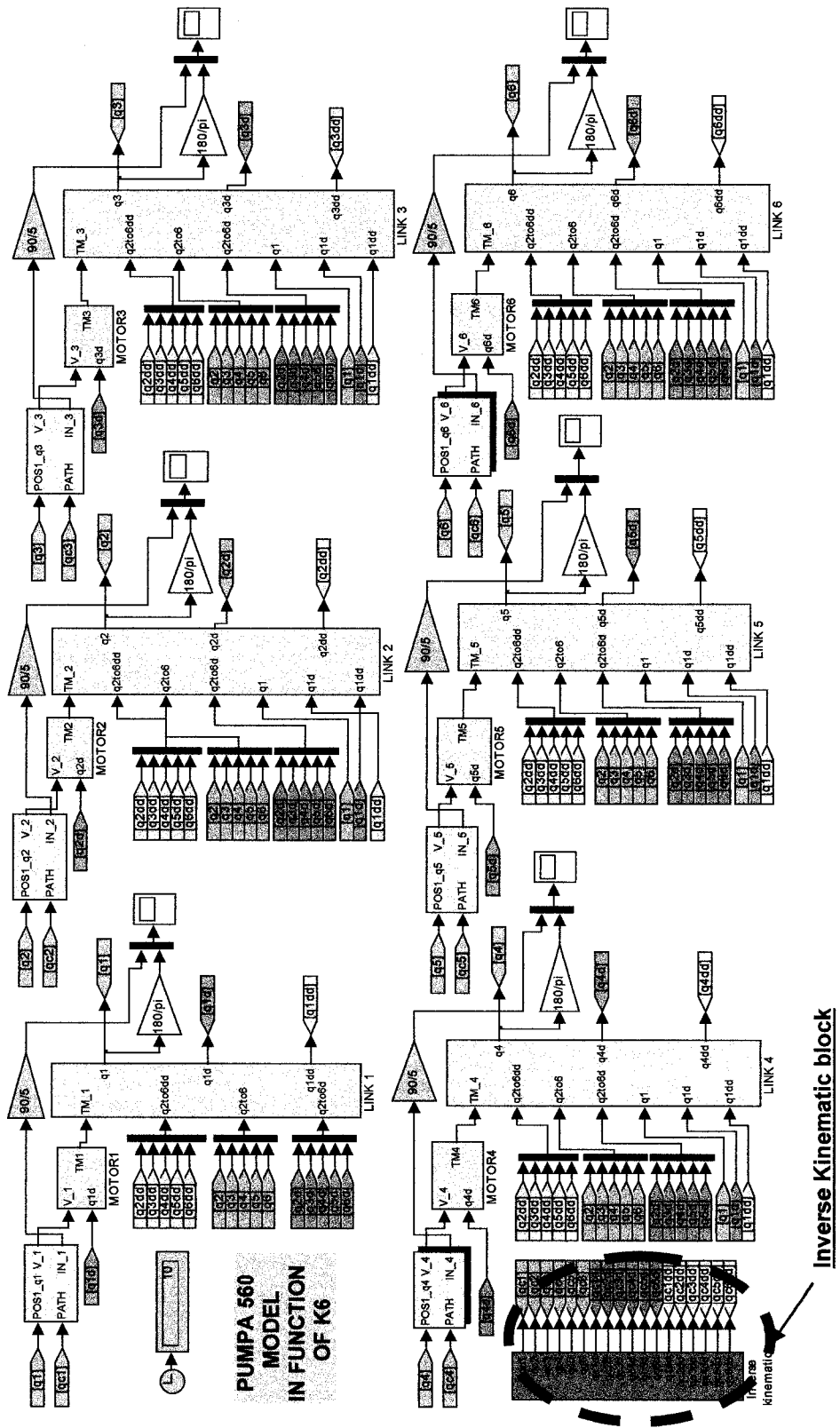
Figure 6.44: Schematic diagram of the PUMA 560 robot

129

Using the DH parameters from Table 5.5, the PUMA 560 kinematic model was created using the UROCA kinematic software. See Figure 6.45.
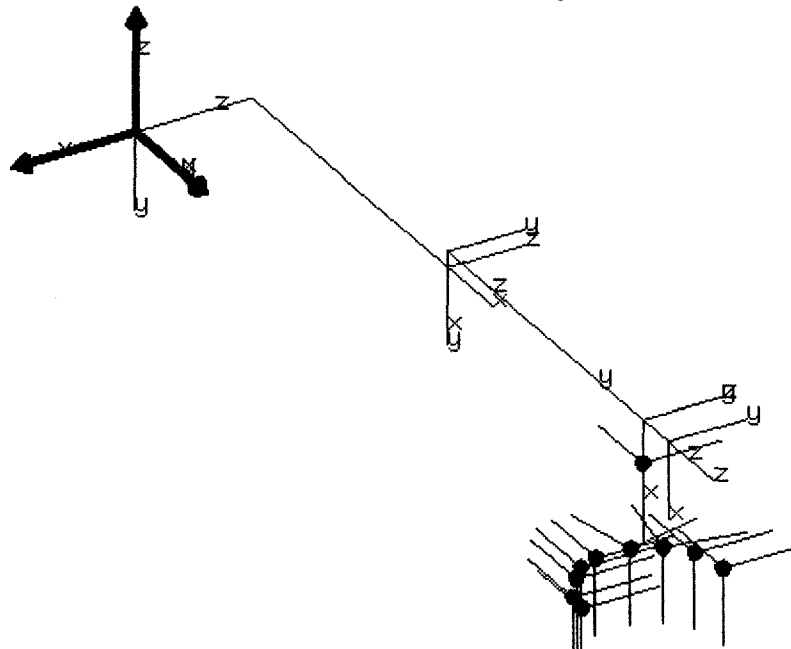
Figure 6.45: PUMA 560 robot path in UROCA software

The created path contains ten points (1-2-3-4-5-6-7-8-9-HOME). The resulting inverse kinematic solution for each point in the path is given in Table 6.2. This information is used in a PUMA 560 simulation, as an input path integrated in an inverse kinematic block, shown in Figure 6.44.

Table 6.2: PUMA 560 robot path

Points	1	2	3	4	5	6	7	8	9
θ_1	11.176	11.065	9.65	7.323	3.746	1.647	0.281	-1.578	-1.822
θ_2	0.777	-8.112	-12.695	-15.546	-16.905	-16.499	-15.04	-11.779	-8.37
θ_3	29.244	48.622	59.137	65.932	69.261	68.248	64.708	56.998	49.202
θ_4	0	0	0	0	0	0	0	0	0
θ_5	59.979	49.49	43.558	39.614	37.644	38.247	40.332	44.781	49.167
θ_6	11.176	11.065	19.65	-4.677	3.746	1.647	-0.281	-1.578	-1.822

The response of the PUMA 560 robot using the reconfigurable PI controller for each joint is presented in Figure 6.46. It is very clear that system stabilizes quickly.

130
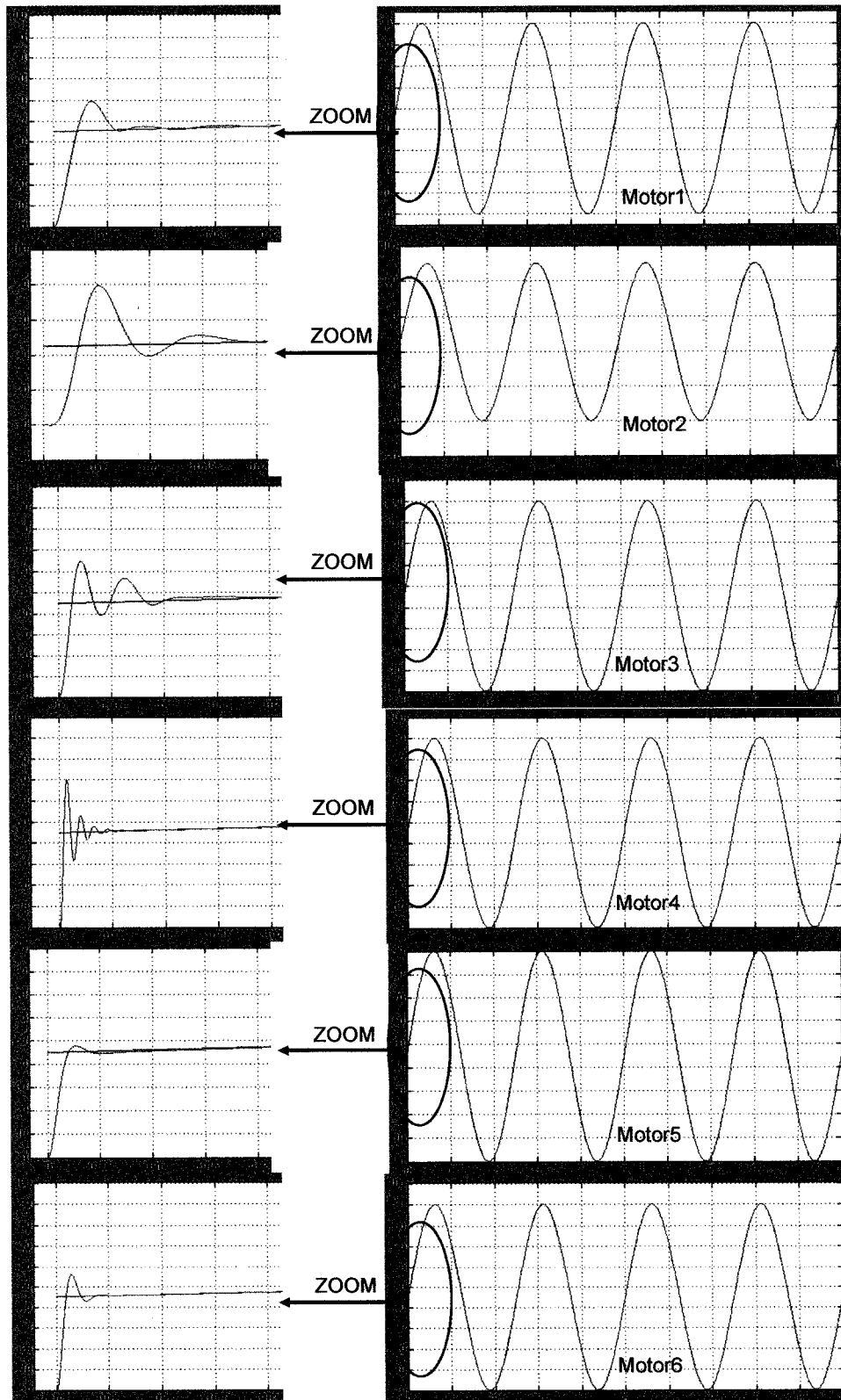
Figure 6.46: The response of the PUMA 560 joint positions using the PI reconfigurable controller

131

6.4. Procedure for Representing Robots using all Six Reconfigurable Modules

There are six steps for defining robot kinematics, dynamics and control using all eight reconfigurable modules.

The schematic diagram of the PUMA 560 robot can be easily changed for any other robot from the RPF group of robots. Then freely call this schematic diagram the Reconfigurable Robot Platform (RRP).

STEP_1: Ensure the selected robot belongs to the RPF group of robots.

STEP_2: Using the UROCA software for modeling robots, select joint coordinate systems, link lengths, link offsets, and joint limits form the selected robot manufacturer. This procedure is explained in Chapter 2, and described in detail in Figure 2.25. This will produce the robot kinematic model, which can be used for creating different paths for specific applications. These paths will be used in Step_6 for the joint position control simulation.

STEP_3: The kinematic model contains information that can be used for automatic generation of its Jacobian matrix using (RPFJM), singularity matrix using (RPGSM), and workspace using (RRW).

STEP_4: By adding the mass of each link, and knowing all kinematic information (D-H parameters), the robot dynamic model can be calculated using the RPFDM module.

STEP_5: For calculation of robot actuator dynamics, information about the motors is needed. This information is listed in Chapter 6, Table 6.1. Using RPFDM+, the complete dynamic model of the selected robot is calculated.

STEP_6: Using Reconfigurable Robot Platform (RRP) can change expressions for each link dynamic. In a separate simulation all the motor parameters can be

132

input, and by running the simulation all six PI controllers will be automatically generated. This procedure is graphically presented in Figure 6.47.
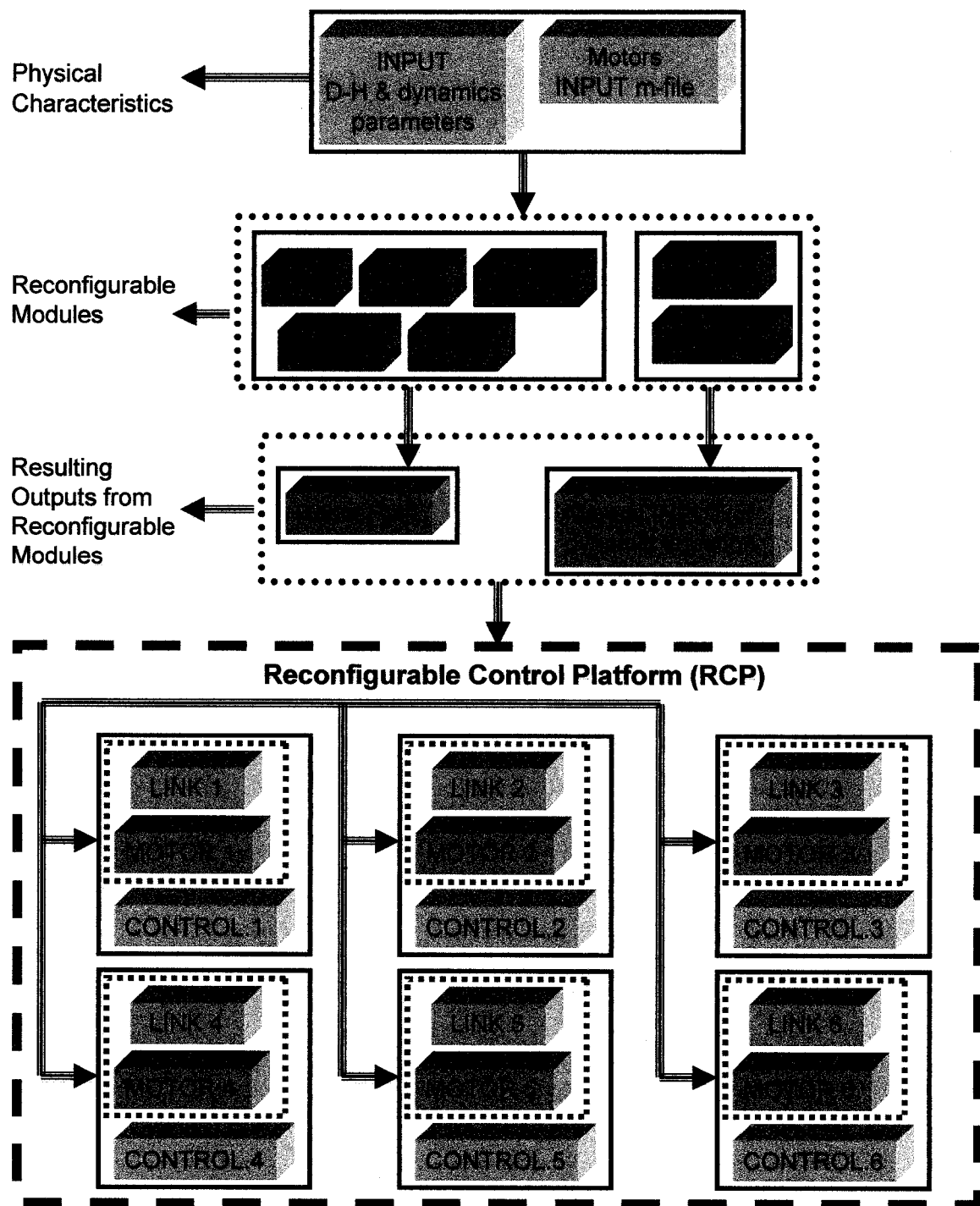
Figure 6.47: Automatic robot plant and control generation using manual input of dynamic equations

133

CHAPTER SEVEN

7. FUTURE WORK

The first step in a RPF model extension will be to eliminate the Pieper's condition. This means that the model is not limited to those robots with spherical wrists. With this extension, a new reconfigurable robot model can be used for robots with offset wrists. Mathematically this means: $a_4 \neq 0$, $a_5 \neq 0$ and $d_5 \neq 0$. This idea is presented in Figure 7.1.
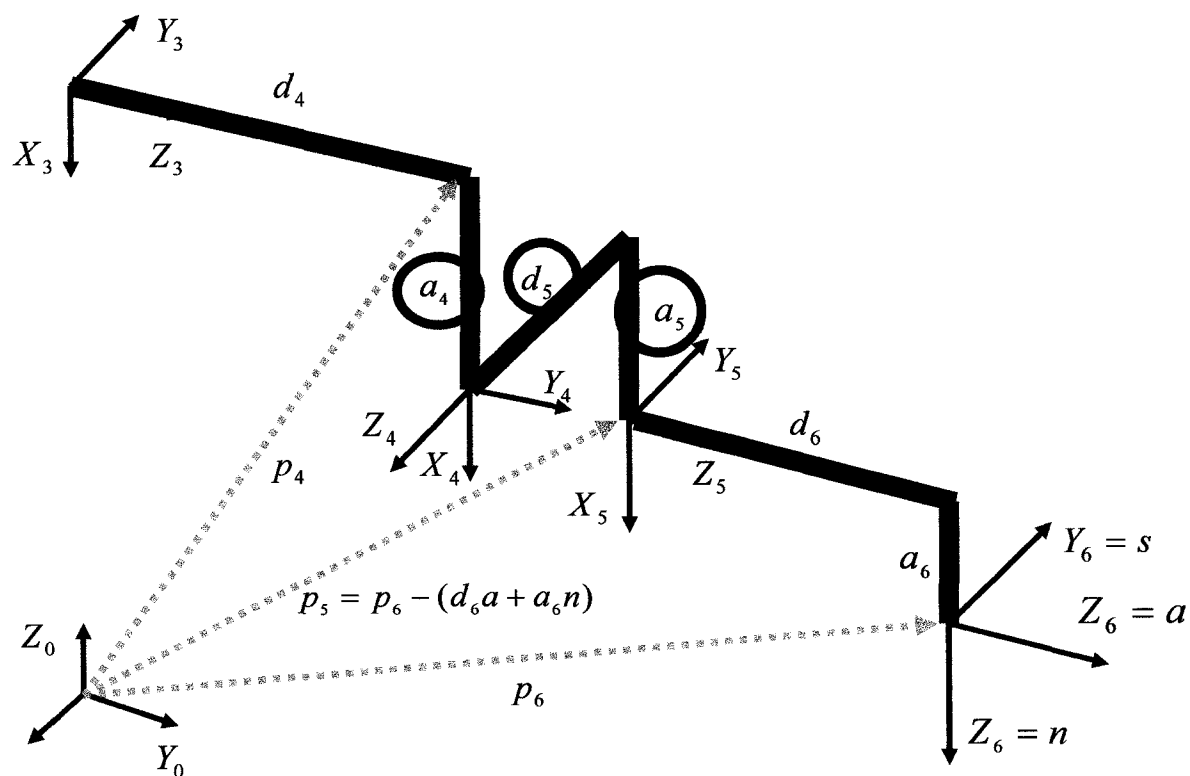
Figure 7.1: Robot offset wrist

The proposed D-H parameters with the ability to add three model parameters are presented in Table 7.1.

134

Table 7.1: D-H Parameters for robots with offset wrists

Joint	θ_i	d_i	a_i	α_i
1	θ_1	d_1	a_1	$\pm 90°$
2	θ_2	d_2	a_2	$\pm 180°;0$
3	θ_3	d_3	a_3	± 90
4	θ_4	d_4	a_4	± 90
5	θ_5	d_5	a_5	± 90
6	θ_6	d_6	a_6	$\pm 180°;0$

Additional kinematic calculations for this model will need to use the recursive numerical method proposed by Pashkevich A., 1997. Using this method the vector Z_4 can be calculated, which produces a value for d_5. To calculate a_4, vector X_4 must be calculated. This procedure is shown in the following equations:

$$Z_5 = Z_6 \cos \alpha_6 = aK_6 \tag{181}$$

$$X_5 = X_6 \cos \theta_6 = n \cos \theta_6 \tag{182}$$

$$Y_5 = Z_5 \times X_5 \tag{183}$$

$$Z_5 \parallel Y_4 \Rightarrow Y_4 = -Z_5 K_5 \tag{184}$$

$$X_4 = Y_4 \times Z_4 \tag{185}$$

Again using the recursive numerical method proposed by Pashkevich A., 1997, a_5 can be calculated. With these three solutions, the RPF model will be extended to all 6R robots with offset wrists.

The dynamic computation for this extended model requires more computational power than the average PC provides. Three new parameters will increase the computational complexity, but add more capability for modeling other robots.

135

A kinematics and dynamics model of rigid and elastic robotic systems was developed by Filipovic M., at al., (2007). Adding the elastic characteristics of the robot manipulator is possible future extension of the GPFDM+ model.

Using the idea of an integral manifold, a reduced-order model of the robot with flexible joints was derived. The controller was designed for the rigid robot model by corrective control to compensate the effects of the flexible joint (Spong M. W., at al., 1987).

The most important future step is to use a BlockBuilder for Simulink, for automatic translation of each robot link dynamics from MAPLE 10 code to Simulink Reconfigurable Robot Platform (RRP). This procedure will completely automate robot modeling and control.

One can say: "***From the robot physical model to the resulting controller is now one step, requiring only defining the robot and running the simulation***"!

The automatic robot plant and controller generation using the eight reconfigurable models and Block Builder for Simulink is graphically shown in Figure 7.2.

Block Builder for Simulink will be used to replace the manual input of the dynamic equations. This will minimize the time for robot plant development.
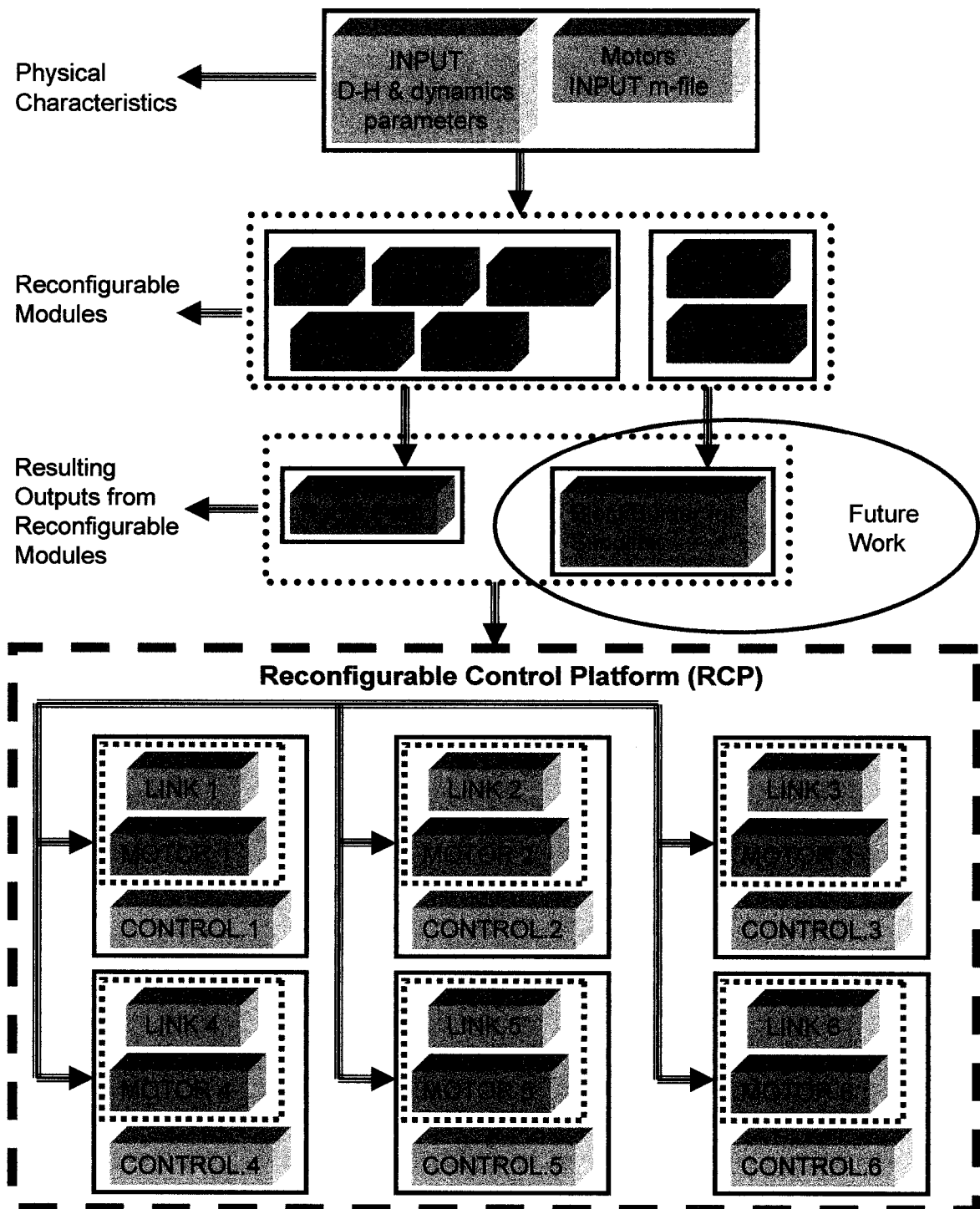
Figure 7.2: Automatic robot plant and control generation using Block Builder for Simulink

137

This process can also be reversed. Using the reconfigurable kinematic, dynamic and control modules, new reconfigurable machines can be produced. Using the developed modules for designing new reconfigurable automated machines, allows them to perfectly match a new environment. The Meta model of a reconfigurable robot can be built such that it satisfies all kinematic characteristics of the previously developed unified model. This means that each joint has the ability to easily change its positive direction and to increase or decrease links lengths and offsets. This research is a bridge between current industrial practice and future global trends. See Figure 7.3.
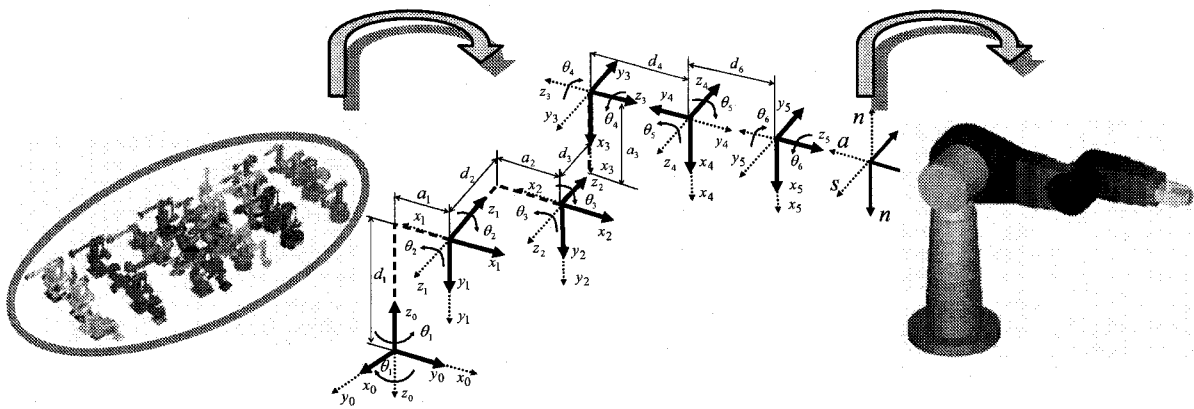
Figure 7.3: Bridge between current industrial practices and future global trends

The reconfigurable modules can be used for a current manufacturing system and for the future reconfigurable industry. This methodology can be applied to any automated machine, to develop reconfigurable modules and reconfigurable machines.

138

CHAPTER EIGHT

8. CONCLUSIONS

From the industrial experience in the Flow Software Technologies, and literature review, most of the simulation and off-lining programming software packages are designed to provide only robot kinematic. The inverse kinematic solution is done separately for a single group of robots. These software systems usually have library of some robots, and if the user needs a new robot they have the option to buy it or to model it from scratch. This process is often complex and tedious. These simulation and off-lining programming software systems cannot be used to perform any reconfigurable control process. These problems are solved in this research providing a comprehensive basis for new reconfigurable control system called UROCA (Unified Reconfigurable Open Control Architecture). Using the similarities between different robotic systems, a unified generic PUMA -Fanuc kinematic model has been developed. The generalized approach for systematic modeling and solving (UKMS) was used for modeling robots from the GPF group of robots and solving their direct and inverse kinematics.

For easy calculation of the Jacobian of different robotic systems, the Reconfigurable PUMA -Fanuc Jacobian Matrix (RPFJM) was developed. The computation was done using the recursive Newton-Euler method and many trigonometric simplifications. This procedure was done first manually, which helps to get simplified and organized results. Maple 10 ® software was subsequently used for the computation and validation of the results. The Jacobian matrix was developed earlier for this PUMA model, (Leathy M. B., *et al.*, 1987). This example is used to prove the validity of the RPFJM, and all elements are in Appendix B. Similarly another example was done for Fanuc model and all elements are presented in Appendix C.

139

By decoupling the (RPFJM) matrix, the Reconfigurable PUMA -Fanuc Singularity Matrix (RPFSM) was developed. This module was computed using the combination of two methods: recursive Newton-Euler method and the simple vector cross product method. The RPFSM was tested for the PUMA robots and the results were compared with the literature (Cheng F. T., *et al.*, 1997), (Oenny D., *et al.*, 2000), and (Yuan J., 2001). This comparison shown validity of the RPFSM model. Two examples are shown in Appendix E and Appendix F.

The calculation of robot the work envelope was done using the reconfigurable modeling approach. The 2D and 3D boundary workspace was created using the specially developed method called Filtering Boundary Points (FBP). This model was named Reconfigurable Robot Workspace (RRW).

Applying directly the recursive Newton-Euler method for computing the dynamics of the RPF model without any simplifications and output organization produced a result that need manual organization of the mass matrix A, matrix of Coriolis torque B, matrix of centrifugal torque C, and vector of gravity torque G. The needed manual organization and calculation procedure is extremely difficult and almost impossible. Such calculation requires expensive computational facilities. These problems are solved in this research by using the new developed Automatic Separation Method (ASM). This method avoids calculation complexity and reaches the final goal of the dynamic equation. Therefore it was possible to develop a feasible calculation of direct and inverse dynamics of different robotic systems using the Generic PUMA -Fanuc Dynamic Model (GPFDM). Using trigonometric simplification rules the general dynamic model was reduced further. The physical simplification conditions were not implemented because of the differences between robotic systems, but they can easily be added according to the user needs. Using the automatic generation method (ASM), each element of the mass matrix A, matrix of Coriolis torque B, matrix of centrifugal torque C, and vector of gravity torque G is produced. This model is extended to incorporate the

140

robotic actuator dynamics. Coupling GPFDM and dynamics of the motors the complete electro-mechanical model named GPFDM+ is presented.

The design of Reconfigurable Control Platform (RCP) for PUMA 560 and sizing of DC motors were provided in detail. For the RCP the different control strategies were used for controller development of joint position control. The best result was produced with reconfigurable "PI" controller for joint position control. This controller was designed as a function of robot motor parameters. Simulation was done using Matlab/Simulink ® software.

The RPF model and its seven solutions: UKMS (Unified Kinematic Modeler and Solver), RGPFJM (Reconfigurable Generic PUMA -Fanuc Jacobian Matrix), RPFSM (Reconfigurable PUMA -Fanuc Singularity Matrix), RRW (Reconfigurable Robot Workspace), RPFDM (Reconfigurable PUMA -Fanuc Dynamic Model), RPFDM+ (Reconfigurable PUMA -Fanuc Dynamic Model Plus) and RCP (Reconfigurable Control Platform) are graphically shown in Figure 8.1.
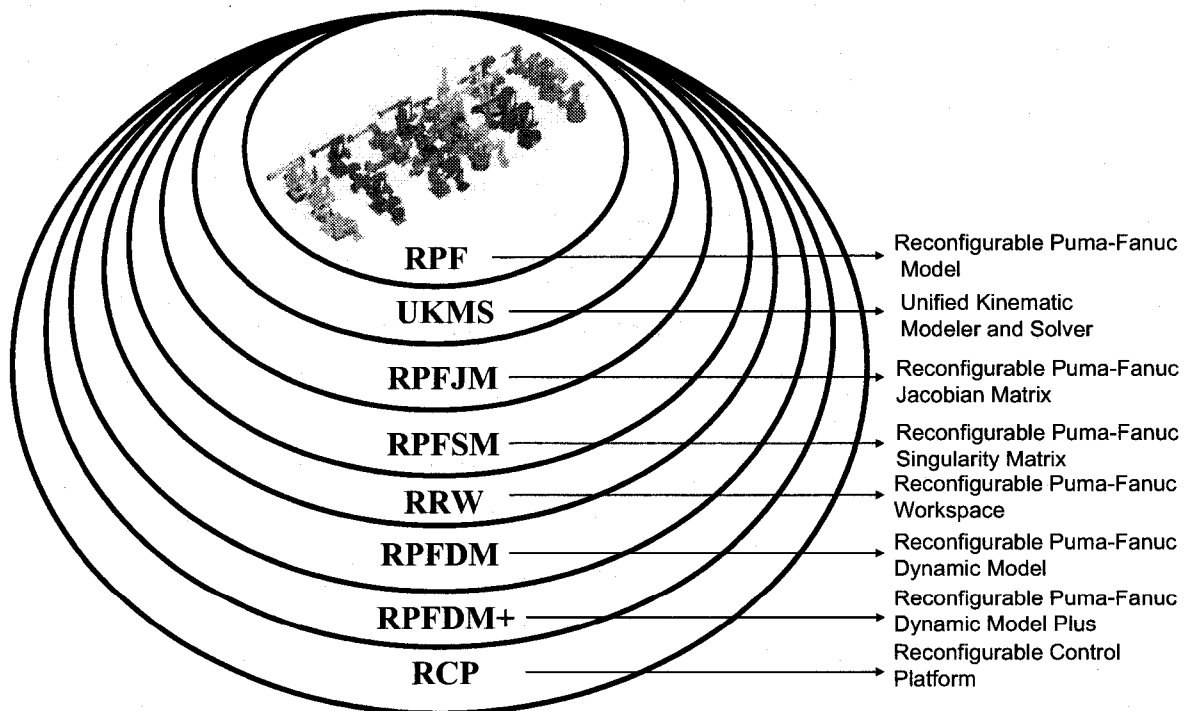

Figure 8.1: The GPF model and its seven reconfigurable solutions

141

For all eight reconfigurable modules different examples were performed. The examples of ABB IRB1400 and Fanuc ARCMate120iL robots were used to show the capability of UKMS and verify inverse kinematic results. The same robots were used for showing the capability of RRW model. For the validation of RPFDM, RPFDM+, and RCP a PUMA 560 robot was used.

All eight reconfigurable modules can be reconfigured by changing configuration parameters K_1, K_2, K_3, K_4, K_5, and K_6.

The results of the various analyses conducted in this research proved the thesis and the advantages of modeling robots and manufacturing systems using the "Unified Reconfigurable Open Control Architecture" (UROCA) philosophy. This was demonstrated for kinematics, dynamics and control of "PUMA -Fanuc" like structures.

The globalization of industry means that customers and production will commonly exist worldwide. To support this new trend, development of new machines and software, that will be quickly and easily changeable and adaptable to satisfy new customer needs, can be achieved by applying a reconfigurable methodology, as presented in this work. Using the developed reconfigurable kinematic, dynamic and control modules, the new reconfigurable machines can be produced so that they perfectly match in a new environment. Building a meta model of a reconfigurable robot can be achieved by using entirely developed reconfigurable modules.

This research is a bridge between current industrial practices and future global trends. The reconfigurable modules can be used for a current manufacturing system and for the future reconfigurable industry.

REFERENCES

Abdel-Malek K., Yeh Haran-Jou and Khairaliah N., (1999), "Workspace, Void, and Volume Determinantion of the General 5DOF Manipulator", Mechanical Structures and Mechanisms, Vol. 27, No. 1, pp. 89-115.

Abdel-Malek K., Yeh Haran-Jou, and Othman S., (2000), "Interior and Exterior Boundaries to the Workspace of Mechanical Manipulator", Robotics and Computer Integrated Manufacturing, Vol. 16, pp. 365-376.

Armstrong B., Oussama K., and Burdick J., (1986), "The Explicit Dynamic and Inertia Parameters of the PUMA 560 Arm", International Conference on Robotics and Automation, pp. 510-518.

Anderson J. R., (1990), "Dynamic damping control: implementation issues and simulation results", IEEE International Conference on Robotics and Automation, Vol. 1, pp. 68-77.

Anderson J. R. and Spong M. W., (1988), "Hybrid impedance control of robotic manipulators", IEEE International Conference on Robotics and Automation, Vol.4, pp. 1073-80.

Anon. (1999), Igrip Deneb; help file.

Burdick J. W., (1986), "An Algorithm for Generation of Efficient Manipulator Dynamic Equations", IEEE International Conference on Robotics and Automation, vol. 3, pp. 212-218.

Benhabib B., Zak G., and Lipton M.G., (1989), "A generalized kinematic modeling method for modular robots," Journal of Robotic Systems Vol.6, No.5, pp.545-571.

Balkan M. T., Ozgoren M. A. K., Arikan S., and Baykurt H. M., (2001), "A kinematic structure-based classification and compact equations for six-dof industrial robotic manipulators", Mechanism and Machine Theory Vol. 36, pp. 817-832.

Balkan M. T., Ozgoren M. A. K., Arikan S., and Baykurt H. M., (2000), "A method of inverse kinematics solution including singular and multiple configurations for a class of robotic manipulators", Mechanism and Machine Theory Vol.35, pp.1221-1237.

Bekir K. and Serkan A., (2000), "An improved approach to the solution of inverse kinematics problems for robot manipulators", Engineering Application of Artificial Intelligence Vol.13, pp.159-164.

Corke P. I. (1998), "A Symbolic and Numeric Procedure for Manipulator Rigid-Body Dynamic Significance Analysis and Simplification", Robotica, Vol. 16, Iss. 5, pp. 589-594.

Corke P. I., and Armstrong B., (1995), "A meta-study of PUMA 560 dynamics: A critical appraisal of literature data", Robotica, Vol. 13, pp. 253-258.

Corke P. I., and Armstrong B., (1994), "A Search for Consensus Among Model Parameters Reported for the PUMA 560 Robot", Proc. IEEE Conf. Robotics and Automation, pp. 1608-1613.

Corke P. I., (1994), "The Unimation PUMA servo system", MTM-226 report, CSIRO Division of Manufacturing Technology, Australia.

Ceccarelli M., and Vinciguerra A., (1995), "On the Workspace of the General 4R Manipulators", The International Journal of Robotics Research, Vol. 14, No. 2, pp. 152-160.

Ceccarelli M., (1996), "A Formulation for the Workspace Boundary of General N-revolute Manipulators", Mechanisms and Machine Theory, Vol. 31, No. 5, pp. 637-646.

144

Chen I. M. and Yang G., (1996), "Configuration Independent Kinematics for Modular Robots," Proc. IEEE Int'l Conf. Robotics and Automation, Minneapolis, MN, pp.1440-1445.

Chapelle F., and Bidaud P., (2001), "A Closed Form for Inverse Kinematics Approximation of General 6R Manipulators using Genetic Programming", IEEE International Conference on Robotics and Automation, Seoul, Korea, pp. 3364-3369.

Cheng F. T., Tzung-Liang H., York-Yin S., and Tsing-Hua C. (1997), "Study and Resolution of Singularities for a 6-DOF PUMA Manipulators", IEEE Transactions on Systems, Man, and Cybernetics-part B: Cybernetics, Vol. 27, No. 2, pp.332-343.

Djuric A. M., (1999), "Economical Industrial Workcell Modeling Simulation and Layout Design"; Master Thesis, University of Windsor; Windsor, Canada.

Djuric A. M. and ElMaraghy W. H., (2006), "Generalized Reconfigurable 6-Joint Robot Modeling", Transactions of the CSME, vol. 30, no. 4, pp. 533-565.

Djuric A. M. and ElMaraghy W. H., (2007), "A Unified Reconfigurable Robots Jacobian", Proc. of the 2nd Int. Conf. on Changeable, Agile, Reconfigurable and Virtual Production pp. 811-823.

Djuric A. M., (2007), "Reconfigurable MAPLE 10® Program for Calculation of the 6R - Joint Robot Dynamics", Industrial and Manufacturing (IMS) Center , University of Windsor, Technical Document number 2007-01.

Dixon W. E., Moses D., Walker I. D., and Dawson D. M., (2001), "A Simulink-Based Robotic Toolkit for Simulation and Control of the PUMA 560 Robot Model", IEEE International Conference on Intelligent Robots and Systems, pp. 2202-2207.

Denavit J. and Hartenberg R. S, (1955), "A kinematic notation for lower-pair mechanisms based on matrices", Journal of Applied Mechanics Vol. 77, pp. 215-221.

ElBeheiry E. M., ElMaraghy W., and ElMaraghy H., (2004), "The structured design of a reconfigurable control process", Proc. 14th International CIRP Design Seminar, Cairo, Egypt

Electro-Craft Corp., (1973), DC Motors, Speed Controls, Servo Systems, Second Edition .

Featherstone R., and Orin D., (2000), "Robot Dynamics: Equations and Algorithms", IEEE Int. Conf. Robotics & Automation Magazine, vol. 1, pp. 826-834.

Fu K. S., Gonzalez R.C., and Lee C.S.G., (1987), "Robotics: control, sensing, vision, and intelligence", McGraw-Hill Inc., pp.12-82.

Fischer I.S., (2000), "A geometric method for determining joint rotations in the inverse kinematics of robotic manipulators", Journal of Robotic Systems Vol.17, No.2, pp.107-117.

Fu H., Yang L. and Zhou C., (1998), "A computer-aided geometric approach to inverse kinematics", Journal of Robotic Systems Vol.15, No.3, pp.131-143.

Fu H., Yang L. and Zhang J., (2000), "A set of geometric invariants for kinematic analysis of 6R manipulators", The International Journal of Robotics Research Vol.19, No.8, pp.784-792.

Fijany A. and Antal K. Bejczy (1988), "Efficient Jacobian Inversion for the Control of Simple Robot Manipulators", IEEE, Vol., No., pp. 999-1007.

Filipovic M., Potkonjak V. and Vukobratovic M., (2007), "Humanoid robotic system with and without elasticity elements walking on an   immobile/mobile platform", Journal of Intelligent & Robotic Systems, Vol. 48, pp. 157–186.

Gu Y. L. and Ho J. S., (1990), "A Unified Kinematic Presentation and its Application to Robot Control", IEEE, pp. 98-103.

Gogu G. (2002), "Families of 6R orthogonal robotic manipulators with only isolated and pseudo-isolated singularities", Mechanism and Machine Theory, Vol. 37, No. 11, pp.1347-1375.

Goldenberg A. A. and Chan L., (1988), "An Approach to Real-Time Control of Robots in Task Space. Application to Control of PUMA   560 Without VAL-II", IEEE Transactions on Industrial Electronics, Vol. 35, No. 2, pp. 231-238.

Groover P. M., (1987) "Automation, Production Systems, and Computer-Integrated manufacturing" Printed and published by the Prentice-Hall Inc., Englewood Cliffs, New Jersey.

Hansen J. A., Gupta K. C., and Kazerounian S. M. K., (1983), "Generation and Evaluation of the Workspace of a Manipulator", The International Journal of Robotics Research, Vol. 2, No. 3, pp. 22-31.

Hayes M. J. D., Husty M. L., and Zsombor-Murray P. J. (2002), "Singular Configurations of Wrist-Partitioned 6R Serial Robots: a Geometric Perspective for Users", Transactions, Canadian Society of Mechanical Engineers, Vol. 26, No. 1, pp.41-55.

Her M. G., Chen C. Y., Hung Y. C., Karkoub M., (2002), "Approximating a Robot Inverse Kinematics Solution Using Fazzy Logic Tuned by Genetic Algorithms", International Journal of Advanced Manufacturing Technology Vol.20, No.5, pp. 375-380.

Hsia T. C., Lasky T. A., and Guo Z. Y., (1988), "Robust Independent Robot Joint Control: Design and Experimentation", IEEE Robotics and Automation, Vol.3, pp. 1329-1334.

Izaguirre A., Minoru H., Richard P. P., Vincent H., (1992), "A New Computational Structure for Real-Time Dynamics", The International Journal of Robotics Research, Vol. 11, No. 4, pp. 346-361.

Ju M. S., and Mansour J. M., (1989), "Comparison of Methods for Developing the Dynamics of Rigid Body Systems", The International Journal of Robotic Research, Vol. 8, No. 6, pp. 19-27.

Kelmar L. and Khosla P., (1988), "Automatic generation of kinematics for a reconfigurable modular manipulator system", Proceedings of IEEE Conference on Robotics and Automation, Philadelphia, PA, pp.663-668.

Kohil D., and Spanos J., (1985), "Workspace Analysis of Mechanical Manipulators Using Polynomial Discriminants", Transaction of ASME, Journal of Mechanisms, and Automation Design, Vol. 107, pp. 209-215.

Kohil D., and A. H. Soni, (1975), "Kinematic analysis of spatial mechanisms via successive screw displacements", ASME Journal of Engineering for Industry 2(B), pp.739-747.

Katupitiya J., Radajewski R., Sanderson J., Tordon M., (1997), "Implementation of a PC Based Controller for a PUMA Robot", Mechatronics and Machine Vision in Practice, IEEE, pp. 14-19.

Kokotovic V., Grabowski J., Amin V., and Lee J., (1999) "Electro Hydraulic Power Steering System", SAE Technical Papers, Document Number: 1999-01-0404.

Kwon S. J., Youm Y.I, and Wan Kyun Chung, (1991), "General Algorithm for Automatic Generation of the Workspace for N-link Redundant Manipulators", IEEE, Vol. 2, pp. 1722-1725.

148

Leva A., and Bascetta L., (2006), "On the design of the feed forward compensator in two-degree-of-freedom controllers", Mechatronics, Vol. 16, pp. 533-546.

Leathy M. B., Nugent Jr. M., Valavanis K. P., and Saridis G. N., (1986), "Efficient Dynamic for a PUMA -600", Vol. 3, pp. 519- 524, IEEE.

Leathy M. B., Nugent Jr. L. M., Saridis G. N., and Valavanis K. P. (1987), "Efficient PUMA Manipulator Jacobian Calculation and Inversion", Journal of Robotic Systems, Vol. 4, No. 2, pp.185-197.

Legnani G., Casolo F., Righettini P. and Zappa B., (1996) "A homogeneous matrix approach to 3D kinematics and dynamics – I. theory", Mechanism and Machine Theory Vol.31, No.5, pp. 573-587.

Legnani G., F. Casolo, P. Righettini and B. Zappa, (1996), "A homogeneous matrix approach to 3D kinematics and dynamics –II. Theory", Applications to chains of rigid bodies and serial manipulators, Mechanism and Machine Theory, Vol.31, No.5, pp. 589-605.

Lee C. S. G., and Ziegler M., (1984), "A geometric approach in solving the inverse kinematics of PUMA robots", IEEE Transactions on Aerospace and Electronic Systems Vol.20, No.6, pp. 695-706.

Manseur R. and Doty K. L., (1996), "Structural kinematics of 6Revolute-axis robot manipulators", Mechanism and Machine Theory Vol.31, No.5, pp.647-657.

Manseur R. and Doty K. L., (1992) "Fast inverse kinematics of five-revolute-axis robot manipulators", Mechanism and Machine Theory Vol.27, No.5, pp. 587-5977.

Manseur R. and Doty K. L., (1989), "A robot manipulator with 16 real inverse kinematics solutions sets", The International Journal of Robotics Research Vol.8, No.5, pp. 75-79.

Manseur R. and Doty K. L., (1988), "A fast algorithm for inverse kinematic analysis of robot manipulators", The International Journal of Robotics Research Vol.7, No.3, pp.52-63.

Matsumaru T., (1995), "Design and Control of the Modular Robot System: TOMMS", IEEE International Conference on Robotics and Automation, Nagoya, Japan, pp.2125-2131.

Moreira N., Alvito P. and Lima P., (1996), "First Step Towards an Open Control architecture for a PUMA 560", Proceedings of the CONTROLO, 2nd. Portuguese Conf. on Automatic Control.

Nof S. Y., "Handbook of Industrial Robotics", Second Edition, New York: John Wiley & Sons, 1999.

Nathery J. F. and Spong M., (1994), "Robotica: A Mathematica package for Robot Analysis", IEEE Robotics & Automation Magazine, Vol. 1, Iss. 1, pp.13-20.

Nagy P. V., (1988), "The PUMA 560 Industrial Robot: Inside-Out", Robots 12, pp. 4-67.

Orin D. E. and Schrader W. W. (1984), "Efficient Computation of the Jacobian for Robot Manipulators", The International Journal of Robotics Research, Vol. 3, No. 4, pp. 66-75.

Oenny D., Marcelo H. A., and Ser Y. L. (2000), "Singularity Handling on PUMA in Operational Space Formulation", Transactions, Canadian Society of Mechanical Engineers, ISER, pp. 491-500.

Owens J. P., (1994), "Workspace, A Microcomputer Industrial Robot Simulator and off Line Programming System", Next Steps for Industrial Robotics, IEE Colloquium, The Institution of Electrical Engineers, London, UK.

Owens J. P., (1990), "Industrial Robot Simulation", Ph. D. dissertation, Department of Electrical and Electronic Engineering, University of Newcastle Upon Tyne, UK.

Pieper D. L, (1968), "The kinematics of manipulators under computer control", Ph.D. dissertation, Dept. of Mechanical Engineering, Stanford University.

Pennock G. R. and Yang A. T., (1985), "Application of dual-number matrices to the inverse kinematics problem of robot manipulators", ASME Journal of Mechanisms, Transmissions and Automation in Design Vol.107, pp.201-208.

Park H. S., and Cho H. C., (1991), "General Design Conditions for an Ideal Robotic Manipulator Having Simple Dynamics", The International Journal of Robotics Research, Vol. 10, No. 1, pp. 21-29.

Palaz H., Kurugollu F. and Bucak I. O., (1993), "Parallel Processing of the Newton-Euler Equations of Robot Arm Motion on a Network of TMS320C25 Processors", Conference Proceedings, ISIE'93 - Budapest, IEEE International, pp. 352-357.

Pashkevich A., (1997), "Real-time inverse kinematics for robots with offset and reduced wrist", Control Engineering Practice, Vol.5, No.10, pp.1443-1450.

Paul P. R., (1981), "Robot manipulator: mathematics, programming and control", MIT Press, Cambridge, MA.

Podhorodeski R. P. and Nokleby S. B., (2000), "Reconfigurable Main-Arm for Assembly of all Revolute-only KS Branches," J. of Robotic Systems, Vol. 17, No. 7, pp. 365-373.

Rajagopalan R., (1996), "Distributed Computation of Inverse Dynamics of Robots", IEEE Comput. Soc. Press., pp. 106-112.

151

Sokolov A. and Sandor J. Toth, (1999), "New Approach of Dynamic simulation of PUMA 560 Implemented in LabVIEW", Periodica Polytechica Ser. Mech. Eng., Vol. 43, No. 2, pp. 121-130.

Spanos J., and Kohil D., (1985), "Workspace Analysis of Regional Structures of Manipulators", Transaction of ASME, Journal of mechanisms, and Automation Design, Vol. 107, pp. 216-222.

Spong M. W. and Vidyasagar M. (1989), "Robot Dynamics and Control", J. Wiley and Son, New York.

Spong M. W., Khorasani K., Kokotovic Petar V., (1987), "An Integral Manifold Approach to the Feedback Control of Flexible Joint Robots", IEEE Journal of Robotic and Automation, Vol. RA-3, No. 4, pp. 291-300.

Shaik M. A. and Datreis P., (1986), "A Worksapce Optimization Approach to Manipulator Linkage Design", IEEE, pp. 75-81.

Tarn T., Bejczy A. K., Yun X., and Li Z., (1991), "Effect of Motor Dynamics on Nonlinear Feedback Robot Arm Control", IEEE Transactions on Robotics and Automation, Vol. 7, No. 1, pp. 114-122.

Tewari A., (2002), "Modern Control Design With Matlab and Simulink", John Wiley & Sons, Ltd.

Tourassis V. D. and Ang M. H. Jr, (1989), "A modular architecture for inverse robot kinematics", IEEE Transaction of Robotics and Automation Vol.5, No.5, pp.555-568.

Tourassis V. D. and Ang M. H. Jr, (1995), "Task decoupling in robot manipulators", Journal of Intelligent and Robotic Systems, Vol. 14, No. 3, pp.283-302.

Tsai L. W., (1985), "Solving the kinematics of the most general six-and five-degree-of freedom manipulators by continuation methods", ASME Journal of

Mechanisms, Transmissions and Automation in Design, Vol.107, No.2, pp.189-200.

Uicker J. J. Jr., Denavit J., and Hartenberg R. S., (1964), "An iterative method for the displacement analysis of spatial mechanisms", ASME, Journal of Applied Mechanics 31(E), pp. 309-314.

Vukobratovic M., Stokic D., Kircanski N., Kircanski M., Hristic D., Karan B., Vujic D., Djurovic M., (1986), "Introduction to Robotics", Institute "Mihailo Pupin", Belgrade, Serbia.

Vivas A., and Mosquera V., (2005), "Predictive Functional Control of a PUMA robot", ACSE Conference, 19-21 December 2005, CICC, Cairo, Egypt

Walker M. W., and Orin D. E., (1982), "Efficient Dynamic Computer Simulation of Robotic Mechanisms", Journal of Dynamic Systems, Measurement, and Control, Vol. 104, pp. 205-210.

Workspace 5®, User Manual, 2000.

Yang A. T., and R. Freudenstein, (1964), "Application of dual number quaternian algebra to the analysis of spatial mechanisms", ASME, Journal of Applied Mechanics, Vol. 31, Series E, pp. 152-157.

Yuan J. (2001), "Local SVD Inverse of Robot Jacobian", Robotica, Vol. 19, pp.79-86.

Yoshida K., Ikeda N., and Mayed H., (1992), "Experimental Study of the Identification Methods for an Industrial Robot Manipulator", IEEE/RSJ International Conference on Intelligent Robots and Systems, Vol. 1, pp. 236-270.

Yamakita M., Hoshino Y., Morimoto K., Furuta K., (1991), "Parallel Implementation of Newton-Euler Algorithm with One Step ahead Prediction", IEEE International Conference on Robotics and Automation, Vol. 2, pp. 1842-1849 .

Zhang H., and Sikka P., (1991), "Characterization of the Workspace for the Planar Robot Manipulator", IEEE, Vol. 1, pp. 158-161.

APPENDIX A: REDUCED RPFJM EQUATIONS

$$J_{11} = -K_1K_2K_3a_1 \sin\theta_4 \cos\theta_5 \cos\theta_6 + K_1K_2K_3K_4K_5a_1 \cos\theta_4 \sin\theta_6$$
$$-K_1K_2K_3a_2 \sin\theta_4 \cos\theta_4 \cos\theta_5 \cos\theta_6 + K_1K_2K_3K_4K_5a_2 \cos\theta_2 \cos\theta_4 \sin\theta_6$$
$$-K_1K_2K_3a_3 \cos(\theta_2 + K_2\theta_3)\sin\theta_4 \cos\theta_5 \cos\theta_6 + K_1K_4K_5d_6 \sin(\theta_2 + K_2\theta_3)\sin\theta_4 \cos\theta_6$$
$$+K_1d_2 \cos(\theta_2 + K_2\theta_3)\cos\theta_4 \cos\theta_5 \cos\theta_6 + K_1K_2K_3K_4d_2 \sin(\theta_2 + K_2\theta_3)\sin\theta_5 \cos\theta_6$$
$$+K_1K_4K_5d_2 \cos(\theta_2 + K_2\theta_3)\sin\theta_4 \sin\theta_6 + K_1K_2d_3 \cos(\theta_2 + K_2\theta_3)\cos\theta_4 \cos\theta_5 \cos\theta_6$$
$$+K_1K_3K_4d_3 \sin(\theta_2 + K_2\theta_3)\sin\theta_5 \cos\theta_6 + K_1K_2K_4K_5d_3 \cos(\theta_2 + K_2\theta_3)\sin\theta_4 \sin\theta_6$$
$$-K_1d_4 \sin(\theta_2 + K_2\theta_3)\sin\theta_4 \cos\theta_5 \cos\theta_6 + K_1K_4K_5d_4 \sin(\theta_2 + K_2\theta_3)\cos\theta_4 \sin\theta_6$$
$$-K_1d_6 \sin(\theta_2 + K_2\theta_3)\cos\theta_4 \cos\theta_5 \sin\theta_6 + K_1K_2K_3K_4d_6 \cos(\theta_2 + K_2\theta_3)\sin\theta_5 \sin\theta_6$$
$$+K_1K_2K_3K_4K_5a_3 \cos(\theta_2 + K_2\theta_3)\cos\theta_4 \sin\theta_6$$

$$J_{12} = K_2a_2 \sin\theta_3 \cos\theta_4 \cos\theta_5 \cos\theta_6 - K_2K_3K_4a_2 \cos\theta_3 \sin\theta_5 \cos\theta_6$$
$$+K_2K_4K_5a_2 \sin\theta_3 \sin\theta_5 \sin\theta_6 - K_2K_3K_4a_3 \sin\theta_5 \cos\theta_6 + K_2K_3d_4 \cos\theta_4 \cos\theta_5 \cos\theta_6$$
$$+K_2K_3K_4K_5d_4 \sin\theta_4 \sin\theta_6 - K_2K_3d_6 \sin\theta_4 \cos\theta_5 \sin\theta_6 - K_2K_3K_4K_5d_6 \cos\theta_4 \cos\theta_6$$

$$J_{13} = -K_3K_4a_3 \sin\theta_5 \cos\theta_6 + K_3K_4K_5d_4 \sin\theta_4 \sin\theta_6$$
$$+K_3d_4 \cos\theta_4 \cos\theta_5 \cos\theta_6 - K_3d_6 \sin\theta_4 \cos\theta_5 \sin\theta_6 - K_3K_4K_5d_6 \cos\theta_4 \cos\theta_6$$

$$J_{14} = -K_4d_6 \sin\theta_5 \sin\theta_6, J_{15} = K_5d_6 \cos\theta_6, J_{16} = 0$$

$$J_{21} = K_1K_2K_3K_4K_5K_6a_1 \cos\theta_4 \cos\theta_6 + K_1K_2K_3K_6a_1 \sin\theta_4 \cos\theta_5 \sin\theta_6$$
$$+K_1K_2K_3K_4K_5K_6a_2 \cos\theta_2 \cos\theta_4 \cos\theta_6 + K_1K_2K_3K_6a_2 \cos\theta_2 \sin\theta_4 \cos\theta_5 \sin\theta_6$$
$$+K_1K_2K_3K_4K_5K_6a_3 \cos(\theta_2 + K_2\theta_3)\cos\theta_4 \cos\theta_6$$
$$+K_1K_2K_3K_6a_3 \cos(\theta_2 + K_2\theta_3)\sin\theta_4 \cos\theta_5 \sin\theta_6$$
$$+K_1K_5K_6a_6 \cos\theta_4 \sin\theta_5 \sin(\theta_2 + K_2\theta_3) + K_1K_2K_3K_4K_5K_6a_6 \cos(\theta_2 + K_2\theta_3)\cos\theta_5$$
$$-K_1K_2K_3K_4K_6d_2 \sin(\theta_2 + K_2\theta_3)\sin\theta_5 \sin\theta_6$$
$$-K_1K_6d_2 \cos(\theta_2 + K_2\theta_3)\cos\theta_4 \cos\theta_5 \sin\theta_6$$
$$+K_1K_4K_5K_6d_2 \cos(\theta_2 + K_2\theta_3)\sin\theta_4 \cos\theta_6$$
$$-K_1K_2K_6d_3 \cos(\theta_2 + K_2\theta_3)\cos\theta_4 \cos\theta_5 \sin\theta_6$$
$$-K_1K_3K_4K_6d_3 \sin(\theta_2 + K_2\theta_3)\sin\theta_5 \sin\theta_6 + K_1K_2K_4K_6d_3 \cos(\theta_2 + K_2\theta_3)\sin\theta_4 \cos\theta_6$$
$$+K_1K_6d_4 \sin(\theta_2 + K_2\theta_3)\sin\theta_4 \cos\theta_5 \sin\theta_6 + K_1K_4K_5K_6d_4 \sin(\theta_2 + K_2\theta_3)\cos\theta_4 \cos\theta_6$$
$$-K_1K_6d_6 \sin(\theta_2 + K_2\theta_3)\cos\theta_4 \cos\theta_5 \cos\theta_6$$
$$+K_1K_2K_3K_4K_6d_6 \cos(\theta_2 + K_2\theta_3)\sin\theta_5 \cos\theta_6 - K_1K_4K_5K_6d_6 \sin(\theta_2 + K_2\theta_3)\sin\theta_4 \sin\theta_6$$

155

$$J_{22} = -K_2 K_6 a_2 \sin\theta_3 \cos\theta_4 \cos\theta_5 \sin\theta_6$$
$$+ K_2 K_3 K_4 K_6 a_2 \cos\theta_3 \sin\theta_5 \sin\theta_6 + K_2 K_4 K_5 a_2 \sin\theta_3 \sin\theta_4 \cos\theta_6$$
$$+ K_2 K_3 K_4 K_6 a_3 \sin\theta_5 \sin\theta_6 + K_2 K_3 K_5 K_6 a_6 \sin\theta_4 \sin\theta_5$$
$$+ K_2 K_3 K_4 K_5 d_4 \sin\theta_4 \cos\theta_6 - K_2 K_3 K_6 d_4 \cos\theta_4 \cos\theta_5 \sin\theta_6$$
$$- K_2 K_3 K_6 d_6 \sin\theta_4 \cos\theta_5 \cos\theta_6 + K_2 K_3 K_4 K_5 K_6 d_6 \cos\theta_4 \sin\theta_6$$

$$J_{23} = K_3 K_4 K_6 a_3 \sin\theta_5 \sin\theta_6 + K_3 K_5 K_6 a_6 \sin\theta_4 \sin\theta_5 - K_3 K_6 d_4 \cos\theta_4 \cos\theta_5 \sin\theta_6$$
$$+ K_3 K_4 K_5 K_6 d_4 \sin\theta_4 \cos\theta_6 - K_3 K_6 d_6 \sin\theta_4 \cos\theta_5 \cos\theta_6 + K_3 K_4 K_5 K_6 d_6 \cos\theta_4 \sin\theta_6$$

$$J_{24} = -K_4 K_5 K_6 a_6 \cos\theta_5 - K_4 K_6 d_6 \sin\theta_5 \cos\theta_6, J_{25} = -K_5 K_6 d_6 \sin\theta_6, J_{26} = K_6 a_6$$

$$J_{31} = -K_1 K_2 K_3 K_5 K_6 a_1 \sin\theta_4 \sin\theta_5 - K_1 K_2 K_3 K_5 K_6 a_2 \cos\theta_2 \sin\theta_4 \sin\theta_5$$
$$- K_1 K_2 K_3 K_5 K_6 a_3 \cos(\theta_2 + K_2\theta_3)\sin\theta_4 \sin\theta_5 + K_1 K_5 K_6 d_2 \cos(\theta_2 + K_2\theta_3)\cos\theta_4 \sin\theta_5$$
$$- K_1 K_2 K_3 K_4 K_5 K_6 d_2 \sin(\theta_2 + K_2\theta_3)\cos\theta_5 + K_1 K_2 K_5 K_6 d_3 \cos(\theta_2 + K_2\theta_3)\cos\theta_4 \sin\theta_5$$
$$- K_1 K_3 K_4 K_5 K_6 d_3 \sin(\theta_2 + K_2\theta_3)\cos\theta_5 - K_1 K_5 K_6 d_4 \sin(\theta_2 + K_2\theta_3)\sin\theta_4 \sin\theta_5$$
$$+ K_1 K_6 a_6 \sin(\theta_2 + K_2\theta_3)\cos\theta_4 \cos\theta_5 \sin\theta_6 - K_1 K_2 K_3 K_4 K_6 a_6 \cos(\theta_2 + K_2\theta_3)\sin\theta_5 \sin\theta_6$$
$$- K_1 K_4 K_5 K_6 a_6 \sin(\theta_2 + K_2\theta_3)\sin\theta_4 \cos\theta_6$$
$$J_{32} = K_2 K_5 K_6 a_2 \sin\theta_3 \cos\theta_4 \sin\theta_5 + K_2 K_3 K_4 K_5 K_6 a_2 \cos\theta_3 \cos\theta_5$$
$$+ K_2 K_3 K_4 K_5 K_6 a_3 \cos\theta_5 + K_2 K_3 K_6 a_6 \sin\theta_4 \cos\theta_5 \sin\theta_6 + K_2 K_3 K_4 K_5 K_6 a_6 \cos\theta_4 \cos\theta_6$$
$$+ K_2 K_3 K_5 K_6 d_4 \cos\theta_4 \sin\theta_5$$

$$J_{33} = K_3 K_4 K_5 K_6 a_3 \cos\theta_5 + K_3 K_6 a_6 \sin\theta_4 \cos\theta_5 \sin\theta_6 + K_3 K_4 K_5 K_6 a_6 \cos\theta_4 \cos\theta_6$$
$$+ K_3 K_5 K_6 d_4 \cos\theta_4 \sin\theta_5$$

$$J_{34} = K_4 K_6 a_6 \sin\theta_5 \sin\theta_6, J_{35} = -K_5 K_6 a_6 \cos\theta_6, J_{36} = 0$$

$$J_{41} = K_1 \sin(\theta_2 + K_2\theta_3)\cos\theta_4 \cos\theta_5 \cos\theta_6 - K_1 K_2 K_3 K_4 \cos(\theta_2 + K_2\theta_3)\sin\theta_5 \cos\theta_6$$
$$+ K_1 K_4 K_5 \sin(\theta_2 + K_2\theta_3)\sin\theta_4 \sin\theta_6$$

$$J_{42} = K_2 K_3 \sin\theta_4 \cos\theta_5 \cos\theta_6 - K_2 K_3 K_4 K_5 \cos\theta_4 \sin\theta_6$$

$$J_{43} = K_3 \sin\theta_4 \cos\theta_5 \cos\theta_6 - K_3 K_4 K_5 \cos\theta_4 \sin\theta_6,$$

$$J_{44} = K_4 \sin\theta_5 \cos\theta_6, J_{45} = K_5 \sin\theta_6, J_{46} = 0$$

$$J_{51} = -K_1 K_6 \sin(\theta_2 + \theta_3)\cos\theta_4 \cos\theta_5 \sin\theta_6$$
$$+ K_1 K_2 K_3 K_4 K_6 \cos(\theta_2 + K_2\theta_3)\sin\theta_5 \sin\theta_6 + K_1 K_4 K_5 K_6 \sin(\theta_2 + K_2\theta_3)\sin\theta_4 \cos\theta_6$$

$$J_{52} = -K_2 K_3 K_6 \sin\theta_4 \cos\theta_5 \sin\theta_6 - K_2 K_3 K_4 K_5 K_6 \cos\theta_4 \cos\theta_6$$

$$J_{53} = -K_3 K_6 \sin\theta_4 \cos\theta_5 \sin\theta_6 - K_3 K_4 K_5 K_6 \cos\theta_4 \cos\theta_6, J_{54} = -K_4 K_6 \sin\theta_5 \sin\theta_6$$

$$J_{55} = K_5 K_6 \cos\theta_6, J_{56} = 0$$

156

$$J_{61} = K_1 K_5 K_6 \sin(\theta_2 + K_2\theta_3)\cos\theta_4 \sin\theta_5 + K_1 K_2 K_3 K_4 K_5 K_6 \cos(\theta_2 + K_2\theta_2)\cos\theta_5$$

$$J_{62} = K_2 K_3 K_5 K_6 \sin\theta_4 \sin\theta_5 , J_{63} = K_3 K_5 K_6 \sin\theta_4 \sin\theta_5 , J_{64} = -K_4 K_5 K_6 \cos\theta_5$$

$$J_{65} = 0 , J_{66} = K_6$$

APPENDIX B: REDUCED RPJM EQUATIONS

$J_{11} = a_2 \sin\theta_4 \cos\theta_4 \cos\theta_5 \cos\theta_6 + a_2 \cos\theta_2 \cos\theta_4 \sin\theta_6$
$+ a_3 \cos(\theta_2 + \theta_3)\sin\theta_4 \cos\theta_5 \cos\theta_6 + a_3 \cos(\theta_2 + \theta_3)\cos\theta_4 \sin\theta_6$
$+ d_2 \cos(\theta_2 + \theta_3)\cos\theta_4 \cos\theta_5 \cos\theta_6 + d_2 \sin\theta_5 \cos\theta_6 + d_2 \cos(\theta_2 + \theta_3)\sin\theta_4 \sin\theta_6$
$+ d_4 \sin(\theta_2 + \theta_3)\sin\theta_4 \cos\theta_5 \cos\theta_6 + d_4 \sin(\theta_2 + \theta_3)\cos\theta_4 \sin\theta_6$
$+ d_6 \sin(\theta_2 + \theta_3)\cos\theta_4 \cos\theta_5 \sin\theta_6 + d_6 \cos(\theta_2 + \theta_3)\sin\theta_5 \sin\theta_6$
$+ d_6 \sin(\theta_2 + \theta_3)\sin\theta_4 \cos\theta_6$

$J_{12} = a_2 \sin\theta_3 \cos\theta_4 \cos\theta_5 \cos\theta_6 + d_4 \cos\theta_4 \cos\theta_5 \cos\theta_6 + a_2 \cos\theta_3 \sin\theta_5 \cos\theta_6$
$+ a_3 \sin\theta_5 \cos\theta_6 - a_2 \sin\theta_3 \sin\theta_5 \sin\theta_6 - d_4 \sin\theta_4 \sin\theta_6 - d_6 \sin\theta_4 \cos\theta_5 \sin\theta_6$
$+ d_6 \cos\theta_4 \cos\theta_6$

$J_{13} = d_4 \cos\theta_4 \cos\theta_5 \cos\theta_6 + a_3 \sin\theta_5 \cos\theta_6 - d_4 \sin\theta_4 \sin\theta_6 - d_6 \sin\theta_4 \cos\theta_5 \sin\theta_6$
$+ d_6 \cos\theta_4 \cos\theta_6$

$J_{14} = d_6 \sin\theta_5 \sin\theta_6$

$J_{15} = d_6 \cos\theta_6$

$J_{16} = 0$

$J_{21} = a_2 \cos\theta_2 \cos\theta_4 \cos\theta_6 - a_2 \cos\theta_2 \sin\theta_4 \cos\theta_5 \sin\theta_6 + a_3 \cos(\theta_2 + \theta_3)\cos\theta_4 \cos\theta_6$
$- a_3 \cos(\theta_2 + \theta_3)\sin\theta_4 \cos\theta_5 \sin\theta_6 - d_2 \sin(\theta_2 + \theta_3)\sin\theta_5 \sin\theta_6$
$+ d_2 \cos(\theta_2 + \theta_3)\cos\theta_4 \cos\theta_5 \sin\theta_6 + d_2 \cos(\theta_2 + \theta_3)\sin\theta_4 \cos\theta_6$
$- d_4 \sin(\theta_2 + \theta_3)\sin\theta_4 \cos\theta_5 \sin\theta_6 + d_4 \sin(\theta_2 + \theta_3)\cos\theta_4 \cos\theta_6$
$+ d_6 \sin(\theta_2 + \theta_3)\cos\theta_4 \cos\theta_5 \cos\theta_6 + d_6 \cos(\theta_2 + \theta_3)\sin\theta_5 \cos\theta_6$
$- d_6 \sin(\theta_2 + \theta_3)\sin\theta_4 \sin\theta_6$

$J_{22} = -a_2 \sin\theta_3 \cos\theta_4 \cos\theta_5 \sin\theta_6 - a_2 \cos\theta_3 \sin\theta_5 \sin\theta_6 - a_2 \sin\theta_3 \sin\theta_4 \cos\theta_6$
$- a_3 \sin\theta_5 \sin\theta_6 - d_4 \sin\theta_4 \cos\theta_6 - d_4 \cos\theta_4 \cos\theta_5 \sin\theta_6 - d_6 \sin\theta_4 \cos\theta_5 \cos\theta_6$
$- d_6 \cos\theta_4 \sin\theta_6$

$J_{23} = -a_3 \sin\theta_5 \sin\theta_6 - d_4 \cos\theta_4 \cos\theta_5 \sin\theta_6 - d_4 \sin\theta_4 \cos\theta_6 - d_6 \sin\theta_4 \cos\theta_5 \cos\theta_6$
$- d_6 \cos\theta_4 \sin\theta_6$

$J_{24} = d_6 \sin\theta_5 \cos\theta_6$

$J_{25} = -d_6 \sin\theta_6$

$J_{26} = 0$

158

$$J_{31} = a_2 \cos\theta_2 \sin\theta_4 \sin\theta_5 + a_3 \cos(\theta_2 + \theta_3)\sin\theta_4 \sin\theta_5 - d_2 \cos(\theta_2 + \theta_3)\cos\theta_4 \sin\theta_5$$
$$- d_2 \sin(\theta_2 + \theta_3)\cos\theta_5 + d_4 \sin(\theta_2 + \theta_3)\sin\theta_4 \sin\theta_5$$

$$J_{32} = a_2 \sin\theta_3 \cos\theta_4 \sin\theta_5 - a_2 \cos\theta_3 \cos\theta_5 - a_3 \cos\theta_5 + d_4 \sin\cos\theta_4 \sin\theta_5$$

$$J_{33} = d_4 \cos\theta_4 \sin\theta_5 - a_3 \cos\theta_5$$

$$J_{34} = 0$$

$$J_{35} = -K_5 K_6 a_6 \cos\theta_6$$

$$J_{36} = 0$$

$$J_{41} = -\sin(\theta_2 + \theta_3)\cos\theta_4 \cos\theta_5 \cos\theta_6 - \cos(\theta_2 + \theta_3)\sin\theta_5 \cos\theta_6 + \sin(\theta_2 + \theta_3)\sin\theta_4 \sin\theta_6$$

$$J_{42} = \sin\theta_4 \cos\theta_5 \cos\theta_6 + \cos\theta_4 \sin\theta_6$$

$$J_{43} = \sin\theta_4 \cos\theta_5 \cos\theta_6 + \cos\theta_4 \sin\theta_6$$

$$J_{44} = -\sin\theta_5 \cos\theta_6$$

$$J_{45} = \sin\theta_6$$

$$J_{46} = 0$$

$$J_{51} = \sin(\theta_2 + \theta_3)\cos\theta_4 \cos\theta_5 \sin\theta_6 + \cos(\theta_2 + \theta_3)\sin\theta_5 \sin\theta_6 + \sin(\theta_2 + \theta_3)\sin\theta_4 \cos\theta_6$$

$$J_{52} = -\sin\theta_4 \cos\theta_5 \sin\theta_6 + \cos\theta_4 \cos\theta_6$$

$$J_{53} = -\sin\theta_4 \cos\theta_5 \sin\theta_6 + \cos\theta_4 \cos\theta_6$$

$$J_{54} = \sin\theta_5 \sin\theta_6$$

$$J_{55} = \cos\theta_6$$

$$J_{56} = 0$$

$$J_{61} = -\sin(\theta_2 + \theta_3)\cos\theta_4 \sin\theta_5 + \cos(\theta_2 + \theta_3)\cos\theta_5$$

$$J_{62} = \sin\theta_4 \sin\theta_5$$

$$J_{63} = \sin\theta_4 \sin\theta_5$$

$$J_{64} = \cos\theta_5$$

$$J_{65} = 0$$

$$J_{66} = 1$$

$$J_{12} = -a_2 \sin\theta_3 \cos\theta_4 \cos\theta_5 \cos\theta_6 - d_4 \cos\theta_4 \cos\theta_5 \cos\theta_6 - a_2 \cos\theta_3 \sin\theta_5 \cos\theta_6$$
$$- a_3 \sin\theta_5 \cos\theta_6 + a_2 \sin\theta_3 \sin\theta_5 \sin\theta_6 + d_4 \sin\theta_4 \sin\theta_6 + d_6 \sin\theta_4 \cos\theta_5 \sin\theta_6$$
$$- d_6 \cos\theta_4 \cos\theta_6$$

$$J_{13} = d_4 \cos\theta_4 \cos\theta_5 \cos\theta_6 + a_3 \sin\theta_5 \cos\theta_6 - d_4 \sin\theta_4 \sin\theta_6 - d_6 \sin\theta_4 \cos\theta_5 \sin\theta_6$$
$$+ d_6 \cos\theta_4 \cos\theta_6$$

$$J_{14} = d_6 \sin\theta_5 \sin\theta_6$$

$$J_{15} = d_6 \cos\theta_6$$

$$J_{16} = 0$$

$$J_{21} = -a_1 \cos\theta_4 \cos\theta_6 + a_1 \sin\theta_4 \cos\theta_5 \sin\theta_6 - a_2 \cos\theta_2 \cos\theta_4 \cos\theta_6$$
$$+ a_2 \cos\theta_2 \sin\theta_4 \cos\theta_5 \sin\theta_6 - a_3 \cos(-\theta_2 + \theta_3)\cos\theta_4 \cos\theta_6$$
$$+ a_3 \cos(-\theta_2 + \theta_3)\sin\theta_4 \cos\theta_5 \sin\theta_6 - d_2 \sin(-\theta_2 + \theta_3)\sin\theta_5 \sin\theta_6$$
$$+ d_4 \sin(-\theta_2 + \theta_3)\sin\theta_4 \cos\theta_5 \sin\theta_6 - d_4 \sin(-\theta_2 + \theta_3)\cos\theta_4 \cos\theta_6$$
$$- d_6 \sin(-\theta_2 + \theta_3)\cos\theta_4 \cos\theta_5 \cos\theta_6 - d_6 \cos(-\theta_2 + \theta_3)\sin\theta_5 \cos\theta_6$$
$$+ d_6 \sin(-\theta_2 + \theta_3)\sin\theta_4 \sin\theta_6$$

$$J_{22} = a_2 \sin\theta_3 \cos\theta_4 \cos\theta_5 \sin\theta_6 + a_2 \cos\theta_3 \sin\theta_5 \sin\theta_6 + a_2 \sin\theta_3 \sin\theta_4 \cos\theta_6$$
$$+ a_3 \sin\theta_5 \sin\theta_6 + d_4 \sin\theta_4 \cos\theta_6 + d_4 \cos\theta_4 \cos\theta_5 \sin\theta_6 + d_6 \sin\theta_4 \cos\theta_5 \cos\theta_6$$
$$+ d_6 \cos\theta_4 \sin\theta_6$$

$$J_{23} = -a_3 \sin\theta_5 \sin\theta_6 - d_4 \cos\theta_4 \cos\theta_5 \sin\theta_6 - d_4 \sin\theta_4 \cos\theta_6 - d_6 \sin\theta_4 \cos\theta_5 \cos\theta_6$$
$$- d_6 \cos\theta_4 \sin\theta_6$$

$$J_{24} = d_6 \sin\theta_5 \cos\theta_6$$

$$J_{25} = -d_6 \sin\theta_6$$

$$J_{26} = 0$$

$$J_{31} = -a_1 \sin\theta_4 \sin\theta_5 - a_2 \cos\theta_2 \sin\theta_4 \sin\theta_5 - a_3 \cos(-\theta_2 + \theta_3)\sin\theta_4 \sin\theta_5$$
$$- d_4 \sin(-\theta_2 + \theta_3)\sin\theta_4 \sin\theta_5$$

$$J_{32} = -a_2 \sin\theta_3 \cos\theta_4 \sin\theta_5 + a_2 \cos\theta_3 \cos\theta_5 + a_3 \cos\theta_5 - d_4 \cos\theta_4 \sin\theta_5$$

$$J_{33} = d_4 \cos\theta_4 \sin\theta_5 - a_3 \cos\theta_5$$

$$J_{34} = 0$$

$$J_{35} = 0$$

$$J_{36} = 0$$

$$J_{41} = \sin(-\theta_2 + \theta_3)\cos\theta_4\cos\theta_5\sin\theta_6 + \cos(-\theta_2 + \theta_3)\sin\theta_5\cos\theta_6$$
$$- \sin(-\theta_2 + \theta_3)\sin\theta_4\sin\theta_6$$

$$J_{42} = -\sin\theta_4\cos\theta_5\cos\theta_6 - \cos\theta_4\sin\theta_6$$

$$J_{43} = \sin\theta_4\cos\theta_5\cos\theta_6 + \cos\theta_4\sin\theta_6$$

$$J_{44} = -\sin\theta_5\cos\theta_6$$

$$J_{45} = \sin\theta_6$$

$$J_{46} = 0$$

$$J_{51} = -\sin(-\theta_2 + \theta_3)\cos\theta_4\cos\theta_5\sin\theta_6 - \cos(-\theta_2 + \theta_3)\sin\theta_5\sin\theta_6$$
$$- \sin(-\theta_2 + \theta_3)\sin\theta_4\cos\theta_6$$

$$J_{52} = \sin\theta_4\cos\theta_5\sin\theta_6 - \cos\theta_4\cos\theta_6$$

$$J_{53} = -\sin\theta_4\cos\theta_5\sin\theta_6 + \cos\theta_4\cos\theta_6$$

$$J_{54} = \sin\theta_5\sin\theta_6$$

$$J_{55} = \cos\theta_6$$

$$J_{56} = 0$$

$$J_{61} = \sin(-\theta_2 + \theta_3)\cos\theta_4\sin\theta_5 - \cos(-\theta_2 + \theta_3)\cos\theta_5$$

$$J_{62} = -\sin\theta_4\sin\theta_5$$

$$J_{63} = \sin\theta_4\sin\theta_5$$

$$J_{64} = \cos\theta_5$$

$$J_{65} = 0$$

$$J_{66} = 1$$

APPENDIX D: REDUCED RECONFIGURABLE PUMA -

FANUC SINGULARITY MATRIX (RPFSM)

$$J_{11} = K_2 d_2 \cos(\theta_2 + K_2\theta_3)\cos\theta_4 \cos\theta_5 \cos\theta_6 + K_1 K_2 d_3 \cos(\theta_2 + K_2\theta_3)\cos\theta_4 \cos\theta_5 \cos\theta_6$$
$$- K_1 K_2 K_3 a_2 \sin\theta_4 \cos\theta_4 \cos\theta_5 \cos\theta_6 - K_1 K_2 K_3 a_3 \cos(\theta_2 + K_2\theta_3)\sin\theta_4 \cos\theta_5 \cos\theta_6$$
$$- K_1 d_4 \sin(\theta_2 + K_2\theta_3)\sin\theta_4 \cos\theta_5 \cos\theta_6 + K_1 K_2 K_3 K_4 d_2 \sin\theta_5 \cos\theta_6$$
$$+ K_1 K_3 K_4 d_3 \sin(\theta_2 + K_2\theta_3)\sin\theta_5 \cos\theta_6 + K_1 K_4 K_5 d_2 \cos(\theta_2 + K_2\theta_3)\sin\theta_4 \sin\theta_6$$
$$+ K_1 K_2 K_4 K_5 d_3 \cos(\theta_2 + K_2\theta_3)\sin\theta_4 \sin\theta_6 + K_1 K_2 K_3 K_4 K_5 a_1 \cos\theta_4 \sin\theta_6$$
$$+ K_1 K_2 K_3 K_4 K_5 a_2 \cos\theta_2 \cos\theta_4 \sin\theta_6 + K_1 K_2 K_3 K_4 K_5 a_3 \cos(\theta_2 + K_2\theta_3)\cos\theta_4 \sin\theta_6$$
$$+ K_1 K_4 K_5 d_4 \sin(\theta_2 + K_2\theta_3)\cos\theta_4 \sin\theta_6$$
$$J_{12} = K_2 a_2 \sin\theta_3 \cos\theta_4 \cos\theta_5 \cos\theta_6 + K_2 K_3 d_4 \cos\theta_4 \cos\theta_5 \cos\theta_6$$
$$- K_2 K_3 K_4 a_2 \cos\theta_3 \sin\theta_5 \cos\theta_6 - K_2 K_3 K_4 a_3 \sin\theta_5 \cos\theta_6 + K_2 K_4 K_5 a_2 \sin\theta_3 \sin\theta_5 \sin\theta_6$$
$$+ K_2 K_3 K_4 K_5 d_4 \sin\theta_4 \sin\theta_6$$

$$J_{13} = K_3 d_4 \cos\theta_4 \cos\theta_5 \cos\theta_6 - K_3 K_4 a_3 \sin\theta_5 \cos\theta_6 + K_3 K_4 K_5 d_4 \sin\theta_4 \sin\theta_6$$

$$J_{14} = 0$$

$$J_{15} = 0$$

$$J_{16} = 0$$

$$J_{21} = K_1 K_2 K_3 K_4 K_5 K_6 a_1 \cos\theta_4 \cos\theta_6 + K_1 K_2 K_3 K_6 a_1 \sin\theta_4 \cos\theta_5 \sin\theta_6$$
$$+ K_1 K_2 K_3 K_4 K_5 K_6 a_2 \cos\theta_2 \cos\theta_4 \cos\theta_6 + K_1 K_2 K_3 K_6 a_2 \cos\theta_2 \sin\theta_4 \cos\theta_5 \sin\theta_6$$
$$+ K_1 K_2 K_3 K_4 K_5 K_6 a_3 \cos(\theta_2 + K_2\theta_3)\cos\theta_4 \cos\theta_6$$
$$+ K_1 K_2 K_3 K_6 a_3 \cos(\theta_2 + K_2\theta_3)\sin\theta_4 \cos\theta_5 \sin\theta_6$$
$$- K_1 K_2 K_3 K_4 K_6 d_2 \sin(\theta_2 + K_2\theta_3)\sin\theta_5 \sin\theta_6 - K_1 K_6 d_2 \cos(\theta_2 + K_2\theta_3)\cos\theta_4 \cos\theta_5 \sin\theta_6$$
$$+ K_1 K_4 K_5 K_6 d_2 \cos(\theta_2 + K_2\theta_3)\sin\theta_4 \cos\theta_6 - K_1 K_2 K_6 d_3 \cos(\theta_2 + K_2\theta_3)\cos\theta_4 \cos\theta_5 \sin\theta_6$$
$$- K_1 K_3 K_4 K_6 d_3 \sin(\theta_2 + K_2\theta_3)\sin\theta_5 \sin\theta_6 + K_1 K_2 K_4 K_6 d_3 \cos(\theta_2 + K_2\theta_3)\sin\theta_4 \cos\theta_6$$
$$+ K_1 K_6 d_4 \sin(\theta_2 + K_2\theta_3)\sin\theta_4 \cos\theta_5 \sin\theta_6 + K_1 K_4 K_5 K_6 d_4 \sin(\theta_2 + K_2\theta_3)\cos\theta_4 \cos\theta_6$$
$$J_{22} = -K_2 K_6 a_2 \sin\theta_3 \cos\theta_4 \cos\theta_5 \sin\theta_6 + K_2 K_3 K_4 K_6 a_2 \cos\theta_3 \sin\theta_5 \sin\theta_6$$
$$+ K_2 K_4 K_5 a_2 \sin\theta_3 \sin\theta_4 \cos\theta_6 + K_2 K_3 K_4 K_6 a_3 \sin\theta_5 \sin\theta_6 + K_2 K_3 K_4 K_5 d_4 \sin\theta_4 \cos\theta_6$$
$$- K_2 K_3 K_6 d_4 \cos\theta_4 \cos\theta_5 \sin\theta_6$$
$$J_{23} = K_3 K_4 K_6 a_3 \sin\theta_5 \sin\theta_6 - K_3 K_6 d_4 \cos\theta_4 \cos\theta_5 \sin\theta_6 + K_3 K_4 K_5 K_6 d_4 \sin\theta_4 \cos\theta_6$$

$$J_{24} = 0$$

162

$J_{25} = 0$

$J_{26} = 0$

$J_{31} = -K_1 K_2 K_3 K_5 K_6 a_1 \sin\theta_4 \sin\theta_5 - K_1 K_2 K_3 K_5 K_6 a_2 \cos\theta_2 \sin\theta_4 \sin\theta_5$
$\qquad - K_1 K_2 K_3 K_5 K_6 a_3 \cos(\theta_2 + K_2\theta_3)\sin\theta_4 \sin\theta_5 + K_1 K_5 K_6 d_2 \cos(\theta_2 + K_2\theta_3)\cos\theta_4 \sin\theta_5$
$\qquad - K_1 K_2 K_3 K_4 K_5 K_6 d_2 \sin(\theta_2 + K_2\theta_3)\cos\theta_5 + K_1 K_2 K_5 K_6 d_3 \cos(\theta_2 + K_2\theta_3)\cos\theta_4 \sin\theta_5$
$\qquad - K_1 K_3 K_4 K_5 K_6 d_3 \sin(\theta_2 + K_2\theta_3)\cos\theta_5 - K_1 K_5 K_6 d_4 \sin(\theta_2 + K_2\theta_3)\sin\theta_4 \sin\theta_5$

$J_{32} = K_2 K_5 K_6 a_2 \sin\theta_3 \cos\theta_4 \sin\theta_5 + K_2 K_3 K_4 K_5 K_6 a_2 \cos\theta_3 \cos\theta_5 + K_2 K_3 K_4 K_5 K_6 a_3 \cos\theta_5$
$\qquad + K_2 K_3 K_5 K_6 d_4 \cos\theta_4 \sin\theta_5$

$J_{33} = K_3 K_5 K_6 d_4 \cos\theta_4 \sin\theta_5 + K_3 K_4 K_5 K_6 a_3 \cos\theta_5$

$J_{34} = 0$

$J_{35} = 0$

$J_{36} = 0$

$J_{41} = K_1 \sin(\theta_2 + K_2\theta_3)\cos\theta_4 \cos\theta_5 \cos\theta_6 - K_1 K_2 K_3 K_4 \cos(\theta_2 + K_2\theta_3)\sin\theta_5 \cos\theta_6$
$\qquad + K_1 K_4 K_5 \sin(\theta_2 + K_2\theta_3)\sin\theta_4 \sin\theta_6$

$J_{42} = K_2 K_3 \sin\theta_4 \cos\theta_5 \cos\theta_6 - K_2 K_3 K_4 K_5 \cos\theta_4 \sin\theta_6$

$J_{43} = K_3 \sin\theta_4 \cos\theta_5 \cos\theta_6 - K_3 K_4 K_5 \cos\theta_4 \sin\theta_6$

$J_{44} = K_4 \sin\theta_5 \cos\theta_6$

$J_{45} = K_5 \sin\theta_6$

$J_{46} = 0$

$J_{51} = -K_1 K_6 \sin(\theta_2 + \theta_3)\cos\theta_4 \cos\theta_5 \sin\theta_6 + K_1 K_2 K_3 K_4 K_6 \cos(\theta_2 + K_2\theta_3)\sin\theta_5 \sin\theta_6$
$\qquad + K_1 K_4 K_5 K_6 \sin(\theta_2 + K_2\theta_3)\sin\theta_4 \cos\theta_6$

$J_{52} = -K_2 K_3 K_6 \sin\theta_4 \cos\theta_5 \sin\theta_6 - K_2 K_3 K_4 K_5 K_6 \cos\theta_4 \cos\theta_6$

$J_{53} = -K_3 K_6 \sin\theta_4 \cos\theta_5 \sin\theta_6 - K_3 K_4 K_5 K_6 \cos\theta_4 \cos\theta_6$

$J_{54} = -K_4 K_6 \sin\theta_5 \sin\theta_6$

$J_{55} = K_5 K_6 \cos\theta_6$

$J_{56} = 0$

$J_{61} = K_1 K_5 K_6 \sin(\theta_2 + K_2\theta_3)\cos\theta_4 \sin\theta_5 + K_1 K_2 K_3 K_4 K_5 K_6 \cos(\theta_2 + K_2\theta_2)\cos\theta_5$

$J_{62} = K_2 K_3 K_5 K_6 \sin\theta_4 \sin\theta_5$

$$J_{63} = K_3 K_5 K_6 \sin\theta_4 \sin\theta_5$$

$$J_{64} = -K_4 K_5 K_6 \cos\theta_5$$

$$J_{65} = 0$$

$$J_{66} = K_6$$

164

APPENDIX E: REDUCED RECONFIGURABLE PUMA

SINGULARITY MATRIX

$J_{11} = d_2 \cos(\theta_2 + \theta_3) \cos\theta_4 \cos\theta_5 \cos\theta_6 + a_2 \sin\theta_4 \cos\theta_4 \cos\theta_5 \cos\theta_6$
$+ a_3 \cos(\theta_2 + \theta_3) \sin\theta_4 \cos\theta_5 \cos\theta_6 + d_4 \sin(\theta_2 + \theta_3) \sin\theta_4 \cos\theta_5 \cos\theta_6 + d_2 \sin\theta_5 \cos\theta_6$
$+ d_2 \cos(\theta_2 + \theta_3) \sin\theta_4 \sin\theta_6 + a_2 \cos\theta_2 \cos\theta_4 \sin\theta_6$
$+ a_3 \cos(\theta_2 + \theta_3) \cos\theta_4 \sin\theta_6 + d_4 \sin(\theta_2 + \theta_3) \cos\theta_4 \sin\theta_6$

$J_{12} = a_2 \sin\theta_3 \cos\theta_4 \cos\theta_5 \cos\theta_6 + d_4 \cos\theta_4 \cos\theta_5 \cos\theta_6$
$+ a_2 \cos\theta_3 \sin\theta_5 \cos\theta_6 + a_3 \sin\theta_5 \cos\theta_6 - a_2 \sin\theta_3 \sin\theta_5 \sin\theta_6 - d_4 \sin\theta_4 \sin\theta_6$

$J_{13} = d_4 \cos\theta_4 \cos\theta_5 \cos\theta_6 + a_3 \sin\theta_5 \cos\theta_6 - d_4 \sin\theta_4 \sin\theta_6$

$J_{14} = 0$

$J_{15} = 0$

$J_{16} = 0$

$J_{21} = a_2 \cos\theta_2 \cos\theta_4 \cos\theta_6 - a_2 \cos\theta_2 \sin\theta_4 \cos\theta_5 \sin\theta_6 + a_3 \cos(\theta_2 + \theta_3) \cos\theta_4 \cos\theta_6$
$- a_3 \cos(\theta_2 + \theta_3) \sin\theta_4 \cos\theta_5 \sin\theta_6 - d_2 \sin(\theta_2 + \theta_3) \sin\theta_5 \sin\theta_6$
$+ d_2 \cos(\theta_2 + \theta_3) \cos\theta_4 \cos\theta_5 \sin\theta_6 + d_2 \cos(\theta_2 + \theta_3) \sin\theta_4 \cos\theta_6$
$- d_4 \sin(\theta_2 + \theta_3) \sin\theta_4 \cos\theta_5 \sin\theta_6 + d_4 \sin(\theta_2 + \theta_3) \cos\theta_4 \cos\theta_6$

$J_{22} = -a_2 \sin\theta_3 \cos\theta_4 \cos\theta_5 \sin\theta_6 - a_2 \cos\theta_3 \sin\theta_5 \sin\theta_6$
$- a_2 \sin\theta_3 \sin\theta_4 \cos\theta_6 - a_3 \sin\theta_5 \sin\theta_6 - d_4 \sin\theta_4 \cos\theta_6 - d_4 \cos\theta_4 \cos\theta_5 \sin\theta_6$

$J_{23} = -a_3 \sin\theta_5 \sin\theta_6 - d_4 \cos\theta_4 \cos\theta_5 \sin\theta_6 - d_4 \sin\theta_4 \cos\theta_6$

$J_{24} = 0$

$J_{25} = 0$

$J_{26} = 0$

$J_{31} = a_2 \cos\theta_2 \sin\theta_4 \sin\theta_5 + a_3 \cos(\theta_2 + \theta_3) \sin\theta_4 \sin\theta_5 - d_2 \cos(\theta_2 + \theta_3) \cos\theta_4 \sin\theta_5$
$- d_2 \sin(\theta_2 + \theta_3) \cos\theta_5 + d_4 \sin(\theta_2 + \theta_3) \sin\theta_4 \sin\theta_5$

$J_{32} = a_2 \sin\theta_3 \cos\theta_4 \sin\theta_5 - a_2 \cos\theta_3 \cos\theta_5 - a_3 \cos\theta_5 + d_4 \cos\theta_4 \sin\theta_5$

$J_{33} = d_4 \cos\theta_4 \sin\theta_5 - a_3 \cos\theta_5$

$J_{34} = 0$

165

$J_{35} = 0$

$J_{36} = 0$

$J_{41} = -\sin(\theta_2 + \theta_3)\cos\theta_4 \cos\theta_5 \cos\theta_6 - \cos(\theta_2 + \theta_3)\sin\theta_5 \cos\theta_6 + \sin(\theta_2 + \theta_3)\sin\theta_4 \sin\theta_6$

$J_{42} = \sin\theta_4 \cos\theta_5 \cos\theta_6 + \cos\theta_4 \sin\theta_6$

$J_{43} = \sin\theta_4 \cos\theta_5 \cos\theta_6 + \cos\theta_4 \sin\theta_6$

$J_{44} = -\sin\theta_5 \cos\theta_6$

$J_{45} = \sin\theta_6$

$J_{46} = 0$

$J_{51} = \sin(\theta_2 + \theta_3)\cos\theta_4 \cos\theta_5 \sin\theta_6 + \cos(\theta_2 + \theta_3)\sin\theta_5 \sin\theta_6 + \sin(\theta_2 + \theta_3)\sin\theta_4 \cos\theta_6$

$J_{52} = -\sin\theta_4 \cos\theta_5 \sin\theta_6 + \cos\theta_4 \cos\theta_6$

$J_{53} = -\sin\theta_4 \cos\theta_5 \sin\theta_6 + \cos\theta_4 \cos\theta_6$

$J_{54} = \sin\theta_5 \sin\theta_6$

$J_{55} = \cos\theta_6$

$J_{56} = 0$

$J_{61} = -\sin(\theta_2 + \theta_3)\cos\theta_4 \sin\theta_5 + \cos(\theta_2 + \theta_2)\cos\theta_5$

$J_{62} = \sin\theta_4 \sin\theta_5$

$J_{63} = \sin\theta_4 \sin\theta_5$

$J_{64} = \cos\theta_5$

$J_{65} = 0$

$J_{66} = 1$

166

APPENDIX F: REDUCED RECONFIGURABLE FANUC

SINGULARITY MATRIX

$J_{11} = -a_2 \sin\theta_4 \cos\theta_4 \cos\theta_5 \cos\theta_6 - a_3 \cos(-\theta_2 + \theta_3)\sin\theta_4 \cos\theta_5 \cos\theta_6$
$- d_4 \sin(-\theta_2 + \theta_3)\sin\theta_4 \cos\theta_5 \cos\theta_6 - a_1 \cos\theta_4 \sin\theta_6 - a_2 \cos\theta_2 \cos\theta_4 \sin\theta_6$
$- a_3 \cos(-\theta_2 + \theta_3)\cos\theta_4 \sin\theta_6 - d_4 \sin(-\theta_2 + \theta_3)\cos\theta_4 \sin\theta_6$

$J_{12} = -a_2 \sin\theta_3 \cos\theta_4 \cos\theta_5 \cos\theta_6 - d_4 \cos\theta_4 \cos\theta_5 \cos\theta_6 - a_2 \cos\theta_3 \sin\theta_5 \cos\theta_6$
$- a_3 \sin\theta_5 \cos\theta_6 + a_2 \sin\theta_3 \sin\theta_5 \sin\theta_6 + d_4 \sin\theta_4 \sin\theta_6$

$J_{13} = d_4 \cos\theta_4 \cos\theta_5 \cos\theta_6 + a_3 \sin\theta_5 \cos\theta_6 - d_4 \sin\theta_4 \sin\theta_6$

$J_{14} = 0$

$J_{15} = 0$

$J_{16} = 0$

$J_{21} = -a_1 \cos\theta_4 \cos\theta_6 + a_1 \sin\theta_4 \cos\theta_5 \sin\theta_6 - a_2 \cos\theta_2 \cos\theta_4 \cos\theta_6$
$+ a_2 \cos\theta_2 \sin\theta_4 \cos\theta_5 \sin\theta_6 - a_3 \cos(-\theta_2 + \theta_3)\cos\theta_4 \cos\theta_6$
$- a_3 \cos(-\theta_2 + \theta_3)\sin\theta_4 \cos\theta_5 \sin\theta_6 + d_4 \sin(-\theta_2 + \theta_3)\sin\theta_4 \cos\theta_5 \sin\theta_6$
$- d_4 \sin(-\theta_2 + \theta_3)\cos\theta_4 \cos\theta_6$

$J_{22} = a_2 \sin\theta_3 \cos\theta_4 \cos\theta_5 \sin\theta_6 + a_2 \cos\theta_3 \sin\theta_5 \sin\theta_6 + a_2 \sin\theta_3 \sin\theta_4 \cos\theta_6$
$+ a_3 \sin\theta_5 \sin\theta_6 + d_4 \sin\theta_4 \cos\theta_6 + d_4 \cos\theta_4 \cos\theta_5 \sin\theta_6$
$J_{23} = -a_3 \sin\theta_5 \sin\theta_6 - d_4 \cos\theta_4 \cos\theta_5 \sin\theta_6 - d_4 \sin\theta_4 \cos\theta_6$

$J_{24} = 0$

$J_{25} = 0$

$J_{26} = 0$

$J_{31} = -a_1 \sin\theta_4 \sin\theta_5 - a_2 \cos\theta_2 \sin\theta_4 \sin\theta_5 - a_3 \cos(-\theta_2 + \theta_3)\sin\theta_4 \sin\theta_5$
$- d_4 \sin(-\theta_2 + \theta_3)\sin\theta_4 \sin\theta_5$

$J_{32} = -a_2 \sin\theta_3 \cos\theta_4 \sin\theta_5 + a_2 \cos\theta_3 \cos\theta_5 + a_3 \cos\theta_5 - d_4 \cos\theta_4 \sin\theta_5$

$J_{33} = d_4 \cos\theta_4 \sin\theta_5 - a_3 \cos\theta_5$

$J_{34} = 0$

$J_{35} = 0$

$J_{36} = 0$

$J_{41} = \sin(-\theta_2 + \theta_3)\cos\theta_4 \cos\theta_5 \cos\theta_6 + \cos(-\theta_2 + \theta_3)\sin\theta_5 \cos\theta_6 - \sin(-\theta_2 + \theta_3)\sin\theta_4 \sin\theta_6$

$J_{42} = -\sin\theta_4 \cos\theta_5 \cos\theta_6 - \cos\theta_4 \sin\theta_6$

$J_{43} = \sin\theta_4 \cos\theta_5 \cos\theta_6 + \cos\theta_4 \sin\theta_6$

$J_{44} = -\sin\theta_5 \cos\theta_6$

$J_{45} = \sin\theta_6$

$J_{46} = 0$

$J_{51} = -\sin(-\theta_2 + \theta_3)\cos\theta_4 \cos\theta_5 \sin\theta_6 - \cos(-\theta_2 + \theta_3)\sin\theta_5 \sin\theta_6$
$- \sin(-\theta_2 + \theta_3)\sin\theta_4 \cos\theta_6$

$J_{52} = \sin\theta_4 \cos\theta_5 \sin\theta_6 - \cos\theta_4 \cos\theta_6$

$J_{53} = -\sin\theta_4 \cos\theta_5 \sin\theta_6 + \cos\theta_4 \cos\theta_6$

$J_{54} = \sin\theta_5 \sin\theta_6$

$J_{55} = \cos\theta_6$

$J_{56} = 0$

$J_{61} = \sin(-\theta_2 + \theta_3)\cos\theta_4 \sin\theta_5 - \cos(-\theta_2 + \theta_3)\cos\theta_5$

$J_{62} = -\sin\theta_4 \sin\theta_5$

$J_{63} = \sin\theta_4 \sin\theta_5$

$J_{64} = \cos\theta_5$

$J_{65} = 0$

$J_{66} = 1$

168

APPENDIX G: REDUCED RECONFIGURABLE PUMA 560

DYNAMIC PARAMETERS

$$a_{11} = 2.57 + 1.38\cos^2\theta_2 + 0.3\sin^2(\theta_2 + \theta_3) + 0.744\cos\theta_2\sin(\theta_2 + \theta_3)$$

$$a_{12} = 0.69\sin\theta_2 - 0.134\cos(\theta_2 + \theta_3) - 0.00397\sin(\theta_2 + \theta_3)$$

$$a_{13} = -0.134\cos(\theta_2 + \theta_3) - 0.00397\sin(\theta_2 + \theta_3)$$

$$a_{14} = 0$$

$$a_{15} = 0$$

$$a_{16} = 0$$

$$a_{21} = a_{12}$$

$$a_{22} = 6.79 + 0.744\sin\theta_3$$

$$a_{23} = 0.33 + 0.372\sin\theta_3 - 0.011\cos\theta_3$$

$$a_{24} = 0$$

$$a_{25} = 0$$

$$a_{26} = 0$$

$$a_{32} = a_{23}$$

$$a_{33} = 1.16$$

$$a_{34} = -0.00125\sin\theta_4\sin\theta_5$$

$$a_{34} = 0.00125\cos\theta_4\cos\theta_5$$

$$a_{36} = 0$$

$$a_{41} = a_{14}$$

$$a_{42} = a_{24}$$

$$a_{43} = a_{34}$$

$$a_{44} = 0.2$$

$$a_{45} = 0$$

$$a_{46} = 0$$

169

$$a_{51} = a_{15}$$

$$a_{52} = a_{25}$$

$$a_{53} = a_{35}$$

$$a_{55} = 0.18K_6$$

$$a_{56} = 0$$

$$a_{61} = a_{16}$$

$$a_{62} = a_{26}$$

$$a_{63} = a_{36}$$

$$a_{64} = a_{46}$$

$$a_{65} = a_{56}$$

$$a_{66} = 0$$

$$b_{112} = -2.76\sin\theta_2\cos\theta_2 + 0.744\cos(2\theta_2 + \theta_3) + 0.6\sin(\theta_2 + \theta_3)\cos(\theta_2 + \theta_3)$$
$$- 0.0213 + 0.0426\sin^2(\theta_2 + \theta_3)$$

$$b_{113} = 0.744\cos\theta_2\cos(\theta_2 + \theta_3) + 0.6\sin(\theta_2 + \theta_3)\cos(\theta_2 + \theta_3)$$
$$+ 0.022\cos\theta_2\sin(\theta_2 + \theta_3) - 0.0213 + 0.0426\sin^2(\theta_2 + \theta_3)$$

$$b_{114} = -0.0025\sin(\theta_2 + \theta_3)\cos(\theta_2 + \theta_3)\sin\theta_4\sin\theta_5 + 0.00086\cos\theta_4\sin\theta_5$$
$$- 0.00248\cos\theta_2\cos(\theta_2 + \theta_3)\sin\theta_4\sin\theta_5$$

$$b_{115} = -0.0025\sin^2(\theta_2 + \theta_3)\sin\theta_5 + 0.0025\sin(\theta_2 + \theta_3)\cos(\theta_2 + \theta_3)\cos\theta_4\cos\theta_5$$
$$- 0.00248\cos\theta_2\cos(\theta_2 + \theta_3)\sin\theta_5 + 0.00248\cos\theta_2\cos(\theta_2 + \theta_3)\cos\theta_4\cos\theta_5$$
$$+ 0.00086\sin\theta_4\cos\theta_5$$

$$b_{116} = 0$$

$$b_{123} = 0.267\sin(\theta_2 + \theta_3) - 0.00758\cos(\theta_2 + \theta_3)$$

$$b_{124} = 0$$

$$b_{125} = 0$$

$$b_{126} = 0$$

$$b_{134} = b_{124}$$

$$b_{135} = b_{125}$$

170

$$b_{136} = b_{126}$$

$$b_{145} = 0$$

$$b_{146} = 0$$

$$b_{156} = 0$$

$$b_{212} = 0$$

$$b_{213} = 0$$

$$b_{214} = 0.00164 \sin(\theta_2 + \theta_3) - 0.0025 \cos(\theta_2 + \theta_3) \cos\theta_4 \sin\theta_5$$
$$+ 0.00248 \sin\theta_2 \cos\theta_4 \sin\theta_5 + 0.0003 \sin(\theta_2 + \theta_3) - 0.0006 \sin(\theta_2 + \theta_3) \sin^2\theta_4$$

$$b_{215} = -0.0025 \cos(\theta_2 + \theta_3) \sin\theta_4 \cos\theta_5 + 0.00248 \sin\theta_2 \sin\theta_4 \cos\theta_5$$
$$- 0.000642 \cos(\theta_2 + \theta_3) \sin\theta_4$$

$$b_{216} = 0$$

$$b_{223} = 0.022 \sin\theta_3 + 0.744 \cos\theta_3$$

$$b_{224} = -0.00248 \cos\theta_3 \sin\theta_4 \sin\theta_5$$

$$b_{225} = -0.0025 \sin\theta_5 + 0.00248 \cos\theta_3 \cos\theta_4 \sin\theta_5 - 0.00248 \sin\theta_3 \sin\theta_4$$

$$b_{226} = 0$$

$$b_{234} = -0.00248 \cos\theta_3 \sin\theta_4 \sin\theta_5$$

$$b_{235} = -0.0025 \sin\theta_5 + 0.00248 \cos\theta_3 \cos\theta_4 \sin\theta_5 - 0.00248 \sin\theta_3 \sin\theta_4$$

$$b_{236} = 0$$

$$b_{245} = 0$$

$$b_{246} = 0$$

$$b_{256} = 0$$

$$b_{312} = 0$$

$$b_{313} = 0$$

$$b_{314} = -0.0025 \cos(\theta_2 + \theta_3) \cos\theta_4 \sin\theta_5 + 0.00164 \sin(\theta_2 + \theta_3) + 0.0003 \sin(\theta_2 + \theta_3)$$
$$+ 0.0006 \cos\theta_2 \sin(\theta_2 + \theta_3) \sin^2\theta_4$$

$$b_{315} = -0.0025 \cos(\theta_2 + \theta_3) \sin\theta_4 \cos\theta_5 - 0.000642 \cos(\theta_2 + \theta_3) \sin\theta_4$$

$$b_{316} = 0$$

171

$$b_{323} = 0$$

$$b_{324} = 0$$

$$b_{325} = -0.0025 \sin \theta_5$$

$$b_{326} = 0$$

$$b_{334} = 0$$

$$b_{335} = -0.0025 \sin \theta_5$$

$$b_{336} = 0$$

$$b_{345} = -0.0025 \sin \theta_4 \cos \theta_5$$

$$b_{346} = 0$$

$$b_{356} = 0$$

$$b_{412} = -0.00164 \sin(\theta_2 + \theta_3) + 0.0025 \cos(\theta_2 + \theta_3) \cos \theta_4 \sin \theta_5$$
$$- 0.00248 \sin \theta_2 \cos \theta_4 \sin \theta_5 - 0.0003 \sin(\theta_2 + \theta_3) + 0.0006 \sin(\theta_2 + \theta_3) \sin^2 \theta_4$$

$$b_{413} = 0.0025 \cos(\theta_2 + \theta_3) \cos \theta_4 \sin \theta_5 - 0.00164 \sin(\theta_2 + \theta_3) - 0.0003 \sin(\theta_2 + \theta_3)$$
$$- 0.0006 \cos \theta_2 \sin(\theta_2 + \theta_3) \sin^2 \theta_4$$

$$b_{414} = 0$$

$$b_{415} = -0.00064 \cos(\theta_2 + \theta_3) \cos \theta_4$$

$$b_{416} = 0$$

$$b_{423} = 0$$

$$b_{424} = 0$$

$$b_{425} = 0.00064 \sin \theta_4$$

$$b_{425} = 0$$

$$b_{426} = 0$$

$$b_{435} = 0.00064 \sin \theta_4$$

$$b_{445} = 0$$

$$b_{446} = 0$$

$$b_{456} = 0$$

172

$$b_{512} = 0.0025\cos(\theta_2 + \theta_3)\sin\theta_4\cos\theta_5 - 0.00248\sin\theta_2\sin\theta_4\cos\theta_5$$
$$+ 0.000642\cos(\theta_2 + \theta_3)\sin\theta_4$$

$$b_{513} = 0.0025\cos(\theta_2 + \theta_3)\sin\theta_4\cos\theta_5 + 0.000642\cos(\theta_2 + \theta_3)\sin\theta_4$$

$$b_{514} = 0.00064\cos(\theta_2 + \theta_3)\cos\theta_4$$

$$b_{515} = 0$$

$$b_{516} = 0$$

$$b_{523} = 0.0025\sin\theta_5$$

$$b_{524} = -0.00064\sin\theta_4$$

$$b_{525} = 0$$

$$b_{526} = 0$$

$$b_{534} = -0.00064\sin\theta_4$$

$$b_{535} = 0$$

$$b_{536} = 0$$

$$b_{545} = 0$$

$$b_{546} = 0$$

$$b_{556} = 0$$

$$b_{612} = 0$$

$$b_{613} = 0$$

$$b_{614} = 0$$

$$b_{615} = 0$$

$$b_{616} = 0$$

$$b_{623} = 0$$

$$b_{624} = 0$$

$$b_{625} = 0$$

$$b_{626} = 0$$

$$b_{634} = 0$$

$$b_{635} = 0$$

173

$b_{636} = 0$

$b_{645} = 0$

$b_{646} = 0$

$b_{656} = 0$

$c_{11} = 0$

$c_{12} = 0.69\cos\theta_2 + 0.134\sin(\theta_2 + \theta_3) - 0.0238\sin\theta_2$

$c_{13} = 0.267\sin(\theta_2 + \theta_3) - 0.00758\cos(\theta_2 + \theta_3)$

$c_{14} = 0$

$c_{15} = 0$

$c_{16} = 0$

$c_{21} = 2.76\sin\theta_2 \cos\theta_2 - 0.744\cos(2\theta_2 + \theta_3) + 0.6\sin(\theta_2 + \theta_3)\cos(\theta_2 + \theta_3)$
$+ 0.0213 + 0.0426\sin^2(\theta_2 + \theta_3)$

$c_{22} = 0$

$c_{23} = 0.011\sin\theta_3 + 0.394\cos\theta_3$

$c_{24} = 0$

$c_{25} = 0$

$c_{26} = 0$

$c_{31} = -0.392\cos\theta_2 \cos(\theta_2 + \theta_3) - 0.3\sin(\theta_2 + \theta_3)\cos(\theta_2 + \theta_3)$
$- 0.011\cos\theta_2 \sin(\theta_2 + \theta_3) + 0.0165 + 0.0213\sin^2(\theta_2 + \theta_3)$

$c_{32} = 0.011\sin\theta_3 + 0.392\cos\theta_3$

$c_{33} = 0$

$c_{34} = -0.00125\cos\theta_4 \sin\theta_5$

$c_{35} = -0.00125\cos\theta_4 \sin\theta_5$

$c_{36} = 0$

$c_{41} = 0.00125\sin(\theta_2 + \theta_3)\cos(\theta_2 + \theta_3)\sin\theta_4 \sin\theta_5 - 0.00043\cos\theta_4 \sin\theta_5$
$+ 0.00124\cos\theta_2 \cos(\theta_2 + \theta_3)\sin\theta_4 \sin\theta_5$

$c_{42} = 0.00124\cos\theta_3 \sin\theta_4 \sin\theta_5$

174

$c_{43} = 0$

$c_{44} = 0$

$c_{45} = 0$

$c_{46} = 0$

$c_{51} = 0.00125 \sin^2(\theta_2 + \theta_3) \sin \theta_5 - 0.00125 \sin(\theta_2 + \theta_3) \cos(\theta_2 + \theta_3) \cos \theta_4 \cos \theta_5$
$+ 0.00124 \cos \theta_2 \cos(\theta_2 + \theta_3) \sin \theta_5 - 0.00124 \cos \theta_2 \cos(\theta_2 + \theta_3) \cos \theta_4 \cos \theta_5$
$- 0.00043 \sin \theta_4 \cos \theta_5$

$c_{52} = 0.00125 \sin \theta_5 - 0.00124 \cos \theta_3 \cos \theta_4 \sin \theta_5 + 0.00124 \sin \theta_3 \sin \theta_4$

$c_{53} = -0.00125 \sin \theta_5$

$c_{54} = 0$

$c_{55} = 0$

$c_{56} = 0$

$c_{61} = 0$

$c_{62} = 0$

$c_{63} = 0$

$c_{64} = 0$

$c_{65} = 0$

$c_{66} = 0$

$G_1 = 0$

$G_2 = (-4.421632 \cos \theta_2 + 1.5266816 \sin^2 \theta_2 - 2.2108160 \cos(\theta_1 + \theta_2) \cos \theta_2$
$+ 0.7633408 \sin(\theta_1 + \theta_2))g$

$G_3 = (-0.048768 \sin^2(\theta_2 + \theta_3) + 0.048768 \cos \theta_1 \cos^2(\theta_2 + \theta_3) + 0.097536 \cos(\theta_2 + \theta_3))g$

$G_4 = 0.0692912(2 \cos^2 \theta_4 + \cos(\theta_2 + \theta_3) \cos \theta_4 + \cos \theta_1 \sin(\theta_2 + \theta_3) \sin \theta_4) \sin(\theta_2 + \theta_3))g$

$G_5 = 0$

$G_6 = 0.0073125 K_6 (-\sin(\theta_2 + \theta_3) \sin \theta_4 \sin^2 \theta_6 + \cos(\theta_2 + \theta_3) \sin \theta_5 \sin \theta_6 \cos \theta_6$
$+ \sin(\theta_2 + \theta_3) \cos \theta_4 \cos \theta_5 \sin \theta_6 \cos \theta_6 - K_6 \cos \theta_1 \cos^2(\theta_2 + \theta_3) \cos \theta_4 \cos^2 \theta_5 \sin \theta_6$
$- \sin \theta_1 \cos^2(\theta_2 + \theta_3) \cos \theta_4 \cos^2 \theta_5 \cos \theta_6)g$

175

VITA AUCTORIS

NAME:	Ana M. Djuric
PLACE OF BIRTH	Uzice, Serbia
YEAR OF BIRTH	1966
EDUCATION	Belgrade University, Belgrade, Serbia 1985-1993 Dipl. of Mechanical Engineering
	University of Windsor, Windsor, Canada 1997-1999 M. A. Sc.
	University of Windsor, Windsor, Ontario, Canada 2003-2007 Ph.D.

176

PUBLICATIONS

Ana M. Djuric, ElMaraghy, W. H, ElBeheiry, E. M., 2004, "Unified integrated modelling of robotic systems", NRC International Workshop on Advanced Manufacturing, June 2004, London, Canada.

Ana M. Djuric and W. H. ElMaraghy (2006). "Generalized Reconfigurable 6-Joint Robot Modeling", Transactions of the CSME, Vol. 30, No. 4, pp. 533-565

Ana M. Djuric and W. H. ElMaraghy, (2007) "A Unified Reconfigurable Robots Jacobian", Proc. of the 2nd Int. Conf. on Changeable, Agile, Reconfigurable and Virtual Production pp. 811-823

Ana M. Djuric, (2007), "Reconfigurable MAPLE 10® Program for Calculation of the 6R - Joint Robot Dynamics", Industrial and Manufacturing (IMS) Center, University of Windsor, Technical Document number 2007-01.